

Mineral self-organization in extreme geochemical environments: *implications for prebiotic chemistry and life detection*

Ilektra E. Kotopoulou

Ph.D Thesis



UGR

Universidad
de Granada



erc
European Research Council
Established by the European Commission



CSIC
CONSEJO SUPERIOR DE INVESTIGACIONES CIENTÍFICAS

IACt
INSTITUTO ANDALUZ DE CIENCIAS DE LA TIERRA

Mineral self-organization in extreme geochemical environments: implications for prebiotic chemistry and life detection

Ilektra E. Kotopoulou

**This dissertation is submitted for the degree of
*Doctor of Philosophy***



Thesis Supervisor, Prof. Juan Manuel Garcia-Ruiz

April 2020

**Universidad de Granada (UGR)
Consejo Superior de Investigaciones Científicas (CSIC)
Instituto Andaluz de Ciencias de la Tierra (IACT)
Laboratorio de Estudios Cristalográficos (LEC)**

Editor: Universidad de Granada. Tesis Doctorales
Autor: Electra Kotopoulou
ISBN: 978-84-1306-539-7
URI: <http://hdl.handle.net/10481/62931>

Publications associated with this doctoral thesis

Publicaciones asociadas a esta tesis doctoral

- 1. E Kotopoulou**, M Lopez-Haro, JJ Calvino Gamez, JM Garcia-Ruiz. Nanoscale anatomy of Fe-silica self-organized membranes: implications for prebiotic chemistry. *Angew. Chem.* (submitted)
- 2. E Kotopoulou**, AD Huertas, JM Garcia-Ruiz, JM Dominguez-Vera, JM Lopez-Garcia, I Guerra-Tschuschke, F Rull. A Polyextreme Hydrothermal System Controlled by Iron: The Case of Dallol at the Afar Triangle. *ACS Earth and Space Chemistry* Cover 2019, 3, 90-99.
- 3.** JM García-Ruiz, E Nakouzi, **E Kotopoulou**, L Tamborrino, O Steinbock. Biomimetic mineral self-organization from silica-rich spring waters. *Science Advances* 2017, e1602285.

Other publications NOT directly associated with this doctoral thesis

Otras publicaciones NO directamente asociadas a esta tesis doctoral

- 1. E Kotopoulou**, A Godelitsas, J Göttlicher, R Steininger, R Price, D.A Fike, J. P. Amend, W.P Gilhooly III, G Druschel, P Nomikou, PN Gamaletsos, S Lozios. Geochemistry and nanomineralogy of Fe-sulfides from As-rich shallow-sea hydrothermal sediments. *Marine Chemistry* (under review).
- 2.** E Margariti, ET Stathopoulou, Y Sanakis, **E Kotopoulou**, P Pavlakis, A Godelitsas. A geochemical approach to fossilization processes in Miocene vertebrate bones from Sahabi, NE Libya. *Journal of African Earth Sciences* 2019, 149, 1-18.
- 3.** F. Otálora, A Mazurier, JM Garcia-Ruiz, MJ Van Kranendonk, **E Kotopoulou**, A El Albani, CJ Garrido. A crystallographic study of crystalline casts and pseudomorphs from the 3.5 Ga Dresser Formation, Pilbara Craton (Australia). *Journal of Applied Crystallography* 2018, 51, 1050-1058.

'Αθηνᾶ ∞ Alexander

Funding

This thesis was developed within the European Research Council under the Programme (FP7/2007-2013)/ERC Grant Agreement 340863 (Prometheus) and from MINECO, ref CGL2016-78971-P, AEI/FEDER, UE”.

ABSTRACT

The overarching goal of this thesis was to investigate the role of mineral self-organization and abiotic mineral precipitation in early Earth geochemistry, prebiotic chemistry and life detection, by focusing on two case studies: a) the precipitation and nanoscale characterization of iron-silica self-organized, filamentous membranes, grown from both synthetic and natural solutions, and b) the geochemistry and mineral precipitation at the polyextreme hydrothermal system of Dallol, the physicochemical conditions of which impose a limit to the habitable space of life.

Iron-silica filamentous self-organized membranes, known as chemical gardens, form spontaneously by mixing an alkaline, silicate, solution with an iron-salt seed/solution as a result of osmosis, buoyancy and reaction-diffusion processes. These membranes exhibit a series of astonishing physicochemical properties, relevant for prebiotic chemistry and life detection. Particularly they: i) behave as fuel cells, generating an electrochemical potential of the range of 550 mV, owing to the ion and pH gradients across the membrane wall, ii) can catalyze the formation of amino-/carboxylic acids and RNA nucleobases from organics that were available on early Earth (i.e. formamide (CH_3NO) and pyruvate ($\text{CH}_3\text{COCO}_2^-$), iii) function as an effective shield against UV radiation, and iv) grow into tubular, life-reminiscent morphologies, similar to biologic iron filaments.

So far, they have been synthesized in the laboratory and we currently lack insight on the plausibility of their formation in natural environments. At the same time and despite their relevance for prebiotic chemistry, little is known about the structure and mineralogy of these, nanocomposite, membranes at the nanoscale. The first part of this thesis aims to address these issues by studying the structure and mineralogy of iron-silica membranes at the nanoscale, and by exploring their precipitation from natural hyperalkaline, silica-rich water (Ney spring, CA, USA), analogous to aqueous environments of early Earth.

Focused ion beam (FIB)-milled sections of iron-silica membranes, grown from both synthetic (i.e. model membranes) and natural solutions (i.e. natural membranes), were studied using advanced electron microscopy tools. To mimic the early Earth anoxic environments, membrane growth and following nanoscale study were also performed in oxygen-free conditions. The obtained results showed that iron-silica self-organization brings two different surfaces together in one membrane; an outer amorphous silica wall and an inner iron-rich wall. The latter is composed of akaganeite, goethite and magnetite, of large surface areas and inter-/intra-particle porosity. In fact, the building

of the membrane resembles that of a heterogeneous catalyst. Moreover, it was observed that under certain conditions these membranes can exhibit a bilayer structure, where the external silica layers enclose the iron nanoparticles.

Moreover, iron-silica membranes were grown from natural water deriving from a serpentinization setting (i.e, Ney spring, California), supporting the geochemical plausibility of their precipitation in natural environments. The mixing of the Ney water with ferrous iron salts resulted in the typical tubular Fe-silica garden formation. The nanoscale study of the natural Fe(II)-silica membranes showed similar features to the model ones in terms of morphology, structure and mineralogy. In fact, additional surface area measurements suggest that membranes grown from natural waters hold even higher catalytic potential than the model ones. On the contrary, natural Fe(III)-silica membranes (produced with ferric iron salts) breached, soon after their formation due to abundant CO₂ gas release, giving rise to a convection cell that lasted for several minutes. This behavior increases the availability of the surface area of both sides of the membranes (silicate-rich and iron-rich), and quickly releases any newly forming molecules in the solution, enhancing their role as catalysts in geochemical scenarios.

Considering their geochemically plausible precipitation in early Earth hydrothermal systems, where abiotic organics were also produced, iron-silica membranes could have assisted in the generation and organization of the first biologically relevant organic molecules. At the same time, the morphological and mineralogical resemblance of the iron-silica tubular membranes, obtained from purely inorganic reactions, to biogenic iron filaments found in cherts and considered as the oldest remnants of life on this planet, further blurs the boundaries between geochemical and biological morphologies. Thus, the iron-silica membranes present a noteworthy duality; on the one hand these inorganic membranes should not be misinterpreted as remnants of life, while on the other hand, they probably played a critical role in the geochemical origin of life itself.

The study of extreme geochemical environments, i.e. geological sites where extreme physicochemical conditions limit or inhibit life's existence, may provide: i) key information about the early Earth mineral scenery in which life emerged, and ii) help differentiate purely abiotic self-organized mineral assemblies from those formed under the control and/or influence of biological activity. In the search of modern analogue-sites for the study of inorganic mineral formation/precipitation, polyextreme environments and particularly highly acidic and highly saline

environments make the most promising candidates. This is because the combination of extreme salinity with acidity is thought to impose a geochemical barrier to life.

In this framework, the second part of this thesis deals with the geochemistry and mineralogy of a polyextreme hydrothermal system located in the Danakil depression of the Afar Triangle (NE Ethiopia), known as Dallol. The hydrothermal springs of Dallol discharge hypersaline ($> 30\%$), hyperacidic (near to zero pH), oxygen-free (CO_2 -rich) brines containing up to 150 g/L of iron; the fumarolic fields of Dallol emit mainly CO_2 , SO_2 , H_2S gases. Dallol comprises the most acidic natural environment of Earth and the combination of hyperacidity with hypersalinity is most likely imposing a geochemical barrier to life.

In situ measurements, geological mapping, hydrochemical and stable isotopic analysis (hydrogen-oxygen, carbon, nitrogen, argon) of the brines and gases, and mineralogical analysis of the precipitates resulted in the detailed geochemical description of Dallol, presented for the first time in this study. Our results demonstrated that Dallol is a hydrothermal system under the control of iron. The generation of the hyperacidity, the brine evolution, the impressive color palette and the mineral paragenesis are controlled by inorganic processes, related to ferrous iron oxidation and iron complexation with chlorides and sulfates. To determine the redox state across the aqueous system of Dallol, the concentration of the Fe(II) and Fe(III) species was measured in different spring solutions and related pools, by using UV-Vis spectroscopy. Also, UV-Vis and Raman spectroscopies were used for the identification of the iron species responsible for the colors of the brines. The mineralogy of precipitates, patterns and biomorphic structures was resolved by using a series of techniques (PXRD, micro-Raman, FESEM-EDS, TEM). In situ incubations of isotopically-labeled compounds were performed for the detection of biologic activity in the pools and fixed filters of the brines were microscopically studied. However, no microorganisms were detected and recent microbiological studies confirmed the absence of microbial activity from the entire site of Dallol, supporting the findings presented here. Owing to these extremely reducing and sterile conditions, Dallol constitutes a unique, in vivo, laboratory for the abiotic precipitation, self-organization and progressive oxidation of iron minerals, relevant for geochemical processes taking place at early Earth and Martian environments.

In a nutshell, the study of inorganic mineral precipitation and mineral self-organization in extreme geochemical environments may provide insight on the mineral processes that occurred on early Earth and most probably paved the geochemical pathway to life. Given that inorganic mineral

precipitation and mineral self-organization commonly produce morphologically and chemically similar structures to biologic ones, their study has direct implications on fossil life detection in the rock record of Earth and Earth-like planets.

RESUMEN

El objetivo principal de esta tesis es entender el papel que haya jugado el auto-ensamblaje mineral y la precipitación de minerales abiótica en la geoquímica de la Tierra primitiva, la química prebiótica y la detección de vida. Para ello, se ha llevado a cabo un estudio detallado de dos sistemas de interés sobre: *a)* la formación de membranas auto-organizadas de hierro-sílice en disoluciones modelo (preparadas en el laboratorio) y naturales; *b)* la geoquímica y formación mineral en las condiciones poli-extremas del sistema hidrotermal del Dallol (Etiopía), cuyas condiciones fisico-químicas hacen prácticamente imposible la existencia de vida. Las membranas tubulares auto-organizadas de hierro y sílice, también conocidas como jardines de sílice, se forman espontáneamente en disoluciones alcalinas que contienen silicato y una sal de hierro. Su formación se debe a procesos de osmosis, flotabilidad y difusión. Estas membranas poseen propiedades fisicoquímicas muy relevantes para la química prebiótica y la detección de vida: *i)* se comportan como pilas de combustible, generando un potencial electroquímico de unos 550 mV debido a la difusión de iones y el gradiente de pH entre las paredes de las membranas; *ii)* catalizan la formación de aminoácidos y nucleobases de ARN a partir de moléculas orgánicas presentes en la Tierra primitiva (*i.e.*, formamida (CH_3NO) y piruvato ($\text{CH}_3\text{COCO}_2^-$); *iii)* protegen de la radiación UV; y *iv)* crecen en forma de tubo con morfología similar a la de los filamentos de hierro de origen biológico. Hasta ahora, los jardines de sílice sólo se han obtenido en el laboratorio y no se conoce si su precipitación suele ocurrir en aguas naturales. Además, y a pesar de su gran relevancia para la química prebiótica y la detección de vida, se conoce muy poco sobre su estructura y mineralogía a escala nanométrica.

La primera parte de esta tesis doctoral aborda el estudio de la estructura y mineralogía de las membranas de hierro-sílice a escala nanométrica y de su precipitación en disoluciones naturales altamente alcalinas y ricas en sílice recolectados de los manantiales de Ney (CA, USA), considerados como análogos a ambientes acuosos de la Tierra primitiva. Se han obtenido jardines en disoluciones preparadas en el laboratorio (*i.e.*, membranas modelo) y en disoluciones naturales (*i.e.*, membranas naturales). Para imitar los ambientes anóxicos que prevalecieron en la Tierra primitiva, también se realizó la síntesis y caracterización de estas membranas en condiciones anaeróbicas. La estructura interna de las membranas, diseccionadas mediante haces de iones focalizados (FIB, del inglés Focused Ion Beam), se ha caracterizado con microscopía electrónica de alta resolución. Se ha observado que las membranas se componen de dos tipos de capas bien diferenciadas: una capa externa rica en sílice amorfa y otra capa interna rica en hierro. La capa

interna se compone de minerales como akaganeíta, goetita y magnetita que disponen de una gran área específica debida a la porosidad inter- e intraparticular.

Después del crecimiento de la membrana tubular, y cuando el sistema ha alcanzado el equilibrio (~70h), difusión de CO₂ atmosférico en el sistema reduce el pH alcalino inicial lo cual induce la formación de una capa de sílice sobre la cara interna de la membrana tubular. De esta forma, se genera una membrana en bicapa, en la que una capa rica en hierro está recubierta por dos capas de sílice. Hasta el momento, esta importantísima característica de membrana bicapa no ha sido reportado debida a las limitaciones de las técnicas utilizadas. Lo cual demuestra una vez más la importancia de estudiar los procesos a escala manométrica.

Por otro lado, la disolución de sales de hierro ferroso en el agua de Ney (aguas naturales extraídas de zonas de serpentinización) dio lugar a la formación típica de jardines de sílice, los tubos. Además de las similitudes morfológicas, estas membranas naturales presentan también propiedades mineralógicas y estructurales muy similares a las de las membranas modelo. Incluso se ha observado que las membranas naturales poseen mayor área específica que las membranas modelo, lo que favorecería una mayor capacidad catalítica. Sin embargo, las membranas naturales de hierro se rompen durante su formación, debido a la aparición de zonas de convección generadas por el desprendimiento de grandes cantidades de CO₂. Este proceso favorece la disponibilidad de ambas superficies (la externa rica en sílice y la interna rica en hierro) y facilita la liberación de especies generadas en el interior de la membrana, lo que aumentaría la actividad catalítica en ambientes geoquímicos específicos. Teniendo en cuenta su más que posible formación en ambientes hidrotermales de la Tierra primitiva, donde además se general moléculas orgánicas abióticas, es lógico pensar que los jardines de sílice han podido jugar un papel importante en la formación de los primeros sistemas biológicos. Sin embargo, las similitudes morfológicas y estructurales entre los jardines tubulares puramente inorgánicos y los filamentos de hierro biogénicos en rocas y precipitados ricos en sílice, considerados los restos biológicos más antiguos de la Tierra, demuestran que la frontera entre lo mineral y lo vivo es aún más difusa de lo que se pensaba. Por lo tanto, con las membranas de hierro-sílice existe una dualidad reseñable: a pesar de que podrían haber jugado un papel muy importante en el origen geoquímico de la vida, ponen de manifiesto que su morfología no puede ser un criterio inequívoco para distinguir lo biológico de lo inorgánico.

Por otro lado, el estudio de la formación mineral en ambientes geoquímicos extremos (*i.e.*, donde las condiciones fisico-químicas hacen poco viable o incluso inexistente la vida) permite obtener: *i*)

información relevante sobre el escenario mineral donde surgió la vida en la Tierra; *ii*) patrones para diferenciar entre minerales puramente abióticos y minerales formados bajo la influencia de organismos vivos. En este sentido, ambientes naturales con condiciones poli-extremas, y específicamente con valores extremos de pH y salinidad, son ideales para estudiar la formación mineral en condiciones abióticas.

Por lo tanto, la segunda parte de la tesis se centra en estudiar la geoquímica y mineralogía de un sistema poli-extremo único en el mundo, Dallol, localizado en la depresión de Danakil, en el valle del Rift (Etiopía). Dallol es un sistema hidrotermal con temperaturas de 108 °C, hipersalinidad (> 30%) e hiperacidez (con valores de pH próximos a 0), además de altas concentraciones de hierro (150 g L⁻¹) y anaerobiosis. Las fumarolas de Dallol emiten principalmente gases de CO₂, SO₂, H₂S. Estas condiciones tan extremas del Dallol pueden suponer una barrera natural para el desarrollo de vida.

Mediante experimentos *in situ* en Dallol se ha estudiado en detalle la actividad hidrotermal, se ha llevado a cabo el análisis de isótopos estables (hidrógeno-oxígeno, carbón, nitrógeno y argón) de las salmueras y gases emitidos y se ha analizado minuciosamente la mineralogía de los precipitados. Los resultados obtenidos han permitido describir, por primera vez, la geoquímica de Dallol y han puesto de manifiesto la importancia del hierro en este sistema hidrotermal. El estado de oxidación del hierro en distintos manantiales se determinó midiendo las concentraciones de Fe(II) y Fe(III) mediante espectroscopia UV-vis. Asimismo, se identificaron los complejos de Fe responsables del color de las salmueras mediante espectroscopias UV-Vis y Raman. La identificación de los precipitados y estructuras biomorficas se llevó a cabo mediante una combinación de técnicas complementarias incluyendo difracción de rayos X (PXRD), microscopía Raman y microscopias electrónicas de alta resolución (FESEM-EDS y TEM). Hemos demostrado que la hiperacidez, la evolución de las salmueras, la impresionante paleta de colores y la precipitación mineral están controlados por procesos puramente inorgánicos, relacionados con la oxidación del Fe y la formación de complejos con cloruros y sulfatos. De hecho, la ausencia de microorganismos en las aguas de Dallol se ha demostrado mediante experimentos *in situ* de marcaje isotópico con ¹⁸O y ¹³C-urea en las salmueras y estudio microscópico de los filtros de las salmueras. La ausencia de vida en las aguas de Dallol ha sido confirmada recientemente por otro grupo de investigación. Por lo tanto, todas estas condiciones extremas hacen de Dallol un lugar único y un laboratorio natural para el estudio de precipitación abiótica, auto-organización y oxidación progresiva de hierro, procesos que tuvieron lugar en la Tierra primitiva y en Marte.

En resumen, el estudio de procesos de precipitación de minerales y auto-ensamblaje en condiciones (geo)químicas extremas, como son la formación de membranas de hierro-sílice y los precipitados hidrotermales de Dallol, es primordial para avanzar nuestro entendimiento de los procesos abióticos y prebióticos, y la relación entre ambas, que ocurrieron en la tierra primitiva y que dieron lugar a la vida en nuestro planeta. Además, comprender bien estos procesos nos ayudara a reconocerlos mejor en el registro de rocas de nuestro planeta, pero también de otros cuerpos estelares.

TABLE OF CONTENTS

| | |
|---|-----------|
| ABSTRACT | 6 |
| RESUMEN | 10 |
| 1. Introduction..... | 18 |
| 1.1. Mineral self-organization | 19 |
| 1.2. Extreme geochemical environments | 21 |
| 1.3. Mineral self-organization and its relevance to prebiotic chemistry and life detection | |
| 25 | |
| 1.3.1. Me-silica membranes growth and physicochemical properties | 25 |
| 1.3.2. Iron-silica self-organized membranes | 30 |
| 1.3.3. Mineral precipitation at polyextreme conditions | 33 |
| 1.4. Thesis objectives | 35 |
| 1.5. Thesis outline..... | 37 |
| References | 38 |
| 2. Iron-silica self-organized membranes: geochemical plausibility, nanoscale | |
| characterization and catalytic behavior | 49 |
| 2.1. Summary | 50 |
| 2.2. Experimental and analytical part | 51 |
| 2.3. Results and discussion | 55 |
| 2.3.1. Fe-silica membranes formation from the Ney water..... | 55 |
| 2.3.2. Microscopic and spectroscopic study at the nanoscale: model vs natural membranes. | |
| 64 | |
| 2.3.3. Catalytic potential of the self-organized Fe-silica membranes | 68 |
| 2.3.4. Fe-silica membranes formation and nanoscale characterization in anoxic conditions | |
| 70 | |

| | |
|--|------------|
| 2.3.5. Inorganic Fe-silica membranes and their biologic counterparts: a life detection issue | 73 |
| 2.4. Findings and concluding remarks | 76 |
| References | 79 |
| 3. Geochemistry and mineralogy of the polyextreme hydrothermal system of Dallol, NE Ethiopia | 86 |
| 3.1. Summary | 87 |
| 3.3. Results and discussion | 94 |
| 3.3.1. The hydrothermal system of Dallol | 94 |
| 3.3.2. Hydrochemistry | 97 |
| 3.3.3. Acidity and iron speciation | 99 |
| 3.3.4. Mineralogy of iron, self-organized, precipitates | 106 |
| 3.3.5. Isotopic study | 109 |
| 3.3.6. Biogeochemical investigation | 110 |
| 3.3.7. Microbiologic review | 113 |
| 3.3.8. Dallol, an analogue-site for abiotic iron mineral precipitation | 115 |
| 3.3.9. Fe-silica self-organized membranes grown from the Dallol spring water | 116 |
| 3.4. Findings and concluding remarks | 118 |
| References | 121 |
| 4. General conclusions, limitations and open questions | 126 |
| 4.1. Iron-silica membranes geochemical plausibility and catalytic potential | 127 |
| 4.1.1. On the Fe-silica membranes precipitation in natural environments | 129 |
| 4.1.2. Fe-silica membranes and microfossils | 131 |
| 4.2. The polyextreme hydrothermal system of Dallol; an analogue-site for abiotic iron minerals' formation and oxidation | 132 |
| 4.2.1. Analogue-site | 132 |

| | |
|--|------------|
| 4.2.2. Dallol hydrothermal brine: un utterly complex fluid | 133 |
| References | 134 |
| APPENDIX | 139 |
| I. Supplementary Information | 139 |
| II. Publications directly related to this thesis | 147 |
| III. Publications non related to this thesis | 150 |

Chapter 1

Introduction

In the multidisciplinary scientific world, it is not uncommon that for the same scientific terms different interpretations are given by the different academic disciplines. For example, the term ‘*self-organization*’ in social sciences refers to the functional differentiation and reflexivity of social-cognitive network systems (Leydesdorff, 2003; Halley and Winkler, 2008), while in biology it usually refers to the ability of biomolecules to establish supermolecular hierarchical organization without external intervention, e.g. protein folding (Scott et al., 2001). Likewise, a metamorphic petrologist might consider as ‘*extreme*’ a geochemical environment of ultra-high pressure (e.g., 1 GPa) or temperature (e.g., 1000 °C), whereas for a microbiologist extreme conditions may merely refer to 38MPa pressure (corresponding to an ocean depth of 3800 m) and 121 °C temperature. As the title indicates, this dissertation that deals with ‘mineral self-organization in extreme geochemical environments’ stands between geochemistry, mineralogy, materials science, and astrobiology. Therefore, to avoid confusion allow me to start unraveling the thesis scope by defining the terms ‘mineral self-organization’ and ‘extreme’ geochemical environments, and continue by explaining the implications these might have for early Earth environments, prebiotic chemical reactions and life detection in the rock record.

1.1. Mineral self-organization

Self-organization in precipitation reactions far from equilibrium is the phenomenon during which chemical cocktails organize spontaneously, i.e. without the intervention of external directing influences, into low symmetry patterns of different complexity. These non-equilibrium conditions are normally obtained by a permanent feed of fresh reactants (Nicolis and Prigogine, 1977). While, self-assembly operates at the nano-microscopic level and results from atomic or cluster interactions leading to well-ordered equilibrium structures characterized by a minimum of free energy, such as crystals, mesophases, lipid membranes or carbon nanotubes, self-organization occurs at a macroscopic level when a system, kept far from equilibrium, dissipates energy (Haken 1977). The classic textbook example of chemical self-organization is the Liesegang rings (Liesegang, 1896)(Figure 1A). This is a type of rhythmic pattern characterized by a macroscopic (millimeter to centimeter-scale) spatial arrangement of precipitate aggregates, each made up of a large number of crystallites of various sizes. These chemical oscillations result from the coupling between diffusion of a dissolved reactant and the nucleation, growth and/or ripening of the precipitate product. Other well-studied examples are the Belousov-Zhabotinsky oscillating reactions, the Turing patterns and silica self-organized nanostructures, namely silica gardens and biomorphs (Figure 1B-D)(Turing, 1952; Petrov et al., 1993; Garcia-Ruiz et al., 2003; 2009; Kellermeier et al., 2013; Nakouzi and

Steinbock, 2016). Such self-organized systems hold great promise for modern materials science because they provide an alternative route for the fabrication of advanced materials, for example, autocatalytic membranes and self-healing materials (Nakouzi and Steinbock, 2016). But, more importantly, more and more studies consider chemical self-organization a plausible pathway to biologic self-organization (Russell et al., 1994; Monnard and Deamer, 2002; Hanczyc et al., 2003; Garcia-Ruiz et al., 2020).

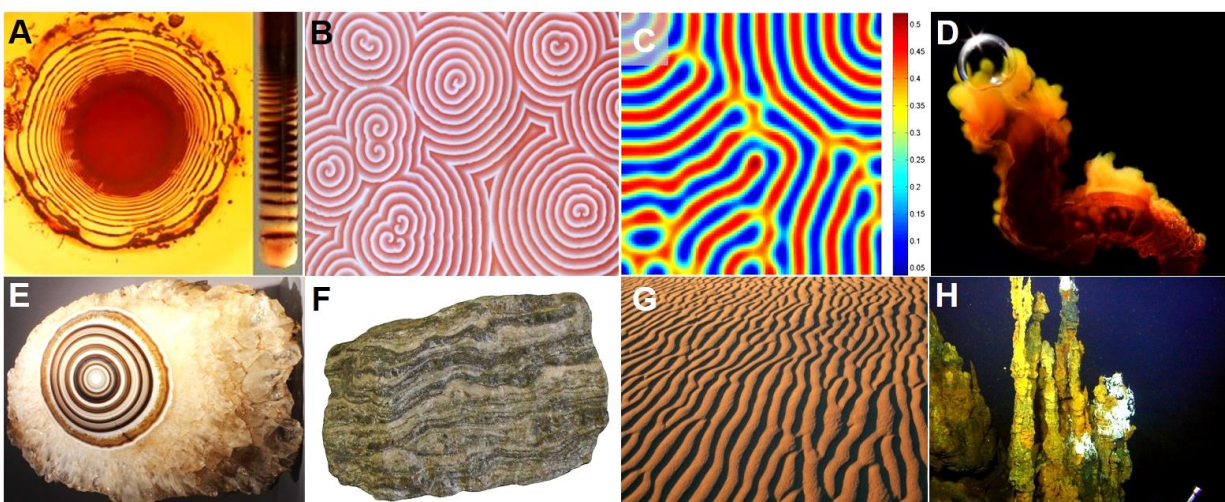


Figure 1. Self-organization patterns in chemical and Earth systems. **A.** Liesegang rings. **B.** Belousov-Zhabotinsky oscillation reaction. **C.** Turing patterns. **D.** Bubbled-guided filamentous iron-silica gardens (image by Stephane Querbes). **E.** Sardonix agate (Natural History museum of Paris). **E.** Gneiss foliation (source Britannica). **F.** Aeolian ripples in sand dune. **H.** Hydrothermal chimneys from the Brothers Volcano, New Zealand (NOAA).

A number of rhythmic and/or hierarchical patterns resulting from self-organized processes have been observed in geological systems (Fig. 1E-H), both in macro- and micro-scales, although the term ‘self-organization’ is not frequently used by Earth scientists. Rocks and minerals often exhibit rhythmic patterns, whereby their chemical composition and/or physical properties vary repetitively across a spatial transect. Some of these patterns are the result of systematic variations in the external environment that generated the deposit, i.e. gravitation is traditionally considered to be the fundamental order-creating force in geology, while many other physical/chemical forces can be responsible for reaction-transport feedbacks giving rise to in-situ structure formation (e.g. Chen et al. 1990, Ortoleva et al. 1990). Self-organizing examples that have been proposed for mineral systems are the banding/zoning in agates, geodes, concretions and orbicules, the foliation in gneiss, the boudins in metamorphic rocks, but also Liesegang-like secondary (diagenetic) sedimentary structures showing bands of (authigenic) minerals that are arranged in a regular repeating pattern,

aeolian ripple marks found in sand dunes or hydrothermal whiskers and chimneys (Anderson, 1990; Ortoleva, 1994; Merino and Wang, 2001, Russell et al., 2010; Wang et al., 2015; Ding et al., 2016).

1.2. Extreme geochemical environments

Before life's appearance on Earth, mineral precipitation and growth was abiotic. Once life emerged and expanded on planet Earth, geochemistry-mineralogy and biology have interacted bidirectionally, both indirectly (e.g., providing template and concentration surfaces, nucleation sites, pH-Eh interfaces etc.) and directly (biomineralization). As a result, the search for modern geochemical environments where mineral formation is dictated by inorganic processes is of paramount importance for understanding the early Earth geochemical conditions in which life have emerged, and for differentiating between inorganic and biologically-induced mineral precipitation processes. The latter has direct implications in life detection studies on Earth and other planets/moons. Thus, the study of extreme geochemical environments, i.e., geological sites where extreme physicochemical values limit or inhibit life's existence, may provide key answers to help distinguish self-organized mineral assemblies from those formed under the control and/or influence of biological activity. A review of extreme geochemical environments is given below (Fig. 2).

pH

Extreme geochemical environments may show separately or combined extreme values of pH, temperature, pressure, water activity-salinity, radiation gradients, oxygen and metals/metalloids concentrations (e.g., As, Hg, Cu, Fe), that may impose energetic and nutrient limits on life. Extreme low pH values are to be expected in volcanic environments, such as, the Kawah Ijen Volcano in Indonesia (0.4 pH)(Delmelle y Bernard, 1994) and AMD (acid mine drainage) pits like in Rio Tinto in Spain (~1 pH)(Fernández-Remolar et al., 2005), whereas high pH values are commonly encounter in soda lakes, such as, the Magadi in Kenya (10.9 pH)(Eugster, 1980), as well as in terrestrial and submarine serpentinization sites like the Samail springs, Oman (11-12 pH)(Chavagnac et al., 2013) or the Lost City hydrothermal field, Pacific ocean (11.6)(Kelley et al., 2005). The lowest and highest reported pH values are from a mine in Iron Mt, California (-3.6) and a red mud pit lake in Gorka, Poland (13.3) respectively (Nordstrom et al., 2000; Czop et al., 2011). Currently, the most extreme acidophile and alkaliphile can survive at pH 0 and pH 12.5, respectively (pH_{opt} 0.7 and 11). The lowest pH_{min} -0.06 was observed for two hyperacidophilic Archaea (*Picrophilus oshimae* and *P. torridus*, pH_{opt} 0.7), isolated from a solfataric hot spring in Noboribetsu (Hokkaido, Japan) (Schleper et al., 1996). In contrast, the highest pH_{max} of 12.5 was

observed for an alkaliphilic, aerobic, mesophilic bacterium (*Serpentinomonas* sp. B1, $\text{pH}_{\text{opt}} 11$), isolated from a terrestrial serpentinizing system, The Cedars (Suzuki et al., 2014).

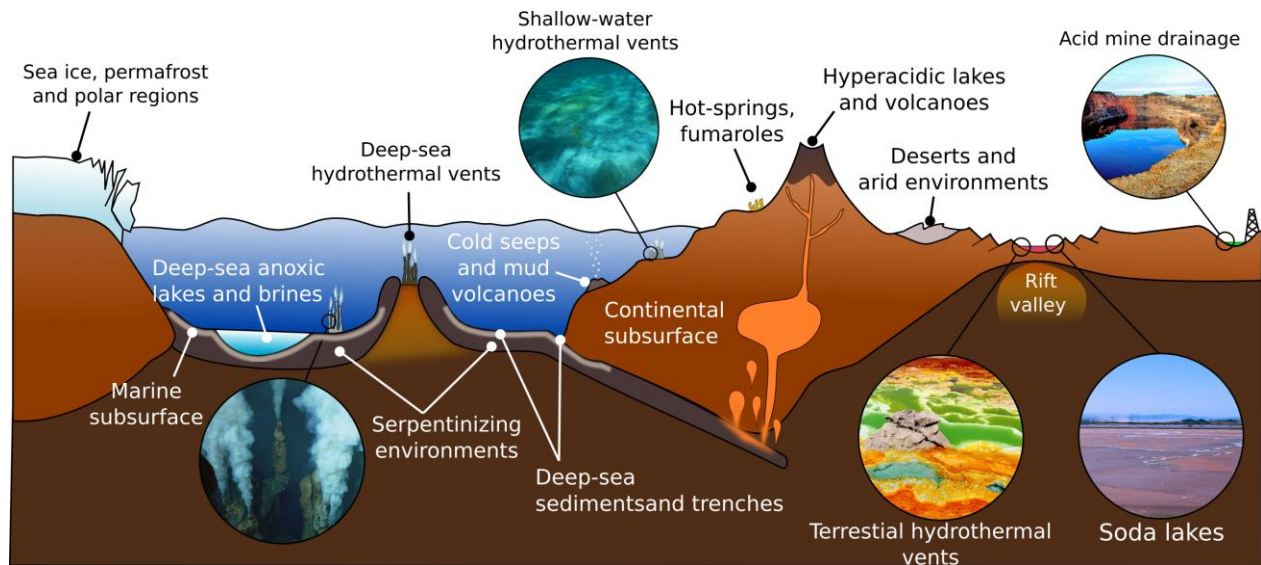


Figure 2. Idealized cross section of Earth's crust showing natural and manmade extreme environments, and their most common (approximate) geodynamic locations (modified after Merino et al., 2019).

Salinity

Saline environments comprise a large portion of the Earth and range from the marine environment (3-4% salinity), hot springs (up to 10.5% salinity), and to soda lakes (up to 37.1% salinity), and even salt inclusions (up to 49.7% salinity) (Scambelluri et al., 1997). Salinity can also vary significantly on smaller scales, for example, in tidal pools (Morris and Taylor, 1983), or on salt mineral grains due to water deliquescence (Davila et al., 2008). A wide range of different ions, including Na^+ , Cl^- , SO_4^{2-} , Ca^{2+} , and Mg^{2+} can contribute to total salinity in the environment (Oren, 2013). The ionic composition can significantly influence water activity, especially in presence of high concentrations chaotropic salts (MgCl_2 , CaCl_2), like in the athalassic deep-sea hypersaline anoxic basins of the Mediterranean Sea (Yakimov et al., 2015) or the geothermal lakes of Danakil, Ethiopia (Gaet' Ale)(Pérez and Chebude, 2017). In addition, water availability in terrestrial saline environments is further influenced by precipitation rates relative to evaporation, resulting in increasing concentration of salts (Finlayson et al., 2018). Concerning microorganisms, the current highest salinity record holder is *Halarsenatibacter silvermanii* strain SLAS-1T, isolated from the alkaline hypersaline Searles Lake (CA, United States) ($\text{salinity}_{\text{opt}} 35\% \text{ NaCl}$) (Blum et al., 2009). The theoretical water activity minima for halophilic archaea and bacteria is 0.611 aw while it is

0.632 aw for fungi (Stevenson et al., 2015). In comparison, the water activity of NaCl saturated solutions is estimated to be 0.755 aw while pure water is 1 aw (Hallsworth et al., 2007; Stevenson et al., 2015). However, when there are high concentrations of the chaotropic MgCl₂ or CaCl₂, the water activity is lowered even more (e.g., 0.3 aw for a saturated MgCl₂ solution). For example, environmental surveys reported microbial communities in the brines of two athalassic deep-sea hypersaline anoxic basin (DHAB), Discovery (MgCl₂ 5M, T = 14.5 °C).

Temperature

The temperature on Earth's surface ranges from -98.6 (East Antarctica) (Scambos et al., 2018) up to 495 °C (deep-sea hydrothermal vents) (McDermott et al., 2018), while much higher temperatures are reached in magma-influenced subsurface environments. Fluid temperatures above 100 °C are possible whenever the combination of hydrothermal or magmatic activity is present together with high pressure, for example, in the deep subsurface near volcanoes or at deep-sea hydrothermal vents. In the absence of geothermal influence, the highest surface temperature reported on Earth is 71 °C, in the Lut Desert (Iran) (Mildrexler et al., 2011). The current temperature extreme that microbial life can survive extends from -25 °C (T_{min}, *Deinococcus geothermalis* DSM 11300) (Frösler et al., 2017) to 130 °C (T_{max}, “*Geogemma barossii*” 121) (Kashefi and Lovley, 2003). The temperature range in which microorganisms are reported to be metabolically active is currently between -20 °C (an enrichment culture from the Siberian permafrost soil) (Rivkina et al., 2000) and 122 °C (*Methanopyrus kandleri* 116; Takai et al., 2008). The upper temperature limit of life might lay near 150 °C, due primarily to the instability of macromolecules above this temperature, while thermodynamic considerations suggest that life might be impossible below - 40 °C (Price and Sowers, 2004). In comparison, the lowest temperature in which a pure culture isolate is capable of growing is -15 °C with 18% salinity (*Planococcus halocryophilus* Or1; Mykytczuk et al., 2012, 2013). In contrast, there are very few halothermophiles, with a combined temperature range of 17–70 °C (T_{opt} = 50–65 °C) and salinity range 2.9–29.2 % (salinity_{opt} = 11.7–26.3 % NaCl) (Mesbah and Wiegel, 2005) and in general an absence of strains in high temperature (>60 °C) and high salinity sites (30% NaCl)(Merino et al., 2019).

Pressure

On Earth's surface, pressure ranges from 0.1 to 112 MPa, with higher pressures observed at the subduction zones (e.g., 900 MPa at the top of a subducting plate, Mariana Forearc)(Mottl et al., 2004), in polar regions and subsurface environments (e.g., Miettinen et al., 2015). It is estimated

that microbial life could be supported at subduction zone forearcs with pressures ~ 340 MPa (Plümper et al., 2017) and the current record holder is *Thermococcus piezophilus*, a thermophilic Archaeon able to survive up to 125 MPa ($P_{\text{opt}} = 50$ MPa, $P_{\text{growth range}} = 0.1\text{--}125$ MPa) (Dalmasso et al., 2016). In contrast to high pressure environments, the low pressure found at high altitude in mountain formations (0.0033 MPa at the summit of Mount Everest) is unlikely to affect microbial survival per se, and the lowest pressure is found in space vacuum or low Earth orbit (10^{-13} to 10^{-10} MPa) (Horneck et al., 2010).

Radioactivity

Apart from natural radioactivity deriving from the radioactive decay of ^{238}U , ^{235}Th and ^{40}K , the most extreme radiation levels are produced from human-made radioactive-contaminated sites. These range from 0.5 Bq/kg at the Great Lakes, United States (Trapeznikov, 1983) to 109 Bq/kg at Hanford Site in Richland, WA, United States (Fredrickson et al., 2004). Concerning other types of ionizing radiation, UV and gamma rays can impact microbial cells via direct and indirect (e.g., the formation of reactive oxygen species) mechanisms. Radiation-resistant microorganisms have been shown to resist up to 30 kGy of γ -radiation, in the case of a thermophilic bacterium *Thermococcus gammatolerans* EJ3 (Jolivet et al., 2003) and a mesophilic bacterium *Deinococcus hohokamensis* (Rainey et al., 2005) and 100–1000 J/m² of UV254, in a xerotolerant bacterium *Psychrobacter pacificensis* LOS3S-03b (La Duc et al., 2007).

Polyextreme environments, where more than two physicochemical extremes meet are relatively rare in the surface of the modern Earth. In fact, so far, no strains have been discovered to grow under the joint extremes of high temperature, salinity, and pH, raising the question of whether life is possible under polyextreme conditions (Harrison et al., 2013).

This dissertation examines mineral systems that self-organize in nanoscale, without the intervention of biological activity. The studied mineral self-organization takes place in extreme geochemical conditions in terms of fluid chemistry, i.e., pH, iron and silica concentrations, and in relation to the chemical limits on the habitable space of life. Emphasis is given in: **a**) mineral membranes that self-organize in presence of iron salts, grown from both laboratory and natural alkaline, silica-rich solutions, **b**) iron mineral precipitation processes in natural, polyextreme environments that may impose a physicochemical limit to the habitable space of life.

For the first case, I studied the precipitation and nanoscale characterization of Fe-silica membranes grown from both sodium (tri)silicate solution (i.e. model membranes) and from natural water from the Ney spring (CA, USA) (i.e. natural membranes). The Ney spring discharges hyperalkaline (pH >12), silica-rich water ($\text{SiO}_2 > 0.65\text{M}$) originating from a serpentinization system. The extremely high pH value of Ney's water arises from serpentinization, a geological process known to produce alkaline, reducing conditions and simple abiotic organic molecules, whereas the high-silica content is due to percolation of the alkaline fluids through silica-rich volcanic rocks. As for the second case, I studied iron geochemistry and mineral precipitation at the terrestrial, hyperacidic (pH <1), hypersaline (w.a. < 0.4), anoxic hydrothermal vents of Dallol (NE Ethiopia). Although these modern settings (alkaline fluids and acidic hydrothermal vents) are under the control of the current atmospheric, biologic and geodynamic processes they can be considered as analogue-sites for early Earth mineral self-organized systems, as explained in the following paragraphs.

1.3. Mineral self-organization and its relevance to prebiotic chemistry and life detection

1.3.1. Me-silica membranes growth and physicochemical properties

One of the most critical steps on the emergence of life on early Earth was the concentration and oligomerization of the biologically relevant organic molecules. But, the information available about water bodies/primitive oceans on Hadean Earth strongly suggests that concentrations of the abiotic building blocks (e.g. amides, lipids, amino acids, etc.) were too dilute for significant oligomerization to occur. To solve this conundrum, absorption on mineral surfaces has been put forward as a plausible mechanism for the significant concentration of the first organic molecules (Deamer et al., 2002; Hanczyc et al., 2003; Hazen and Sverjensky, 2010; Dalai et al., 2016; Gillams and Jia, 2018). In this context, multiple studies examined the role of mineral surfaces in the chemical polymerization reactions that might have taken place at early Earth and in the formation of a proto-cellular membrane by allowing amphiphilic molecules, such as fatty acids, to interact with clays, silica, pyrite, iron-oxides, iron-sulfides etc., assisting the formation of a vesicle (Ferris and Ertem, 1992; Monnard and Deamer, 2002; Hanczyc et al., 2003; Martin and Russell, 2003; Hanczyc et al., 2007; Cleaves II and al., 2012; Sahai et al., 2017). Based on these, and other works (Monnard et al., 2000), it is now generally accepted that mineral-mediated membranes may have provided a geochemical pathway to the transition from inorganic chemistry to biology (Deamer et al., 2002; Hanczyc et al., 2003, Garcia-Ruiz et al., 2020).

Among all mineral-mediated pathways that have been explored so far, those related to inorganic, self-organized, Me-/sulfide/silica(te) membranes, known as chemical gardens, hold a special place.

These membranes have been paralleled to hydrothermal chimneys and might have served as electron/proton conductors and redox catalysts at the early hydrothermal systems which have been proposed as possible niches for the emergence of metabolism (Russell et al., 1994; Martin and Russell, 2003; Barge et al., 2019). Me-silica membranes constitute a remarkable example of spontaneous, inorganic compartmentalization and present a series of intriguing properties. The typical silica garden experiment, i.e. immersing a Me-salt pellet in a water glass solution, results in the spontaneous growth of filamentous, tubular, weed-like shapes that look like biologic features. In fact, it was due to their reminiscence of living forms that they were described as iron trees by Glauber in the 17th century and were later related, for morphological reasons, to the origin of life (Glauber, 1646; Traube, 1867; Leduc, 1911).

Since those studies, a large body of literature has reported on the formation and physicochemical properties of the silica membranes precipitated with a variety of metal salts, among others, those of copper, cobalt, iron, nickel, magnesium, calcium and zinc (Coatman et al., 1980; Collins et al., 1999; Balköse, et al., 2002; Cartwright et al., 2002; Uechi et al., 2004; Pagano et al., 2007a; Pagano et al., 2007b; Pagano et al., 2008; Parmar et al., 2009; Cartwright et al., 2011; Barge et al., 2012; Glaab et al., 2012; Glaab et al., 2016).

In general, self-organization of metal-silica membranes takes place spontaneously when an alkaline, silicate-rich solution reacts with a concentrated metal-source (e.g. soluble metal-salt particle or metal-salt solution), due to a reaction/diffusion-controlled precipitation process (Thouvenel-Romans 2003 Cartwright et al., 2012; Glaab et al., 2012; Kellermeier et al., 2013) (Fig.3). Me-silica membranes exhibit two main morphological types: i) a film that is either growing in hollow, twisted, tubes resembling bacterial filaments that may extend over several decimeters in length, while their diameter is limited to a few millimeters and their walls are only some tens of microns in width (Fig. 3A, C), or, in closed structures that expand through subsequent self-healing breaches (Fig. 3B) and, ii) conjoint vesicles that may extend over several decimeters in diameter and tens of microns in width, exhibiting a botryoidal texture (Fig. 3D-E) (Parmar et al., 2010; Cartwright et al., 2011; Barge et al., 2012; Barge et al., 2015a; Barge et al., 2016; Kellermeier et al., 2013; Nakouzi and Steinbock, 2016; Glaab et al., 2016; Glaab et al., 2017; Bizzarri et al., 2018).

The first type (filamentous or self-healing film) can be obtained by using both solid reactant seeds or solutions. As shown by Cartwright, et al., (2002) high silica concentration favors the rupture of the membrane that leads to the jetting of the inner Me-solution and the branching of the forming

tubes, whereas low silica concentration only forms a gelatinous, more plastic membrane and does not create a tube. Apart from the typical chemistry class experiment, the solid reactant seed can be replaced with a corresponding solution that can be injected at constant flow rates or, at constant driving pressures (Thouvenel-Romans and Steinbock, 2003; Pagano et al., 2008; Makki and Steinbock, 2012; Batista et al., 2014; Wang et al., 2017) or by precipitation at the air-fluid interface when a buoyant metal ion solution is pumped to the surface of a silicate solution (Hussein et al., 2016). In Haudin et al. (Haudin et al., 2014; 2015) experiments complex morphologies were obtained by injecting one of the reacting species into a thin solution layer of its complementary ion (Fig. 3C). Furthermore, one-dimensional membranes similar in composition to chemical gardens have been grown in microfluidic devices (Batista and Steinbock, 2015). On the contrary the second morphological type (vesicles) occurs when mixing two sols, i.e. by injecting microdrops (volume $<2 \mu\text{L}$) of the iron solution into the silicate one, and vice versa (Kotopoulou et al., 2017; Bizzari et al., 2018).

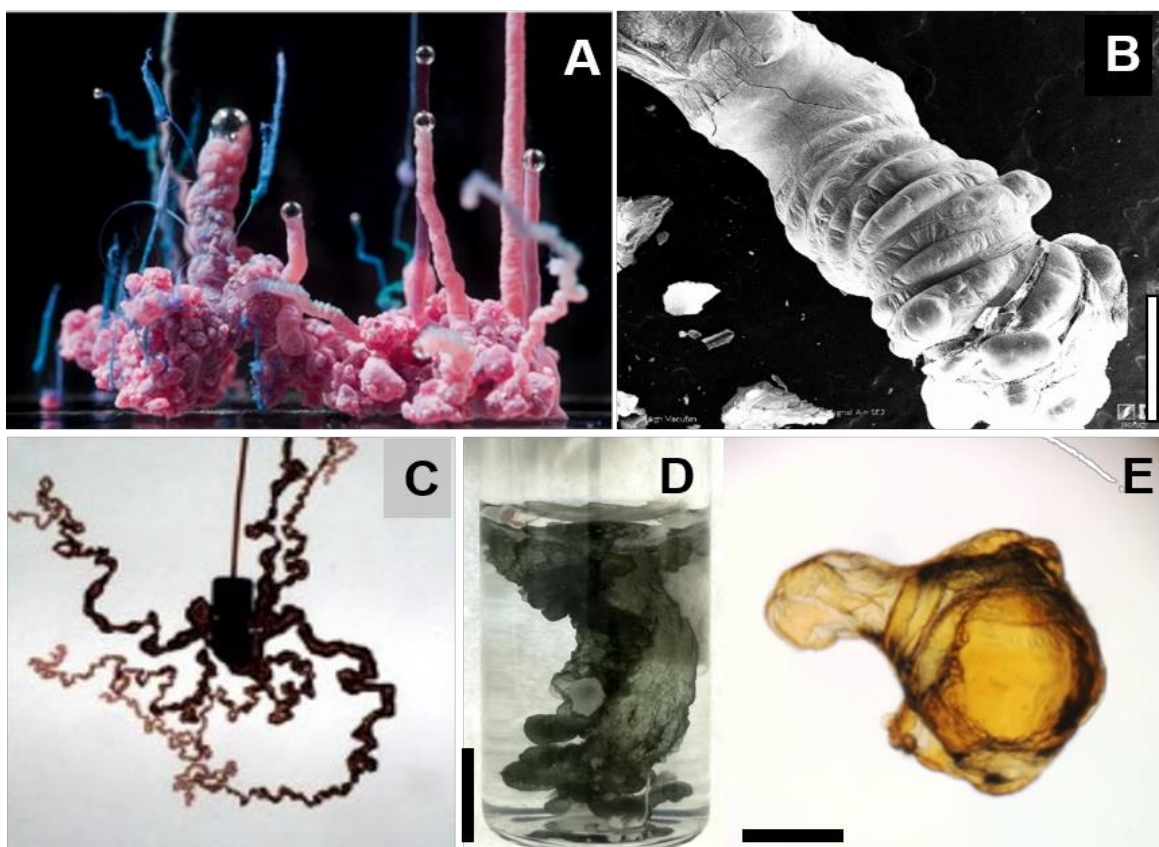


Figure 3. Different morphological types of Me-silica membranes. **A.** Tubular Co-silica membranes produced by immersing a CoCl_2 seed in water glass (image courtesy of S. Querbes) **B.** SEM image of an Fe(III)-silica tubule, scale is 0.5 mm. **C.** Spiral filamentous morphologies of quasi 2D membranes produced by injecting a cobalt chloride sol into sodium silicate in a Hele-Shaw cell at a fixed flow rate. Field of view is $15 \times 15 \text{ cm}$. (after Haudin et al., 2014). **D-E.** Vesicle

morphologies of Fe(II)- and Fe(III)-silica membranes occurring by mixing of the alkaline silicate with Fe(II)-chloride and Fe(III)-chloride solutions respectively. Scales: D 1 cm, E, 200 μm .

In all cases, the growth of the membrane begins with the dissolution of the metal salt, which gives rise to the formation of a colloidal metal (hydr)oxide film around the dissolving seed particle (in the case of pellets) or around the injection tip (in the case of solutions), and the subsequent rapture of this membrane due to an osmotically driven flow of water. From the breach site, buoyant salt water outflows and rapidly reacts at the liquid interface with the alkaline silicate solution to form a new precipitate that compartmentalizes the two reaction environments (Fig.4A-D) (Coatman et al., 1980; Cartwright et al., 2002; Kellermeier et al., 2013). The initial membrane grows by a reaction-transport-mediated process that not only stretches the membrane but also simultaneously thickens it. As the membrane ages, this feature is partially lost, and one can observe the formation of cracks in the now brittle material. It is from these cracks directly exposing the two reactive liquids to each other, that the self-healing membranes form a new layer, sealing the previous and creating a scar-like rim (Nakouzi and Steinbock, 2016).

This leads to the formation of a diaphragm membrane with compartmentalized spaces, separating two very distinct chemical environments in terms of pH and ions concentrations (Fig.4E). The drastic chemical variations between the inner volume of the acidic metal salt solution and the surrounding highly alkaline sol of sodium silicate, render iron-silica membranes fascinating laboratory models for studying spontaneously created gradients in self-organized systems, as well as, their application in materials science and biogeochemistry.

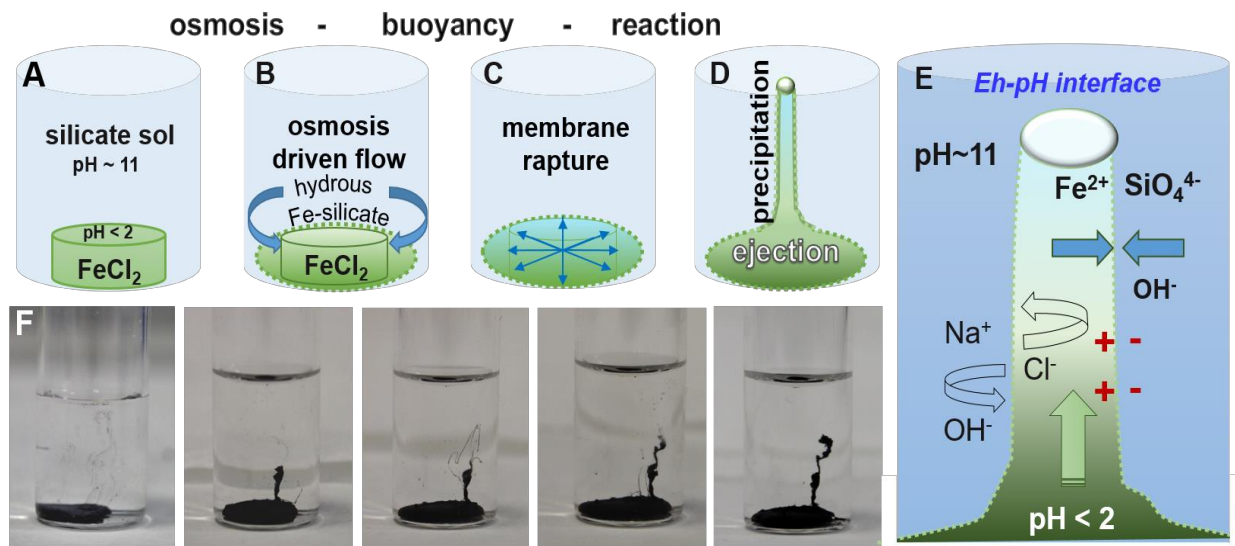


Figure 4. Me-silica membranes growth in the case of a reacting Me-salt seed with a sodium silicate sol. **A.** Upon addition of a silica solution to a Fe-metal salt pellet, a film of hydrated metal silicate is immediately formed over the surface of the crystals (green dotted line). **B.** Osmosis causes water to diffuse through this barrier (blue arrows) and dissolve the enclosed solid salt. **C.** This increases the internal pressure and leads to swelling of the flexible membrane, until a critical stage is reached and rupture occurs. **D-F.** At this point, the outer layer breaks, and a jet of concentrated metal salt solution is ejected into the surrounding medium. Owing to buoyancy, the lighter acidic salt solution ascends vertically into the heavier alkaline silica sol and rapidly solidifies due to simultaneous precipitation of metal hydroxide and/or silicate at the interface between the chemically distinct environments creating a wall around the initially liquid jet. This eventually leads to filamentous-like tubules. **E.** Fe-silica membrane where pH and ion gradients generate an electrochemical voltage that remains active for several hours.

To investigate this Glaab et al., (Glaab et al., 2012) produced tubes with a large enough diameter to allow the in situ measurement of ion concentrations in the interior of these tubes using electrodes (Fig.5A-D). These measurements demonstrated that an electrochemical potential across the membrane was generated, which persisted over periods of up to days. Interestingly, iron-silica membranes produced from Fe(III)-salt pellets exhibited the highest potential, of ~550 mV (Glaab et al., 2016). Similarly, Barge et al., (2015) measured the electrical potential and current across membranes precipitated both by injection and solution interface methods in Fe-sulfide and Fe-oxyhydroxide reaction systems. They demonstrated that by linking multiple experiments in series they could produce sufficient electrical energy to light an external light emitting diode (LED). Both studies evidence that iron membranes operate far from equilibrium and highlight the battery-like nature of the iron mineral membranes, showing their potential as self-catalyzed chemical reactors.

Owing to the generated pH-Eh interface, these membranes have been paralleled to hydrothermal chimneys (Martin and Russell, 2003; McGlynn et al., 2012; Barge et al., 2014), although the precipitation mechanism is quite different, i.e. in chemical gardens the cations directly react with silicate (or other anions) and hydroxide ions to yield metal-silica(te) hydrates, whereas, mineral precipitation in chimneys occurs due to pressure/temperature decrease and mixing with seawater. Nonetheless, these membranes are thought to have served as electron/proton conductors and redox catalysts at the early Earth hydrothermal environments (Russell et al., 1994; Martin et al., 2008; Barge et al., 2019) that have been shown to generate abiotic organics, and have been proposed as possible niches for the emergence of metabolism (McCollom and Seewald, 2007; Ménez et al., 2018; Klein et al., 2019). Apart from their possible role in proto-biochemistry, Me-silica membranes have raised interest due to their potential use as Brønsted acid catalysts, photocatalysts

(Collins, et al., 1999; Pagano et al., 2008) and/or microreactors (Maselko and Strizhak, 2004). Particularly the study of the physicochemical properties of the iron tubular gardens may elucidate ferrotube and whisker formation and the mechanisms of iron and steel corrosion (Stone & Goldstein, 2004).

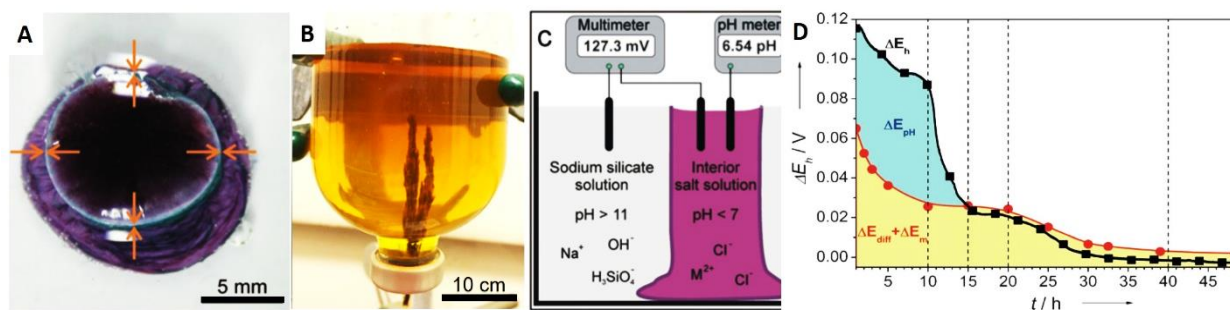


Figure 5. **A.** Top view of a membrane tube, showing its open end, formed upon slow addition of silica solution to a tablet of CoCl_2 . **B.** Chemical gardens precipitated by injection method in iron-hydroxide reaction systems, after Barge et al., 2019. **C.** Scheme of the experimental setup used for in situ measurements of pH and DEh. **D.** Electrochemical potentials in CoCl_2 -based silica gardens. The overall cell potential (DEh) results from a combination of diffusion (DE_{diff}) and membrane (DE_{m}) potentials as well as a third pH-induced contribution (DE_{pH})(after Glaab et al., 2012).

1.3.2. Iron-silica self-organized membranes

Although a wide variety of synthetic Me-membranes can be produced those produced with Fe(II)/(III) soluble particles/solutions and with silicate anions, are by far the most relevant for early Earth geochemistry, prebiotic chemistry and life detection. Iron, the second most abundant metal (after aluminum) and the fourth most abundant element in the Earth's crust (Rudnick and Fountain, 1995) that has been readily available in early Earth (in the reduced form), being a primary component of the Precambrian oceans, sediments and hydrothermal precipitates (Rudnick and Fountain, 1995; Rasmussen et al., 2015; Halevy et al., 2017). The role of ferrous iron in prebiotic chemistry was recently highlighted by Muchowska et al., (2019) that demonstrated that by mixing it with pyruvate ($\text{CH}_3\text{COCO}_2^-$) and glyoxylate (two products of abiotic CO_2 reduction) they can build up nine of the eleven intermediates of the biological Krebs cycle, including all five universal metabolic precursors, supporting the theory for a geochemical origin of the metabolism. Furthermore, owing to iron's abundance and availability, as well as, iron's rich coordination chemistry, the living organisms were evolved to use iron for a series of crucial cell processes, such as oxygen transport and storage or electron transfer reactions (Crichton and Boelaert, 2001; Sanchez et al., 2017).

With respect to the Me-silica membranes made with iron salts/salt solutions, they have been found to show the highest battery-like performance, generating more than 550 mV that endures for several hours (Glaab et al., 2012; Barge et al., 2015). In addition, iron membranes are able to yield biologically relevant organics (amino acids, carboxylic acids, nucleobases) by formamide condensation (CH_3NO) (Bizzari et al., 2018) and the formation of amino acids in presence of pyruvate ($\text{CH}_3\text{COCO}_2^-$) (Barge et al., 2019) as will be explicated below. Last but not least, filamentous Fe-silica membranes are implicated in the detection of the earliest forms of life. This is because of their morphological and chemical resemblance to putative biologic iron filaments found in cherts and in silica-rich hydrothermal precipitates, including those reported as the earliest forms of life of 4 Ga age (Dodd et al., 2017, McMahon, 2019; Johannessen et al., 2020).

Formamide (CH_3NO), the simplest carboxylic acid amide, although it is not naturally occurring on modern Earth, it has been detected in dense clouds of molecular gas and dust in star-forming regions and in several comets. Apart from this sources it is thought to have been present in early Earth by the hydrolysis of hydrogen cyanide (HCN) (Niether et al., 2016) or by the conversion of aqueous acetonitrile (ACN) to formamide via hydrogen cyanide (HCN), by exposure to radioactive minerals (Adam et al., 2018). This molecule that is proposed as an alternative solvent to overcome the ‘water paradox’, is a critical intermediate product in Miller-type reactions and a nucleotide precursor that has been demonstrated to condense into carboxylic acids, several amino acids, as well as into purines and pyrimidines in presence of minerals (Miyakawa et al. 2002; Mulkidjanian et al. 2012; Adande et al., 2013; Ferris et al. 2015; Pino et al., 2015; Bada et al., 2016; Neither et al., 2016; Saladino et al., 2016; Saladino et al., 2009; Saladino et al., 2012; Saladino et al., 2019).

In a recent study (Bizzarri et al., 2018) co-precipitated Fe-silica membranes with formamide, by injecting microdrops of Fe-salt solutions into a silicate solution that was previously doped with formamide. They noticed that the Fe-membranes catalyzed the condensation of formamide yielding the four nucleobases of RNA, three amino acids and several carboxylic acids in a single experiment, at 80 ° C. Adding to this, it was shown that these membranes are also capable of providing UV radiation shielding to the produced molecules (Saladino et al., 2016). Thus it is speculated that the inorganic Fe-silica membranes and vesicles could have catalyzed the formation of life-relevant organic molecules, while shielding them from the high levels of UV radiation that prevailed during the Hadean (Cockell, 2000; Segura et al., 2003; Saladino et al., 2019).

At the same time pyruvate is of particular interest in prebiotic chemistry because in extant metabolic networks it undergoes various reactions leading to amino acids, sugars, cofactors, and lipids (Novikov and Copley, 2013). Cody et al. (2000) have shown that small amounts of pyruvate can be produced under simulated hydrothermal vent conditions from alkyl thiols and carbon monoxide in the presence of iron sulfides at 250 °C. Further, it has been shown that pyruvate and other α -keto acids can later react to form a variety of products including lactate, β -hydroxy ketones, thiols (in the presence of iron-sulfide), and the amino acid alanine (in the presence of ammonia). Recently, Barge et al., (2019) showed that pyruvate can undergo reductive amination in the presence of mixed-valence iron oxyhydroxides to form the amino acid alanine, as well as the reduced product lactate. In particular they showed that the maximum yield of alanine was observed when the iron oxyhydroxide mineral contained 1:1 Fe(II):Fe(III), under alkaline conditions, and at moderately warm temperatures; conditions that may be found, for example, in iron-containing sediments near an alkaline hydrothermal vent system.

Yet, to fully understand the remarkable physicochemical properties of the Fe-silica membranes, their putative role in prebiotic chemical reactions, their precipitation in early Earth environments and to be able to distinguish them from their biologic tubular counterparts, it is paramount to have a detailed characterization of their internal anatomy, i.e. mineral chemistry and structure. Previous studies reported that these membranes are composed of a mixture of amorphous (metal)silicate/silica and crystalline iron hydroxides/oxides (Balköse et al., 2002; Parmar et al., 2010; Makki and Steinbock, 2012; Barge et al., 2011; 2012; 2015a; 2016; 2019; Glaab et al., 2012; 2016; Glaab et al., 2017). However, we still lack information about the precise mineral phases building these nanocomposite membranes and how these phases are distributed/organized at the nanoscale.

So far, Fe-silica membranes have been grown from synthetic solutions and it is not known whether Fe-silica membranes can precipitate from natural solutions relevant for the early Earth (Hadean-Archean) aqueous settings. Moreover, it is not known whether the remarkable physicochemical properties of the model Fe-silica membranes can be extended to the natural ones.

This thesis aims to provide insight on the mineral chemistry and structure of the Fe-silica membranes at the nanoscale, and the implications these might have for the catalytic behavior of the membranes. In addition, the geochemical plausibility of the Fe-silica membranes growth from natural solutions will be investigated in various physicochemical conditions and discussed in

relation with the early Earth environments. These experiments will be coupled with detailed characterization at the nanoscale and comparison with the model membranes.

1.3.3. Mineral precipitation at polyextreme conditions

Modern geochemical settings where mineral precipitation is purely abiotic are seldom found. This is not surprising considering that microbial life has been encountered in all types of geological settings, from the deep subsurface and submarine hydrothermal vents to the ice cups and acid mine drainage pits (Rampelotto, 2013; Merino et al., 2019). At the same time, there is no rock record from the Hadean, the lifeless period of the planet, when mineral precipitation was purely inorganic. Thus, we lack insight on the mineral self-organization processes that prevailed in Hadean-Early Archean (4.1-3.8 Ga) and formed the geochemical niches for the emergence and spreading of life.

In the search of modern analogue-sites for the study of inorganic mineral formation/precipitation, polyextreme environments and particularly highly acidic and highly saline environments make the most promising candidates. This is because the combination of extreme salinity with acidity is thought to impose a geochemical barrier to life (Charisson et al., 2013, Merino et al., 2019). Stemming from this, the second part of the thesis examines the geochemical processes that control mineral precipitation at the polyextreme hydrothermal system of Dallol, NE Ethiopia. Although the bibliographic record about Dallol was limited, focusing on the geodynamical and geophysical characteristics of Dallol within the Afar Triangle, the very few studies that provided some geochemical evidence (Darrah et al., 2013; Franzson et al., 2015) reported on a geochemically unique hydrothermal system, developed onto the evaporitic sequence of Danakil depression. Hyperacidic, hypersaline, anoxic, Fe-rich brines of more than 100 °C temperature are discharging from the springs of the hydrothermal system. Hence, it became evident that Dallol would make an ideal candidate-site for the investigation of mineral self-organization and precipitation in life-limiting conditions.

The dome of Dallol lies in the Danakil depression at the extension of the Main Ethiopian Rift (MER), at the Afar Triangle (see chapter 4 Fig. 2). This depression, situated 120 m bmsl, is a vast salty plain composed of more than 2 km deposit of evaporites following several marine transgressions of the Red Sea, during the evolution of the MER since Miocene to Quaternary (Holwerda and Hutchinson, 1968). In this region, where the crustal thickness does not exceed the 14km, the Red Sea, the Gulf of Aden, and the MER produce a triple junction zone associated with mantle plume activity and basaltic intrusive and extrusive magmatism (Makris and Ginzburg, 1987;

Wolfenden et al., 2004) As a result, several volcanic chains are forming, mainly represented by basaltic shield volcanoes, among them the Erta Ale range. The Dallol dome along with the neighboring areas of the Black and Gaet' Ale Lakes (the latter also known as Yellow Lake) (Master, 2016; Pérez and Chebude, 2017) are the most recent expressions at the northwestern part of the Erta Ale volcanic range, following from SE to NW the Hayli Gubbi, Ale Bagu, Erta Ale, Borale, Dalafilla, Alu and Gada Ale volcanoes (Nobile et al., 2012; Pagli et al., 2012). The dome of Dallol consists of protruding bedded-halite and anhydrite layers dipping gently outwards outlining an elliptical structure elongated in E-W direction, partially covered by overimposed geothermal deposits (López-García et al., 2020). A central depression of 1 km in diameter gives to the Dallol dome a crater-like appearance (Holwerda and Hutchinson, 1968; Talbot, 2008; Franzson et al., 2015). The volcano-like morphology, geothermal activity and location of the dome has led many authors to refer to this structure as the “Dallol volcano” (Edelmann et al., 2010; Darrah et al., 2013; Keir et al., 2013; Tadiwos, 2013; Wunderman, 2013; Corti et al., 2015).

However, volcanic materials have never been found on the dome or its immediate surroundings. Dallol has not yet developed into a volcano; it is a hydrothermal system resulting from the interaction of upwelling magma, confined in a shallow magmatic chamber 2.4 km deep below the segment of Dallol, and the evaporitic sequence, created from successive transgressions of the Red Sea, the most recent placed at 32 kya (Hovland et al., 2006; Nobile et al., 2012). The Dallol dome is exclusively composed of salt deposits coming from uplifted primary halite beds controlled by the presence of a shallow magmatic chamber, and derived halokinetic processes (López-García et al., 2020).

Intense geothermal activity, which occasionally includes phreatic explosions and is mainly controlled by poorly understood interactions between magma, deep hydrated salts and groundwater, results in the world-renowned colorful acidic brine ponds, fumaroles, small geysers, salt deposits, and other hydro-geothermal manifestations (Holwerda and Hutchinson, 1968; Hovland et al., 2006; Talbot, 2008; Franzson et al., 2015; Warren, 2015a; Varet, 2018). The result of such interactions is a polyextreme environment with brines exhibiting low pH (≤ 0), high salt contents ($> 30\%$) and high temperature (up to $\sim 110^{\circ}\text{C}$). Other minor geothermal-related structures are located around the Dallol dome (see chapter 4 Fig. 2). These include the Round Mountain to the west, the Black Mountain in the southwest, the Horseshoe Mountain in the east and the Yellow Lake (Ga'et Ale) southeast, as well as many other small bubbling springs and ponds of geothermal origin (López-García et al., 2020).

1.4. Thesis objectives

The scope of this thesis is to investigate the importance of mineral self-organization and inorganic mineral precipitation for the early Earth geochemistry, prebiotic chemistry and life detection, by focusing on two case-studies: a) iron-silica, self-organized, membranes and their role in prebiotic chemistry and life detection, and b) iron geochemical cycling and abiotic iron mineral precipitation at the polyextreme hydrothermal system of Dallol. Following, the thesis objectives are presented with respect to each subject.

a) Inorganic, self-organized, Fe-silica membranes compartmentalize chemically distinct reaction environments, behave as fuel cells, provide UV radiation shielding to the molecules of the interior, and catalyze the formation of nucleobases, amino acids and carboxylic acids by formamide condensation. These remarkable properties raise the following questions: i) what is the nanoscale anatomy of the Fe-silica membranes and how is it related to their catalytic behavior? ii) can Fe-silica membranes grow from natural solutions and, if yes, how do they compare with the model membranes? iii) under which geochemical conditions their growth might have been plausible in early Earth? iv) provided that they precipitated in the early Earth environments, what could have been their role in prebiotic chemistry? v) how are these inorganic Fe-silica filamentous membranes similar/different to biogenic iron filaments found in cherts? Therefore, the objectives of the thesis were to:

- Investigate the mineralogy and structure of model Fe-silica membranes at the nanoscale by using advanced electron microscopy tools.
- Explore the precipitation of Fe-silica membranes with natural solutions that mimic early Earth aqueous environments
- Conduct a macroscopic-microscopic-nanosopic and spectroscopic comparison of model and natural Fe-silica membranes
- Perform the growth and ex-situ analysis of membranes at the nanoscale in anaerobic conditions simulating their growth in the early Earth environments
- Present a model for the Fe-silica membranes precipitation in the early Earth geochemical settings

- Compare the inorganic iron-silica filamentous membranes to putative iron bacterial filaments found in cherts

b) By studying the geochemistry and mineral precipitation at the polyextreme hydrothermal system of Dallol, I intend to provide insight on the geochemical processes that control iron mineral precipitation in polyextreme conditions and answer the following questions: i) which are the geochemical processes that produce the combination of hyperacidity, hypersalinity and iron enrichment in the hydrothermal system of Dallol? How does Dallol compare to other hyperacidic sites known from crater lakes and volcanic systems? ii) how are the spectacular colors of the site generated? Are they related to biologic activity or to inorganic processes? iii) what is the mineralogy of the precipitates, the self-organized patterns and biomorphic structures found in the dome? Therefore, the objectives were to:

- Perform in situ measurements (pH-Eh, T, O₂, CO₂), stable isotopic study of the fluids (oxygen-hydrogen-dissolved inorganic carbon), dissolved and free gases (oxygen, nitrogen, argon and carbon stable isotopes) and hydrochemical analysis of the Dallol hydrothermal brines for understanding the fluid chemistry of the brines.
- Compare the hydrochemical characteristics of Dallol to other hyperacidic sites.
- To determine the redox state across the aqueous system of Dallol by measuring the concentration of Fe(II) and Fe(III), in different spring solutions and related pools.
- Identify the Fe aqueous and solid species responsible for the colors of the pools by using Raman and UV-Vis spectroscopies.
- Look for in situ autotrophic and heterotrophic biologic activity in the brines of Dallol by performing isotopically-labelled incubations and conduct microscopic study of fixed filters of the brines for the detection of microorganisms.
- Resolve the mineralogy of precipitates, patterns and biomorphic structures by using a series of techniques (PXRD, in situ Raman, micro-Raman, FESEM-EDS, TEM).
- Explore the precipitation of natural Fe-silica membranes by replacing the synthetic Fe-chloride solution with pristine Dallol water.

1.5.Thesis outline

The overall structure of the study takes the form of four chapters, including this first introductory chapter that is laying out the scope and the objectives of this work. Chapter two presents the results of the geochemical plausibility and nanoscale characteristics of the iron-silica membranes, while the third chapter presents the findings of iron mineral self-organization in the polyextreme conditions of Dallol, Ethiopia. The main conclusions of this work, as well as, research limitations and open questions are discussed in chapter four. Each chapter, apart from the introductory and concluding ones, is structured as follows: summary and graphical abstract, materials and methods, results and discussion. Materials and methods do not form a separate chapter. Instead, experimental protocols and analytical techniques used for each case study are presented within the corresponding chapters. At the end of the thesis an appendix is shown, followed by the published results and the curriculum vitae.

References

- Adam, Z.R., Hongo, Y., Cleaves, H.J. et al., 2018. Estimating the capacity for production of formamide by radioactive minerals on the prebiotic Earth. *Sci Rep* 8, 265. <https://doi.org/10.1038/s41598-017-18483-8>.
- Adande, G.R., Woolf, N.J., Ziurys, L.M., 2013. Observations of interstellar formamide: availability of a prebiotic precursor in the galactic habitable zone. *Astrobiology* 13, 439-453.
- Anderson, R.S., 1990. Eolian ripples as examples of self-organization in geomorphological systems, *Earth-Science Reviews*, 29, 77-96.
- Bada, J.L., Chalmers, J.H., Cleaves, H.J., 2016. Is formamide a geochemically plausible prebiotic solvent? *Physical chemistry chemical physics : PCCP* 18, 20085-20090.
- Balköse, D., Özkan, F., Köktürk, U., Ulutan, S., Ülkü, S., Nişli, G., 2002. Characterization of Hollow Chemical Garden Fibers from Metal Salts and Water Glass. *Journal of Sol-Gel Science and Technology* 23, 253-263.
- Barge, L.M., Abedian, Y., Russell, M.J., Doloboff, I.J., Cartwright, J.H., Kidd, R.D., Kanik, I., 2015a. From Chemical Gardens to Fuel Cells: Generation of Electrical Potential and Current Across Self-Assembling Iron Mineral Membranes. *Angewandte Chemie* 54, 8184-8187.
- Barge, L.M., Cardoso, S.S., Cartwright, J.H., Cooper, G.J., Cronin, L., De Wit, A., Doloboff, I.J., Escribano, B., Goldstein, R.E., Haudin, F., Jones, D.E., Mackay, A.L., Maselko, J., Pagano, J.J., Pantaleone, J., Russell, M.J., Sainz-Diaz, C.I., Steinbock, O., Stone, D.A., Tanimoto, Y., Thomas, N.L., 2015b. From Chemical Gardens to Chemobrionics. *Chemical reviews* 115, 8652-8703.
- Barge, L.M., Cardoso, S.S., Cartwright, J.H., Doloboff, I.J., Flores, E., Macias-Sanchez, E., Sainz-Diaz, C.I., Sobron, P., 2016. Self-assembling iron oxyhydroxide/oxide tubular structures: laboratory-grown and field examples from Rio Tinto. Proceedings. *Mathematical, physical, and engineering sciences* 472, 20160466.
- Barge, L.M., Doloboff, I.J., Russell, M.J., VanderVelde, D., White, L.M., Stucky, G.D., Baum, M.M., Zeytounian, J., Kidd, R., Kanik, I., 2014. Pyrophosphate synthesis in iron mineral films and membranes simulating prebiotic submarine hydrothermal precipitates. *Geochimica et Cosmochimica Acta* 128, 1-12.
- Barge, L.M., Doloboff, I.J., White, L.M., Stucky, G.D., Russell, M.J., Kanik, I., 2012. Characterization of iron-phosphate-silicate chemical garden structures. *Langmuir : the ACS journal of surfaces and colloids* 28, 3714-3721.
- Batista, B.C., Cruz, P., Steinbock, O., 2014. From Hydrodynamic Plumes to Chemical Gardens: The Concentration-Dependent Onset of Tube Formation, *Langmuir*, 30, 9123-9129.
- Batista, B.C., Steinbock, O., 2015. Growing Inorganic Membranes in Microfluidic Devices: Chemical Gardens Reduced to Linear Walls, *J. Phys. Chem. C*, 119, 27045-27052.

- Bizzarri, B.M., Botta, L., Perez-Valverde, M.I., Saladino, R., Di Mauro, E., Garcia Ruiz, J.M., 2018. Silica metal-oxide vesicles catalyze comprehensive prebiotic chemistry. *Chem. Eur. J.* 2018, 24, 8126.
- Blum, J. S., Han, S., Lanoil, B., Saltikov, C., Witte, B., Tabita, F. R., et al., 2009. Ecophysiology of “Halarsenatibacter silvermanii” strain SLAS-1 T, gen. nov., sp. nov., a facultative chemoautotrophic arsenate respirer from salt-saturated Searles Lake, California. *Appl. Environ. Microbiol.* 75, 1950–1960. doi: 10.1128/AEM.02614-08.
- Cartwright, J.H.E., Escribano, B., Sainz-Díaz, C.I., 2011. Chemical-Garden Formation, Morphology, and Composition. I. Effect of the Nature of the Cations. *Langmuir : the ACS journal of surfaces and colloids* 27, 3286-3293.
- Cartwright, J.H.E., Garia-Ruiz, J.M., Novella, M.L., Otálora, F., 2002. Formation of Chemical Gardens. *J. Colloid Interface Sci.* 256, 351-359.
- Chavagnac, V., Ceuleneer, G., Monnin, C., Lansac, B., Hoareau, G., and Boulart, C., 2013. Mineralogical assemblages forming at hyperalkaline warm springs hosted on ultramafic rocks: A case study of Oman and Ligurian ophiolites, *Geochem. Geophys. Geosyst.*, 14, 2474– 2495, doi:10.1002/ggge.20146.
- Chen, W., Ghaith, A., Park, A., Ortoleva, P., 1990. Diagenesis Through Coupled Processes: Modeling Approach, Self-Organization, and Implications for Exploration, in *Prediction of Reservoir Quality through Chemical Modeling*, AAPG Special Volumes.
- Cleaves II, H.J., al., e., 2012. Mineral–organic interfacial processes: potential roles in the origins of life. *Chem. Soc. Rev.* 41, 5502–5525.
- Coatman, R.D., Thomas, N.L., Double, D.D., 1980. Studies of the growth of "silicate" gardens. *Journal of Materials Science* 15, 2017-2026 .
- Collins, C., Zhou, W., Klinowski, J., 1999. A unique structure of $\text{Cu}_2(\text{OH})_3\cdot\text{NH}_3$ crystals in the 'silica garden' and their degradation under electron beam irradiation. *Chemical Physics Letters* 306, 145-148.
- Corti, G., Bastow, I. D., Keir, D., and Pagli, C., 2015. “Rift-related morphology of the Afar Depression,” in *Landscapes and Landforms of Ethiopia*, ed. P. Billi, (Dordrecht: Springer Science+Business Media), 251–274. doi: 10.1007/978-94-017-8026-1.
- Czop, M., Motyka, J., Sracek, O., and Szuwarzyński, M., 2011. Geochemistry of the hyperalkaline Gorka pit lake (pH > 13) in the Chrzanow region, southern Poland. *Water Air Soil Pollut.* 214, 423–434. doi: 10.1007/s11270-010- 0433-x.
- Dalai, P., Kaddour, H., Sahai, N., 2016. Incubating Life: Prebiotic Sources of Organics for the Origin of Life. *Elements* 12, 401-406.
- Dalmasso, C., Oger, P., Selva, G., Courtine, D., L’Haridon, S., Garlaschelli, A., et al., 2016. Thermococcus piezophilus sp. nov., a novel hyperthermophilic and piezophilic archaeon with a broad pressure range for growth, isolated from a deepest hydrothermal vent at the Mid-Cayman Rise. *Syst. Appl. Microbiol.* 39, 440–444. doi: 10.1016/j.syapm.2016.08.003

- Darrah, T.H., Tedesco, D., Tassi, F., Vaselli, O., Cuoco, E., Poreda, R.J., 2013. Gas chemistry of the Dallol region of the Danakil Depression in the Afar region of the northern-most East African Rift. *Chemical Geology* 339, 16-29.
- Davila, A. F., Gómez-Silva, B., de los Rios, A., Ascaso, C., Olivares, H., McKay, C. P., et al. (2008). Facilitation of endolithic microbial survival in the hyperarid core of the Atacam Desert by mineral deliquescence. *J. Geophys. Res. Biogeosci.* 113:G1. doi: 10.1029/2007JG000561.
- Deamer, D.W., Dworkin, J.P., Sandford, S.A., Bernstein, M.P., Allamandola, L.J., 2002. The first cell membranes. *Astrobiology* 2, 371-382.
- Delmelle, P., Bernard, A., 1994. Geochemistry, mineralogy, and chemical modeling of the acid crater lake of Kawah Ijen Volcano, Indonesia, *Geochimica et Cosmochimica Acta*, 58, 2445-2460.
- Ding, Y., Batista, B., Steinbock, O., Cartwright, J.H.E., Cardoso, S.S.S., 2016. Growth of wavy membranes in chemical gardens, *Proceedings of the National Academy of Sciences* 113, 9182-9186; DOI: 10.1073/pnas.1607828113.
- Dodd, M.S., Papineau, D., Grenne, T., Slack, J.F., Rittner, M., Pirajno, F., O'Neil, J., Little, C.T., 2017. Evidence for early life in Earth's oldest hydrothermal vent precipitates. *Nature* 543, 60-64.
- Edelmann, J., Roscoe, R., and Roscoe, R., 2010. Volcano tourism in Ethiopia and the Danakil Rift Zone, in *Volcano and Geothermal Geotourism, Sustainable Geo-Resources for Leisure and Recreation*, eds P. Erfurt-Cooper, and M. Cooper, (Abingdon: Taylor and Francis), 59–67.
- Ferris, J.P., Ertem, G., 1992. Oligomerization reactions of ribonucleotides: the reaction of the 5'-phosphorimidazolide of nucleosides on montmorillonite and other minerals. *Orig. Life Evol. Biosph.* 22, 369-381
- Fernández-Remolar, D.C., Morris, R.V., Gruener, J.E., Amils, R., Knoll, A.H., , 2005. The Río Tinto Basin, Spain: Mineralogy, sedimentary geobiology, and implications for interpretation of outcrop rocks at Meridiani Planum, Mars. *Earth Planet. Sci. Lett.* 240, , 149-167.
- Finlayson, C. M., Milton, R., Prentice, C., and Davidson, N. C. (eds), 2018. *The Wetland Book II, Distribution, Description, and Conservation*. Berlin: Springer.
- Franzson, H., Helgadóttir, H. M., and Óskarsson, F., 2015. Surface exploration and first conceptual model of the Dallol geothermal area, northern Afar, Ethiopia, in *Proceedings World Geothermal Congress 2015*, Melbourne, 11.
- Frösler, J., Panitz, C., Wingender, J., Flemming, H.-C., and Rettberg, P., 2017. Survival of *Deinococcus geothermalis* in Biofilms under Desiccation and Simulated Space and Martian Conditions. *Astrobiology* 17, 431–447. doi: 10.1089/ast.2015.1431.
- García-Ruiz, J.M., Hyde, S.T., Carnerup, A.M., Christy, A.G., Van Kranendonk, M.J., Welham, N.J., 2003. Self-assembled silica-carbonate structures and detection of ancient microfossils. *Science* 302, 1194-1197.
- García-Ruiz, J.M., Melero-Garcia, E., Hyde, S.T., 2009. Morphogenesis of self-assembled nanocrystalline materials of barium carbonate and silica. *Science* 323, 362-365.

- García-Ruiz, J.M., Nakouzi, E., Kotopoulou, E., Tamborrino, L., Steinbock, O., 2017. Biomimetic mineral self-organization from silica-rich spring waters. *Science Advances* 3, e1602285.
- García-Ruiz, J.M., van Zuilen, M., Bach, W., 2020. Mineral self-organization on a lifeless planet, *Physics of Life Reviews*, in press.
- Gillams, R.J., Jia, T.Z., 2018. Mineral Surface-Templated Self-Assembling Systems: Case Studies from Nanoscience and Surface Science towards Origins of Life Research. *Life* 8.
- Glaab, F., Kellermeier, M., Kunz, W., Morallon, E., Garcia-Ruiz, J.M., 2012. Formation and evolution of chemical gradients and potential differences across self-assembling inorganic membranes. *Angewandte Chemie* 51, 4317-4321.
- Glaab, F., Rieder, J., Garcia-Ruiz, J.M., Kunz, W., Kellermeier, M., 2016. Diffusion and precipitation processes in iron-based silica gardens. *Physical chemistry chemical physics : PCCP* 18, 24850-24858.
- Glaab, F., Rieder, J., Klein, R., Choquesillo-Lazarte, D., Melero-Garcia, E., Garcia-Ruiz, J.M., Kunz, W., Kellermeier, M., 2017. Precipitation and Crystallization Kinetics in Silica Gardens. *Chemphyschem : a European journal of chemical physics and physical chemistry* 18, 338-345.
- Glauber, J.R., 1646. *Furni Novi Philosophici*, Amsterdam.
- Haken, H., 1977 (ed.). *Synergetics- An introduction, Non equilibrium phase transitions and self-organization in physics, chemistry, biology*. Springer-Verlag.
- Halevy, I., Alesker, M., Schuster, E.M., Popovitz-Biro, R., Feldman, Y., 2017. A key role for green rust in the Precambrian oceans and the genesis of iron formations. *Nature Geoscience* 10, 135-139.
- Halley, J.D. and Winkler, D.A., 2008. Consistent concepts of self-organization and self-assembly. *Complexity*, 14: 10-17. doi:10.1002/cplx.20235.
- Hallsworth, J. E., Yakimov, M. M., Golyshin, P. N., Gillion, J. L. M., D'Auria, G., De Lima Alves, F., et al., 2007. Limits of life in MgCl₂-containing environments: chaotropy defines the window. *Environ. Microbiol.* 9, 801–813. doi: 10.1111/j.1462-2920.2006.01212.x.
- Hanczyc, M.M., Fujikawa, S.M., Szostak, J.W., 2003. Experimental models of primitive cellular compartments: encapsulation, growth, and division. *Science* 302, 618-622.
- Hanczyc, M.M., Mansy, S.S., Szostak, J.W., 2007. Mineral surface directed membrane assembly. *Origins of life and evolution of the biosphere*, 37, 67-82.
- Harrison, J. P., Gheeraert, N., Tsigelnitskiy, D., and Cockell, C. S., 2013. The limits for life under multiple extremes. *Trends Microbiol.* 21, 204–212. doi: 10.1016/j.tim.2013.01.006.
- Haudin, F., Cartwright, J.H.E., Brau, F., De Wit., A. 2014. Spiral precipitation in confined chemical gardens, *Proceedings of the National Academy of Sciences*, 111, 17363-17367; DOI: 10.1073/pnas.1409552111.
- Haudin, F., Cartwright, J.H.E., and De Wit. A., 2015. Direct and Reverse Chemical Garden Patterns Grown upon Injection in Confined Geometries, *The Journal of Physical Chemistry C*, 119, 15067-15076 DOI: 10.1021/acs.jpcc.5b00599.

- Hazen, R.M., Sverjensky, D.A., 2010. Mineral surfaces, geochemical complexities, and the origins of life. *Cold Spring Harbor perspectives in biology* 2, a002162.
- Holwerda, J. G., and Hutchinson, R. W., 1968. Potash-bearing evaporites in the Danakil area, Ethiopia. *Econ. Geol.* 63, 124–150. doi: 10.2113/gsecongeo.63.2.124.
- Horneck, G., Klaus, D. M., and Mancinelli, R. L., 2010. Space microbiology. *Microbiol. Mol. Biol. Rev.* 74, 121–156. doi: 10.1128/MMBR.00016-09.
- Hussein, S., Maselko, J., Pantaleone, J.T., 2016. Growing a Chemical Garden at the Air–Fluid Interface, *Langmuir* 2016, 32, 3, 706-711.
- Jolivet, E., L’Haridon, S., Corre, E., Forterre, P., and Prieur, D., 2003. Thermococcus gammatolerans sp. nov., a hyperthermophilic archeon from a deep-sea hydrothermal vent that resists ionizing radiation. *Int. J. Syst. Evol. Microbiol.* 53, 847–851. doi: 10.1099/ijs.0.02503-0
- Kashefi, K., and Lovley, D. R., 2003. Extending the upper temperature limit for life. *Science* 301:934. doi: 10.1126/science.1086823.
- Keir, D., Bastow, I. D., Pagli, C., and Chambers, E. L., 2013. The development of extension and magmatism in the Red Sea rift of Afar. *Tectonophysics* 607, 98–114. doi: 10.1016/j.tecto.2012.10.015.
- Kellermeier, M., Glaab, F., Melero-Garcia, E., Garcia-Ruiz, J.M., 2013. Experimental techniques for the growth and characterization of silica biomorphs and silica gardens. *Methods in enzymology* 532, 225-256.
- Kelley, D.S., Karson, J.A., Früh-Green, G.L., et al., 2005. A Serpentinite-Hosted Ecosystem: The Lost City Hydrothermal Field. *Science*, 307, 1428-1434, DOI: 10.1126/science.1102556.
- Klein, F., Grozeva, N.G., Seewald, J.S., 2019. Abiotic methane synthesis and serpentinization in olivine-hosted fluid inclusions. *Proceedings of the National Academy of Sciences* 116, 17666.
- Kotopoulou, E., Perez-Valverde, M.I., Garcia-Ruiz, J.M., 2017. Exploring the Geological Relevance of Iron-Silica Self-assembled Membranes, *Macla*, 22, 77-79.
- La Duc, M. T., Bernardini, J. N., Kempf, M. J., Newcombe, D. A., Lubarsky, M., and Venkateswaran, K., 2007. Microbial diversity of Indian ocean hydrothermal vent plumes: microbes tolerant of desiccation. Peroxide Exposure, and Ultraviolet and g-Irradiation. *Astrobiology* 7, 416–431. doi: 10.1089/ast.2006.0060.
- Leduc, S., 1911. *The Mechanism of Life*, Rebman, London.
- Leydesdorff, L., 2001. *A sociological theory of communication: The self-organization of the knowledge-based society*. Universal publishers, USA, 2nd edition. ISBN: 1-58112-695-6.
- Liesegang, R.E., 1896. *Photogr. Archiv.* 21, 221.
- López-García J.M., Moreira, D., Benzerara, K., Grunewald, O., and López-García, P., 2020. Origin and Evolution of the Halo-Volcanic Complex of Dallol: Proto-Volcanism in Northern Afar (Ethiopia). *Front. Earth Sci.* 7:351. doi: 10.3389/feart.2019.00351.

- Makki, R., Steinbock, O., 2012. Nonequilibrium synthesis of silica-supported magnetite tubes and mechanical control of their magnetic properties. *J. Am. Chem. Soc.* 134, 15519-15527.
- Makris, J., Ginzburg, A., 1987. The Afar Depression: transition between continental rifting and sea-floor spreading. *Tectonophysics* 141, 199-214.
- Martin, W., Russell, M.J., 2003. On the origins of cells: a hypothesis for the evolutionary transitions from abiotic geochemistry to chemoautotrophic prokaryotes, and from prokaryotes to nucleated cells. *Phil. Trans. R. Soc. B* 358, 59-85.
- Martin, W., Baross, J., Kelley, D., Russell, M.J., 2008. Hydrothermal vents and the origin of life. *Nature Reviews Microbiology* 6, 805-814.
- Maselko, J., Strizhak, P., 2004. Spontaneous Formation of Cellular Chemical System that Sustains Itself far from Thermodynamic Equilibrium, *J. Phys. Chem. B*, 108, 4937-4939.
- McCollom, T.M., Ritter, G., Simoneit, B.R.T., 1999. Lipid Synthesis Under Hydrothermal Conditions by Fischer-Tropsch-Type Reactions. *Origins of life and evolution of the biosphere* 29, 153-166.
- McCollom, T.M., Seewald, J.S., 2007. Abiotic Synthesis of Organic Compounds in Deep-Sea Hydrothermal Environments. *Chem. Rev.* 107, 382-401.
- McDermott, J. M., Sylva, S. P., Ono, S., German, C. R., and Seewald, J. S., 2018. Geochemistry of fluids from Earth's deepest ridge-crest hot-springs: piccard hydrothermal field, Mid-Cayman Rise. *Geochim. Cosmochim. Acta* 228, 95–118. doi: 10.1016/j.gca.2018.01.02.
- McGlynn, S.E., Kanik, I., Russell, M.J., 2012. Peptide and RNA contributions to iron–sulphur chemical gardens as life's first inorganic compartments, catalysts, capacitors and condensers. *Philosophical Transactions of the Royal Society A*, 370, 3007-3022.
- McMahon, S., 2019. Earth's earliest and deepest purported fossils may be iron-mineralized chemical gardens. *Proc. R. Soc. B* 286, 20192410.
- Ménez, B., Pisapia, C., Andreani, M., Jamme, F., Vanbellingen, Q.P., Brunelle, A., Richard, L., Dumas, P., Refregiers, M., 2018. Abiotic synthesis of amino acids in the recesses of the oceanic lithosphere. *Nature* 564, 59-63.
- Merino, E., Wang, Y. 2001. Geochemical self-organization in rocks: occurrences, observations, modeling, testing – with emphasis on agate genesis In *Non-Equilibrium Processes and Dissipative Structures in Geoscience, Self-Organization Yearbook Vol. 11:* (eds Krug, H. -J. & Kruhl, J. H.) 13–45 (Duncker & Humblot, 2001).
- Merino, N., Aronson, H.S., Bojanova, D.P., Feyhl-Buska, J., Wong, M.L., Zhang, S., Giovannelli, D., 2019. Living at the Extremes: Extremophiles and the Limits of Life in a Planetary Context, *Frontiers in Microbiology*, 10, 780.
- Mesbah, N., and Wiegel, J., 2005. “Halophilic thermophiles: a novel group of extremophiles,” in *Microbial Diversity: Current Perspective and Potential Applications*, eds T. Satyanarayana, and B.

- N. Johri (New Delhi: International Publishing House Pvt. Ltd.), 91–118 doi: 10.1196/annals.1419.028.
- Miettinen, H., Kietäväinen, R., Sohlberg, E., Numminen, M., Ahonen, L., and Itävaara, M., 2015. Microbiome composition and geochemical characteristics of deep subsurface high-pressure environment, Pyhäsalmi mine Finland. *Front. Microbiol.* 6:1203. doi: 10.3389/fmicb.2015.0120.3
- Mildrexler, D. J., Zhao, M., and Running, S. W., 2011. Satellite finds highest land skin temperatures on Earth. *Bull. Am. Meteorol. Soc.* 92, 855–860. doi:10.1175/2011BAMS3067.1
- Monnard, P.A., Deamer, D.W., 2002. Membrane self-assembly processes: steps toward the first cellular life. *The Anatomical record* 268, 196-207.
- Morris, S., and Taylor, A. C., 1983. Diurnal and seasonal variation in physicochemical conditions within intertidal rock pools. *Estuar. Coast. Shelf Sci.* 17, 339–355. doi: 10.1016/0272-7714(83)90026-4.
- Muchowska, K.B., Varma, S.J., Moran, J., 2019. Synthesis and breakdown of universal metabolic precursors promoted by iron. *Nature* 569, 104-107.
- Mykytczuk, N. C. S., Foote, S. J., Omelon, C. R., Southam, G., Greer, C. W., and Whyte, L. G., 2013. Bacterial growth at -15 °C; molecular insights from the permafrost bacterium *Planococcus halocryophilus* Or1. *ISME J.* 7, 1211–1226. doi: 10.1038/ismej.2013.8.
- Mykytczuk, N. C. S., Wilhelm, R. C., and Whyte, L. G., 2012. *Planococcus halocryophilus* sp. nov., an extreme sub-zero species from high arctic permafrost. *Int. J. Syst. Evol. Microbiol.* 62, 1937–1944. doi: 10.1099/ijss.0.035782-0.4
- Nakouzi, E., Steinbock, O., 2016. Self-organization in precipitation reactions far from the equilibrium, *Science Advances*, e1601144.
- Nicolis, G, Prigogine I., 1977, Self-organization in nonequilibrium systems. From dissipative structures to order through fluctuations. Wiley-Blackwell.
- Niether, D. Afanasenkau, J. K. Dhont, S. Wiegand, Accumulation of formamide in hydrothermal pores to form prebiotic nucleobases, 2016, *Proc. Natl. Acad. Sci. USA.*, 113, 4272–4277.
- Nobile, A., Pagli, C., Keir, D., Wright, T. J., Ayele, A., Ruch, J., et al., 2012. Dike-fault interaction during the 2004 Dallol intrusion at the northern edge of the Erta Ale Ridge (Afar, Ethiopia). *Geophys. Res. Lett.* 39, 2–7. doi: 10.1029/2012GL053152.
- Nordstrom, D.K., Alpers, C.N., Ptacek, K.J., Blowers, D.W., 2000. Negative pH and Extremely Acidic Mine Waters from Iron Mountain, California. *Environ. Sci. Technol.* 34, 254-258.
- Novikov, Y., and Copley, S., 2013. Reactivity landscape of pyruvate under simulated hydrothermal vent conditions, *Proceedings of the National Academy of Sciences*, 110, 13283-13288; DOI: 10.1073/pnas.130492311013283-13288.
- Oren, A., 2013. “Life in magnesium- and calcium-rich hypersaline environments: salt stress By Chaotropic Ions,” in *Polyextremophiles. Cellular Origin, Life in Extreme Habitats and*

- Astrobiology, eds J. Seckbach, A. Oren, and H. Stan-Lotter (Dordrecht: Springer), 215–232. doi: 10.1007/978-94-007-6488-0.
- Ortoleva P., Chen W., 1990. Self-Organization in Far-from-Equilibrium Reactive Porous Media Subject to Reaction Front Fingering. In: Walgraef D., Ghoniem N.M. (eds) *Patterns, Defects and Materials Instabilities*. NATO ASI Series (Series E: Applied Sciences), vol 183. Springer, Dordrecht.
- Pagano, J.J., Bánsági, T., Steinbock, O., 2007a. Tube Formation in Reverse Silica Gardens. *The Journal of Physical Chemistry C* 111, 9324-9329.
- Pagano, J.J., Bánsági, T., Steinbock, O., 2007b. Tube Formation in Reverse Silica Gardens *J. Phys. Chem. C* 111, 9324-9329.
- Pagano, J.J., Jr., T.B., Steinbock, O., 2008. Bubble-templated and flow-controlled synthesis of macroscopic silica tubes supporting zinc oxide nanostructures. *Angewandte Chemie* 47, 9900–9903.
- Pagli, C., Wright, T. J., Ebinger, C. J., Yun, S.-H., Cann, J. R., Barnie, T., et al., 2012. Shallow axial magma chamber at the slow-spreading Erta Ale Ridge. *Nat. Geosci.* 5, 284–288. doi: 10.1038/ngeo1414.
- Parmar, K., Chaturvedi, H.T., Akhtar, M.W., Chakravarty, S., Das, S.K., Pramanik, A., Ghosh, M., Panda, A.K., Bandyopadhyaya, N., Bhattacharjee, S., 2009. Characterization of cobalt precipitation tube synthesized through “silica garden” route. *Materials Characterization* 60, 863-868.
- Parmar, K., Pramanik, A.K., Bandyopadhyaya, N.R., Bhattacharjee, S., 2010. Synthesis and characterization of Fe(III)-silicate precipitation tubes. *Materials Research Bulletin* 45, 1283-1287.
- Pérez, E., Chebude, Y., 2017. Chemical Analysis of Gaet’ale, a Hypersaline Pond in Danakil Depression (Ethiopia): New Record for the Most Saline Water Body on Earth. *Aquatic Geochemistry* 23, 109-117.
- Petrov, V., Gáspár, V., Masere, J. et al. Controlling chaos in the Belousov—Zhabotinsky reaction. *Nature* 361, 240–243 (1993). <https://doi.org/10.1038/361240a0>.
- Plümper, O., King, H. E., Geisler, T., Liu, Y., Pabst, S., Savov, I. P., et al., 2017. Subduction zone forearc serpentinites as incubators for deep microbial life. *Proc. Natl. Acad. Sci. U.S.A.* 114, 4324–4329. doi: 10.1073/pnas.1612147114.
- Price, P. B., and Sowers, T., 2004. Temperature dependence of metabolic rates for microbial growth, maintenance, and survival. *Proc. Natl. Acad. Sci. U.S.A.* 101, 4631–4636. doi:10.1073/pnas.0400522101.
- Rivkina, E. M., Friedmann, E. I., McKay, C. P., and Gilichinsky, D. A., 2000. Metabolic activity of Permafrost Bacteria below the freezing point. *Appl. Environ. Microbiol.* 66, 3230–3233. doi: 10.1128/AEM.66.8.3230-3233.2000.
- Rasmussen, B., Krapež, B., Muhling, J.R., Suvorova, A., 2015. Precipitation of iron silicate nanoparticles in early Precambrian oceans marks Earth’s first iron age. *Geology* 43, 303-306.

- Rudnick, R.L., Fountain, D.M., 1995. Nature and composition of the continental crust: A lower crustal perspective. *Reviews of Geophysics* 33, 267-309.
- Russell, M.J., Daniel, R.M.D., Hall, A.J., Sherringham, J.A., 1994. A Hydrothermally Precipitated Catalytic Iron Sulphide Membrane as a First Step Toward Life. *J Mol Evol* 39, 231-243.
- Sahai, N., Kaddour, H., Dalai, P., Wang, Z., Bass, G., Gao, M., 2017. Mineral Surface Chemistry and Nanoparticle-aggregation Control Membrane Self-Assembly. *Scientific reports* 7, 43418.
- Saladino, R., Botta, G., Bizzarri, B.M., Di Mauro, E., Garcia Ruiz, J.M., 2016. A Global Scale Scenario for Prebiotic Chemistry: Silica-Based Self-Assembled Mineral Structures and Formamide. *Biochemistry* 55, 2806-2811.
- Saladino, R., Crestini, C., Ciciriello, F., Pino, S., Costanzo, G., Di Mauro, E., 2009. From formamide to RNA: the roles of formamide and water in the evolution of chemical information. *Research in microbiology* 160, 441-448.
- Saladino, R., Crestini, C., Pino, S., Costanzo, G., Di Mauro, E., 2012. Formamide and the origin of life. *Physics of life reviews* 9, 84-104.
- Saladino, R., Di Mauro, E., Garcia-Ruiz, J.M., 2019. A Universal Geochemical Scenario for Formamide Condensation and Prebiotic Chemistry. *Chem. Eur. J.* 25, 3181 – 3189.
- Sánchez, M., Sabio, L., Gálvez, N., Capdevila, M., Dominguez-Vera, J.M., 2017. Iron chemistry at the service of life. *Life*, 69, 382-388.
- Scambelluri, M., Piccardo, G., Philippot, P., Robbiano, A., and Negretti, L. (1997). High salinity fluid inclusions formed from recycled seawater in deeply subducted alpine serpentinite. *Earth Planet. Sci. Lett.* 148, 485–499. doi: 10.1016/S0012-821X(97)00043-5.
- Scambos, T. A., Campbell, G. G., Pope, A., Haran, T., Muto, A., Lazzara, M., et al., 2018. Ultralow surface temperatures in East Antarctica from satellite thermal infrared mapping: the coldest places on earth. *Geophys. Res. Lett.* 45, 6124–6133. doi: 10.1029/2018GL078133.
- Schleper, C., Puhler, G., Klenk, H.-P., and Zillig, W., 1996. *Picrophilus oshimae* and *Picrophilus torridus* fam. nov., gen. nov., sp. nov., two species of hyperacidophilic, thermophilic, heterotrophic, aerobic archaea. *Int. J.* 46, 814–816. doi: 10.1099/00207713-46-3-814.
- Scott, C., Franks, N.R., Sneyd, J., Bonabeau, E., Deneubourg, J-L., and Theraula, G., 2001. *Self-Organization in Biological Systems*, Princeton University Press, U.S.A. isbn: 0691012113.
- Stevenson, A., Cray, J. A., Williams, J. P., Santos, R., Sahay, R., Neuenkirchen, N., et al., 2015. Is there a common water-activity limit for the three domains of life. *ISME J.* 9, 1333–1351. doi: 10.1038/ismej.2014.219.
- Stone, D. A., and Goldstein, R. E., 2004. Tubular precipitation and redox gradients on a bubbling template. *Proceedings of the National Academy of Sciences of the United States of America*, 101, 11537–11541. doi:10.1073/pnas.0404544101.

- Suzuki, S., Ishii, S., Wu, A., Cheung, A., Tenney, A., Wanger, G., et al., 2013. Microbial diversity in The Cedars, an ultrabasic, ultrareducing, and low salinity serpentinizing ecosystem. *Proc. Natl. Acad. Sci. U.S.A.* 110, 15336–15341. doi: 10.1073/pnas.1302426110.
- Tadiwos, C., 2013. Dallol volcano and Danakil depression; earth resources and geo-hazards, in Proceedings of the 24th Colloquium of African Geology and 14th Congress of Geological Society of Africa, Aveiro.
- Takai, K., Nakamura, K., Toki, T., Tsunogai, U., Miyazaki, M., Miyazaki, J., et al., 2008. Cell proliferation at 122 C and isotopically heavy CH₄ production by a hyperthermophilic methanogen under high-pressure cultivation. *Proc. Natl. Acad. Sci. U.S.A.* 105, 10949–10954. doi: 10.1073/pnas.0712334105.
- Talbot, C. J., 2008. Hydrothermal salt-but how much? *Mar. Pet. Geol.* 25, 191–202. doi: 10.1016/j.marpetgeo.2007.05.005.
- Thouvenel-Romans, S., Steinbock, O., 2003. Oscillatory Growth of Silica Tubes in Chemical Gardens. *J. Am. Chem. Soc.* 125, 4338-4331.
- Traube, M., 1867. Experimente zur Theorie der Zellenbildung und Endosmose. *Arch. Anat. Physiol.*, 87–165.
- Trapeznikov, A., 1983. Radioactivity in the Canadian environment. *Natl. Res. Counc. Canada* 19250:292.
- Turing, A.L., The chemical basis of morphogenesis, *Phil. Trans. R. Soc. Lond. B*, 237, <http://doi.org/10.1098/rstb.1952.0012>.
- Uechi, I., Katsuki, A., Dunin-Barkovskiy, L., Tanimoto, Y., 2004. 3D-Morphological Chirality Induction in Zinc Silicate Membrane Tube Using a High Magnetic Field. *The Journal of Physical Chemistry B* 108, 2527-2530.
- Varet, J., 2018. Recent and active units of the Danakil Sea (Dagad Salt Plain) and Afdera Lake, in *Geology of Afar (East Africa)* (Cham: Springer International Publishing), 205–226. doi: 10.1007/978-3-319-60865-5_7.
- Wang, Y., Chan, M. & Merino, E., 2015. Self-organized iron-oxide cementation geometry as an indicator of paleo-flows. *Sci Rep* 5, 10792. <https://doi.org/10.1038/srep10792>.
- Wang, Q., Bentley, M. R., Steinbock, O., 2017. Self-Organization of Layered Inorganic Membranes in Microfluidic Devices, *J. Phys. Chem. C*, 121, 26, 14120-14127.
- Wolfenden, E., Ebinger, C., Yirgu, G., Deino, A., and Ayalew, D., 2004, Evolution of the northern Main Ethiopian rift: birth of a triple junction: *Earth and Planetary Science Letters*, v. 224, no. 1-2, p. 213-228.
- Wunderman, R. (ed.), 2013. Report on Dallol (Ethiopia), in *Bulletin of the Global Volcanism Network*, Vol. 38, ed. R. Wunderman, (Washington, DC: Smithsonian Institution). doi: 10.5479/si.GVP.BGVN201305-221041.

Yakimov, M. M., La Cono, V., Spada, G. L., Bortoluzzi, G., Messina, E., Smedile, F., et al., 2015. Microbial community of the deep-sea brine Lake Kryos seawaterbrine interface is active below the chaotropicity limit of life as revealed by recovery of mRNA. *Environ. Microbiol.* 17, 364–382. doi: 10.1111/1462-2920.12587.

Chapter 2

**Iron-silica self-organized membranes: geochemical
plausibility, nanoscale characterization and catalytic
behavior**

2.1. Summary

Fe-silica membranes, commonly known as Fe-silica gardens, were grown in the laboratory using natural hyperalkaline, silica-rich water sampled from the Ney spring in California. The obtained membranes (hereafter referred to as natural membranes) were characterized at the nanoscale using a variety of analytical techniques and their characteristics were compared to synthetic membranes (i.e. model membranes). The role of these membranes as potential catalysts of prebiotic and early life chemical reactions is discussed with respect to their mineral chemistry and bilayer structure. In addition, their morphological and mineralogical resemblance to biogenic iron filamentous structures found in cherts, that may lead to misinterpretation of the origin of some of the Earth's oldest microfossils, is highlighted.

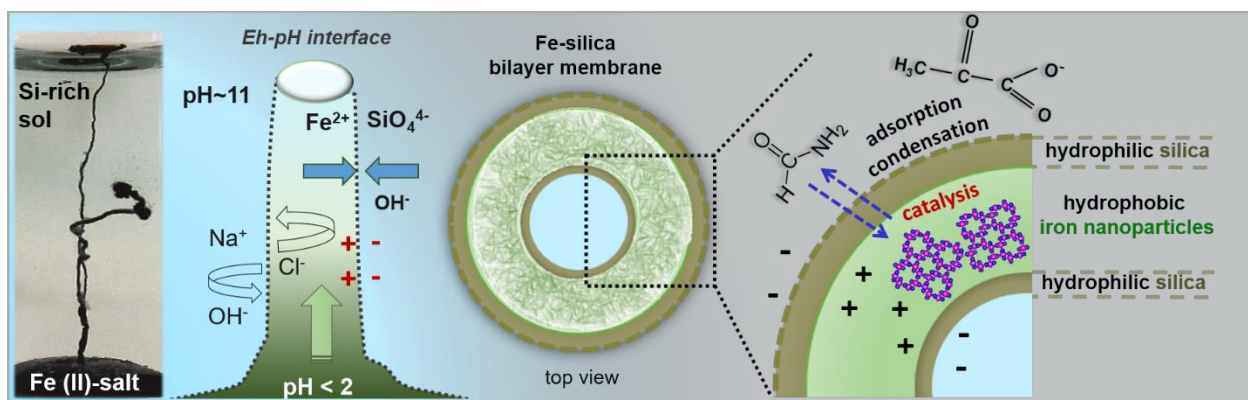


Figure 1. Graphical abstract showing the inorganic Fe-silica bilayer membrane, capable of adsorbing and condensating organic molecules and catalyzing the formation of amino acids, nucleobases and carboxylic acids while providing UV radiation shielding. These membranes, that could have precipitated in the early hydrothermal environments (among other settings), may have provided a template for the concentration and organization of the first biologically relevant organics.

2.2. Experimental and analytical part

Chemical analysis of water

Chemical analysis of the Ney water was performed with a range of quantitative instruments. SiO_2 , Mg^{2+} , Ca^{2+} , Ba^{2+} , Sr^{2+} , Na^+ , Li^+ , K^+ , $\text{B}^{\text{n+}}$, and $\text{Mo}^{\text{n+}}$ concentrations were measured using a Perkin Elmer 7300 Inductively Coupled Plasma Atomic Emission Spectrometer (ICP-AES) operating in the dual view mode. A second measurement of the Ba^{2+} , Li^+ , and $\text{Mo}^{\text{n+}}$ was performed using a Thermo X7 Inductively Coupled Plasma Mass Spectrometer (ICP-MS). Furthermore, anion concentrations (Cl^- , SO_4^{2-} , CO_3^{2-} , HCO_3^-) were determined using ion chromatography. The conductivity and fluoride ion concentration were determined using a Mantech PC-Titrate Autotitrator system. However, the exceedingly high alkalinity of the Aqua de Ney water samples could not be measured using this instrument. Therefore, a manual titration was performed of three aliquots of the Aqua de Ney water with 0.1 N (0.05 M) of sulfuric acid. The water samples required (166 ± 3) mL of the titrant to reach a pH of 4.5. Notice that this value is not solely indicative of the carbonate ion concentration, as the high silica concentration also contributes to the alkalinity.

Membrane precipitation

For the model membrane I placed separately solid pellets of $\text{FeCl}_2 \cdot 4\text{H}_2\text{O}$, FeCl_3 , and $\text{Fe}_2(\text{SO}_4)_3 \cdot 9\text{H}_2\text{O}$ (pellets were prepared using an agate mortar, until reaching the powder fraction, and a press up to 10 tons) in a 4 mL volume glass vial and poured 3 mL of diluted (1:4) commercial water glass (6.25 M “ SiO_2 ”_(aq)). For the natural membrane I replaced the silicate sol with the Ney solution, without dilution and used the same pellets as for the model membrane. Note that the silica concentration of the Ney solution is 0.65M (4230 ppm SiO_2). The experiments were conducted: a) in ambient conditions, b) in anoxic conditions (inside a N_2 atmosphere glove box) and c) at a temperature of 60 and 80 °C. For the anoxic experiments all solutions were prepared and handled inside the glove box with Ar-purged Milli-Q water. The solid pellets were prepared as well inside the glove box with fresh Fe-salt powder, by placing the powder in a pressure cell and by fixing it with a hammer.

Field emission gun scanning electron microscope (FESEM) equipped with an Oxford energy-dispersive X-ray spectrometer (EDS)

Following the formation of the tubular membranes and the termination of the phenomenon, the membranes were studied ex-situ under a field emission gun scanning electron microscope. A

ZEISS SUPRA 40 VP, FESEM-EDS equipped with an Oxford energy-dispersive X-ray spectrometer (EDS) of the Centro de Instrumentación Científica (CIC) of the University of Granada, Spain, operating at 5keV-20KeV was used for the textural and chemical characterization of the sub-micron mineral phases. High resolution images were obtained at 5 kV and at 2 mm working distance, in SE and 15 kV in BS mode, while for the elemental analyses operating conditions were set at 15 kV accelerating voltage and 7.5 mm working distance and the AZtec 3.0 SP1 EDS software was used.

Powder X-ray diffraction (PXRD)

Also, powder X-ray diffraction (PXRD) was performed, to identify the mineral crystalline phases of the membranes, with the X'Pert Pro MPD (PANalytical) diffractometer, powered by a Philips PW3040/60 X-ray generator (Cu-K α) and fitted with an X'Celerator detector, at 40 kV acceleration voltage and a current of 40 mA. Phase identification was carried out with the HighScore Plus Software (PANalytical) and the American Mineralogist Crystal Structure Database.

Raman Spectroscopy

Raman spectra were recorded using a HORIBA Jobin Yvon LabRAM HR UV-VIS spectrometer equipped with an Olympus BX41 optical microscope with binocular and Koehler illumination and a CCD detector at excitation wavelengths of 532 nm (frequency doubled Nd:YAG laser).

Gas Chromatography Mass Spectroscopy (GC-MS)

In the case of the gas production upon reaction of the Fe(III)-, Cu(II)- and Zn(II)- salts with the Ney water, GC-MS was used to identify the gas phase using an Agilent VARIAN (now Bruker) 450 GC 240-MS Ion Trap Mass Spectrometer (40 mL manual injection, gastight syringe). For the measurement standard air samples as well as blank samples of the Ney solution were used.

Ultramicrotome and FESEM-FIB

Following the development of the model and natural membranes, the Fe(II)-silica hollow tubes were extracted and rinsed with deionized water. Ultrathin sections of the tubes were prepared by focus ion beam (FIB) milling, by using a Zeiss Crossbeam Auriga 40 FIB-SEM at the facilities of the Institut de Physique du Globe de Paris (IPGP), France as described in Heaney et al. (2001). The FIB system used a Ga liquid metal ion source which allowed milling, operating at 30 kV acceleration voltage. A thin layer of platinum was deposited on the specimen that was previously

Au coated. Horizontal ultrathin cross sections were prepared at the sample preparation facilities of the Centro de Instrumentacion Científica of the University of Granada. The tubular membranes were embedded in resin blocks and stained with Toluidine Blue for the selection of the areas for ultrathin sectioning. Ultrathin sections were cut by using a microtome with a 35° diamond knife (Reichert Ultra-Cut), dispersed in Milli-Q water and transferred from the water on a formvar C-coated Cu grid.

TEM/STEM/HR-HAADF/EELS

High-resolution high-angle annular dark-field (HR-HAADF), elemental mapping X-ray Energy Dispersive Spectroscopy (XEDS) and electron energy loss spectroscopy (EELS) analyses including the energy loss near-edge fine structure (ELNES) were used to characterize the structure and mineral chemistry of the membranes in nanoscale. The study was performed on a FEI Titan³ Ultimate 60-300 double Cs-corrected, operating at 300 kV at the Servicios Centrales de Investigación Científica y Tecnológica (SC-ICYT), University of Cádiz, Spain. The aberrations of the condenser lenses were corrected up to fourth-order using the Zemlin tableau to obtain a sub-Angstrom electron probe. A condenser aperture of 50 μm yielding an electron probe with a convergence angle of 18 mrad was used and the annular dark-field (ADF) collection angle ranged from 64 to 200 mrad. HR-HAADF image simulation studies were built with RHODIUS, a computer program developed at Cadiz University (Bernal et al., 1998), while, the TEMSIM software was used for HR-HAADF image simulations (Kirkland, 2010).

XEDS acquisitions were performed using the SuperX G2 detector. In order to get a high signal-to-noise ratio a beam current of 0.12 nA and a dwell pixel time of 25 μs were used, which results in a total acquisition time of 3s per frame, recording a total of 100 frames. To extract XEDS elemental maps, O K, Si K and Fe K family lines were used. The XEDS elemental maps were post-filtered using a 3x3 average pixels to improve the visualization.

EELS experiments were performed in the dual spectrum imaging (dual-SI) mode which allows the correlation of analytical and structural information on selected regions of the material under study. In this technique: i) the EELS and HAADF signals are collected simultaneously while the electron beam is scanned across the selected area of the sample; ii) the Dual mode and the zero-loss region are recorded simultaneously with the core-loss signal of the element(s) of interest, which allows a very precise determination of the absolute value of the energies at which the core-loss edges are appearing in the experiment. To perform these analyses a Quantum–Gatan post column Imaging

Filter (GIF) was used equipped with an ultra-fast shutter. A 16.5 mm camera length was used giving a collection semi-angle of 73.5 mrad. The experiments were acquired in Dual EELS-SI mode using an energy dispersion of 0.25 eV, 0.07 nA probe current, and 50 ms acquisition time per EELS spectrum. Si L_{2,3} (90-173.5eV), O K(520-590 eV) and Fe L_{2,3} (690-760 eV) elemental maps were built after removing the background from raw data, using a power law model and a window width of 25 eV. Multiple linear least squares (MLLS) fitting technique was used for the evaluation of the Fe(II)/Fe(III) atomic percentages. Samples were placed on a formvar C-coated Cu-grid and to avoid contaminations were cleaned with oxygen plasma process (25% oxygen and 75% argon) for 5-10 seconds before being placed into the TEM. No change in specimen was observed by TEM after the oxygen plasma cleaning.

BET – Surface Area

The specific surface area of the membrane was determined by the BET method using N₂ adsorption–desorption isotherms measured at 77.4 K with a surface analyzer Belsorp-Max of the BEL JAPAN Inc.III at the facilities of the ISTerre (Insitut des Sciences de la Terre/Institute of Earth Sciences) Grenoble. The N₂ (77.4 K) adsorption–desorption measurements were carried out in a relative pressure range P/P₀ from 0.001 to 0.997 (Pressure sensors on each port: 133 kPa et 1.33 kPa). The annealed samples were outgassed in vacuum at 80 °C for 10 h before measurements. The specific surface areas and distribution of pore size were calculated using the Brunauer–Emmet–Teller (BET) method (Brunauer et al., 1938).

2.3. Results and discussion

2.3.1. Fe-silica membranes formation from the Ney water

The alkaline Ney springs belong to an abandoned spa called Aqua de Ney at the Ney Creek, a tributary of the Sacramento River, in the eastern Klamath Mountains, eight kilometers south of Mount Shasta (Siskiyou County, N. California, USA) (Fig. 1A). The springs are located about three hundred meters downstream of the Fairy falls, and they can be accessed following the Ney Springs Canyon Trail. Only the spring closer to the shore of the creek produces alkaline water. This alkaline spring is today a well, built in a hexagonal shape, located a couple of meters above the creek (Fig.1B). The water leaves the well through an underground connection to another artificial, circular pool closer to the creek that was used as a footbath in the spa created by John Ney in late 19th century.

Ney springs discharge at the Ordovician Trinity sub-terrane, an east-dipping ultramafic sheet composed of serpentized tectonic peridotite (known also as Trinity Ophiolite) with gabbro-dioritic intrusions (Feth et al., 1961; Barnes and O'Neil 1969; Barnes et al., 1974; Brouxel et al., 1988; Irwin, 1994). The geological scenario is completed by the overlain Devonian-Mississippian volcanic and sedimentary units (Redding sub-terrene), the Jurassic granitic plutons, and the Cascade Range Eocene-Quaternary sequence, comprising volcanic and sedimentary deposits (Fig.1A). The Tertiary sequence outcrops with a deeply weathered albite-rich dacitic facies on the southern side of the canyon, at the level of the Ney Springs. The alkaline Ney spring is located in the contact of the Trinity ophiolite complex and the albite-rich dacitic facies of the Tertiary basaltic-andesitic volcanic deposits (Barnes and O'Neil 1969; Brouxel et al., 1988; Irwin, 1994).



Figure 1. Sampling and geological setting of Ney spring. **A.** Simplified geological map of the Ney Springs area (modified from 35). Geological formation acronyms and description: OUM, Ordovician Trinity Ultramafic Sheet; OGB, Ordovician Gabbro and diorite (hornblende gabbro – hornblende diorite - quartz diorite); DC, Early Devonian Comopley Greenstone (andesitic and basaltic volcanic breccia, tuff, pillow lavas); DK, Early-Middle Devonian Kennett Fm. (interbedded dark siliceous shale, rhyolitic tuff and limestone); MB, Mississippian Bragford Fm. (interbedded dark shale, siltstone, sandstone and locally abundant pebble-conglomerate); JGR, Jurassic granitoid plutons (quartz diorite to granite composition); TVS, Eocene-Oligocene volcanic and sedimentary rocks (andesitic and basaltic flows, breccia, tuff, minor rhyolitic tuff and intercalated sedimentary units); QV, Quaternary volcanic rocks (Basaltic and andesitic flows and pyroclastic rocks); QG, Quaternary glacial deposits (glacial debris). **B.** Hexagonal concrete well, next to the Ney Creek, where the alkaline water was collected. **C.** Methane bubbling from the spring.

The Ney springs were sampled in August of 2015 and November of 2017 at the following coordinates: 41° 15' 43" N, 122° 19' 54" W. Since the silica concentration of the water was of interest the samples were collected in plastic bottles to avoid silica dissolution of the glass bottles. The pH value of the water of the Ney spring was measured in situ 11.9 (2015) and 12.3 (2017). The temperature of the water in the Ney well ranged between 14.5 °C (2015) and 12.3 °C (2017), while the water of the creek was at 15.6 °C (2015) and 14 °C (2017). Major and minor elemental composition, in situ and ex situ pH values, and temperature of the water as well as comparison with previous chemical analyses (Feth et al., 1961; Barnes et al., 1972) are indicated in Table 1. The Ney spring water exhibits noticeable chemical properties. First, the alkaline character of the water and second, the very high silica (more than 4.2 g/L) -the highest value of silica reported in the

literature-, boron (256 mg/L) and lithium (5.1 mg/L) concentrations, the combination of which points to a complicated hydrologic origin.

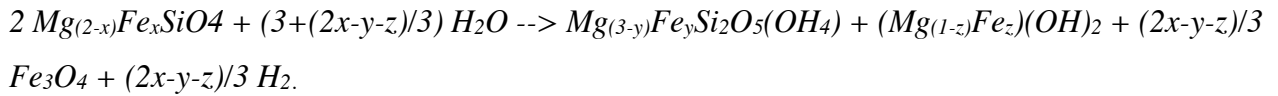
| Reference | Feth et al., 1961 *a/b | Barnes et al., 1972 | This study |
|---|------------------------|---------------------|------------|
| pH | 11.6/ 10.9 | 10.9 | 11.89 |
| conductivity | - | - | 37250 |
| alkalinity (tot as CaCO ₃) | - | - | 13300 |
| T °C | 12.2/ 10 | 10 | 14.5 |
| SiO ₂ | 3970/3400 | 4000 | 4235.6 |
| Ba | - | - | 0.42 |
| B | 242/ 200 | 303 | 256 |
| Ca | 7.3/ 2.5 | 0.6 | <0.4 |
| Mg | 2.6/ 0.9 | 0.3 | 0.2 |
| Na | 10900/ 8710 | 11300 | 11775 |
| K | 135/116 | 220 | 154.5 |
| Li | 3.2/1.5 | - | 5.1 |
| S | 295/439 | 430 | 342 |
| Fe | - | 0.3 | 0.4 |
| Cl ⁻ | 7180/ 5950 | 7500 | 8600 |
| SO ₄ ⁻² | 267/ 172 | 123 | 445 |
| CO ₃ ⁻² | 5560/ 4790 | 5450 | 5399 |
| HCO ₃ ⁻ | - | 586 | <5 |

Table 1. Comparative chemical analysis of the Ney water by Feth et al., 1961 (* a samples were collected in 1958 and b samples in 1957; Barnes et al., 1972 and this study. Elemental concentrations are in ppm, conductivity is in $\mu\text{S}/\text{cm}$.

Different theories for the origin of the Ney spring water have been proposed. The salinity, the relatively high concentration of Na and Cl, the high deuterium value of the water molecule, and the high boron concentration led the first researchers to hypothesize a connection with a connate seawater entrapped in the sediments (Feth et al. 1961). One decade later, new water isotope data were interpreted as “non-meteoric, probably of metamorphic origin with analogies with oilfield brine” (Barnes et al. 1972). More recently, the chemical and d^{37}Cl isotope composition were believed to be controlled by the strong interaction with an underlying serpentinized body (Cullen

2013). Finally, the local ultramafic lithology, the very high pH, the bubbling gas composition that is composed of CH₄ by more than 80% (Mariner et al. 2003; Blank et al., 2017)(Fig.1C) and the serpentine supersaturation suggest serpentinization as the main process that determined the fluid composition (Liakhovitch et al. 2005; Mottl 2009; Boschetti et al. 2013).

Serpentinization is triggered when water interacts with olivine, a silicate mineral, which is a solid solution between two end members, fayalite (the iron-silicate) and forsterite (the magnesium-silicate). The reaction produces magnetite and molecular hydrogen, besides the hydrous minerals serpentine and brucite:



The distribution of Fe in the reaction products, and hence the yield of H₂, is a function of pressure, temperature, and rock composition (Klein et al., 2009; McCollom and Bach, 2009). The presence of brucite imposes a high pH and low silica activity to the interacting waters. Thus, spring waters known to derive from serpentinization processes have pH values as high as 12, even in the contemporary presence of a CO₂-rich atmosphere acting as acidifying agent (Chavagnac et al., 2013). The presence of serpentine and brucite effectively buffer silica concentrations to low values ($3Mg(OH)_2 + 2 SiO_2(aq) = Mg_3Si_2O_5(OH)_4 + H_2O$; ignoring Fe). Hence, the high boron and silica concentration of the Ney water are unusual for this kind of water-rock process, unless to invoke other sources (Boschetti and Toscani 2008; Boschetti et al. 2013a). Oxygen, hydrogen, lithium and boron isotopic study of Boschetti et al., (2018) showed that fossil fluid of seawater origin was affected by both serpentinization and slab dehydration processes that modified the chemical and isotope composition of this early fluid. In particular, the high pH and the serpentine supersaturation agree with the serpentinization reactions, whereas slab dehydration explains the high boron concentration and the low d¹¹B value. Both processes occurred at high temperature and concurred to determine the ¹⁸O-enrichment of this water/slab dehydration water, affected by low-temperature metamorphism and serpentinization processes. According to other studies on modeling and experimental results of serpentinizing fluids (Frost and Beard 2007; Sekine et al. 2015), the high silica activity of the Ney water could be buffered by the serpentine-talc instead of serpentine-brucite pair, following the reaction: *serpentine* + 2SiO₂ → *talc* + H₂O, with the log_(activity) of the dissolved species in Ney at a high pressure (5 kbar), the mean equilibrium temperature is quite similar to the temperature obtained by the slab model. Therefore, most probably this equilibrium

buffered the silica concentration at depth, whereas according to Barnes et al. (1972) and to the low saturation indexes of the silica phases at shallower conditions calculated by Boschetti et al., (2018), the extraordinary enrichment in silica is explained by the flowing of the alkaline water through the dacitic-andesitic rocks, as a result of the dissolution of silica and silica-rich minerals at high pH conditions.

Concerning the methane emitted from the Ney spring, C and H stable isotopes and clumped isotope compositions of CH₄ indicate a methane formation temperature of approximately 50 °C. More importantly, the origin of the methane seems to be dominantly abiotic, likely generated by Fischer-Tropsch type reactions at depth, although possible minor microbial components cannot be excluded (Blank et al., 2017). This finding, along with the hyperalkalinity and the high silica content of the water, render the Ney springs an ideal candidate for investigating the geochemical plausibility of silica self-organized membranes in relation to the serpentinization environments of the early Earth.

Iron-silica membranes were grown from the natural Ney water, herein mentioned as ‘natural’ membranes. As described in the experimental part, soluble pellets of Fe(II)- and Fe(III)-salts were immersed in the Ney water for the membrane growth. In the case of Fe(II)-salt the typical hollow tubes, similar to those produced with model solutions, were obtained (Fig. 2,3).

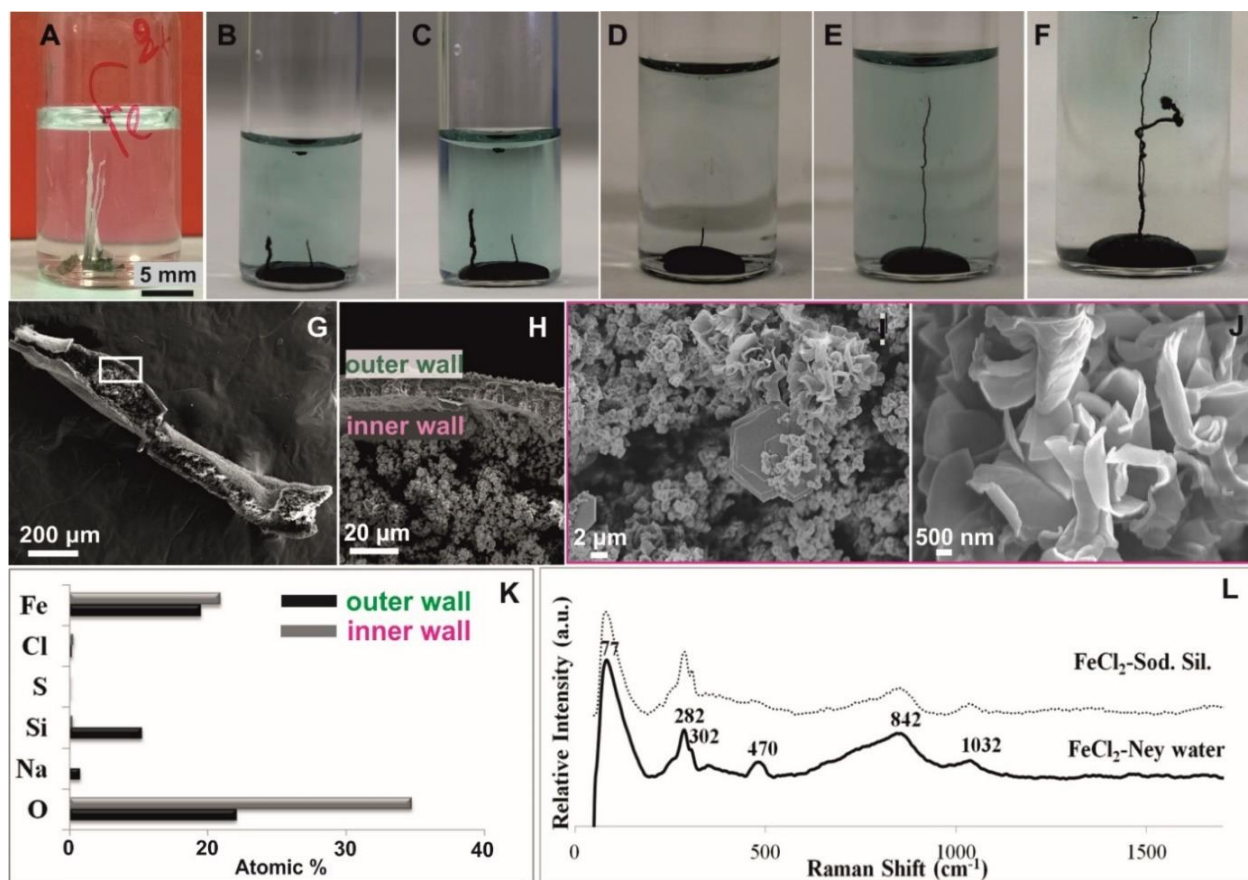


Figure 2. Fe-silica tubular membranes grown from the Ney water. **A.** tubular membrane produced by reaction of the Fe(II)-salt pellet and the model solution. **B-C, D-F.** Fe-silica membrane growth. **G.** SEM image of a section of the membrane. **H.** Zoom in the marked area (white rectangular) of G where the outer smooth and inner complex parts are shown. **I-J.** FESEM images of the internal part of the membrane composed of rosettes and hexagonal platelets of Fe-oxhydroxides. **K.** Comparative histogram for the chemical composition (EDS) of the inner and outer parts. **L.** Comparative Raman spectra of the model and Ney membranes.

These structures reproduce a key feature of classical silica gardens: textural and compositional gradients across the membrane (Pagano et al., 2007; Kellermeier et al., 2013)(Fig. 2). In particular, the outer surface of the membrane, facing towards the silica-rich Ney water, is smooth and rather homogeneous (Fig. 2G-H) while the inner surface consists of micro-rosettes and nano-globules (Fig. 2I-J). Moreover, it is shown that the outer membrane surface is rich in silica and metal silicates while the inner surface is rich in metal-(oxy)hydroxides (Fig. 2K). The formation of tubules in the Ney water is relatively slow (hours) compared to the classical experiments (within seconds to minutes) (Kellermeier et al., 2013)(Fig. 3). The latter result can be attributed to the smaller difference in ionic strength between the inner and outer solution for the case of the Ney experiments, which reduces the strength of the osmotically driven force.

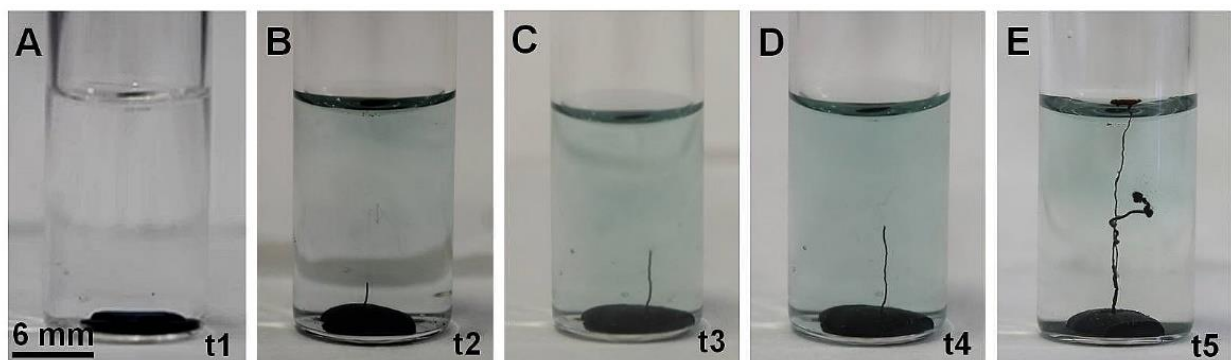


Figure 3. Tubular membrane growth produced by reaction of the Fe(II)-salt pellet ($\text{FeCl}_2 \cdot 4\text{H}_2\text{O}$) with the Ney water. A Formation of the membrane at time $t_1=0$ min. **B** Tubular structure obtained at time $t_2=30$ min. **C** Growth of the tube and continuous fluid jetting at time $t_3=35$ min. **D** Growth of the tube at time $t_4=44$ min. **E** Complete development of the tubular structure at time $t_5= 183$ min.

On the contrary, the experiments performed with the Fe(III)-salts do not give rise to tubular membranes. Instead, they produce a vigorous reaction that releases a large amount of bubbles, leading to the breaching of the membrane soon after its formation and to the creation of a convection cell that remains active for several minutes (Fig. 4). This behavior increases the availability of the surface area of both sides of the membranes (silicate-rich and Fe-rich), and quickly releases any newly forming molecules in the solution, enhancing the role of membranous structures as catalysts in geochemical scenarios (see Introduction)(Barge et al., 2015; Saladino et al., 2016, Barge et al., 2019).

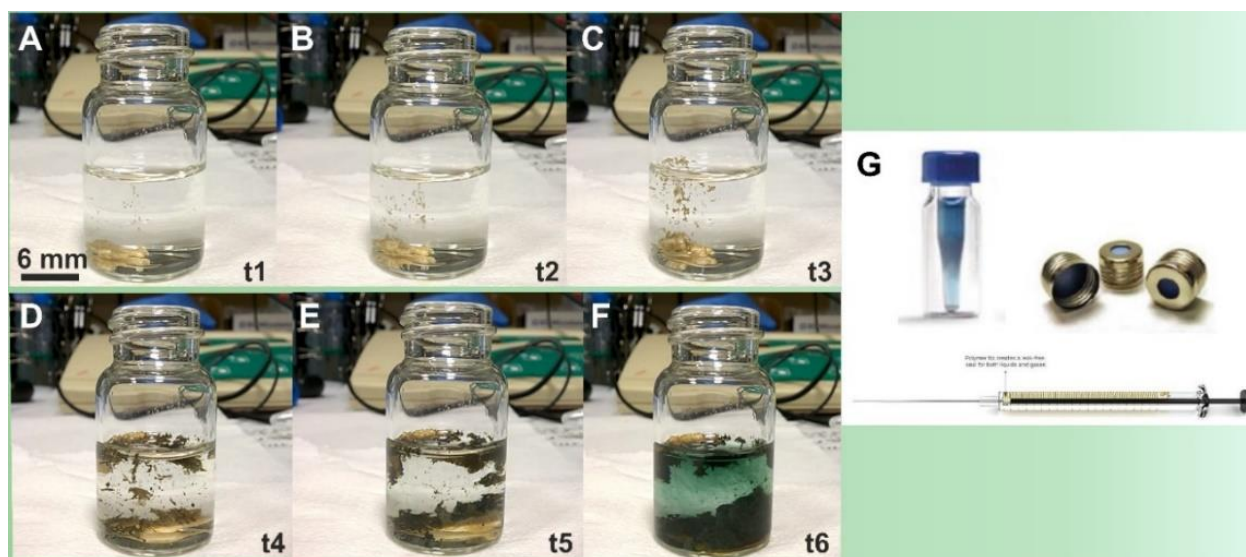


Figure 4. Silica membrane formation and rapture upon reaction of the Ney sol and the Fe(III)-salt. A-F. Immediate rapture of the forming membrane due to CO_2 gas release and establishment of a convection cell that remains active for several minutes; $t_1=5$ sec, $t_2=10$ sec,

t3=25 sec, t4=60 sec, t5=75 sec, t6=120 sec. **G.** The septum vial and the Hamilton syringe used for the gas collection and analysis with GC-MS.

GC-MS was used to analyze the composition of the produced bubbles. This was achieved by placing an Fe(III) micro-pellet inside a septum sealed vial and by injecting the Ney sol with a Hamilton gastight syringe of 100 μ L volume. At the same time another syringe of the same volume was used to collect the released gas (without touching the liquid), produced from the reacting pellet and Ney sol, and directly injected it in the spectrometer. The gas was collected at the beginning of the reaction, during the reaction, and at the end of the reaction, while blank solutions of the Ney sol were also measured. As shown in the chromatograms of Fig. 5 the released gas is CO₂. As soon as the proto metal-silicate membrane forms and expands, the Ney sol (pH 11.9) enters -due to osmosis- inside the dissolving pellet that produces an acidic FeCl₃ sol (pH 1.5). The reaction and mixing of the outer alkaline Ney solution that is rich in carbonate ions (see chemical analysis Table 1) with the acidic iron solution, decreases the pH of the Ney sol and converts the bicarbonate/carbonate species to CO_{2(l)} that are released as CO_{2(g)}. CO₂ concentration was higher during the first 15 sec of the reaction and gradually reduced with time. This is in accordance with the macroscopic observation of abundant bubble release at the beginning of the reaction.

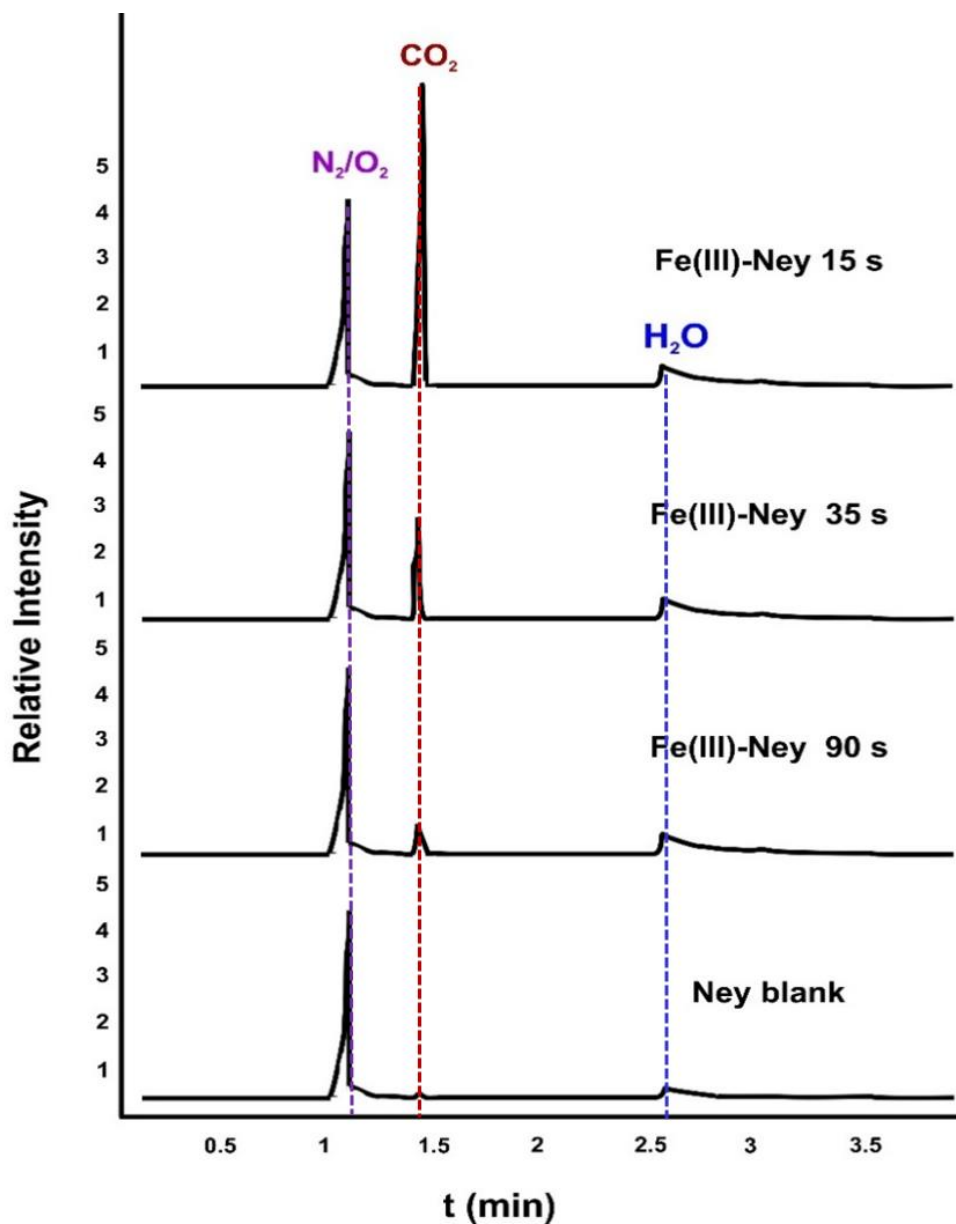


Figure 5. Chromatograms indicating the production of CO_2 (g) upon reaction of the Fe(III) pellets with the Ney water. Note that the CO_2 is obtained from the CO_3^{2-} species as the pH of the Ney solution decreases. CO_2 release is larger during the first 30 sec of the experiment.

2.3.2. Microscopic and spectroscopic study at the nanoscale: model vs natural membranes.

Over the past years a fair amount of studies have focused on the formation mechanisms and properties of Fe-silica membranes (Balköse et al., 2002; Parmar et al., 2010; Makki and Steinbock, 2012; Barge et al., 2012; Barge et al., 2016; Barge et al., 2019; Glaab et al., 2016; Bizzarri et al., 2018). But, we are still lacking chemical and mineralogical information at the nanoscale about these, nanocomposite, structures. Such insight is critical since the composition and structure at the nanoscale determines the physicochemical behavior of these membranes, having among others, direct implications in their function as catalysts (see Introduction). To resolve this issue, a detailed electron microscopic and spectroscopic study of FIB sections obtained from the model membranes, i.e. those made with the sodium silicate solution, and the natural ones, i.e. those made using water obtained from the Ney spring was performed (Fig. 6).

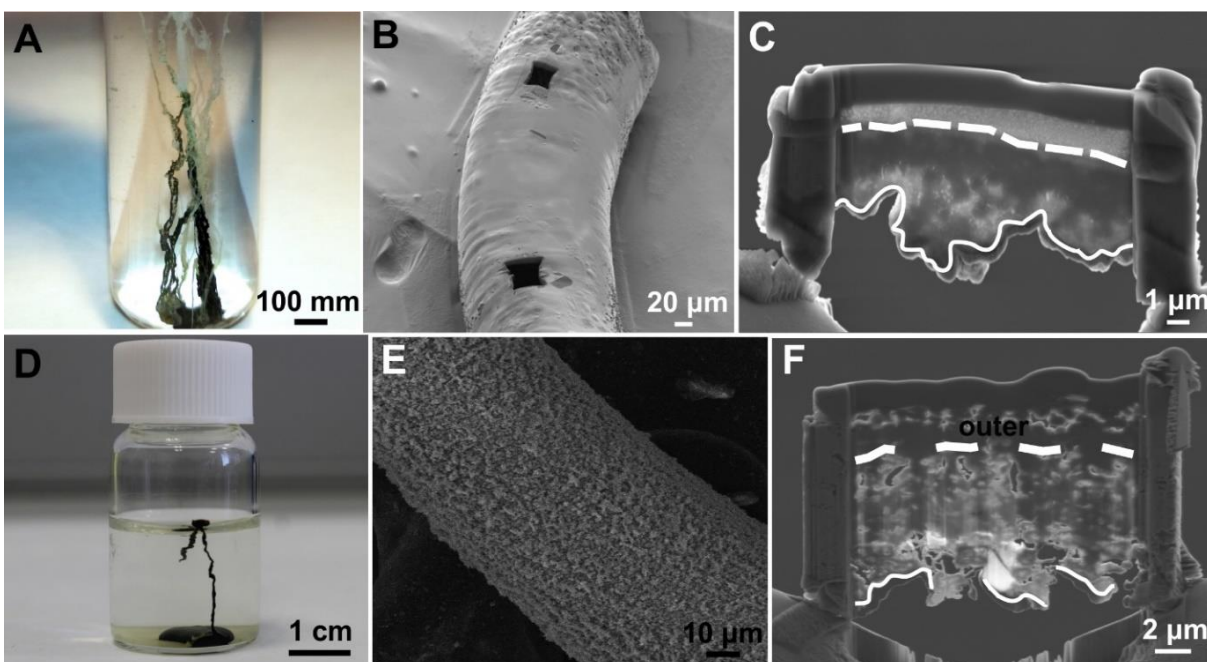


Figure 6. FIB-milled sections of the Fe(II)-silica tubular membranes made with the model sodium silicate solution and the natural Ney water. A. Fe(II)-silica tubular membrane made with the model sol. **B.** SEM image of the model membrane where the areas of the FIB sections are shown. **A. C.** SEM image of the FIB milling section of the natural membrane. The white lines separate the exterior silica layers from the interior Fe-rich layer. **D.** Fe(II)-silica tubular membrane made with the natural sol. **E** SEM image of the natural tubular membrane of **D.** **F.** STEM image of section of the natural membrane prepared by FIB milling. The white lines separate the exterior silica layers from the interior Fe-rich layer.

In the case of the model membranes, detailed observation of the FIB sections showed that the membrane wall is composed of two different layers separated by a sharp boundary (Fig. 6A-C).

Elemental mapping of Si, O, Fe, Cl and Na revealed that the external layer of the membrane is composed of silicon dioxide and the internal one of iron-(oxy)hydroxides/-oxides. A few sodium chloride crystals precipitated on the membrane (Fig. 7A-C). Furthermore, both elemental maps, and line sections, crossing both layers, demonstrate that there is no transition zone between the two layers. Hence, no Fe-silicates are formed in the walls of the membranes as has been previously reported (Cartwright et al., 2002; Glaab et al., 2012).

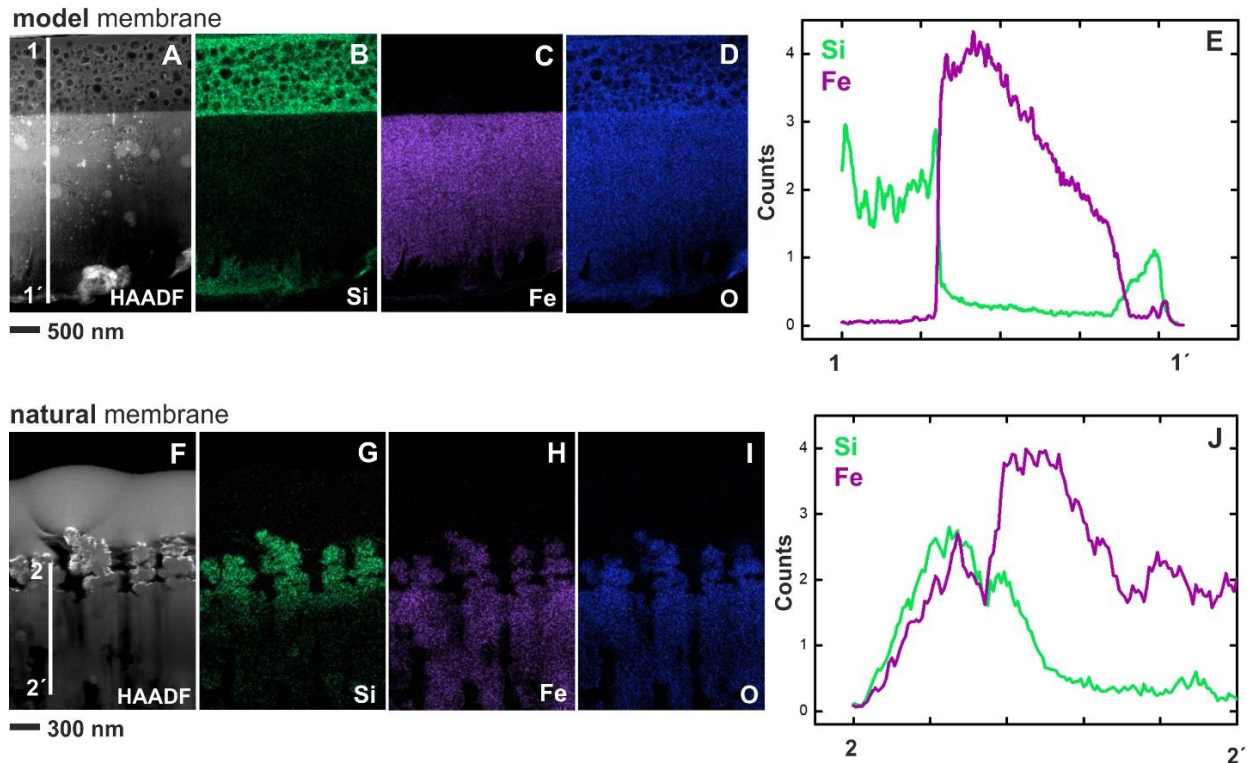


Figure 7. Si, Fe and O elemental maps and lines on the FIB sections of the model and natural membranes where the outer and inner parts are shown. A-D. As seen from the HAADF image and elemental maps the outer part of the membrane is made of SiO_2 and the inner of Fe-oxides/hydroxides. **E.** Si and Fe elemental lines showing the sharp boundary separating the two sides. **F-I.** In the case of the natural membrane there is a HAADF image and elemental maps the outer part of the membrane is made of SiO_2 and the inner of Fe-oxides/hydroxides Si and Fe elemental lines showing the diffusion zone of the membrane.

Si $L_{2,3}$ -edge ELNES characterization (in the energy-loss region 90-200 eV) of the outer layer of the membrane confirmed that the external side is composed of amorphous silica. As indicated in Fig. 8, the spectra show the typical L -edges of silica at 106 eV, 113.5 eV and at 130 eV with respect to the reference sample (Batson, 1991; Neaton et al., 2000). The inner layer of the membrane wall, in close contact with the outer layer is composed of compactly arranged 5-10 nm sized Fe-

(oxy)hydroxide particles. HR-HAADF revealed that these particles correspond to akaganeite (β -FeOOH), containing up to 2% of Cl (Fig. 9A-B). Experimental and simulation data show very high correlation and allow identification of different planes of the akaganeite crystals. Fig. 9B shows the (001) plane of the akaganeite where two series of nanochannels can be identified, having a diameter of 7.5 Å and 3.5 Å, respectively. Moving inwards from the outer wall to the internal part there is a transition to larger crystals that form platelets of 50-150 nm size (Fig. 9A,C), made of rhombohedral goethite (α -FeOOH) and rhombohedral magnetite (Fe_3O_4) (Fig. 9D).

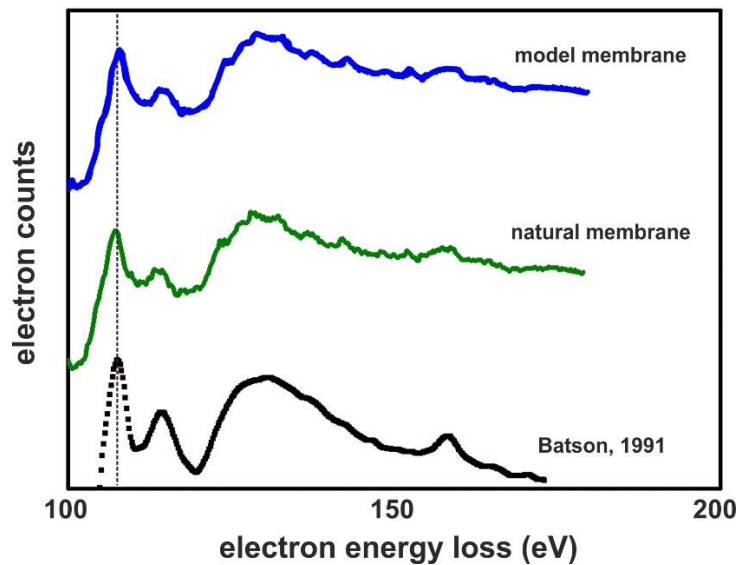


Figure 8. Si $L_{2,3}$ -edge ELNES of the external side of the model and natural membranes matching the α - SiO_2 reference sample (reference after Batson, 1991 EELS Database).

The natural membranes are less rigid and exhibit higher porosity compared to the model membranes. Likewise, the external silica part, i.e. the outer tube wall, is amorphous as confirmed by $L_{2,3}$ -edge ELNES (Fig. 8, 10, but, is thinner than the model membrane ($<1 \mu\text{m}$). EDS mapping indicated a correlation between Si, O and Fe (Fig. 10). However, this spatial correlation does not correspond to a Fe-silicate zone, but, rather to Fe nanoparticles coating the amorphous silica. The internal tube wall is composed of goethite and magnetite platelets with a thickness of ~ 5 - 10 nm and an average length of of ~ 100 - 200 nm (Fig.6 D-F, Fig. 7 F-J, Fig. 10).

Following the tubular membrane growth and allowing the system to reach equilibrium ($\sim 70 \text{ h}$)(Glaab et al., 2016), CO_2 atm diffusion in the sol, lowers the pH of the initially alkaline solution, inducing silica supersaturation and re-precipitation. Consequently, since the tubular membranes are hollow, a thin layer of silica ($<300 \text{ nm}$) re-appears after the iron-rich layer (Fig. 1A-B, E). This

feature, previously overlooked owing to tubes extraction soon after their formation, gives rise to a bilayer membrane where the external silica layers enclose the Fe nanoparticles (Fig. 12)

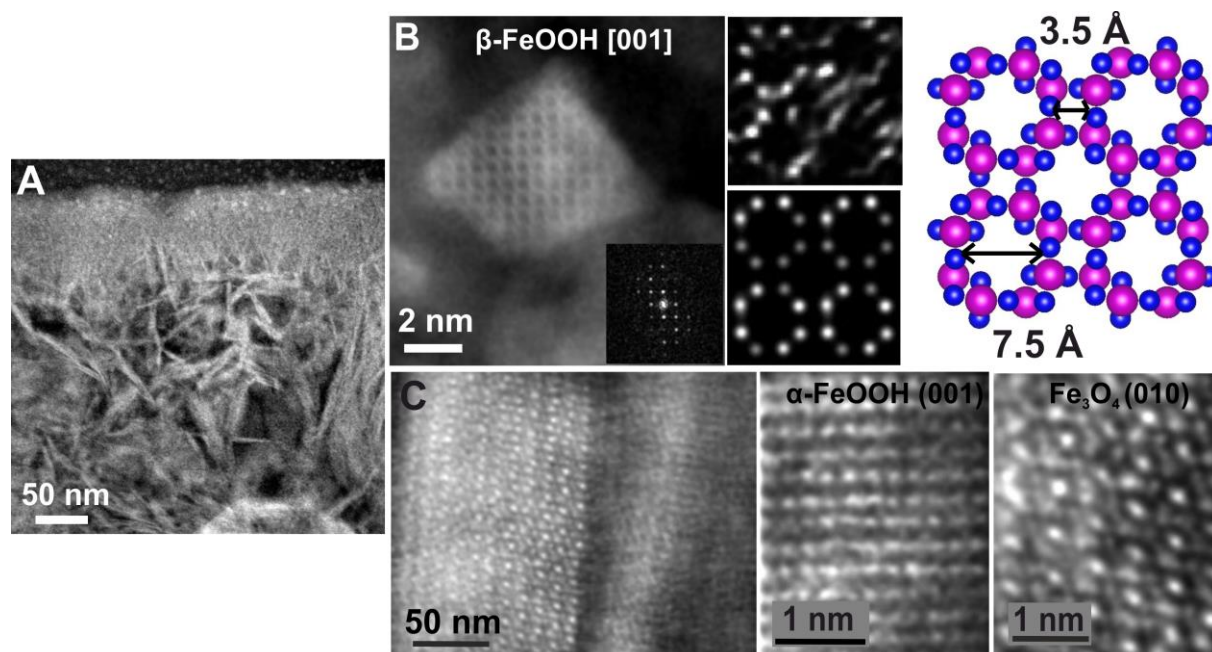


Figure 9. HR-HAADF study and atomic simulations of the internal Fe-rich part of the model membrane. **A.** Medium magnification HAADF image of the Fe-rich layer of the model membrane, where compact size crystals develop to elongated larger crystals forming platelets. **B.** HR-HAADF image of the compact zone and simulation data showing the akaganeite phase, viewed from the [001] direction. Note the size of the nanochannels in the akaganeite structure **C.** HR-HAADF images of the platelets composed of magnetite and goethite.

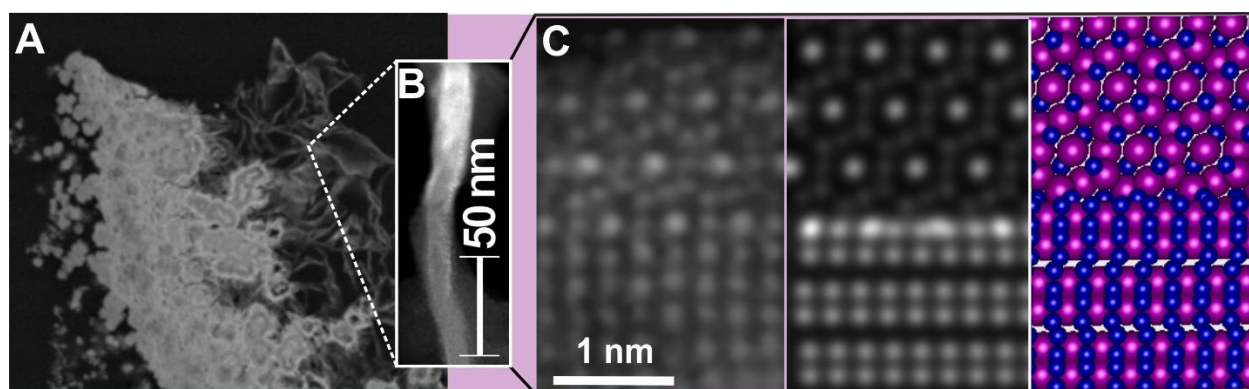


Figure 10. HR-HAADF study and atomic simulations of the internal Fe-rich part of the natural membrane. **A.** Medium magnification STEM image of the horizontal section of the Fe-Ney tubular membrane showing the membrane layers. **B.** Close up of the internal layer of the Fe-platelets. **C.** HR-HAADF image, simulation and structural model of (B) depicting the topotactic transformation of rhombohedral magnetite to rhombohedral goethite.

Specific surface area of model and natural membranes

To estimate the specific surface area (SSA) of the model and natural membranes that is directly related to their catalytic performance Brunauer– Emmet–Teller (BET) (N_2) method was used (Clausen and Fabricius, 2000). Both membranes exhibit high active surface area. As anticipated from the results of the STEM study, the natural membrane has higher SSA, $140 \text{ m}^2/\text{g}$, than the model, $113 \text{ m}^2/\text{g}$ (Fig.11). This can be attributed to the higher intra-particulate porosity of the natural membrane with respect to the model that exhibited a more compact structure. However, it should be mentioned that BET analysis tends to underestimate the SSA in case of particle aggregation, such as in the case of the iron rosettes formed in both membranes, due to certain inaccessibility of non-polar gases (e.g., N_2) to particle boundaries within aggregates (Jeong et al., 2008).

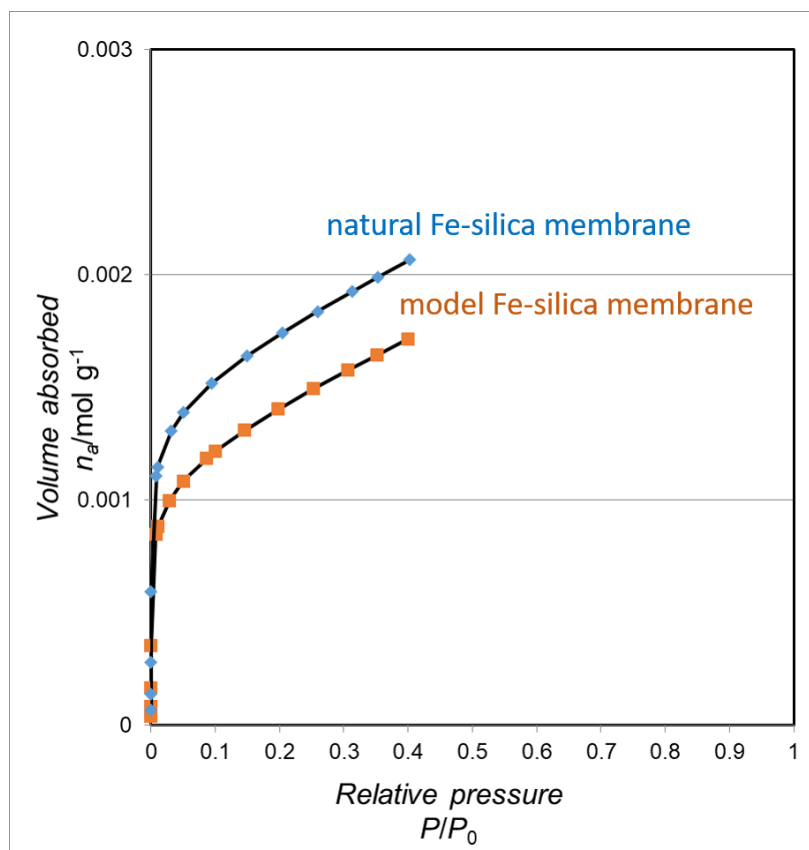


Figure 11. N_2 absorption isotherms of model and natural Fe-silica membranes.

2.3.3. Catalytic potential of the self-organized Fe-silica membranes

The nanoscale study of the FIB-milled sections of both model and natural membranes demonstrated that the composition of the membrane is similar to that of a heterogeneous catalyst; that is iron-

(oxy)-hydroxides dispersed onto a silica amorphous support. In fact, silica is considered an ideal substrate for nanoparticle dispersion in heterogeneous catalysis as it hinders nanoparticle aggregation while increasing the active surface area of the particles (Kensuke et al., 1996; Zhang and Amiridis, 1998; Li et al., 2010 ; Makki and Steinbock, 2012; Suo et al., 2012 ; Králík et al., 2016). Moreover, it has been demonstrated that at alkaline pH the surface charge density of silica is negative and the dissociation of the terminal silanol groups provides an interface where thin films of organics or metals can be adsorbed and concentrated, thus, enhancing condensation reactions (Kensuke et al., 1996; Wang and Caruso, 2004).

At the same time, the iron nanoparticles that constitute the internal wall of the membrane have received great attention for their catalytic and magnetic performance in a range of applications. Particularly, akaganeite, magnetite and goethite can be used in phenol hydroxylation, the Fenton reaction, Michael additions and isomerization, in the manufacturing of electric and magnetic materials, water treatment, labeling and magnetic separation of biological materials, directed drug delivery and more (Huber, 2005; Lefevre et al., 2009; Rusevova et al., 2012). Our study showed that the iron particles of the model and natural Fe-silica membranes exhibit very small particle size (<10 nm), large surface areas, high pore volumes and both micro-interparticle and nano-intraparticle porosity; hence exhibiting high catalytic potential. The natural membranes show higher, interparticle porosity and higher specific surface area as seen from the BET results.

Particularly interesting for the role of the iron-silica membranes in prebiotic chemistry is the fact that iron nanoparticles catalyze the Fischer–Tropsch (FT) synthesis of abiotic organic molecules, which has been shown to take place in submarine hydrothermal vents (McCollom and Seewald, 2007; Foustoukos and Seyfried, 2004; Proskurowski et al., 2008). Adding to this, a recent study demonstrated that during FT-synthesis iron nanoparticles synthesized on a mesoporous silica support -similar to the Fe-silica membranes- exhibit a strong selectivity for the production of CH₄ in presence of H₂ (Jothimurugesan et al., 1998; Zhang et al., 2006; Suo et al., 2012).

Overall, the self-organized Fe-silica bilayer membranes bring together two layers with different physicochemical, mechanical and structural properties. The chemical and mineralogical compartmentalization of the Fe-silica membranes make each layer contribute in a different way in the overall catalytic performance of the membrane. With respect to the yielding of amino acids, carboxylic acids and nucleobases molecules by formamide(CH₃NO) or pyruvate (CH₃COCO₂⁻) condensation onto the membranes (see Introduction), our results support the hypothesis that the

outer silica layer assists the organics adsorption and condensation, while simultaneous precipitation of at least two different iron-oxyhydroxides in the internal wall of the membrane may be responsible for the variety of the organic molecules generated in the internal environment (Saladino et al., 2016; Bizzari et al., 2018, Barge et al., 2019).

Following the membrane growth, equilibration of the outer silica sol with the $\text{CO}_{2\text{atm}}$ and/or evaporation of the alkaline solution, and/or temperature increase will lower the pH of the initially alkaline silicate solution, inducing silica supersaturation and re-precipitation. Therefore, as shown from the study of FIB-milled sections, silica reappears after the iron-oxyhydroxide layer, giving rise to a bilayer membrane, where the external silica hydrophilic layers encapsulate the hydrophobic iron-oxyhydroxides (Fig. 12). This property is particularly interesting considering that amphiphilic molecules, that could be products of FT reactions in hydrothermal systems (McCollom et al., 1999, Rushdi and Simoneit, 2001; Ménez et al., 2018), show high affinity for both silica and iron-oxyhydroxides (Kensuke et al., 1996; Králík et al., 2016).

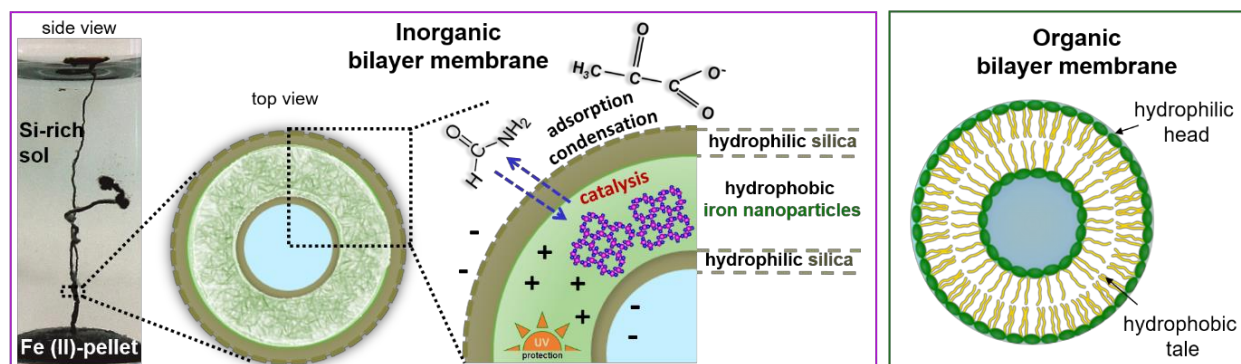


Figure 12. Inorganic Fe-silica bilayer membrane capable of adsorbing and condensing organic molecules and catalyzing the formation of amino acids, nucleobases and carboxylic acids while providing UV radiation shielding. These membranes, that would have precipitated in the early hydrothermal environments, may have provided a template for the concentration and organization of the first organic molecules in a bilayer membrane.

2.3.4. Fe-silica membranes formation and nanoscale characterization in anoxic conditions

Owing to their plausible formation on early Earth environments and their possible key role in catalyzing prebiotic chemical reactions, I investigated Fe(II)-silica membrane precipitation in oxygen-free conditions by growing them inside a N_2 glovebox chamber at ambient temperature, at 60 °C and at 80 °C (see details in the experimental part). Following their formation inside the glovebox chamber the membranes were rinsed with Ar-purged Milli-Q water, were allowed to dry and were placed in an anaerobic TEM cell for the nanoscale study of the specimen in oxygen-free

conditions. The aim of this experiment was to investigate which mineral phases could have been present in membranes forming in the predominantly anoxic environments of the early Earth and, consequently, how this may have affected their catalytic performance.

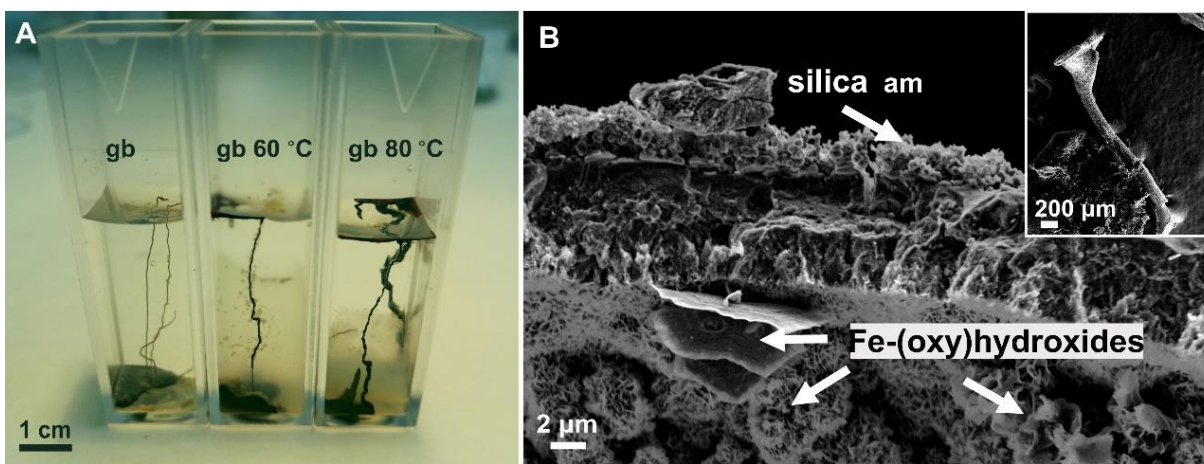


Figure 13. Tubular Fe(II)-silica membranes grown in oxygen-free conditions (N₂ atm. glovebox) and at 60 °C and 80 °C temperature. A. Increasing the temperature induces silica precipitation due to evaporation of the silica sol and produces thicker Fe(II)-silica tubes. **B.** FESEM image of the Fe(II) tubules composed of an outer silica(te) amorphous layer and an inner made of Fe(oxy)hydroxides forming rosettes.

As shown in Fig. 13 typical forms of twisted, hollow tubes were obtained for all temperature steps, composed of an external silica layer and in internal one made of Fe-oxyhydroxides. But, it was observed that with increasing temperature, the tubes became thicker and silica gel precipitated as a result of the slight evaporation and concentration of the silicate solution (due to the temperature increase). This shows that when Fe-silica membranes grow from higher temperature solutions (< 60 °C) they can be quickly embedded in silica gel, thus, exhibiting higher possibilities of preservation.

Due to reported sensitivity of iron-(oxyhydroxides) to the electron beam during the STEM investigation (Pan et al., 2006; Jiang et al., 2015), iron EELS evolution of the samples was tested under the electron beam in a range of 300-80 kV and final working conditions were 80 kV accelerating voltage. Fast EDS mapping allowed identification of areas of interest, i.e. those areas rich in silica, oxygen and iron (Fig. 14 A-D). In those locations dual-ELNES spectra were collected for both iron (*L*_{2,3}-edges) and oxygen (*K*-edges) and MLLS mapping of the iron's oxidation state was performed. MLLS mapping showed that both reduced and oxidized phases are present in the samples (Fig. 13A-D). Fe *L*_{2,3}-edges ELNES spectrum of the reduced area shows a chemical shift towards lower energy, as expected for a divalent material with respect to the trivalent, and the *L*₃

line shows a more complex splitting than that for the trivalent one (Fig.14E). Similar fine structures have been reported for other ferrous minerals, such as, wustite (FeO) and fayalite (Fe₂SiO₄), and the main features of our spectrum match that of the mineral greenalite (Fe₂Fe₃SiO₄) (Garvie and Buseck, 1998; Guggenheim and Eggleton, 1998; Evans et al., 2017).

Dual iron *L*_{2,3}-edges ELNES and oxygen K-edge ELNES spectra of the oxidized area are characteristic of ferric oxyhydroxides and match best with the akaganeite (β-FeOOH) (Chen et al., 2009). The splitting in the pre-peak of this phase (530 eV) indicates a weaker field around the Fe atoms, indicative of a low crystallinity phase, while the weak pre-peak intensity and the shoulder at 532.5 eV may come from the OH⁻ bonding, as suggested by Stichauer, et al., (2001)(Chen et al., 2009).

To sum up, the Fe-silica membranes are composed of amorphous silica and iron oxyhydroxide nanoparticles when precipitation occurs in the presence of oxygen whereas in anoxic conditions Fe(II,III)-silicates, such as, greenalites along with amorphous silica and Fe(II, III)-oxyhydroxides are forming. As shown recently by Barge et al., (2019) pyruvate (CH₃COCO₂⁻), a simple organic molecule of particular relevance for the emergence of metabolism that forms in hydrothermal systems, can undergo reductive amination in the presence of mixed-valence iron-(oxy)hydroxides to form the amino acid alanine, as well as the reduced product lactate. In fact, the maximum yield of alanine was observed when the iron oxyhydroxide mineral contained 1:1 Fe(II):Fe(III), under alkaline conditions. These results demonstrate that Fe-silica membranes may have played a critical role in prebiotic chemical reactions either in the presence of formamide or pyruvate, two organic constituents known to develop complex reaction pathways for the yielding of life relevant organics (Saladino et al., 2012; Novikov and Copley 2013; Muchowska et al., 2019).

Also it's worth noting that greenalites, a group of Al-free, Fe-serpentine are hypothesized to be the main precipitates of the Archean, ferrous- and silica-rich, oceans and they have been identified in many Proterozoic iron formations (Klein, 2005; Beukes and Klein, 1990; Simonson, 2003; Rasmussen et al., 2015; Pufahl et al., 2014; Tosca et al., 2016). Therefore, understanding the interactions between ferrous iron and silica and in this context Fe-silica precipitation, may additionally offer key insight into the redox chemistry of the Precambrian seawater (Siever et al., 1992; Grenne and Slack, 2003; Konhauser et al., 2007; Fischer and Knoll, 2009; Bekker et al., 2014; Rasmussen et al., 2015).

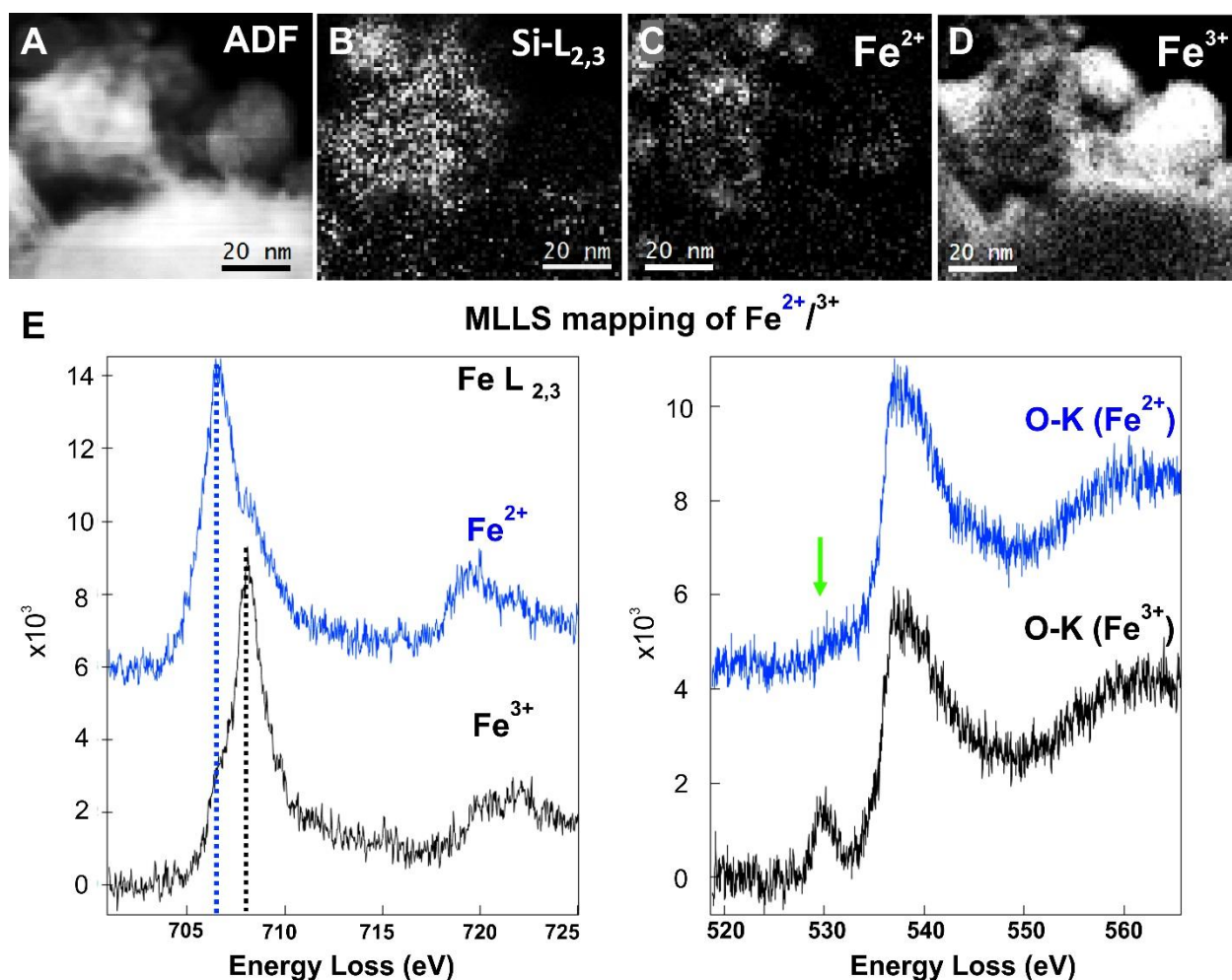


Figure 14. Iron, silicon and oxygen EELS/MLLS mapping of the Fe(II)-silica membrane, prepared and analyzed in anaerobic conditions. A-D. ADF image of an Fe(II)-silica membrane where the Si *K*-edge ELNES mapping and Fe(II)/Fe(III) MLLS mapping are shown. **E.** Iron *L*_{2,3}-edge ELNES of the Fe(II) area (blue line) and Fe(III) area (black line) **F.** Oxygen *K*-edge ELNES spectra of the Fe(II) area (blue line) and Fe(III) area (black line). Note the pre-edge shoulder in the spectrum of the Fe(III) area.

2.3.5. Inorganic Fe-silica membranes and their biologic counterparts: a life detection issue

Although there are several synthetic routes that yield biologically relevant organic compounds such as ribonucleic acids and amino acids, their chemistry is entirely irrelevant in the geological context of early Earth. As discussed previously, Fe-silica membrane formation could have occurred in the geochemical settings of early Earth and these self-organized structures may have played a key role in the catalysis of prebiotic chemical reactions. However, the precipitation of these inorganic membranes can also have important implications for life detection in the rock record of this, and other, planets (McMahon et al., 2019; Johannessen et al., 2020).

A series of tubular structures and filaments, composed of Fe-(oxy)hydroxides such as hematite, ferrihydrite, goethite and magnetite, have been found in cherts and jaspers and were interpreted as microfossils, or remnants of biologic activity (see Little et al., 2004 and references therein;), including those considered to be the earliest forms of life (Dodd et al., 2017). In the absence of silica-forming organisms (e.g. diatoms), these cherts would have formed inorganically, by a silica gel precursor, or, would have been silicified by silicate-rich fluids. Reaction/mixing with Fe-rich salts/-fluids would result in the precipitation of inorganic Fe-silica membranes. As shown here, these inorganic membranes would have been composed by iron-(oxy)hydroxides and silica. In fact, they could have been easily embedded in silica gel, the precipitation of which would be provoked by either a slight acidification or a change in temperature (see Fig. 15 A-B, G). Following diagenesis and or/metamorphic processes, these would not only produce morphologically but also mineralogically indistinguishable inorganic features to the putative biologic ones (Fig, 15).

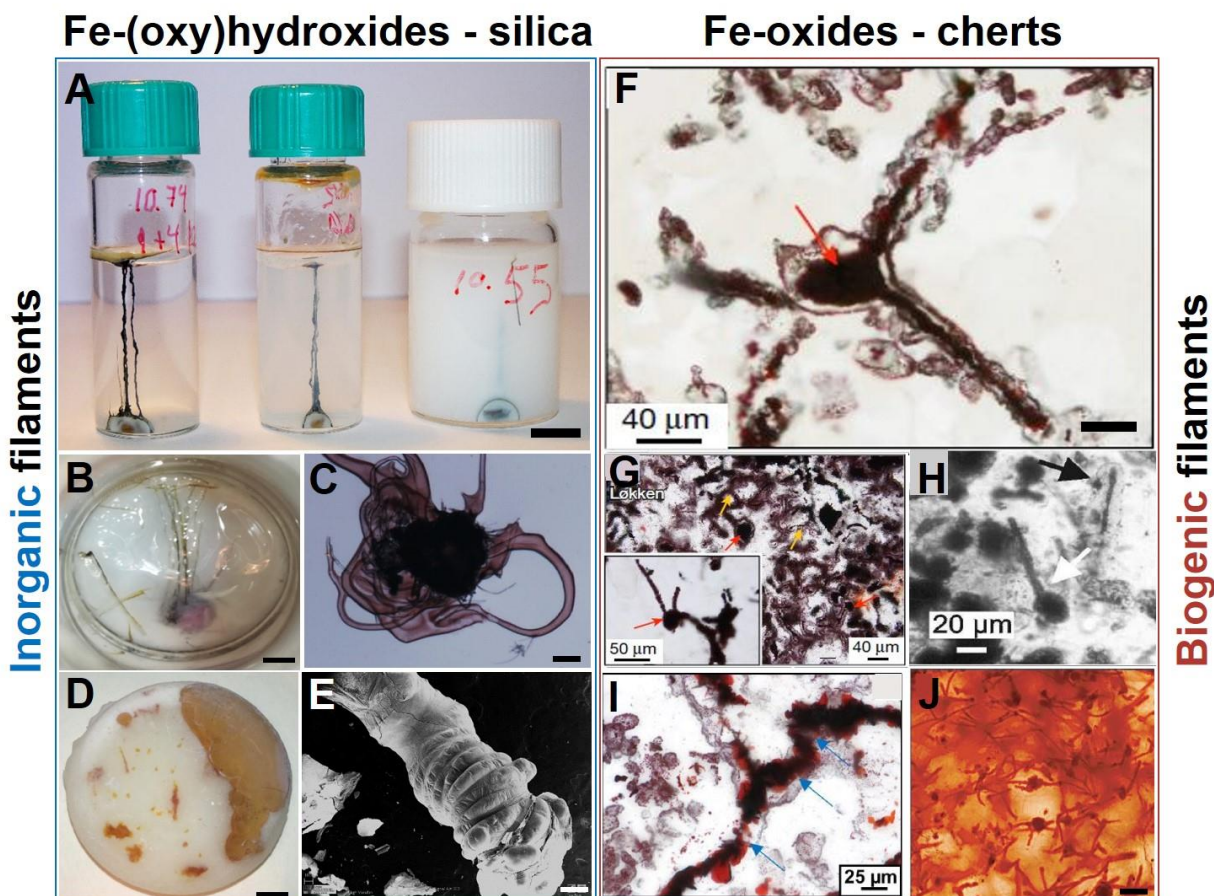


Figure 15. Inorganic tubular iron-silica membranes vs. putative biologic iron filamentous structures in cherts. A-B, D. Fe(III)-silica tubular membranes embedded in silica gel. **C.** Tubular inorganic membranes grown from a single micro-drop of a Me-salt solution The tubes form a complex network of varying angles. **E.** SEM image of an Fe(II)-silica tubular membrane. **F, I.** Transmitted light image of iron-oxide filaments from the Nuvvuagittuq supracrustal belt (NSB)

jasper in Canada (after Dodd et al., 2017). **G.** Photomicrographs taken in plane-polarized light with reflected light of haematite tubes and filaments from the Løkken jasper in Norway (after Dodd et al., 2017). **H.** Transmitted light photomicrographs of small jasper filaments in Figueroa jasper, California (after Little et al., 2004). **J.** Thin-sectioned light micrographs showing porous Si-rich/Fe-poor bands often sparsely colonized by potential appendaged Fe bacteria (after Chi Fru et al., 2015).

As a result, this may lead to misinterpretation of the origin of these filamentous microstructures (McMahon et al., 2019; Johhanessen et al., 2020), taking into account that complimentary isotopic studies to distinguish between inorganic and biological signals are not always clear; isotopic signatures of carbon compounds formed by mineral reactions, such as, Fischer–Tropsch (FT) cycles and siderite decomposition are very similar to those appearing in biological reactions and it is not uncommon for inorganic reactions to overprint the biologic ones (van Zuilen et al., 2002, 2003; McCollom and Seewald, 2006; van Zuilen et al., 2007).

Therefore, it is argued that the Fe-silica membranes that form from a simple chemical cocktail that is not only geochemically plausible, but also, extremely relevant to the aqueous environments of the Hadean-early Archean (see paragraph 4.1.1), could provide an alternative, inorganic, explanation for the occurrence of some of the microstructures considered to be traces of the oldest forms of life on the planet. This issue calls for a detailed geochemical and isotopic characterization of both inorganic and biologic membranes, with respect to their preservation during deformation, diagenetic and metamorphic events.

2.4. Findings and concluding remarks

- Iron-silica membranes, also known as Fe-silica gardens, are inorganic, nanocomposite, filamentous structures arising by mixing a silicate solution with an iron-salt particle/solution due reaction-diffusion controlled precipitation process.
- Owing to the ion and pH gradients generated during membrane growth and compartmentalization, an electrochemical potential is produced across the membrane walls, of the order of 500 mV. Thus, Fe-silica membranes behave as fuel cells and show battery-like properties.
- In addition, they can catalyze the production of amino acids, carboxylic acids and nucleobases by condensating simple organic molecules, such as, formamide and pyruvate that were present in early Earth.
- Despite these intriguing properties, little is known about the structure and organization of the Fe-silica self-organized membranes at the nanoscale. This information will provide insight on their catalytic behavior and potential uses as advanced materials.
- To investigate the geochemical plausibility of the precipitation of these membranes, they were grown for the first time by using natural highly alkaline and silica-rich water from the Ney spring in California; a spring of unique character related to serpentinization and slab subduction processes.
- The formation of the membranes with the Ney water is relatively slow (hours) compared to the model experiments (within seconds to minutes), due to the high ionic strength of the Ney solution, which reduces the strength of the osmotically driven force during the membrane growth.
- Macroscopic, microscopic and spectroscopic comparison of natural Fe(II)-silica membranes to synthetic, showed that they share the typical tubular morphologies of hollow, branching tubes. Moreover, they show the same chemical and mineral distinction between the outer and inner walls; an outer silica-rich wall and an internal Fe-rich wall.

- Fe(III)-silica membranes grown from the Ney water did not form tubules; instead a Fe(III)-silicate film was formed that breached soon after its formation, releasing CO_{2gas} and producing a convection cell that remain active for 1-2 min.
- The nanoscale study of FIB-milled sections of model Fe(II)-silica membranes demonstrated that the composition of the membrane is similar to that of a heterogeneous catalyst; iron-(oxy)-hydroxide nanoparticles dispersed onto a silica amorphous support. In contrast to previous studies our results show that no Fe-silicates are formed in the walls of the membranes that are separated by a sharp boundary.
- The STEM study showed that the iron nanoparticles that constitute the internal wall of the membranes are akaganeite (β -FeOOH), goethite (α -FeOOH) and magnetite (Fe₃O₄) nanosized (5-10 nm) particles that fold into rosettes of 50-150 nm creating intra-particle porosity. Furthermore, they show inter-particle porosity due to their channel-type structure.
- The natural membranes show higher intra-particulate porosity and have higher specific surface area, 140 m²/g, than the model membrane, 113 m²/g, that exhibited a more compact structure, as shown from both the BET analysis and the TEM investigation. Thus the natural membranes are potentially better catalysts than the model ones.
- In addition, nanoscale study of FIB-milled sections of both model and natural membranes revealed their bilayer structure composed of silica layers encapsulating the iron-oxyhydroxides.
- Moreover, Fe(II)-silica membranes were grown inside a glovebox chamber by using Ar-purged solutions and remained in oxygen-free conditions during the TEM-EELS study by placing them inside an anaerobic cell.
- In the case of the anoxic experiment, iron, silicon and oxygen EELS/MLLS mapping of the Fe(II)-silica membrane showed that it is composed of amorphous silica, Fe(II, III)-

oxyhydroxides and Fe(II,III)-silicates, such as, greenalite-group minerals. This results are in accordance with the geochemical modeling of this reaction performed by PHREEQC.

- Considering that similar ferrous iron-silica precipitation reactions were taking place in the ferruginous and silica saturated Precambrian oceans, the nanoscale study of the ferrous iron-silica precipitates in anoxic conditions may additionally provide insight on the formation of the Precambrian iron formations.
- The majority of the putative biogenic iron filaments and microfossils, including those considered as the earliest forms of life on Earth, are found in cherts and jaspers. Apart from showing great morphological resemblance to the inorganic Fe-silica membranes our results show that in addition they share the same structure and mineralogy.
- Fe-silica membranes growth from 60-80 °C temperature solutions accelerated silica gel precipitation and following tube embedment in the silica gel. This implies that Fe-silica membranes possibly forming in low-temperature hydrothermal environments (~80 °C) exhibit higher possibilities of preservation in the sediment record.

References

- Balköse, D., Özkan, F., Köktürk, U., Ulutan, S., Ülkü, S., Nişli, G., 2002. Characterization of Hollow Chemical Garden Fibers from Metal Salts and Water Glass. *Journal of Sol-Gel Science and Technology* 23, 253-263.
- Barnes, I., O'Neil, J.R., 1969. The relationship between fluids in some fresh alpine-type ultramafics and possible modern serpentinization, Western United States. *Geol. Soc. Am. Bull.* 80, 1947–1960.
- Barnes, I., Rapp, J.B., O'Neil, J.R., Sheppard, R.A., Gude III, A.J., 1972. Metamorphic assemblages and the direction of flow of metamorphic fluids in four instances of serpentinization. *Contrib. Mineral. Petrol.* 35, 263-276.
- Barge, L.M., Doloboff, I.J., White, L.M., Stucky, G.D., Russell, M.J., Kanik, I., 2012. Characterization of iron-phosphate-silicate chemical garden structures. *Langmuir : the ACS journal of surfaces and colloids* 28, 3714-3721.
- Barge, L.M., Cardoso, S.S., Cartwright, J.H., Cooper, G.J., Cronin, L., De Wit, A., Doloboff, I.J., Escribano, B., Goldstein, R.E., Haudin, F., Jones, D.E., Mackay, A.L., Maselko, J., Pagano, J.J., Pantaleone, J., Russell, M.J., Sainz-Diaz, C.I., Steinbock, O., Stone, D.A., Tanimoto, Y., Thomas, N.L., 2015b. From Chemical Gardens to Chemobrionics. *Chemical reviews* 115, 8652-8703.
- Barge, L.M., Cardoso, S.S., Cartwright, J.H., Doloboff, I.J., Flores, E., Macias-Sanchez, E., Sainz-Diaz, C.I., Sobron, P., 2016. Self-assembling iron oxyhydroxide/oxide tubular structures: laboratory-grown and field examples from Rio Tinto. *Proceedings. Mathematical, physical, and engineering sciences* 472, 20160466.
- Barge, L.M., Flores, E., Baum, M.M., VanderVelde, D.G., Russell, M.J., 2019. Redox and pH gradients drive amino acid synthesis in iron oxyhydroxide mineral systems, *Proc Natl Acad Sci USA*, 116, 4828-4833; DOI: 10.1073/pnas.1812098116.
- Batson, P.E., 1991. Silicon L_{2,3} core absorption obtained at the buried Al/Si(111) interface. *Physical Review B* 44, 5556-5561.
- Bekker, A., Holland, H.D., Wang, P.L., Rumble III, D., Stein, H.J., Hannah, J.L., Coetzee, L.L., Beukes, N.J., 2004. Dating the rise of atmospheric oxygen. *Nature* 427, 117.
- Bernal, S.; Botana, F. J.; Calvino, J. J.; Lopez-Cartes, C.; Perez-Omil, J. A.; Rodríguez-Izquierdo, J. M., 1998. The interpretation of HREM images of supported metal catalysts using image simulation: Profile view images. *Ultramicroscopy*, 72, 135–164.
- Beukes, N.J., Klein, C., 1990. Geochemistry and sedimentology of a facies transition -from microbanded to granular iron-formation - in the early Proterozoic Transvaal Supergroup, South Africa, *Precambrian Research*, 47, 99-139.
- Bizzarri, B.M., Botta, L., Perez-Valverde, M.I., Saladino, R., Di Mauro, E., Garcia Ruiz, J.M., 2018. Silica metal-oxide vesicles catalyze comprehensive prebiotic chemistry. *Chem. Eur. J.* 2018, 24, 8126.
- Blank, J.G., Stamenković, G.E., Rowe, A.R., Kohl, I., Li, S and Young, E.D., 2017. Methane at the Aqua de Ney hyperalkaline spring (N California, USA): a site of active serpentinization, *Astrobiology Science Conference 2017*, p. 3608.

Boschetti, T., Toscani, L., 2008. Springs and streams of the Taro-Ceno Valleys (Northern Apennine, Italy): reaction path modeling of waters interacting with serpentinized ultramafic rocks. *Chem Geol* 257, 76–91. doi:10.1016/j.chemgeo.2008.08.017.

Boschetti T, Etiope G, Pennisi M, Romain M, Toscani L (2013a) Boron, lithium and methane isotope composition of hyperalkaline waters (Northern Apennines, Italy): terrestrial serpentinization or mixing with brine? *Appl Geochem* 32:17–25. doi:10.1016/j.apgeochem.2012.08.018.

Boschetti T, Etiope G, Toscani L (2013b) Abiotic methane in the hyperalkaline springs of Genova, Italy. *Earth Planet Sci* 7:248–251. doi:10.1016/j.proeps.2013.02.004.

Boschetti, T., Toscani, L., Iacumin, P., Selmo, E., 2017. Oxygen, Hydrogen, Boron and Lithium Isotope Data of a Natural Spring Water with an Extreme Composition: A Fluid from the Dehydrating Slab? *Aquat Geochem*, 23, 299. <https://doi.org/10.1007/s10498-017-9323-9>.

Brouxel, M., Lapierre, H., Michard, A., Albarede, F., 1988. Geochemical study of an early Paleozoic island-arc- back-arc basin system. *Geol Soc Am Bull* 100, 1111-1119.

Cartwright, J.H.E., Garia-Ruiz, J.M., Novella, M.L., Otálora, F., 2002. Formation of Chemical Gardens. *J. Colloid Interface Sci.* 256, 351-359.

Chavagnac, V., Ceuleneer, G., Monnin, C., Lansac, B., Hoareau, G., and Boulart, C., 2013. Mineralogical assemblages forming at hyperalkaline warm springs hosted on ultramafic rocks: A case study of Oman and Ligurian ophiolites, *Geochem. Geophys. Geosyst.*, 14, 2474– 2495, doi:10.1002/ggge.20146.

Chen, S.-Y., Gloter, A., Zobelli, A., Wang, L., Chen, C.-H., Colliex, C., 2009. Electron energy loss spectroscopy and ab initio investigation of iron oxide nanomaterials grown by a hydrothermal process. *Physical Review B*, 79.

Chi Fru, E., Ivarsson, M., Kiliyas, S.P., Frings, P.J., Hemmingsson, C., Broman, C., Bengtson, S., Chatzitheodoridis, E., 2015. Biogenicity of an Early Quaternary iron formation, Milos Island, Greece. *Geobiology*, 13, 225-244.

Clausen, L., Fabricius, I., 2000. BET Measurements: Outgassing of Minerals. *Journal of Colloid and Interface Science* 227, 7-15.

Dodd, M.S., Papineau, D., Grenne, T., Slack, J.F., Rittner, M., Pirajno, F., O'Neil, J., Little, C.T., 2017. Evidence for early life in Earth's oldest hydrothermal vent precipitates. *Nature* 543, 60-64.

Evans, B.W., Kuehner, S.M., Joswiak, D.J., Cressey, G., 2017. Serpentine, Iron-rich Phyllosilicates and Fayalite Produced by Hydration and Mg Depletion of Peridotite, Duluth Complex, Minnesota, USA. *Journal of Petrology* 58, 495-512.

Feth, J.H., Roogers, M., Roberson, C.E., 1961. Aqua de Ney, California, a spring of unique chemical character. *Geochim. Cosmochim. Acta* 22, 75-86.

Fischer, W.W., Knoll, A.H., 2009. An iron shuttle for deepwater silica in Late Archean and early Paleoproterozoic iron formation. *GSA Bulletin* 121, 222-235.

Foustoukos, D.I., Seyfried, W.E., 2004. Hydrocarbons in Hydrothermal Vent Fluids: The Role of Chromium-Bearing Catalysts. *Science* 304, 1002.

- Frost, B.R., Beard, J.S., 2007. On silica activity and serpentinization. *J Petrol* 48, 1351–1368. doi:10.1093/ petrology/egm021.
- Garvie, L.A.J., and Buseck, P.R., 1998. Ratios of ferrous to ferric iron from nanometer-sized areas in minerals, *Nature* 396, 667-670.
- Glaab, F., Kellermeier, M., Kunz, W., Morallon, E., Garcia-Ruiz, J.M., 2012. Formation and evolution of chemical gradients and potential differences across self-assembling inorganic membranes. *Angewandte Chemie* 51, 4317-4321.
- Glaab, F., Rieder, J., Garcia-Ruiz, J.M., Kunz, W., Kellermeier, M., 2016. Diffusion and precipitation processes in iron-based silica gardens. *Physical chemistry chemical physics : PCCP* 18, 24850-24858.
- Glaab, F., Rieder, J., Klein, R., Choquesillo-Lazarte, D., Melero-Garcia, E., Garcia-Ruiz, J.M., Kunz, W., Kellermeier, M., 2017. Precipitation and Crystallization Kinetics in Silica Gardens. *Chemphyschem : a European journal of chemical physics and physical chemistry* 18, 338-345.
- Grenne, T., Slack, J. F., 2003. Paleozoic and Mesozoic silica-rich seawater: Evidence from hematitic chert (jasper) deposits, *Geology* 31, 319–322.
- Guggenheim, S., Eggleton, R.A., 1998. Modulated crystal structures of greenalite and caryopilite; a system with long-range, in-plane structural disorder in the tetrahedra sheet. *The Canadian Mineralogist* ; 36, 163–179. doi: <https://doi.org/>.
- Haiyun Suo, S.W., Chenghua Zhang, Jian Xu, Baoshan Wu, Yong Yang, Hongwei Xiang, Yong-Wang Li, 2012. Chemical and structural effects of silica in iron-based Fischer–Tropsch synthesis catalysts. *Journal of Catalysis* 286, 111-123.
- Hou, W., Wu, B., Yang, Y., Hao, Q., Tian, L., Xiang, H., Li, Y., 2008. Effect of SiO₂ content on iron-based catalysts for slurry Fischer–Tropsch synthesis. *Fuel Processing Technology* 89, 284-291.
- Huber, D.L., 2005. Synthesis, properties, and applications of iron nanoparticles. *Small* 1, 482-501.
- Irwin, W.P., 1994. *U.S. Geological Survey Miscellaneous Investigations, Series Map 1-2148*, scale 1:500,000, 2 sheets.
- Jeong, H.Y., Lee, J.H., Hayes, K.F., 2008. Characterization of synthetic nanocrystalline mackinawite: Crystal structure, particle size, and specific surface area. *Geochimica et Cosmochimica Acta* 72, 493-505.
- Jiang, N., 2016. Electron beam damage in oxides: a review, *Rep. Prog. Phys.* 79 016501
- Johannessen, K.C., McLoughlin, N., Vullum, P.E., Thorseth, I.H., 2020. On the biogenicity of Fe-oxhydroxide filaments in silicified low-temperature hydrothermal deposits: Implications for the identification of Fe-oxidizing bacteria in the rock record. *Geobiology*, 18, 31-53. DOI: 10.1111/gbi.12363.
- Kellermeier, W., Glaab, F., Melero-García, E., García-Ruiz, J.M., 2013. Experimental techniques for the growth and characterization of silica biomorphs and silica gardens in *Methods in Enzymology-Research Methods in Biomineralization Science*, J. J. De Yoreo, Ed. (Burlington: Academic Press, n. 532, 2013), pp. 225-256.

- Kensuke, N., Iwaki, K., Kitano, N., Ohki, A., Maeda, S., 1996. Absorption of enzymes at silica-gel with amphiphilic block copolymers. *Polymer Journal* 28, 911-915.
- Kirkland, E. J., 2010. *Advanced Computing in Electron Microscopy*; Springer.
- Klein, F., Bach, W., Jöns, N., McCollom, T., Moskowitz, B., Berquó, T., 2009. Iron partitioning and hydrogen generation during serpentinization of abyssal peridotites from 15°N on the Mid-Atlantic Ridge, *Geochimica et Cosmochimica Acta*, 73, 6868-6893.
- Klein, C., 2005. Some Precambrian banded iron-formations (BIFs) from around the world: Their age, geologic setting, mineralogy, metamorphism, geochemistry, and origins. *American Mineralogist* 90, 1473–1499.
- Konhäuser KO, Amskold L, Lalonde SV, Posth NR, Kappler A, Anbar A., 2007. Decoupling photochemical Fe(II) oxidation from shallow-water BIF deposition. *Earth and Planetary Science Letters* 258, 87–100.
- Králík, A., Hansen, M., König, B., 2016. Immobilisation of water-oxidising amphiphilic ruthenium complexes on unmodified silica gel. *RSC Advances* 6, 5739-5744.
- Li, Y., Wang, W.-N., Zhan, Z., Woo, M.-H., Wu, C.-Y., Biswas, P., 2010. Photocatalytic reduction of CO₂ with H₂O on mesoporous silica supported Cu/TiO₂ catalysts. *Applied Catalysis B: Environmental* 100, 386-392.
- Liakhovitch, V., Quick, J.E., Gregory, R.T., 2005. Hydrogen and oxygen isotope constraints on hydrothermal alteration of the Trinity peridotite, Klamath Mountains, California. *Int Geol Rev* 47:203–214. doi:10.2747/0020-6814.47.2.203.
- Little, C. T. S., Glynn, S. E., and Mills, R. A., 2004. Four hundred and ninety million year record of bacteriogenic iron oxide precipitation at sea-floor hydrothermal vents. *Geomicrobiology Journal*, 21, 415–429. <https://doi.org/10.1080/01490450490485845>.
- Lefevre, M., Proietti, E., Jaouen, F., Dodelet, J.P., 2009. Iron-based catalysts with improved oxygen reduction activity in polymer electrolyte fuel cells. *Science* 324, 71-74.
- Li, Y., Wang, W.-N., Zhan, Z., Woo, M.-H., Wu, C.-Y., Biswas, P., 2010. Photocatalytic reduction of CO₂ with H₂O on mesoporous silica supported Cu/TiO₂ catalysts. *Applied Catalysis B: Environmental* 100, 386-392.
- Lim, H., Lee, J., Jin, S., Kim, J., Yoon, J., Hyeon, T., 2006. Highly active heterogeneous Fenton catalyst using iron oxide nanoparticles immobilized in alumina coated mesoporous silica. *Chemical communications*, 463-465.
- Makki, R., Steinbock, O., 2012. Nonequilibrium synthesis of silica-supported magnetite tubes and mechanical control of their magnetic properties. *J. Am. Chem. Soc.* 134, 15519-15527.
- Mariner, R.H., Evans, W.C., Presser, T.S., White, L.D., 2003. Excess nitrogen in selected thermal and mineral springs of the Cascade Range in northern California, Oregon, and Washington: sedimentary or volcanic in origin? *J Volcanol Geoth Res* 121, 99–114. doi:10.1016/S0377-0273(02)00414-6.
- Maschmeyer, T., Rey, F., Sankar, G., Thomas, J.M., 1995. Heterogeneous catalysts obtained by grafting metallocene complexes onto mesoporous silica. *Nature* 378, 159-162.

- McCollom, T.M., Ritter, G., Simoneit, B.R.T., 1999. Lipid Synthesis Under Hydrothermal Conditions by Fischer-Tropsch-Type Reactions. *Origins of life and evolution of the biosphere* 29, 153-166.
- McCollom, T.M., Seewald, J.S., 2007. Abiotic Synthesis of Organic Compounds in Deep-Sea Hydrothermal Environments. *Chem. Rev.* 107, 382-401.
- McMahon, S., 2019. Earth's earliest and deepest purported fossils may be iron-mineralized chemical gardens. *Proc. R. Soc. B* 286, 20192410.
- Ménez, B., Pisapia, C., Andreani, M., Jamme, F., Vanbellingen, Q.P., Brunelle, A., Richard, L., Dumas, P., Refregiers, M., 2018. Abiotic synthesis of amino acids in the recesses of the oceanic lithosphere. *Nature* 564, 59-63
- Mottl, M.J., 2009. Highest pH? *Geochemical News* 141. <https://www.geochemsoc.org/publications/geochemicalnews/gn141oct09/highestph/>. Accessed 17 Sep 2017.
- Muchowska, K.B., Varma, S.J., Moran, J., 2019. Synthesis and breakdown of universal metabolic precursors promoted by iron. *Nature* 569, 104-107.
- Neaton, J.B., Muller, D.A., Ashcroft, N.W., 2000. Electronic Properties of the Si/SiO₂ Interface from First Principles. *Physical Review Letters* 85, 1298-1301.
- Kensuke Naka, K.I., Noriaki Kitano, Akira Ohki, Shigeru Maeda, 1996. Absorption of enzymes at silica-gel with amphiphilic block copolymers, *Polymer Journal* 28, 911-915.
- McCollom, T., Bach, W., 2009. Thermodynamic constraints on hydrogen generation during serpentinization of ultramafic rocks, *Geochimica et Cosmochimica Acta*, 73, 856-875.
- Niether, D. Afanasenkau, J. K. Dhont, S. Wiegand, Accumulation of formamide in hydrothermal pores to form prebiotic nucleobases, 2016, *Proc. Natl. Acad. Sci. USA.*, 113, 4272–4277.
- Novikov, Y., Copley S.D., 2013. Reactivity landscape of pyruvate under simulated hydrothermal vent conditions. *Proc Natl Acad Sci USA* 110, 13283–13288.
- Pagano, J.J., Thouvenel-Romans, S., Steinbock, O., 2007. Compositional analysis of copper–silica precipitation tubes. *Phys. Chem. Chem. Phys.* 9, 110-116.
- Pan, Y., Brown, A., Brydson, R., Warley, A., Lic, A., Powell, J., 2006. Electron beam damage studies of synthetic 6-line ferrihydrite and ferritin molecule cores within a human liver biopsy, *Micron*, 37, 403-411.
- Parmar, K., Pramanik, A.K., Bandyopadhyaya, N.R., Bhattacharjee, S., 2010. Synthesis and characterization of Fe(III)-silicate precipitation tubes. *Materials Research Bulletin* 45, 1283-1287.
- Pham, A.L.-T., Lee, C., Doyle, F.M., Sedlak, D.L., 2009. A Silica-Supported Iron Oxide Catalyst Capable of Activating Hydrogen Peroxide at Neutral pH Values. *Environmental Science & Technology* 43, 8930-8935.
- Polshettiwar, V., Len, C., Fihri, A., 2009. Silica-supported palladium: Sustainable catalysts for cross-coupling reactions. *Coordination Chemistry Reviews* 253, 2599-2626.

- Proskurowski, G., Lilley, M.D., Seewald, J.S., Früh-Green, G.L., Olson, E.J., Lupton, J.E., Sylva, S.P., Kelley, D.S., 2008. Abiogenic Hydrocarbon Production at Lost City Hydrothermal Field. *Science* 319, 604.
- Pufahl, P.K., Anderson, S. L., Hiatt, E.E., 2014. Dynamic sedimentation of Paleoproterozoic continental margin iron formation, Labrador Trough, Canada: Paleoenvironments and sequence stratigraphy, *Sedimentary Geology*, 309, 48-65.
- Rasmussen, B., Krapež, B., Muhling, J.R., Suvorova, A., 2015. Precipitation of iron silicate nanoparticles in early Precambrian oceans marks Earth's first iron age. *Geology* 43, 303-306.
- Rostamnia, S., Doustkhah, E., 2014. Nanoporous silica-supported organocatalyst: a heterogeneous and green hybrid catalyst for organic transformations. *RSC Adv.* 4, 28238-28248.
- Rushdi, A.I., Simoneit, B.R.T., 2001. Lipid Formation by Aqueous Fischer-Tropsch-Type Synthesis over a Temperature Range of 100 to 400 °C. *Origins of life and evolution of the biosphere* 31, 103-118.
- Rusevova, K., Kopinke, F.D., Georgi, A., 2012. Nano-sized magnetic iron oxides as catalysts for heterogeneous Fenton-like reactions-Influence of Fe(II)/Fe(III) ratio on catalytic performance. *Journal of hazardous materials* 241-242, 433-440.
- Saladino, R., Botta, G., Bizzarri, B.M., Di Mauro, E., Garcia Ruiz, J.M., 2016. A Global Scale Scenario for Prebiotic Chemistry: Silica-Based Self-Assembled Mineral Structures and Formamide. *Biochemistry* 55, 2806-2811.
- Saladino, R., Crestini, C., Pino, S., Costanzo, G., Di Mauro, E., 2012. Formamide and the origin of life. *Physics of life reviews* 9, 84-104.
- Saladino, R., Di Mauro, E., Garcia-Ruiz, J.M., 2019. A Universal Geochemical Scenario for Formamide Condensation and Prebiotic Chemistry. *Chem. Eur. J.* 25, 3181 – 3189.
- Sekine, Y., et al., 2015. High-temperature water–rock interactions and hydrothermal environments in the chondrite-like core of Enceladus. *Nat Commun* 6:8604. doi:10.1038/ncomms9604. <http://www.nature.com/articles/ncomms9604#supplementary-information>.
- Shin, S., Yoon, H., Jang, J., 2008. Polymer-encapsulated iron oxide nanoparticles as highly efficient Fenton catalysts. *Catalysis Communications* 10, 178-182.
- Siever, R., 1992. The silica cycle in the Precambrian. *Geochimica et Cosmochimica Acta* 56, 3265-3272.
- Simonson, B. M., 2003. Origin and evolution of large Precambrian formations, in *Extreme Depositional Environments: Mega End Members in Geologic Time*, (eds.) Chan, M.A., Archer, W.A., *Geological society of America*, Special Paper 370.
- Stichauer, ., Mirone, A., Turchini, S., Prosperi, T., Zennaro, S., et al., *J. Appl. Phys.* 90, 2511.
- Suo, H., Wang, S., Zhang, C., Xu, J., Wu, B., Yang, Y., Xiang, H., Li, Y.-W., 2012. Chemical and structural effects of silica in iron-based Fischer–Tropsch synthesis catalysts. *Journal of Catalysis* 286, 111-123.
- Tosca, N.J., Guggenheim, S., Pufahl, P.K., 2016. An authigenic origin for Precambrian greenalite: Implications for iron formation and the chemistry of ancient seawater. *GSA Bulletin* 128, 511-530

van Zuilen, M., Lepland, A., Arrhenius, G., 2002. Reassessing the evidence for the earliest traces of life. *Nature* 418, 627–630. <https://doi.org/10.1038/nature00934>.

van Zuilen, M., Chaussidon, M., Rollion-Bard, C., Marty, B., 2007. Carbonaceous cherts of the Barberton Greenstone Belt, South Africa: Isotopic, chemical and structural characteristics of individual microstructures, *Geochimica et Cosmochimica Acta*, 71, 655-669, <https://doi.org/10.1016/j.gca.2006.09.029>.

Wang, Y., Caruso, F., 2004. Enzyme encapsulation in nanoporous silica spheres. *Chemical communications*, 1528-1529.

Zhang, T., Amiridis, M.D., 1998. Hydrogen production via the direct cracking of methane over silica-supported nickel catalysts. *Applied Catalysis A: General* 167, 161-172.

Chapter 3

Geochemistry and mineralogy of the polyextreme hydrothermal system of Dallol, NE Ethiopia

3.1. Summary

One of the latest volcanic features of the Erta Ale range at the Afar Triangle (NE Ethiopia) has created a poly-extreme hydrothermal system located at the Danakil depression, on top of a protovolcano, known as, the dome of Dallol. The interaction of the underlying basaltic magma with the evaporitic salts of the Danakil depression has generated a unique, high temperature (108 °C), hypersaline (> 30 %) hyperacidic (pH values from 0.1 to -1.7), oxygen-free hydrothermal site containing up to 150 g/L of iron. Owing to this combination of physiochemical parameters that is highly probable to impose a barrier to life and to the high iron content, Dallol was selected for study of abiotic mineral precipitation. As demonstrated for the first time in this work, the colorful brine pools and mineral patterns of Dallol derive from the slow oxygen diffusion and progressive oxidation of the dissolved ferrous iron, the iron-chlorine/-sulfate complexation and the evaporation. These inorganic processes induce the precipitation of nanoscale self-organized iron minerals without the intervention of life. Thus, Dallol is the only present-day site we currently know of where we can witness iron mineral self-organization and progressive oxidation as possibly occurred during the complex redox history of the early Earth, when life was neither affecting, nor, inducing mineralization. Finally, Dallol brines were used for the growth of Fe-silica membranes, showing that iron-silica self-organization could have occurred even at the most geochemical extreme settings of the early Earth.

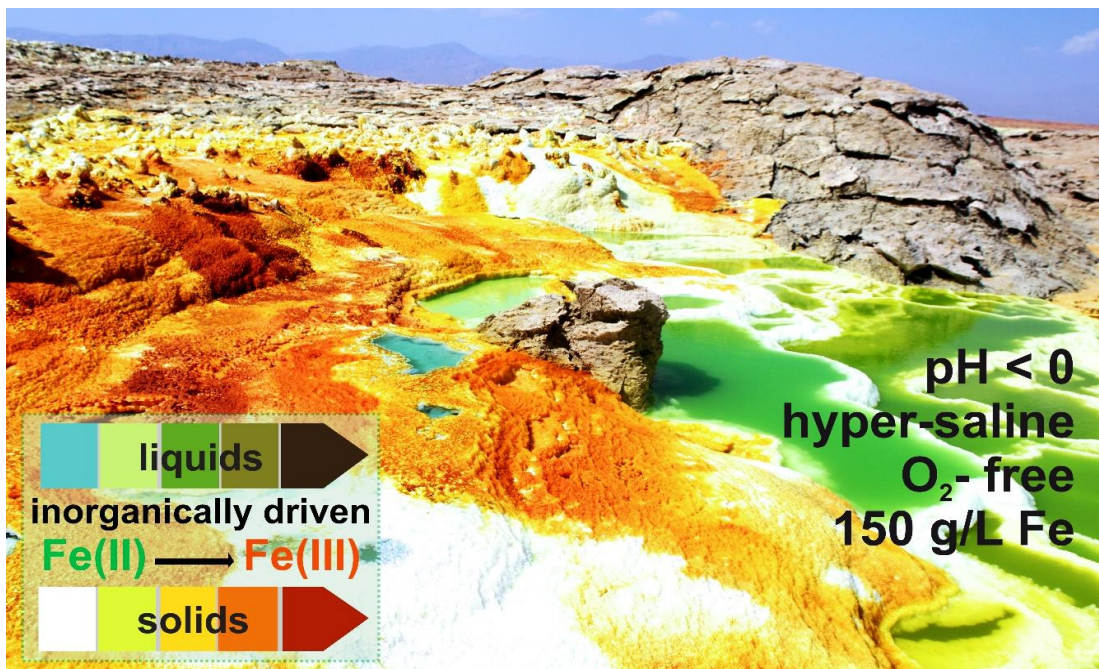


Figure 1. Inorganic iron cycling, oxidation and mineral self-organization at the polyextreme conditions of Dallol.

3.2. Experimental and analytical part

In situ measurements

Temperature (± 0.1 °C) and pH (± 0.1) were measured, both for spring and pools, with a Hanna pHmeter equipped with a glass electrode. Prior to the pH measurement the electrode was soaked in sulfuric acid (97.5%) for 24 h, while, for the pH calibration buffers of pH 4, 2, 1.68 and 0.8 were used. The pH meter was calibrated prior to every measurement and each measurement was repeated 3 times and in different days. Also, dissolved oxygen ($\mu\text{mol/L}$) was measured with the high sensitivity PreSens Fiber Optic Oxygen Meter Fibox 4, of temperature, automatic pressure and salinity compensation and detection limit of 15 ppb dissolved oxygen, 0 – 100 % oxygen. The PreSens system was calibrated with a two-point calibration before each measurement. Temperature, pH and oxygen concentration measurements were repeated three times for the same sampling sites in different days during the fieldtrip.

Sampling and preservation of the anoxic conditions

For the preservation of the pristine conditions of the liquids and to avoid the oxidation during the sample transportation and the measurements, samples of spring and pool water were collected in 12 mL sterile glass vials sealed with a septum tap, covered with parafilm tape and were kept inside a N₂ atm glovebox. Selected efflorescences and precipitates were preserved also in sterile glass septum sealed vials and in re-sealable with ziplock seal bags and were kept inside the glovebox.

Chemical analysis of water

For the determination of the concentration of the anion species we used a 940 Professional IC Vario instrument (Metrohm, Herisau, Switzerland) equipped with a conductivity detector at the Centro de Instrumentación Científica (CIC) of the University of Granada, Spain. An isocratic gradient of Na₂CO₃ (3.6 mM) was used as eluent, keeping an eluent flow at 0.7 mL min⁻¹. The injection loop was 50 μL . Analysis was done in an ionic resin column Metrosep A Supp 7 - 250/4.0. For the rest of the major, minor and trace elements samples were analyzed using an axial inductively coupled plasma optical emission spectrometer (axial ICP-OES Agilent (Varian) 720-ES. ICP analyses were carried out in the Instrumental Technical Services of the Estación Experimental del Zaidín (CSIC). Analytical quality control included analysis of 1 duplicate, 3 blank solutions, as well as, analysis of a series of appropriate reference materials.

Raman and UV-Vis spectroscopies

Raman analysis of the pristine spring and pool water, preserved in oxygen-free conditions, was performed at the laboratory of the Espectroscopía Raman e Infrarroja aplicado a Cosmogeología y Astrobiología (ERICA) of Unidad Asociada UVA-CSIC, Spain. Spectra were recorded with a Horiba-JY Induram spectrometer and a Laser Elforlight G4-30 PSU (532 nm) Cabezal Raman Horiba-JY Superhead, with a Zeiss 20x LF objective. The laser potential was set at 20mW and the water samples were placed vertically with respect to the beam. No sample preparation was required and the samples were not opened during the measurement. For the investigation of the Fe aqueous species I used the UNICAM UV300 spectrometer of the Inorganic Chemistry Department of the University of the Granada, Spain. Sample preparation was carried out inside a N₂ atm glovebox to preserve the oxygen-free conditions. Due to the very high amount of Fe in the liquids, a one-step dilution of 50µL of sample into 1mL of oxygen-free Milli-Q water was done prior to the measurement and samples were placed into quartz cells with septum seal. Spectra were recorded in absorbance mode, between 200-600 nm wavelengths, with a resolution of 1.5 nm.

Isotopic analysis

Isotopic measurements were carried in at the Stable Isotope Laboratory of the Instituto Andaluz de Ciencias de la Tierra (CSIC-UGR, Granada). For the analysis of δD and $\delta^{18}\text{O}$ in water, an aliquot of water (0.7 µl) was injected onto a ceramic column containing a glassy carbon tube at 1450°C to produce H₂ and CO gases (Sharp, 2001). A high-temperature reactor (TC/EA) coupled on-line via a ConFlo III interface to a Delta XP isotope ratio mass spectrometer (Thermo-Finnigan, Bremen). These gases were separated by chromatography using a helium carrier gas stream. To avoid memory effects, each sample was analyzed ten times by discarding the first 5 analyzes and doing average in the last five. Commercial CO and H₂ bottles and 5 different waters, previously calibrated vs. V-SMOW, SLAP and GIPS, were used as internal standards for the oxygen and hydrogen isotopic analyses. The precision was calculated higher than $\pm 0.2\text{‰}$ for the oxygen and $\pm 1\text{‰}$ for the hydrogen, while the standard for reporting oxygen and hydrogen is V-SMOW (Vienna Standard Mean Ocean Water). The isotopic composition of nitrogen, carbon and sulfur was analysed by means of a Carlo Elba NC1500 (Milan, Italy) elemental analyser with a Delta Plus XL (ThermoQuest, Bremen, Germany) mass spectrometer (EA-IRMS). Sulfur samples were mixed with vanadium pentoxide to ensure complete combustion. Internal standard previously calibrated vs IAEA-S1, IAEA-S2, IAEA-S3, NBS-127 y CP-1 for sulfur and NBS-22, IAEA-CH-7, IAEA-CH-6 for carbon were used. The methodology for the *DIC* (dissolved inorganic carbon) analysis is

described in the Supporting Information Methods 1.2. *Dissolved gases*: The ratios O₂/Ar, N₂/Ar, CO₂/Ar, O₂/N₂ and isotopic composition of ¹⁵N/¹⁴N, ¹⁸O/¹⁶O, ¹⁷O/¹⁶O, ³⁶Ar/⁴⁰Ar, ³⁸Ar/⁴⁰Ar were analyzed in a system built specifically for analysis of atmospheric gases by continuous flow. The system employed a Delta V plus (ThermoFinnigan, Bremen, Germany) mass spectrometer configured with 11 faraday cups to simultaneously analyze N₂, O₂, CO₂ and Ar. This allowed the maximum precision in the mixture of atmospheric gases. The precision was calculated for 4 bottles of internal standards vs air and was better than ± 0.03‰ for δ¹⁵N, ± 0.05 δ¹⁷O, ± 0.02 δ¹⁸O, ± 0.06 δ³⁶Ar, ± 0.1 δ³⁸Ar, ± 0.8 for δO₂/N₂ (‰), ± 0.9 for δO₂/Ar (‰), ± 0.56 for δCO₂/Ar (‰).

Powder X-ray Diffraction (HRPXRD)

For the detection of the crystalline phases of the mineral precipitates a high resolution Bruker D8 Advance Series II X-ray diffractometer was utilized, using monochromatic Cu K_{α1} radiation with a primary Ge (111) monochromator and a PSD Lynxeye detector at the facilities of the Laboratorio de Estudios Cristalograficos (LEC) of the Instituto Andaluz de Ciencias de la Tierra (IACT) in Granada, Spain. Samples were run in transmission mode, at 40 kV acceleration voltage and at 40 mA current, for 16 hours from 4 ° to 90 ° 2θ, 0.014° per second. Phase identification was carried out with the Diffrac.Suite software and the American Mineralogist Crystal Structure Database.

Field emission gun scanning electron microscopy (FESEM-EDS)

A ZEISS SUPRA 40 VP, FESEM-EDS equipped with an Oxford energy-dispersive X-ray spectrometer (EDS) of the Centro de Instrumentación Científica (CIC) of the University of Granada, Spain, operating at 5keV-20KeV was used for the textural and chemical characterization of the sub-micron mineral phases. High resolution images were obtained at 5 kV and at 2 mm working distance, in SE and 15 kV in BS mode, while for the elemental analyses operating conditions were set at 15 kV accelerating voltage and 7.5 mm working distance and the AZtec 3.0 SP1 EDS software was used. Biological sample preparation for the SEM study is specified in the Supporting Information Methods 1.3.

micro-Raman

The micro-Raman study of the solids was performed at the laboratory of the Espectroscopía Raman e Infrarroja aplicado a Cosmogeología y Astrobiología (ERICA) of the Unidad Asociada UVA-CSIC, Spain. The spectra were obtained with a Kaiser OSI HoloSpec f/1.8i. CCD Andor DV420A-OE-130 spectrometer equipped with a Research Electro-Optics LSRP-3501, He-Ne 632.8 nm laser

and a Cabezal Raman Kaiser OSI MKII, HFPH-FC-S-632.8 with a Nikon Eclipse E600 microscope with Nikon 50x y 100x LF objectives. The spot size was 38 microns for the 50x objective and 15 microns for the 100x objective.

Transmission electron microscopy: The study in the nanoscale was performed with a Titan X-FEG G2-S/TEM, image C_s -corrector, operating at a 300 kV acceleration voltage at the Centro de Instrumentación Científica (CIC) of the University of Granada, Spain. Samples were placed on a formvar C coated Cu-grid. Z-contrast images were collected using a High-Angle Annular Dark Field (HAADF) detector in Scanning Transmission Mode (STEM), while the chemical composition of the studied phases was obtained with EDX. Also, High-Resolution Transmission Electron Microscopy (HRTEM), along with Fast Fourier Transform Images (FFT), and Selected Area Electron Diffraction (SAED) were performed to investigate the crystal structure of the studied nano-phases.

The (FZ) method for the Fe speciation in the liquids

For the Fe speciation in the liquids I used the equipment described previously by employing ferrozine (FZ) as a Fe(II) chelator, which allows the determination of the Fe(II) concentration by measuring the absorbance at 562 nm in the UV-Vis spectra, due to the formation of the complex $[\text{Fe}^{\text{II}}(\text{FZ})_3]^{2+}$ of a vibrant violet color. The quantitative interpretation of UV-Vis spectra was based on the Beer-Lambert law, where the molar absorptivity ϵ_{562} of the $[\text{Fe}^{\text{II}}(\text{FZ})_3]^{2+}$ complex is 27,900 $\text{M}^{-1}\text{cm}^{-1}$ and on iron standard calibration solutions (Pehkonen, 1995). Subtracting the Fe(II) concentration from the total Fe measured by ICP-OES we obtained the ratio Fe(II)/Fe(III) for springs and pools. Sample preparation was carried out inside a N_2 atm glovebox. Due to the very high amount of Fe in the liquids, a two-step dilution of 10 μL of sample into 1 mL of Ar-purged Milli-Q water (dilution factor 10,000) was performed. Following, 1 mL of 0.01M FZ solution (final dilution factor 11,000) was added, also prepared inside the glovebox with Ar-purged Milli-Q water. Samples were prepared in triplicates and were placed into quartz cells with septum seal for the UV-Vis measurement. To make sure that Fz was always in excess with respect to the Fe(II) amount of the samples, measurements were repeated after collecting a batch of data by increasing ten times the amount of the Fz, without any subsequent increase in the absorbance of the spectra.

Isotopic analysis

For the DIC (Dissolved Inorganic Carbon) an aliquot of sample was injected into 12-ml vials pre-filled with helium and 5 drops of 65% phosphoric acid and shaken in a Vortex agitator for 30 seconds. The vials were left at room temperature for between 15 and 36 hours to obtain a state of equilibrium (Salata, 2000). The CO₂ was separated from other residual gases by chromatography using a helium carrier gas in a Gas Bench (ThermoFinnigan, Bremen, Germany) system interfaced with a mass spectrometer Delta XP isotope ratio mass spectrometer (Thermo-Finnigan, Bremen).

¹⁸O enriched water incubation for detection of primary production: For the evaluation of the GPP¹⁸O, eight 12-ml glass vials were filled. Four replicate samples were immediately fixed (biological activity stopped) with 100 µl of saturated HgCl₂ solution for following analysis of the initial δ¹⁸O(O_{2gas}) values, and stored upside down in darkness. The other four vials, containing beads to ensure mixing, were spiked with 100 µl of 98% H₂¹⁸O. After being closed, these spiked vials were immediately agitated, to ensure that H₂¹⁸O was homogeneously distributed inside the vial. The spiked samples were incubated in situ for 24, and vials were fixed with 100 µl of saturated HgCl₂ solution and stored upside down in darkness. In the stable isotope laboratory, a 4-ml headspace was generated in each vial, by flushing with a helium flow (Mesa et al., 2017). The vials were left for equilibration at room temperature for 24 hours. The δ¹⁸O of the dissolved oxygen in the headspace was measured in a system attached to a Finnigan Delta V Plus isotope ratio mass spectrometer, with precision higher than 0.02 ‰.

Urea incubations: For the isotopic evaluation of the heterotrophic respiration, eight 12-ml glass vials were filled with water. Four vials, containing beads inside to ensure mixing, were spiked with 100 µl of ¹³C-urea (99% enriched in ¹³C) solution (100 mg urea in 12000 µl). After being closed, these spiked vials were immediately agitated, to ensure that urea was homogeneously distributed inside the vial. The spiked samples were incubated in situ for 24 h, and vials were fixed (biological activity stopped) with 100 µl of saturated HgCl₂ solution and stored upside down in darkness. In the laboratory, the samples are analyzed as Dissolved Inorganic Carbon (DIC) (first batch of measurements) (see previous paragraphs). After 4 weeks the measurement was repeated for the same samples (second batch of experiments).

Biological sample preparation for the SEM study

The samples were fixed by adding glutaraldehyde of 2.5% final concentration and were stored at 4 °C overnight to fix the biological material. Following, the samples were filtered with a nylon 0.22 µm pore diameter filter. To remove the salts the filters were washed with 40 mL sterile Milli-Q water that was previously sterilized with a Tuttnauer 3850 autoclave-steam sterilizer and filtered

with a 0.22 μm nylon pore diameter filter. The dehydration procedure involved the washing of the samples with 50%, 70%, and 100% ethanol solution consecutively, previously filtered as described before. The samples were dehydrated by using critical point drying and were carbon coated for the FESEM study.

3.3. Results and discussion

3.3.1. The hydrothermal system of Dallol

The dome of Dallol lies in the Danakil depression at the extension of the Main Ethiopian Rift (MER) of the Afar Triangle (Fig. 2A). This depression, situated 120 m bmsl, is a vast salty plain composed of more than 2 km of evaporites created from successive marine transgressions of the Red Sea, the most recent placed at 32 kya, during the evolution of the MER since Miocene to Quaternary (Holwerda and Hutchinson, 1968). Categorized as BWh (hot desert climate) according to the Köppen classification (Fazzini et al., 2015), with scarce precipitation (up to 144 mm/yr but usually below 50 mm/yr), and a mean annual temperature of 35 °C (Fazzini et al., 2015), the area of Danakil is one of the driest and hottest places on the planet. Danakil belongs to the dry drainage basin of Dinakle with no surficial flow and no, or insignificant, flow out of the drainage system (Berhanu et al., 2014).

However, the karstified Jurassic limestones and sandstones that underlay the evaporitic sequence behave as aquifers enabling the infiltration of meteoritic water from the Danakil Alps to the east and the highlands of the North Ethiopian plateau to the west, via the normal faulting and transverse fractures of the rift zone. In this region of incipient seafloor spreading, where the crustal thickness does not exceed 14 km, the Red Sea, the Gulf of Aden, and the MER produce a triple junction zone associated with mantle plume activity and basaltic intrusive and extrusive magmatism (Ebinger, 2001; Keir et al., 2013; Makris and Ginzburg, 1987; Prodehl, 1991). As a result, several volcanic chains are forming, mainly represented by basaltic shield volcanoes, among them the NNW-SSE Erta Ale range. The Dallol dome along with the neighboring areas of the Black and Gaet' Ale Lakes (the latter also known as Yellow Lake) (Pérez and Chebude, 2017) are the most recent expressions at the northwestern part of the Erta Ale volcanic range; following from SE to NW the Hayli Gubbi, Ale Bagu, Erta Ale, Borale, Dalafilla, Alu and Gada Ale volcanoes (Nobile et al., 2012; Pagli et al., 2012) (Fig. 2A, B). The precise age of the Dallol dome is unknown, probably counting a few hundreds of years, whereas Black and Yellow lakes formed after the phreatic explosions of 1926 and 2005, respectively. Upwelling of basaltic magma confined in a magma chamber just 2.4 km deep below the segment of Dallol intruded the marine evaporitic sequence and created a dome structure lying 60 m bmsl (Carniel et al., 2010; Hovland et al., 2006; Nobile et al., 2012).

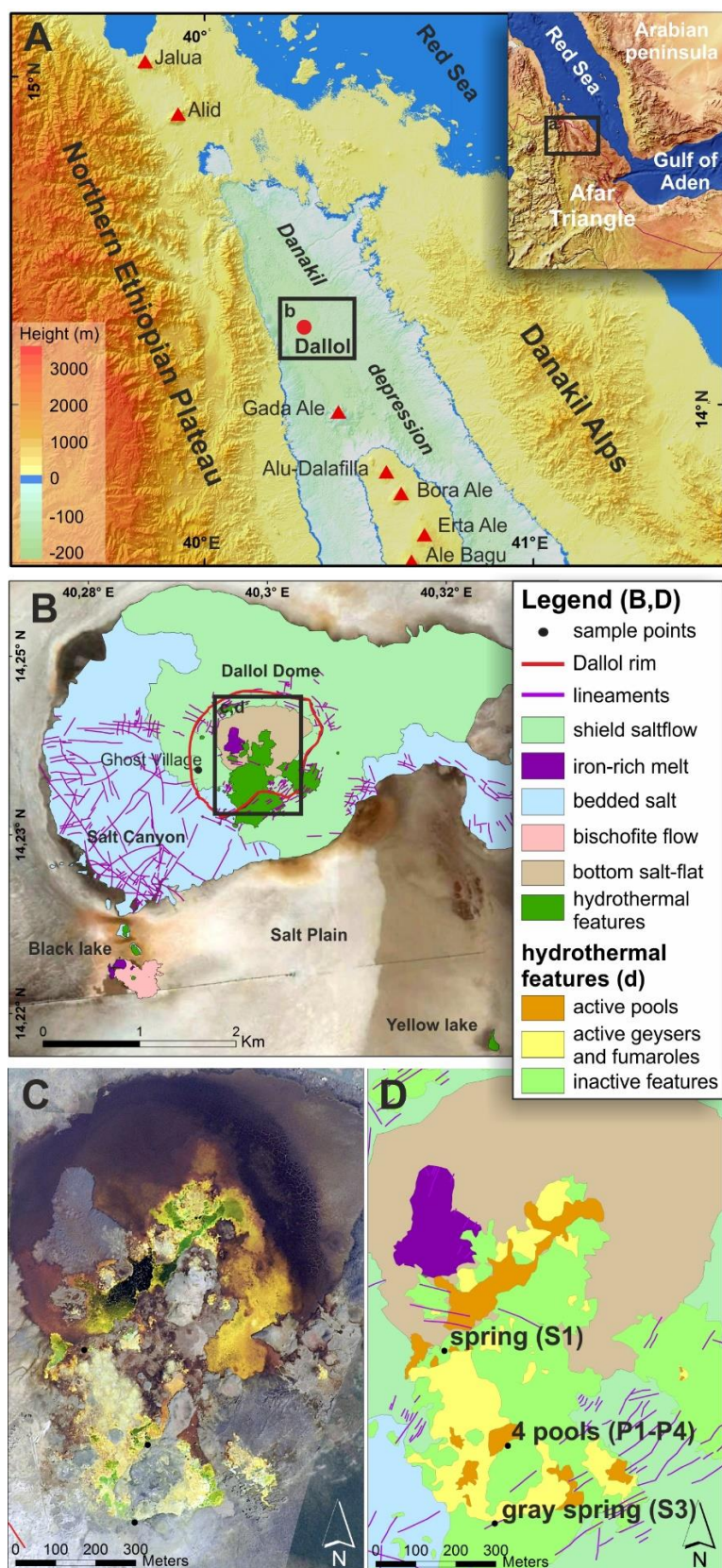


Figure 2. The hydrothermal system of Dallol within the Erta Ale range and maps of the active hydrothermal features of January 2017. A. Dallol dome located in Danakil depression within the Erta Ale volcanic range of the Afar Triangle. B. Geological map of the wider area of the Dallol dome, including Black and Yellow Lakes. C. Aerial image of Dallol dome, showing the active areas in January 2017. D. Map of January 2017 of the hydrothermal activity showing the referred sampling sites within the text, spring (S1), gray spring (S3) and a system of four successive pools (P1-P4).

Dallol has not yet developed into a typical volcano; the crater of the Dallol dome hosts numerous springs, extended fumarolic fields, subaerial and subaqueous hydrothermal springs and acidic brines that produce salt chimneys, pillars, terraces and pools of different, ephemeral, colors (Fig. 3).

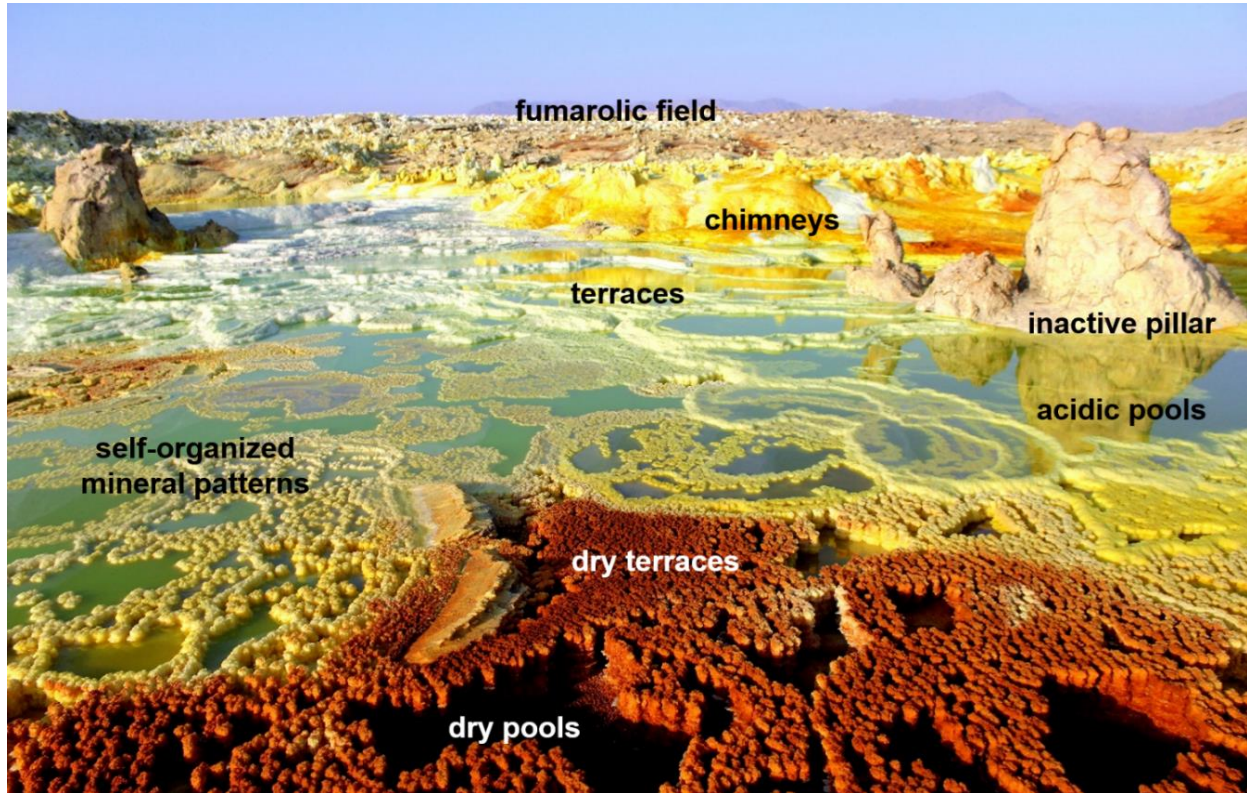


Figure 3. Representative image of the hydrothermal system of Dallol. Fumaroles and active hydrothermal chimneys forming terraces and pools are shown at the background of the image. Moving downwards from the terraces, the oxidation of the Fe mineral precipitates is manifested by the change in the color from white to green, yellow and finally to red. Inactive pillars of past hydrothermal activity are shown at the upper left and right of the image. The height of the right pillar is 1.5 m.

The ascending of magmatic fluids rich in CO_2 , SO_2 , H_2S and acidic gases, together with the boiling of meteoric water and of the seawater trapped in the evaporitic sequence, led to the generation of a hydrothermal system of hyperacidic springs with high content of dissolved CO_2 and chlorides (Carniel et al., 2010; Darrah et al., 2013; Hovland et al., 2006; Nobile et al., 2012). This system is also characterized by an impressive palette of colors that is related to the high iron concentration of the fluids, deriving from the dissolution of the underlying basalt and iron-rich formations (Bonatti et al., 1972).

3.3.2. Hydrochemistry

The hydrothermal system is highly dynamic; active spring sites go inactive and new springs emerge in new locations in the range of days, while the activity is changing in the range of hours within the same site. Eleven spring sites occupying an area of 0.038 km² were active in 2016, whereas eighteen spring sites covering a 0.144 km² area were active in 2017, along NNE trending fissures (Fig. 4).

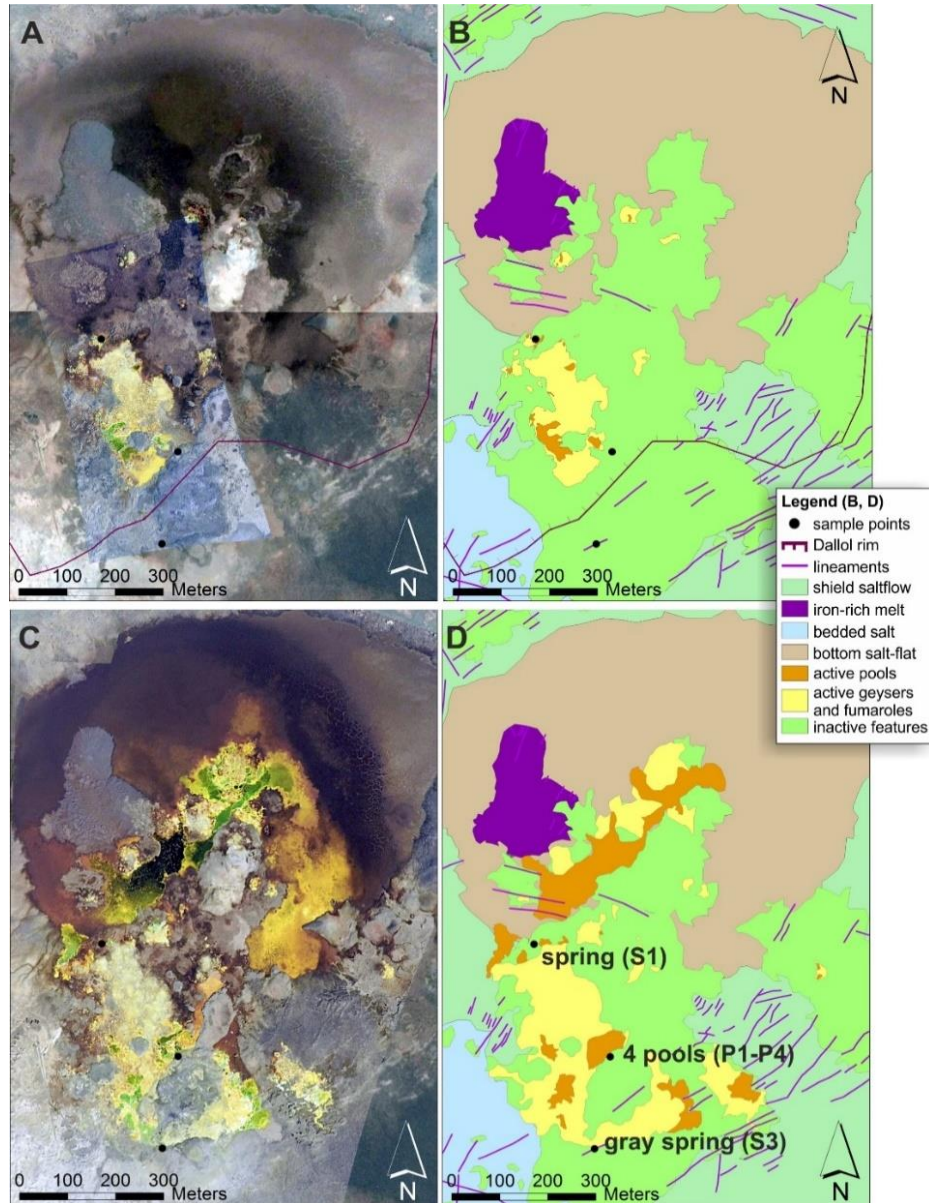


Figure 4. Aerial photographs and related hydrothermal activity maps of Dallol dome for the 2016 and 2017 field campaigns. A, C. Drone images of the dome (by Olivier Grunewald) for January 2016 and 2017 respectively. **B, D.** Activity maps of the dome for January 2016 and 2017 respectively where selected sampling locations are shown. Notice the expansion of the active sites for January 2017.

However, the dominant geochemical characteristics of the system remained within a narrow range of values between the two field campaigns. The springs are discharging oxygen-free, hyperacidic, Fe-rich hydrothermal brines, which are supersaturated with respect to halite. The mean concentrations of the major elements of the spring brines are Cl (251.4 g/L) and Na (92.2 g/L) followed by Fe (22.5 g/L), K (10 g/L), S (as sulfates) (3.6 g/L), Mg (3.7 g/L) and Ca (2.7 g/L), while, the most abundant trace elements are Mn (714 ppm), F (302 ppm), Br (288 ppm), Al (279 ppm) and Zn (54 ppm) (Table 1).

The composition of the gases emitted from the fumarolic fields and the spring complexes of Dallol is dominated by CO₂ (ranging from 70 to 99 %) along with H₂S, N₂, and traces of H₂, Ar, and O₂ (Appendix, table S1)(Darrah et al., 2013). The temperature of the spring water varies between 105.6 (± 0.1) °C and 108.4 (± 0.1) °C. Upon discharge, the spring fluids evaporate and the pressure and temperature decrease abruptly, triggering almost instantaneous precipitation of halite, creating pillars up to few meters in height. As the water flows downstream from the springs, a series of self-organized halite terraces pool the brines, which reduces turbulent flow. The temperature of the upper pools, those closest to the spring, is 85-71 (± 0.1) °C, whereas it drops down to 32 (± 0.1) °C due to increasing equilibration time with the atmosphere and evaporative cooling. The pH values of the spring water are close to zero ranging from 0.16 to -0.5 (± 0.1).

| | S1 | P2 | PS3 | BP1 | YL1 | BL1 | S1** | P1** | BP1** |
|------------------------------------|-------------|-------------|-------------|-------------|-------------|-------------|-------------|-------------|--------------|
| | 2017 | 2017 | 2017 | 2017 | 2017 | 2017 | 2016 | 2016 | 2016 |
| pH | -0.2 | -0.85 | -0.57 | -1.7 | 1.7 | 2.5 | 0.16 | -0.5 | -1.7 |
| T | 106 | 31.8 | 43.1 | 29 | 38.1 | 59.3 | 108.2 | 45 | 31 |
| DO | 0 | 6.8 | 4.4 | - | 111 | - | - | - | - |
| Al | 278 | 579 | 372 | 1664 | - | - | 280 | 358 | 216 |
| Ca | 3055 | 5446 | 8658 | 4873 | 165146 | 6759 | 2264 | 1959 | 1884 |
| Co | 0.5 | 1 | 0.7 | 3.1 | - | - | 0.6 | 1.8 | 2 |
| Cu | 54 | 8 | 2 | 132 | 1 | - | 31 | 22 | 40 |
| Cr | <0.5 | 1.1 | <0.5 | 1.3 | - | - | 0.8 | 0.6 | 1.1 |
| Fe | 18546 | 23856 | 5978 | 100408 | 93 | 1577 | 26445 | 31400 | 153000 |
| K | 10907 | 11454 | 5712 | 40406 | 5078 | 2142 | 9047 | 13711 | 37628 |
| Li | 10 | 11 | 6 | 65 | 30 | 10 | 11 | 14 | 57 |
| Mg | 3679 | 4970 | 3044 | 18865 | 30825 | 108925 | 3765 | 4209 | 15024 |
| Mn | 755 | 759 | 378 | 3592 | 412 | 223 | 673 | 826 | 3710 |
| Na | 91237 | 85623 | 141893 | 12852 | 3302 | 2199 | 93210 | 75494 | 11919 |
| Ni | <0.5 | 8 | <0.5 | 12 | <0.5 | 0.8 | <0.5 | 4 | 9 |
| P | 77 | 25 | 22 | 334 | <0.025 | - | 16.5 | 66 | 286 |
| Si | 49 | 36 | 41 | 14 | 3 | 20 | 31 | 60 | 25 |
| Sb | <0.5 | <0.5 | <0.5 | <0.5 | - | - | <0.5 | <0.5 | <0.5 |
| Sn | 0.9 | <0.5 | 0.7 | <0.5 | - | - | 0.8 | 0.6 | <0.5 |
| Ti | 1.73 | 2.4 | 1.46 | 4.3 | - | - | 0.9 | 1.3 | 4 |
| Th | <0.5 | <0.5 | <0.5 | <0.5 | - | - | <0.5 | <0.5 | <0.5 |
| Tl | <0.5 | <0.5 | <0.5 | <0.5 | - | - | <0.5 | <0.5 | <0.5 |
| V | 20 | 19 | 6 | 95 | - | - | 22 | 25 | 95 |
| Zn | 56 | 66 | 46 | 300 | 16 | <0.025 | 52 | 57 | 204 |
| F⁻ | 292 | 284 | 103 | 150 | 65 | - | 350 | 410 | 180 |
| Cl⁻ | 262678 | 193203 | 209393 | 253050 | 544302 | 309397 | 240000 | 25000 | 380000 |
| Br⁻ | 179 | 230 | 137 | 934 | 6450 | 6317 | 256 | 272 | 1320 |
| SO₄²⁻ | 5033 | 5671 | 10003 | 2017 | 262 | 2507 | 2167 | 6580 | 4620 |
| CO₃²⁻ | <0.5 | <0.5 | <0.5 | <0.5 | <0.5 | <0.5 | <0.5 | <0.5 | <0.5 |
| HCO₃⁻ | <0.5 | <0.5 | <0.5 | <0.5 | <0.5 | <0.5 | <0.5 | <0.5 | <0.5 |

Table 1. Comparative chemical analysis of Dallol brines for the 2016 and 2017 field campaigns. Representative spring (S1) and pool (P2) waters, pool from the gray spring system (PS3) and the most acidic pool (BP) of Dallol dome, and yellow lake (YL1) and black lake (BL1) waters from the mission of 2017. Representative spring (S1**) and pool water (P1**), as well as, the most acidic pool (BP**) of the dome of Dallol from the sampling of 2016. Concentration values are given in ppm, temperature in °C and DO in µmol/L.

3.3.3. Acidity and iron speciation

These hyperacidic values decrease from the upper to the lower pools, the lowest pH value measured in both field missions was -1.7 (± 0.1) (Table 1). Hyperacidic values have been reported as well

for several volcanic crater lakes and hot springs, among them the Kawah Ijen crater lake in Indonesia (pH: ~ 0.3) (Delmelle and Bernard, 2000), the Poas crater in Costa Rica (pH ~ -0.89) (Rodríguez and van Bergen, 2017; Rowe et al., 1992), the Ebeko Volcano in Kuril Islands (pH ~0.2) (Kalacheva et al., 2016), the Copahue in Argentina (pH ~ 0.2) (Agusto et al., 2016; Rodríguez et al., 2016; Varekamp et al., 2009), the Ruapehu in New Zealand (pH ~ 0.6) (Christenson and Wood, 1993), the Nevado del Ruiz, Colombia (pH ~ 1) (Inguaggiato et al., 2015) and the Santa Ana Volcano, El Salvador (pH ~ 0.5) (Colvin et al., 2013). Concerning acid mine effluents, hyperacidic to acidic pH values (0.9-3) have been measured in Rio Tinto in Spain (Fernández-Remolar, 2005), while (Nordstrom et al., 2000) report a much lower value of pH, -3.6, from the Richmond Mine of the Iron Mt in California. Thus, to the best of our knowledge, the hydrothermal system of Dallol is the most acidic natural system. The origin of this acidity is best demonstrated in Fig. 5-6, where SO_4^{2-} , Cl^- , F^- and dissolved Fe concentrations -the main volcanic acidic components- of Dallol are compared to those of other hyperacidic volcano-hydrothermal systems. Dallol fluids exhibit positive anomalies in chlorides (>200 g/L), derived from the interaction of ascending magmatic fluids with the marine evaporites (containing halite, sylvite, carnallite, gypsum, anhydrite), and in dissolved iron originated from the interaction of the magmatic fluids with the underlain basalts and Fe-rich formations.

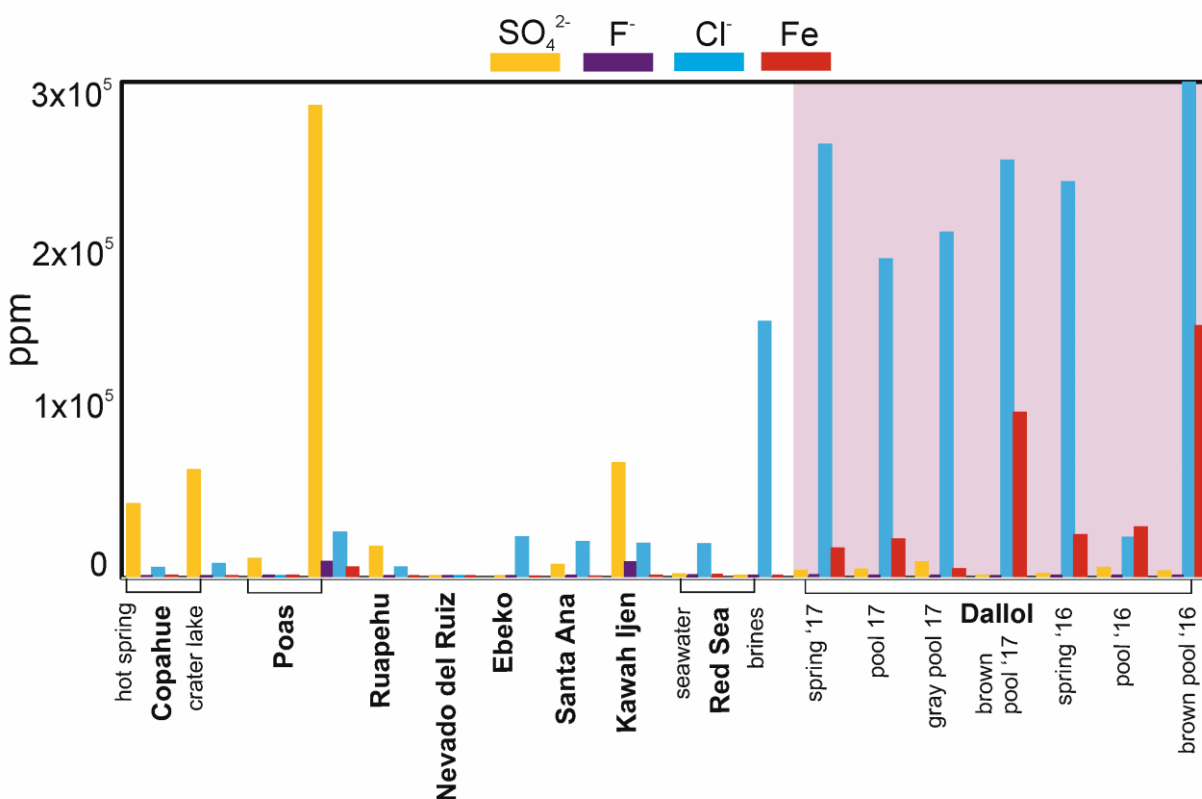


Figure 5. Comparative bar graph of sulfate, chloride, fluoride and iron concentrations of Dallol (purple- shaded area) and other hyperacidic volcanic sites and the Red Sea brines. The values for Copahue (Varekamp et al., 2009), Poas (Rodríguez and van Bergen, 2017; Rowe et al., 1992), Ruapehu (Christenson and Wood, 1993), Nevado del Ruiz (Inguaggiato et al., 2015), Ebeko (Kalacheva et al., 2016), Santa Ana (Colvin et al., 2013), Kawah Ijen (Delmelle and Bernard, 2000), Red Sea brines (Craig, 1969), and Dallol (this study) acidic fluids are shown in ppm.

As indicated also in the triangular diagram of Fig. 6, the sulfate values (~ 5200 ppm) are lower than the mean values of other volcano-hydrothermal systems such as the Poas crater lake system, whereas the mean fluoride concentration (~ 252 ppm) is higher than all the other systems apart from Kawah Ijen volcanic lake, that has a positive anomaly in fluorides.

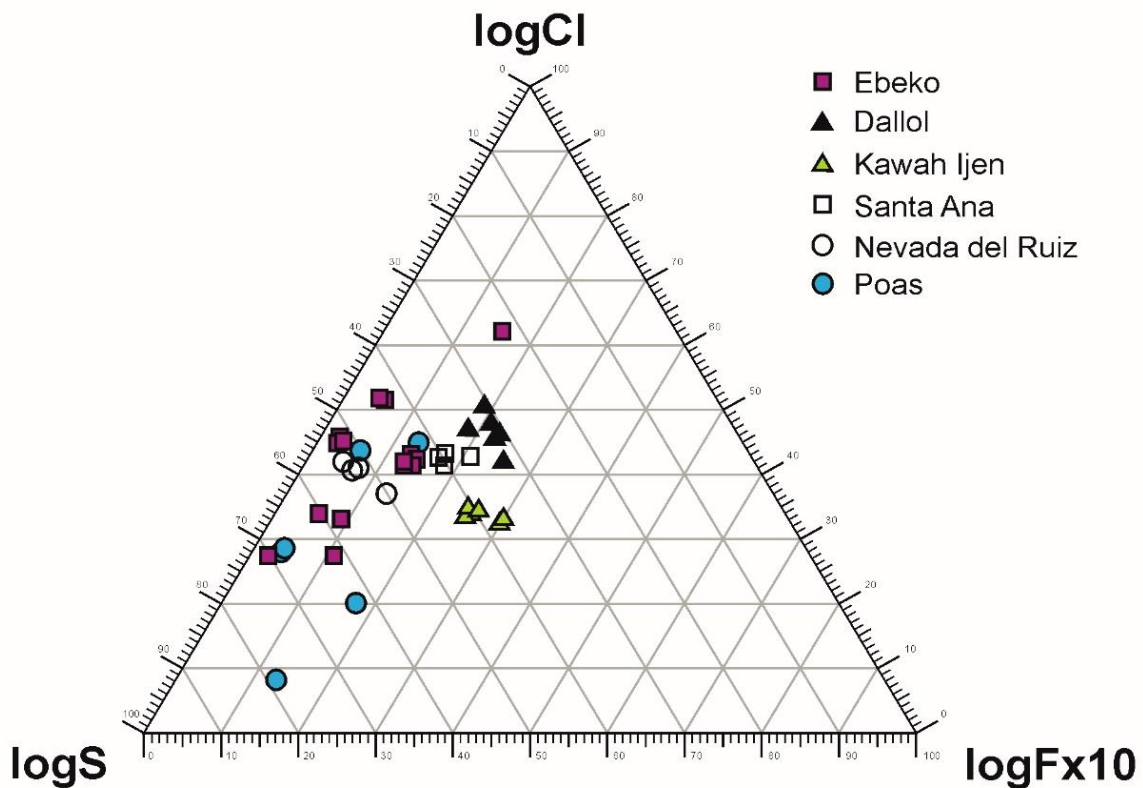


Figure 6. Triangular diagram of S-Cl-Fx10 for Dallol and other hyperacidic volcanic sites (modified after Varekamp et al., 2009). The values for Copahue (Varekamp et al., 2009), Poas (Rodríguez and van Bergen, 2017; Rowe et al., 1992), Ruapehu (Christenson and Wood, 1993), Nevado del Ruiz (Inguaggiato et al., 2015), Ebeko (Kalacheva et al., 2016), Santa Ana (Colvin et al., 2013), Kawah Ijen (Delmelle and Bernard, 2000) are shown in logarithmic scale in ppm.

Consequently, the hyperacidic pH of the Dallol spring water (pH ~ 0) results from: a) the presence of strong acidic gases such as HCl(g), HF(g) in the hydrothermal fluids, and b) the combined enrichment in chlorides and ferrous iron that leads to the formation of acidic Fe(II)-

chlorocomplexes/-sulfates. The gradual oxidation of the latter to Fe(III)-chlorides/-sulfates and consequent concentration in the hydrothermal pools decreases further the pH, down to negative values.

Unlike the Dallol hydrothermal brines, neighboring Black Lake is a magnesium chloride pond of 2.5 (\pm 0.1) pH and 60 °C (\pm 0.1) temperature, while, Yellow Lake is mainly composed of calcium chloride along with magnesium and potassium chlorides of 1.7 (\pm 0.1) pH and 38 °C (\pm 0.1) temperature (Fig. 2B and Table 1). The surrounding area of the salt plain, composed of Na/Ca-K/Mg/Fe-salts and -sulfates, and clays (Warren, 2015) had a pH of 3.5 (\pm 0.1) when flooded with perennial water.

Due to the near zero pH of the spring water and the low dissociation constants of hydrogen sulfide (Millero, 1986; Ohmoto and Lasaga, 1982) the concentration of sulfide in the fluid is practically zero. Sulfur is mainly found around the fumarolic sites as millimeter- to centimeter- dull yellow spheroids made of colloidal and poorly crystalline sulfur formed through atmospheric hydrogen sulfide oxidation dull yellow spheroids made of colloidal and poorly crystalline sulfur formed either by the disproportionation reaction of magmatic SO₂ to elemental sulfur, or, by atmospheric hydrogen sulfide oxidation. On the other hand, sulfates are present in the brines due to the dissolution of the sulfate salts of the evaporitic sequence. Therefore, the aqueous chemistry and the color palette of Dallol should be dominated by the formation of different iron species, in both reduced and oxidized states (Pittwell, 1972).

To determine the redox state across the aqueous system of Dallol the concentration of Fe(II) and Fe(III) was quantified, in different spring solutions and related pools. Fe(II) concentration was determined by employing the external chelator ferrozine and by using UV-Vis spectroscopy, Fe(Tot) was measured by ICP-MS/OES, and Fe(III) was obtained as the difference (Fig. 7). The measured values show that Fe(Tot) is practically ferrous in the spring water and is gradually oxidized to the pools, until is completely converted to ferric iron in the lowest, most concentrated, pools (Fig. 7-8). This gradual oxidation of the Fe(II) is reflected in both the pH and the color of the pools. The pH decreases from -0.79 (\pm 0.1) in pool 1 to -1.32 (\pm 0.1) in pool 4, followed by a change in the color of the pools from light green to dark brown due to hydrolysis and concentrative evaporation of the Fe(III) species that release further H⁺. While, the heat produced by the exothermic Fe(II) oxidation and the increase in the thermal energy by light absorption in the dark brown color pools, are responsible for the increase in temperature from 32 (\pm 0.1) °C in pool 3 to

40 (± 0.1) °C in pool 4. The high consumption rate of oxygen due to oxidation of the Fe(II) and the precipitation of the Fe(III) minerals explains the anoxic conditions in the lowest pools of the hydrothermal field (Fig. 8, pool 4).

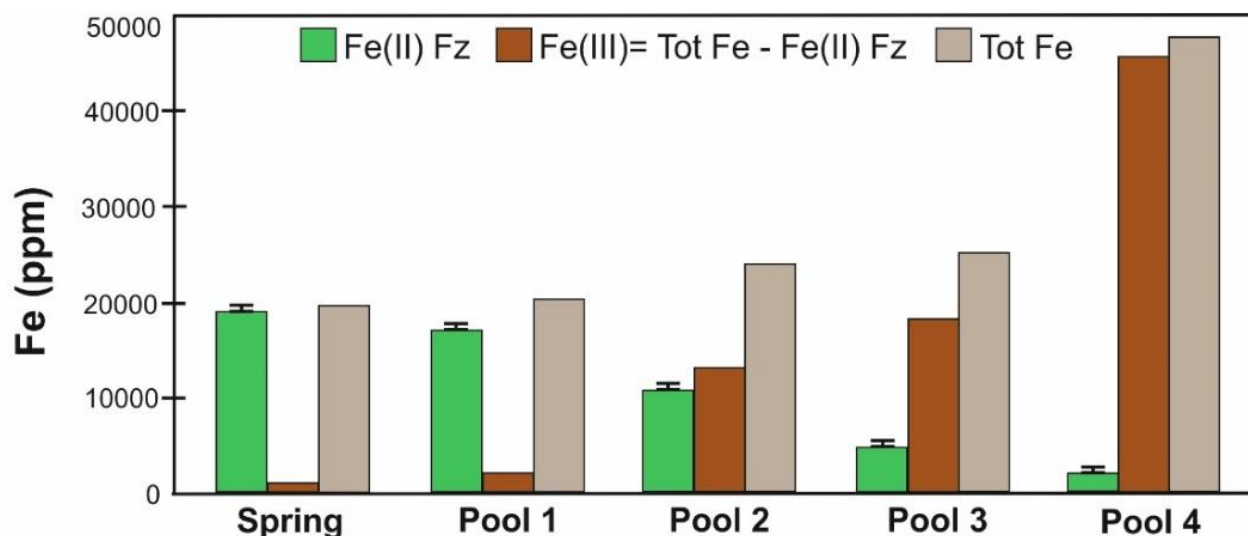
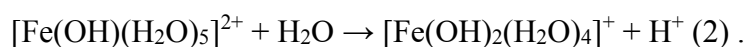
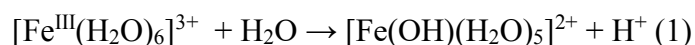


Figure 7. Fe species concentration for the spring water (S1) that is dominated by Fe(II) and four successive pools of Dallol (P1-P4) where Fe(III) is gradually increasing over Fe(II). Fe(II) concentration was measured with UV-Vis by using the Fz method (see Methods), Fe tot was measured by ICP-OES and Fe(III) resulted from the subtraction of Fe(II) from the total Fe. Estimated error for Fe(II) Fz= 5%.

Raman and UV-Vis spectroscopies were used to identify the Fe aqueous species responsible for the colors of the pools. The light green color of the spring and upper pools is owed to ferrous species, mainly associated with the $\nu_1(A_1)$ (Fe-OH₂) stretching band at 370 cm⁻¹ of the [Fe^{II}(H₂O)₆]²⁺ and the broad band around 420-480 cm⁻¹, although, in this region there is an overlap with the deformation modes of the sulfate/bisulfate anions (Fig. 8A, spring and pool 1) (Rudolph et al., 1997; Rull and Sobrón, 1994). Moving from the upper to the lower pools, the [Fe^{II}(H₂O)₆]²⁺ is oxidized and the hexaquairon complex [Fe^{III}(H₂O)₆]³⁺ undergoes hydrolysis to form progressive hydroxo-species, namely [Fe(OH)(H₂O)₅]²⁺ and [Fe(OH)₂(H₂O)₄]⁺ with the accompanying pH drop (equations 1, 2):



Furthermore, the very low pH and the high chloride concentration of the brines, favor the formation of a complex mixture of Fe(III)-chlorides, such as [FeCl₂(H₂O)₅]²⁺ and [FeCl₂(H₂O)₄]⁺ (Heinrich and Seward, 1990; Pittwell, 1972; Stefánsson and Seward, 2008). The latter is the most abundant

and was identified by the 312 cm^{-1} band arising from the $\nu(\text{Fe}^{3+}\text{-Cl})$ stretching vibration in the spectra of the middle and lower pools (Kanno and Iraishi, 1982) (Fig. 9B).

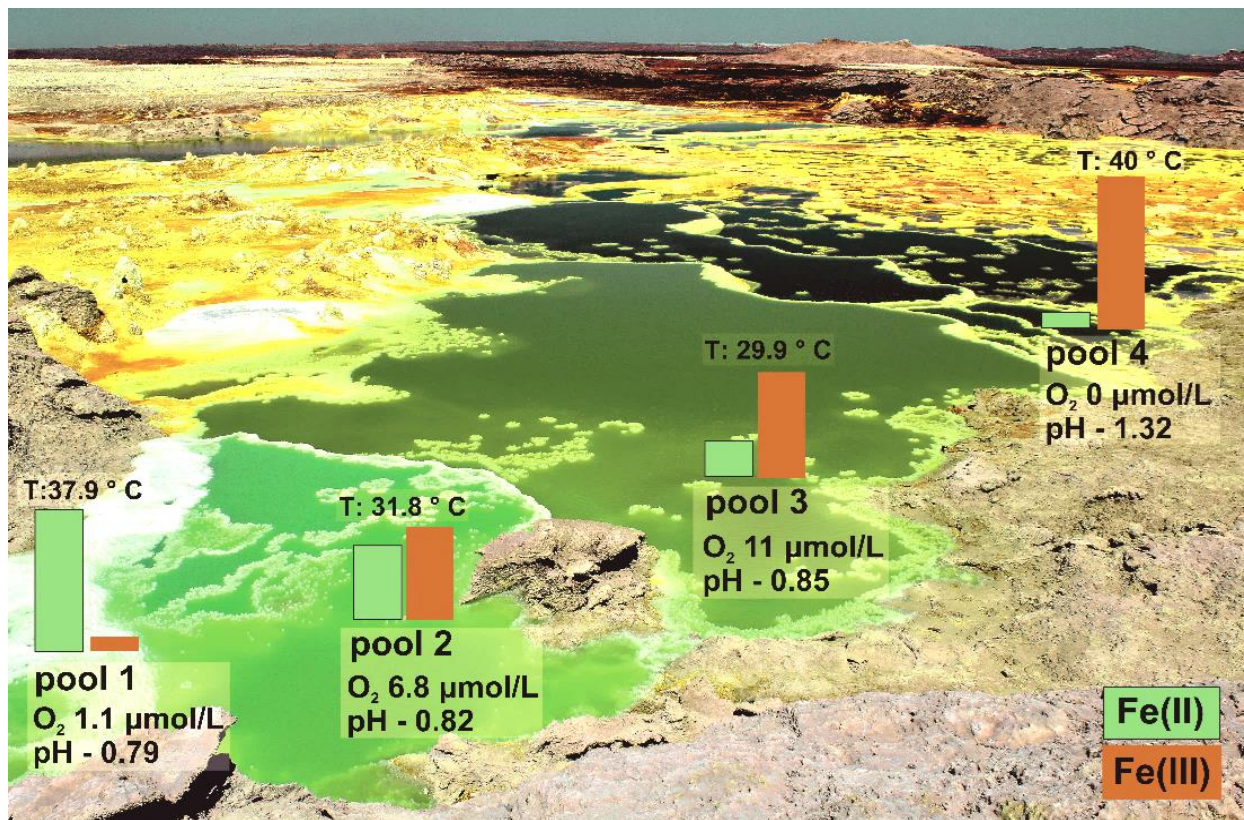


Figure 8. Fe(II)/Fe(III) ratio, pH, O₂ concentration and temperature of four successive pools of a typical spring-terrace system. Pool 1 (P1), the upper pool (oxygen-free spring is at the left of the pool, out of the field of view), is dominated by Fe(II) species of light green color. Moving downstream from the spring to pool 3 (P3), temperature is decreasing and the atmospheric O₂ diffusion results to the formation of Fe(III) species and to pH drop. Ultimately, the lowest pool 4 (P4) is characterized by Fe(III) species the precipitation of which darkens the pool color, lowers further the pH, increases the temperature, and consumes the oxygen.

Note that the intensity of the band at 312 cm^{-1} is increasing from pool 2 to pool 4 as the concentration of Fe(III) is increasing, while, the 370 cm^{-1} band decreases dramatically as the Fe(II) species decrease (Fig. 8A). Likewise, the intensity of the $\nu_1(\text{A}_1)$ vibration of the free SO_4^{2-} at 982 cm^{-1} is decreasing from the spring water to pool 4 and equilibrates with the $\nu(\text{HO-S})$ and the SO_3 vibrations of the bisulfate anion at 875 cm^{-1} and at 1052 cm^{-1} respectively (Fig. 9A, pools 3 & 4) (Rudolph et al., 1997; Rull and Sobrón, 1994). The UV-Vis spectra of springs and pools consist of a broad absorption band centered around 330 nm that becomes more intense as we move from the spring to pool 4 (Fig. 9B). The major electronic transitions for the Fe(III) hydroxo- and chloro-complexes are attributed to ligand-to-metal charge transfers (LMCT). The LMCT absorption of the hydroxo-complexes occurs around 300 nm , whereas, in the chloride-complexes this absorption

intensifies and shifts to lower energies up to 360 nm (Stefánsson and Seward, 2008). Therefore, and in accordance with the Raman study, the UV-Vis spectra show that the Fe(III)-chlorides are practically absent in the spring and the upper pools and become predominant in the lower pools, which explains the intense yellow color. Finally, the lowest pools show darker color due to further oxidation that provokes the precipitation of hydrated yellow iron-oxyhydroxides/-oxides/-sulfates. Two main mineral phases have been identified by X-ray diffraction, Raman spectroscopy, field emission scanning electron microscopy and energy-dispersive analysis, transmission electron microscopy and diffraction: jarosite ($\text{KFe}^{3+}_3(\text{SO}_4)_2(\text{OH})_6$) and akaganeite ($\beta\text{-Fe}^{3+}\text{O}(\text{OH},\text{Cl})$), products of the Fe(III) hydrolysis in the presence of sulfate and chloride, respectively.

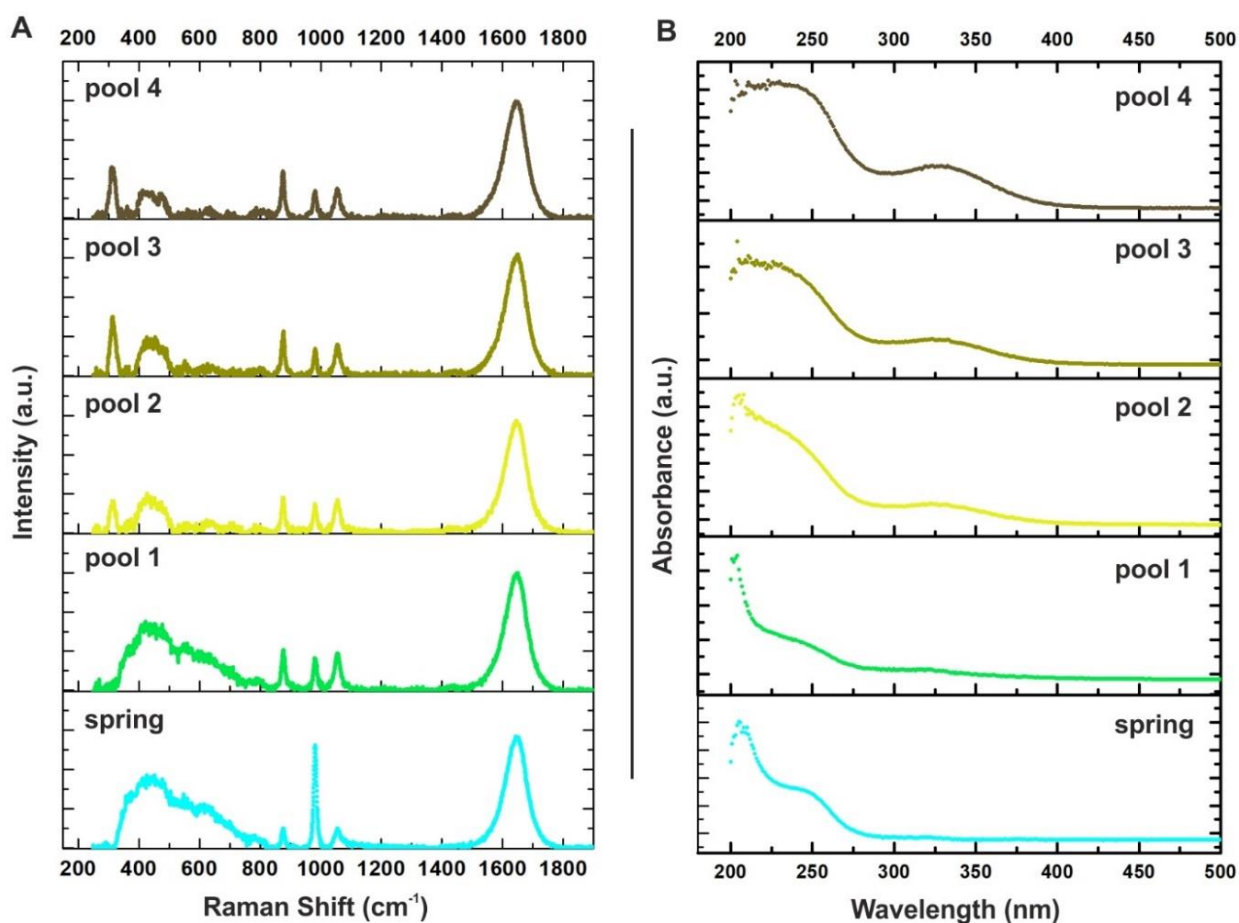


Figure 8. Raman and UV-Vis spectra of the spring water (S1) and the four gradual pools (P1-P4) of Fig. 7. Region of the Raman spectra showing the main vibrations of the Fe aqueous complexes. The concentration of the Fe(III) is increasing gradually from pool 2 to pool 4, as shown by the Fe(III)-Cl stretching vibration band at 312 cm^{-1} . This correlates with the decrease of the intensity of the Fe(II)-OH₂ stretching vibration at 370 cm^{-1} . **B.** UV-absorbance spectra showing the increase of the band centered at 330 nm from the spring and upper pool to the lowest pools, due to Fe(II) oxidation and Cl-complexation.

3.3.4. Mineralogy of iron, self-organized, precipitates

Regarding the solids halite is the dominant macro-crystalline phase found all over the Dallol dome, producing an impressive array of complex mineral patterns (Fig. 10). Among them I would like to underline the following: i) hydrothermal salt-pillars up to 4 meters high, ii) water-lily structures forming in subaqueous springs, iii) flower-like crystals growing in lower pools by extreme evaporation, iv) egg-shaped thin crusts, hollow twisted tubes and pearl-like spheres around active gas gateways, v) various types of efflorescences, and vi) polygonal cracking patterns resembling pieces in a chocolate bar (Fig. 10). Salt pillars and water lilies form by subaerial and subaqueous halite crystallization respectively, due to the cooling of the supersaturated brines. Evaporation and evaporative cooling drive the crystallization of the aforementioned structures except for the “chocolate bar” polygonal cracks, probably formed due to cooling stress, water loss and solidification of a highly viscous sodium chloride, Fe-rich, solution. On top of the halite crystals, microcrystals of Na-/K-/Ca-/Mg-salts, such as, gypsum ($\text{CaSO}_4 \cdot 2\text{H}_2\text{O}$), sodium-sulfates, sylvite (KCl) and carnallite ($\text{KMgCl}_3 \cdot 6\text{H}_2\text{O}$) are precipitating.. Nevertheless, the minor phases of sub-micrometer Fe-(oxy)hydroxides/sulfates, mainly jarosite ($\text{KFe}^{3+}_3(\text{SO}_4)_2(\text{OH})_6$) and akaganeite ($\beta\text{-Fe}^{3+}\text{O}(\text{OH},\text{Cl})$) that form a colorful veil over all the mineral patterns, are those responsible for the color diversity and color evolution of the solids with time (Fig. 8h-m). Far from the active springs and their corresponding pools, the predominant phases are the Fe-oxides mainly represented by hematite (Fe_2O_3) (Fig. 9, 10I-M).

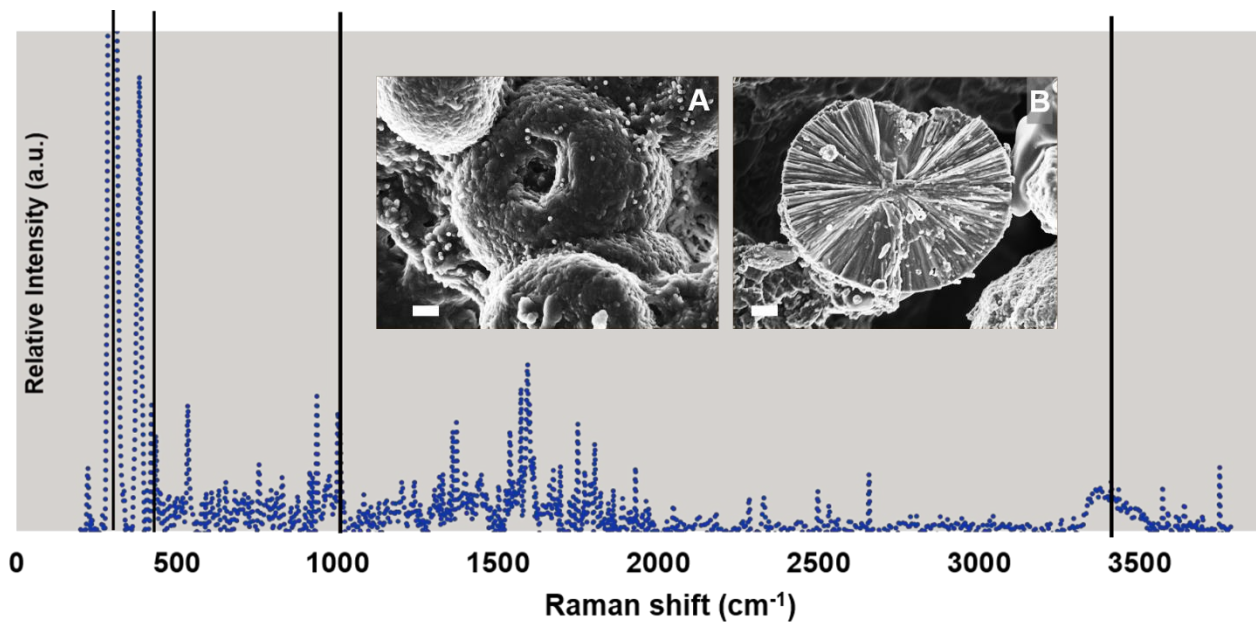


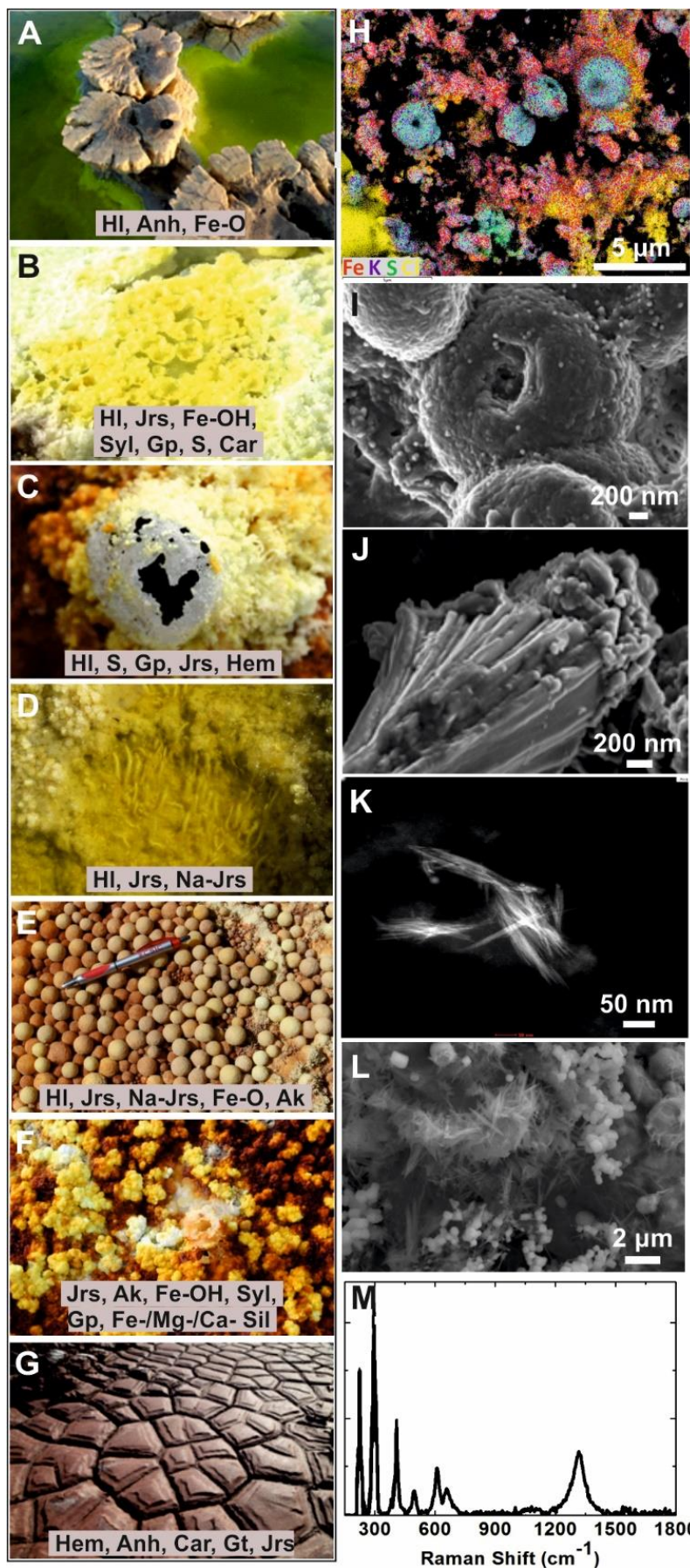
Figure 9. Normalized and background-subtracted Raman spectrum of a brown colored

efflorescence from the Dallol terraces. The characteristic jarosite peaks are marked at 300, 436, 1006 and 3408 cm^{-1} . Typical SEM images of jarosite are shown as well. Scales A, B 200 nm.

Raman scattering from the precipitates did not pick up any organic compounds related to biologic activity, such as bacterial pigments (e.g., carotenoids, chlorophyll) that would produce a set of bands in the region 1000-1600 cm^{-1} and would affect their color (Koyama et al., 1986; Withnall et al., 2003). Therefore, the color of the solids starts as white around the springs, due to the rapid halite crystallization with fluid inclusions, but, turns to yellowish and then to orange and brown as the Fe-oxidation, evaporation, and precipitation of jarosite, akaganeite, hematite and other Fe-oxides takes place as aforementioned. Following aggregation of the Fe-particles, the color intensity is increased to dark-red, brown-purple color. In addition to the sulfur spheroids mentioned above, few nanoparticles of S° and Fe-sulfides were also found dispersed in halite crystals probably deriving from the reduction of Fe(III) trapped in the halite crystals by the hydrogen sulfide gas.

Figure 10. Pictures, microscopic images and mineral composition of different Dallol patterns.

A. Water-lily structures created by subaqueous hydrothermal activity. **B.** Halite flowers with



variable degree of oxidation. **C.** Halite with egg-like shapes forming around gas vents. **D.** Twisted hollow tubes of halite. **E.** Halite pearls. **F.** Efflorescences. **G.** Chocolate bar cracks formed during crystallization of an Fe-rich brine or melt. **H.** FESEM and Fe, K, S, Cl EDX map of a jarosite-rich efflorescence. **I.** FESEM image of jarosite spherules. **J.** FESEM image of part of a jarosite spherule decorated by akaganeite particles. **K.** TEM/HAADF image of the akaganeite nanoparticles. **L.** hematite spindles. **M.** micro-Raman spectrum of the hematite spindles. Mineral abbr.: HI=Halite, Jrs=Jarosite, Na-Jrs=Natrojarosite, Ak=Akaganeite, Gt=Goethite, Fe-OH=Fe-oxyhydroxides, Fe-O=Fe-oxides, Hem=Hematite, Syl=Sylvite, Gp=Gypsum, Anh=Anhydrite, Car=Carnallite, S=Sulfur, Fe-/Mg-/Ca-Sil=Fe-/Mg-/Ca-silicates.

In contrast to other hydrothermal systems, such as Yellowstone, where the color is clearly associated to microbial biofilms (Nugent et al., 2015), the entire color palette of Dallol is the result of inorganic processes. This gradual color variation, ranging from pale green to dark brown and reds, is beautifully displayed in Dallol due to the combined action of the continuous discharge of oxygen-free Fe(II)-rich spring brines, the low solubility of oxygen in high temperature, hyperacidic, hypersaline brines and therefore the slow oxidation of the Fe(II) species. The prevalence of laminar flow in the terrace-pool system and the dominance of diffusion over convection along the entire aqueous pathway from the springs to the pools slow down the dynamics of the system, enabling the discrete display of the stunning colors.

3.3.5. Isotopic study

Dallol spring water has δD values similar to the local meteoric water (-21‰ to -8 ‰ vs V-SMOW) (Craig, 1961; Craig and et al., 1977), while the $\delta^{18}O$ values of the spring water are shifted to more positive values (+5‰ to +8 ‰ vs V-SMOW) indicative of the meteoric water interaction with the underlying evaporites and basaltic flows (Fig. 11) (Appendix, Table S2). The isotopic values of the pool water are both $\delta^{18}O$ and δD enriched as a result of the extreme evaporation rates of the pool water ($\delta^{18}O \sim 10.7\text{‰}$ and $\delta D > +3.2 \text{‰}$). Note that the sample most affected by evaporation corresponds to the lowest, most acidic pool (BP1). Moreover, oxygen isotopic values distinguish Dallol brines from the neighboring sites of Yellow and Black lakes, which exhibit relatively negative $\delta^{18}O$ values (-1‰ to -7 ‰), uncommon for the low latitude of the site (Craig, 1961) (Fig. 11). This indicates different hydrological processes between the geothermal lakes and the system of the dome, that is also reflected in the difference in the hydrochemistry (see Introduction). As shown from other hypersaline systems (Oerter et al., 2018; Sofer and Gat, 1975), the negative δD values of Black and Yellow lakes can be a result of the very high salinity of these Mg-Ca-Cl-rich lakes that are under severe evaporation processes and exhibit complex evolution.

Concerning the dissolved gases of the hydrothermal brines of Dallol, the ratio N_2/Ar shows an excess of N_2 for the spring water indicative of the magmatic influence of the shallow source below the dome, whereas the slightly positive values measured at the pool water result from the subsequent water-atmosphere equilibration (Appendix, Table S3) (Kyser, 1986; Snyder et al., 2003).

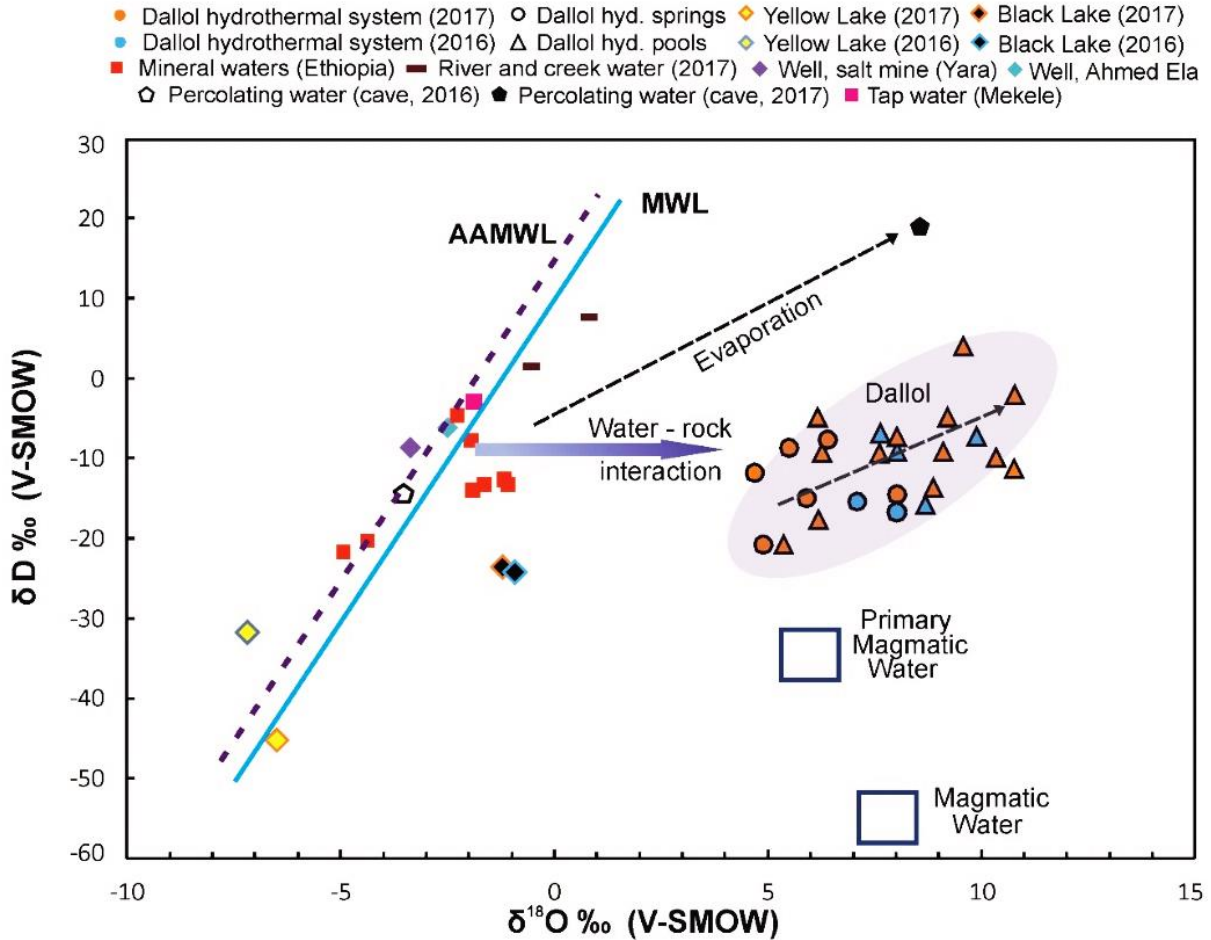


Figure 11. Stable isotope data for the Dallol hydrothermal brines and Black and Yellow Lake waters (2016 and 2017 campaigns). Dallol spring water has $\delta D \text{ ‰}$ values similar to the local meteoric water. The anomalous high $\delta^{18}O$ values of the hot springs indicate the interaction of the meteoric water with the underlying basaltic flows and evaporites. The $\delta^{18}O \text{ ‰}$ and δD values of the Dallol pools are higher due to evaporation processes ($\delta^{18}O > +10 \text{ ‰}$, $\delta D > -10 \text{ ‰}$). Yellow and Black Lake waters exhibit relatively negative values for both δD (-25 ‰ to -48 ‰) and $\delta^{18}O$ (-1 ‰ to -7 ‰) showing distinct hydrological processes with respect to the Dallol dome. MWL: Meteoric Water Line (Craig, 1961); AAMWL: Addis Ababa Meteoric Water Line (Craig and et al., 1977). Magmatic and primary magmatic waters are plotted after (Rye and O'Neil, 1968; Sheppard et al., 1971; Sheppard, 1986).

For the free gases Darrah *et al.*, (Darrah et al., 2013) reported more positive $\delta^{15}N$ values (+2.93 to +4.5) that were interpreted as a source of meta-sediment decomposition. This isotopic evolution of the free gases towards more negative values (see Appendix, Table S1) can be a result of the increased hydrothermal activity over the past years, as shown also in the 2016 and 2017 activity maps of the dome (Fig. 3).

3.3.6. Biogeochemical investigation

The amount of organic matter in the dome is practically zero except for one spring system of grey color explored during the 2017 mission at the SW of the dome (Fig. 2D, S3). The grey color of that spring is owed to amorphous silica and degraded, partially graphitized, organic matter. The silica particles were identified by FESEM as remnants of partially dissolved diatom shells (Fig. 12), while, the measured $\delta^{13}\text{C}$ values of the organic matter (-13‰) are typical of marine algae (Raven et al., 1995). Therefore, both silica and organic matter are considered remnants of fossil diatoms trapped in the evaporitic sequence.

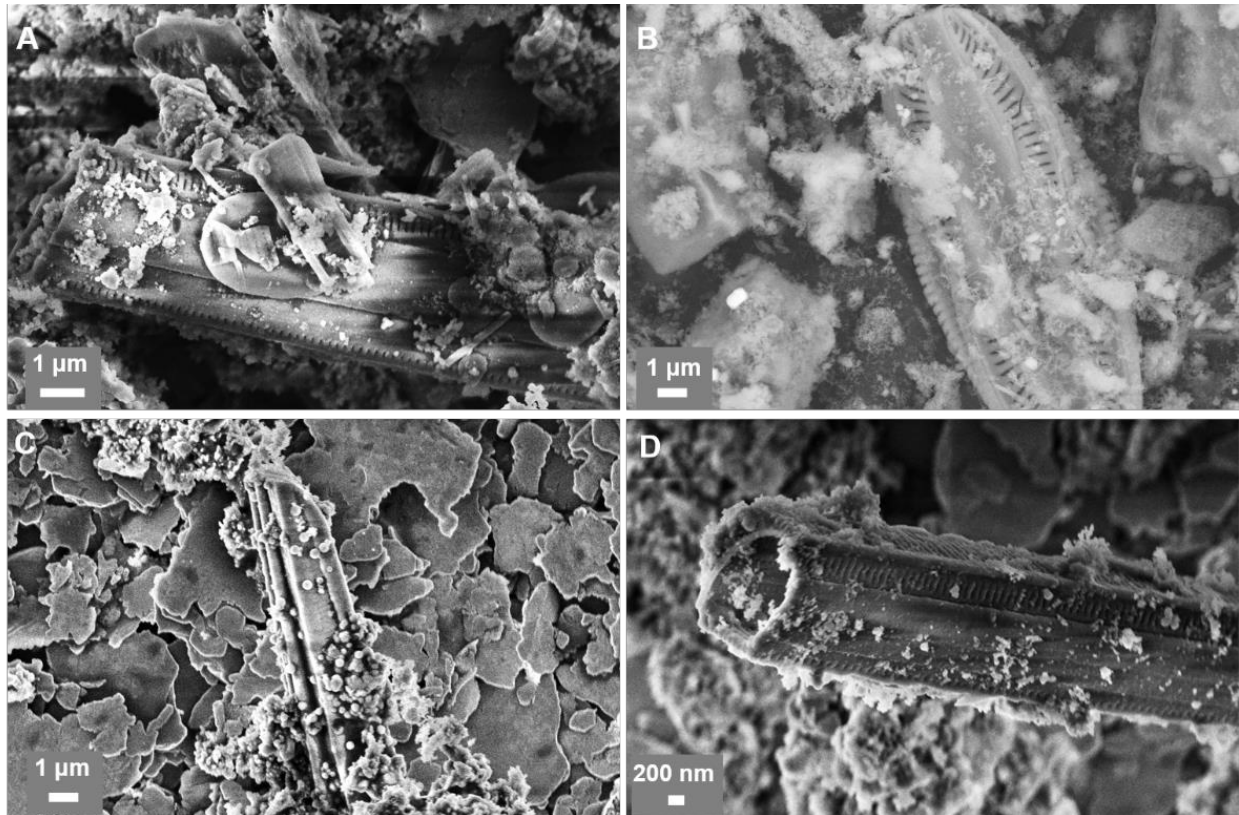


Figure 12. Dissolved diatom shells discharging from the grey spring at the SW of the dome. The diatoms are deriving from the diatomite layers of the Danakil marine evaporitic sequence.

To detect *in situ* the presence of autotrophic and heterotrophic metabolic activity in the hydrothermal pools, incubations of isotopically labeled ^{18}O enriched water and urea- C^{13} respectively were performed, (according to (Grande et al., 1989; Harrison et al., 1985; Mesa et al., 2017; Radajewski et al., 2000; Savidge and Hutley, 1977))(see experimental section for details). The first set of incubations (^{18}O enriched water) was negative for all the samples, confirming the absence of autotrophic activity. The second set of incubations labelled urea with ^{13}C , for the detection of heterotrophic metabolic activity, showed negative results apart from some of the pools that exhibited $\delta^{13}\text{C}$ DIC values exceeding 7000‰ (V-PDB), that should correspond to abundant

biologic activity. The measurement of the positive samples was repeated after four weeks where higher values than the initial were obtained (see Fig. 13A).

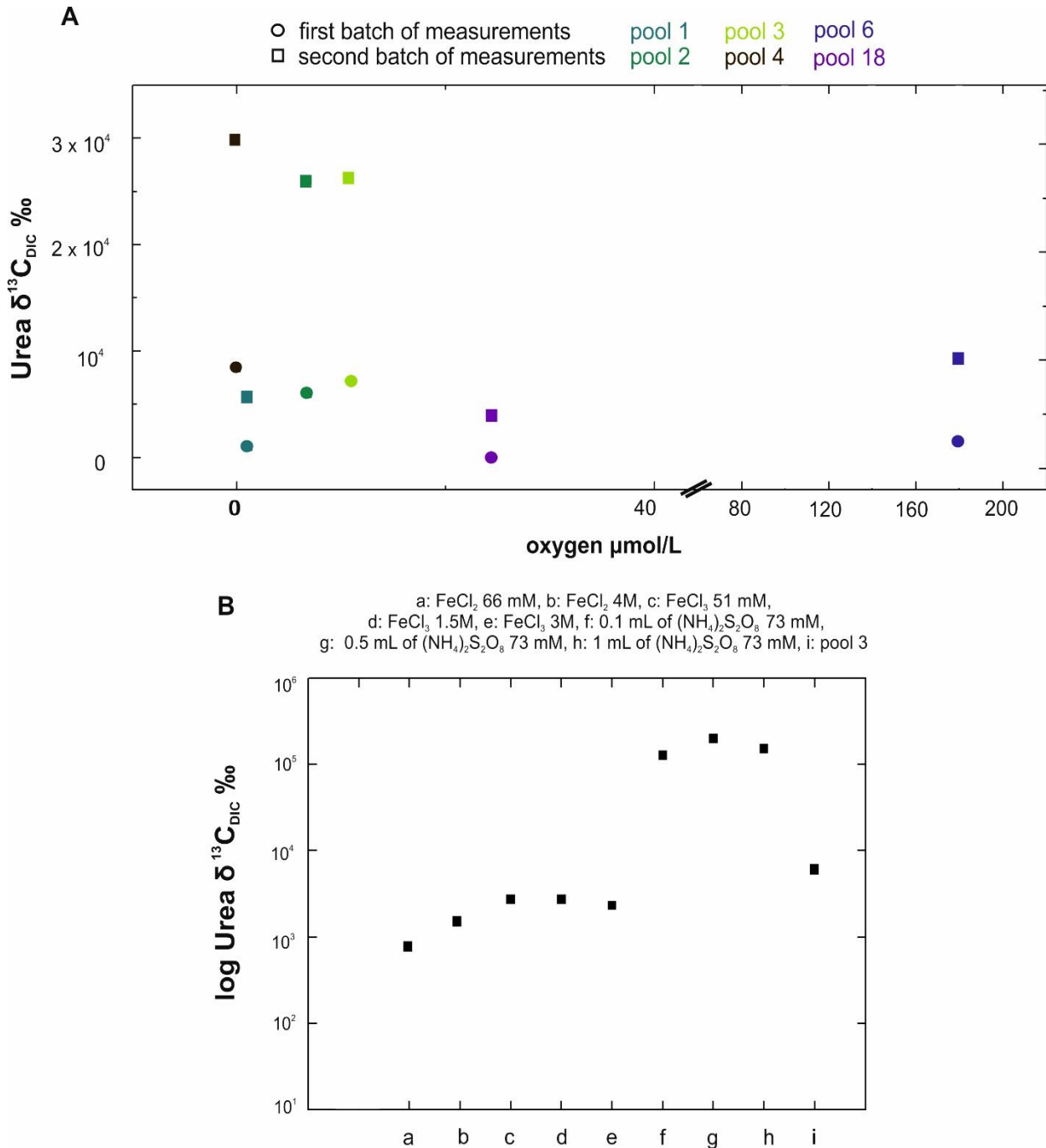


Figure 13. $\delta^{13}\text{C}_{\text{DIC}} \text{ ‰}$ of isotopically labeled Urea for incubations performed in situ and in the laboratory. **A.** First batch and second batch of measurements for pool 1 (P1), pool 2 (P2), pool 3 (P3), pool 4 (P4), pool 6 (P6), pool 18 (P18). **B.** For sterilized FeCl_2 (66 mM), FeCl_2 (4 M), FeCl_3 (51 mM), FeCl_3 (1.5 M), FeCl_3 (3 M), 0.1 ml of $(\text{NH}_4)_2\text{S}_2\text{O}_8$ (73 mM), 0.5 ml of $(\text{NH}_4)_2\text{S}_2\text{O}_8$ (73 mM), 1 ml of $(\text{NH}_4)_2\text{S}_2\text{O}_8$ (73 mM) and sterilized pool (P3).

This isotopic increase cannot be attributed to biologic activity, since after 24 hours of *in situ* incubation and prior to any measurement and the samples were fixed with HgCl_2 (see Methods),

stopping any possible biologic activity. Therefore, the observed increase of $\delta^{13}\text{C}$ CO_2 should occur as a result of inorganic processes. To test the effect of inorganic oxidants in the breaking of urea the same incubation experiment was performed by using sterilized FeCl_2 solutions (66 mM and 4 M), sterilized FeCl_3 solutions (51 mM, 1.5 M and 3 M), sterilized $(\text{NH}_4)_2\text{S}_2\text{O}_8$ solutions (73 mM) and sterilized pool water of Dallol (P3) (Fig. 13B and Appendix Table S4). All the sterile experiments were $\delta^{13}\text{C}$ positive and as illustrated in Fig. 10b, the stronger the oxidant, the higher the value of the measured $\delta^{13}\text{C}$ DIC. Overall, both incubations did not identify traces of biological activity, while it became evident that in such extreme hydrochemical conditions inorganic processes may overprint possible biologic ones.

Likewise, no microorganisms were present in fixed filters of Dallol brines studied by FESEM-EDS (see experimental part for sample preparation and fixation). In one efflorescence sample features resembling bacilli-type bacteria were observed (Fig 14), however considering that these type of bacteria are common contaminants and that they were only encountered in one solid sample, the scenario that they belong to active microorganisms is discarded. Moreover, complementary Raman study of numerous efflorescences and precipitates did not pick up any organic compounds.

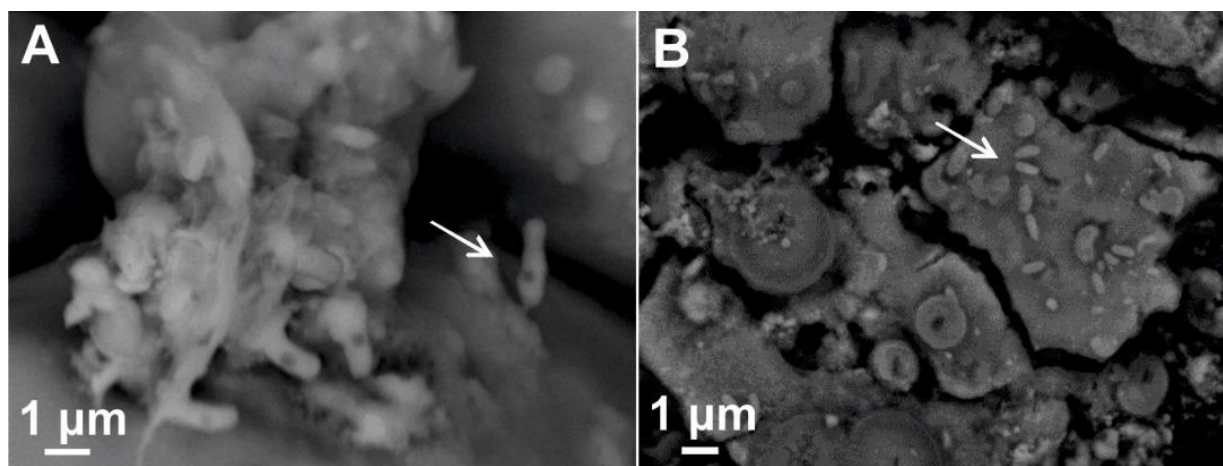


Figure 14. SEM images of brown efflorescences showing features that resemble bacilli bacteria, typical contaminant species during sample handling and preparation.

3.3.7. Microbiologic review

At the same time, two studies were published on the microbiologic investigation of samples from Dallol. Gomez et al., (2019) reported the presence of Nanohaloarchaea from two sites at Dallol, a chimney where spring water of 0.25 pH and 86 °C was discharging and the surrounding pool of 2.42 pH and 47 °C. Nevertheless, there are some points that are raising doubts about both the bulk mineralogical and the microbiologic study they performed. A major criticism concerns the

presence of chlorargyrite (AgCl), wurtzite (ZnS), and pyrolusite (MnO₂) that are reported as main phases along with halite and were identified by bulk XRD. Apart from halite, the rest of the aforementioned minerals have not been encountered by this work after characterizing various samples from all sorts of precipitates and mineral phases of the dome with the use of several techniques (XRD, FESEM-EDS, micro-Raman, HRTEM). With respect to chlorargyrite -a secondary mineral phase at the oxidation of silver mineral deposits- it should be mentioned that Ag is not present in the brines (below detection limit). Moreover, the crystal structure and therefore the XRD pattern of the AgCl is very similar to the NaCl and might appear falsely as a possible match by phase identifications softwares. Similarly, the identification of wurtzite and pyrolusite by powder XRD is challenging, because the mineralogical dominance of halite hinders the identification of the rest of the phases, especially that of minor phases such as wurtzite and pyrolusite. Also none of the other major phases (apart from halite), such as jarosite, gypsum and akaganeite that are precipitating on the chimneys were mentioned in the work by Gomez et al., (2019). Other vague points in the Gomez et al., article are the mismatches in the description of their site 1 that is referred as an active spring and its respective image (Fig. 3 in Gomez et al.,) that demonstrates an inactive, dry chimney, and, in the scales of the SEM and TEM images of the putative nanoarchaea (Gomez et al., 2019, figures 6 and 7). Last but not least, the presence of Nanohaloarchaea is only reported in two samples and without presenting the accession numbers for their sequences, as is commonly done. Therefore, and in light of what has been mentioned so far, both the geochemical and microbiological results by Gomez et al., (2019) are confronted with certain skepticism.

On the other hand, another recent study by Belilla et al, (2019), investigated various samples from different locations of the hydrothermal system of Dallol, the neighboring Salt Canyon and Black and Yellow lakes for the presence of microorganisms. They demonstrated that life existed only in the less extreme locations, i.e. liquid and solid surfaces where only a single parameter, either pH or salinity, showed extreme values. That is in the salt plain/canyon, Lake Assale and not in the dome of Dallol, nor in Black and Yellow Lakes. Consistent with metabarcoding results, and despite the use of various culture media and growth conditions mimicking local environments, cultural approaches did not yield enrichments for any of the Dallol dome, Black and Yellow lake samples. Likewise, multi-parametric fluorescence analysis showed no DNA fluorescence above background for Dallol and Yellow Lake samples (Belilla et al., Fig. S6) and fluorescence-activated cell-sorting (FACS) was only related to salt crystals and silica biomorphic casts resulting from the diatoms dissolution (see Fig.11).

It is well known that life can tolerate or even thrive in extreme conditions. Fascinating organisms can tolerate temperatures as high as 122 °C (*Methanopyrus kandleri*, strain 116) or hyperacidic environments with pH close to zero (*Ferroplasma acidarmanus*) or a combination of both, as for the poly-extremophilic archaea *Sulfolobus acidocaldarius*, that flourishes at 80 °C and pH 3 and the *Picrophilus torridus* that grows optimally at 60 °C and pH 0 (Rampelotto, 2013; Rothschild and Mancinelli, 2001). However, so far, no strains have been discovered to grow under the joint extremes of high temperature, salinity, and pH, raising the question of whether life is possible under polyextreme conditions (Harrison et al., 2013) (Fig. 15). The absence of active microorganisms on Dallol dome and for the Black and Yellow Lakes seems to be related with the hyperacid-hypersaline combinations (pH<3; salt>30%) and the high chaotrophic salt concentration and low water activity (magnesium-rich brines) respectively, as expected. This suggests that that molecular adaptations to simultaneous low-pH and high-salt extremes are incompatible, while high external Cl⁻ concentrations inducing H⁺ and cation (K⁺/Na⁺) import probably disrupt the cell membrane bioenergetics (Merino et al., 2019; Belilla et al., 2019).

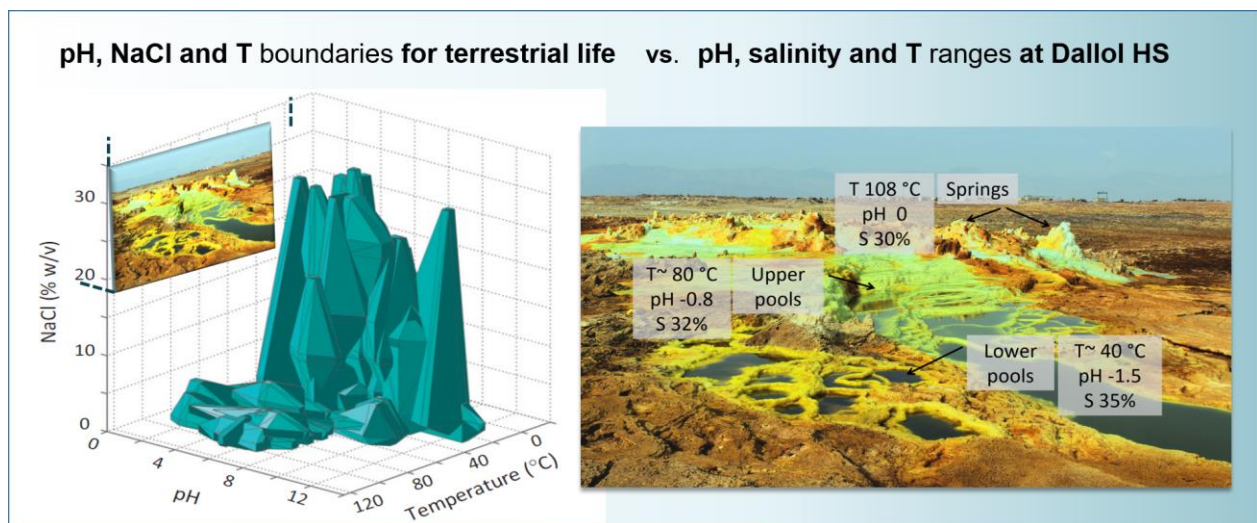


Figure 15. Known boundaries of pH, NaCl (% w/v) and temperature (°C) for terrestrial life versus pH, salinity (% w/v) and temperature (°C) values at the Dallol hydrothermal system (HS). Habitable volumes were estimated using cardinal growth range data obtained for 67 strains of prokaryotic extremophiles, with each polyhedron representing an individual taxon. Notice that no strains have been discovered to grow under the joint extremes of high temperature, salinity, and pH (modified after Harrison et al., 2013).

3.3.8. Dallol, an analogue-site for abiotic iron mineral precipitation

The finding that no microorganisms live in Dallol brines support what is being demonstrated in this thesis, that in Dallol, the geochemical cycling, mineral precipitation and oxidation are

inorganic. This finding makes Dallol a natural laboratory for the self-organization of iron minerals and one of the very few present-day sites where we can witness the progressive oxidation of the iron precipitates as possibly occurred in early Earth, during the transition from anoxic-suboxic to oxygen-rich conditions (Bekker et al., 2004; Canfield, 2005; Halevy et al., 2017; Lyons et al., 2014). Moreover, the mineralogical prevalence of jarosite and related sulfates, and akaganeite and related Fe-oxyhydroxides in the precipitates of Dallol that have been also identified on different Martian geological sites (Amils et al., 2014; Bishop et al., 2015; Klingelhofer et al., 2004), the minor microbiologic and anthropogenic contamination of the dome, as well as, the intense iron corrosion, render Dallol a terrestrial Martian analogue-site of interest for future space missions. Nevertheless, given the plethora of inorganic patterns that are resembling biologic features all around the dome, such as those shown in Fig. 9., it is clear that precipitation processes occurring in hydrothermal vents may give rise to inorganic features that mimic fossil bacterial forms or bioproducts and this has direct implications for life detection studies on Earth and beyond.

3.3.9. Fe-silica self-organized membranes grown from the Dallol spring water

Finally, the chemical resemblance of the Dallol spring water to the acidic Fe-chloride solution used for the growth of the synthetic Fe-silica membranes, coupled with the absence of microorganisms in Dallol brines renders Dallol spring water an ideal solution for exploring natural Fe-silica membrane precipitation. In this context, Fe-silica membranes were grown from the Dallol spring water (pH~0, Fe: 26 g/L, T: 25 °C), modifying the typical protocol described previously, by injecting 1 mL of the pristine Dallol solution into 3 mL of the sodium silicate solution. The spring water had been preserved in oxygen-free conditions inside septum-sealed glass vials (see experimental section and sampling) and the membrane growth experiment was performed inside the glovebox chamber (N₂ atmosphere). For this experiment the silica sol was prepared with the use of Ar-purged Milli-Q water inside the glovebox (1:4 dilution).

By mixing the Dallol water with the silicate sol, consecutive vesicle-type membranes are formed, a typical feature of iron-silica garden growth by microdrops injection (Kotopoulou et al., 2017; Bizzari et al., 2018) (Fig. 16). Aging of the vesicle walls leads to a change of color from light green to dark green. After the formation of the membranes, silica and sodium hydroxide precipitation follows, embedding the membranes.

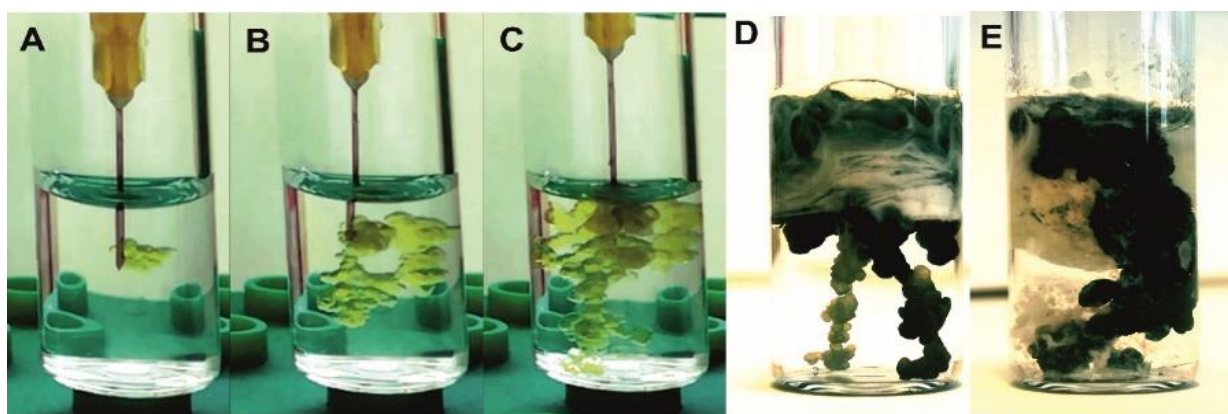


Figure 16. Growth of iron-silica membranes from the anoxic Dallol water in oxygen-free conditions. A-C. Time lapse of the formation of the membranes showing a botryoidal shape obtained from consecutive membrane bursting and re-precipitation. D-E. Final stages of membrane formation where there is a change in the color from light green to dark-green due to membrane wall thickening.

The iron-silica membranes grown from the Dallol water show also the typical compositional and textural gradients across the membrane, as seen by FESEM-EDS and Raman study. As indicated in Fig. 17 the outer membrane wall is rich in silica and sodium hydroxide/chlorides and the inner wall is rich in Fe-(oxy)hydroxides, in agreement to what is observed in the typical membranes (see Introduction). Using Raman spectroscopy, I identified hematite, goethite and akaganeite in the inner membrane wall (Fig. 17).

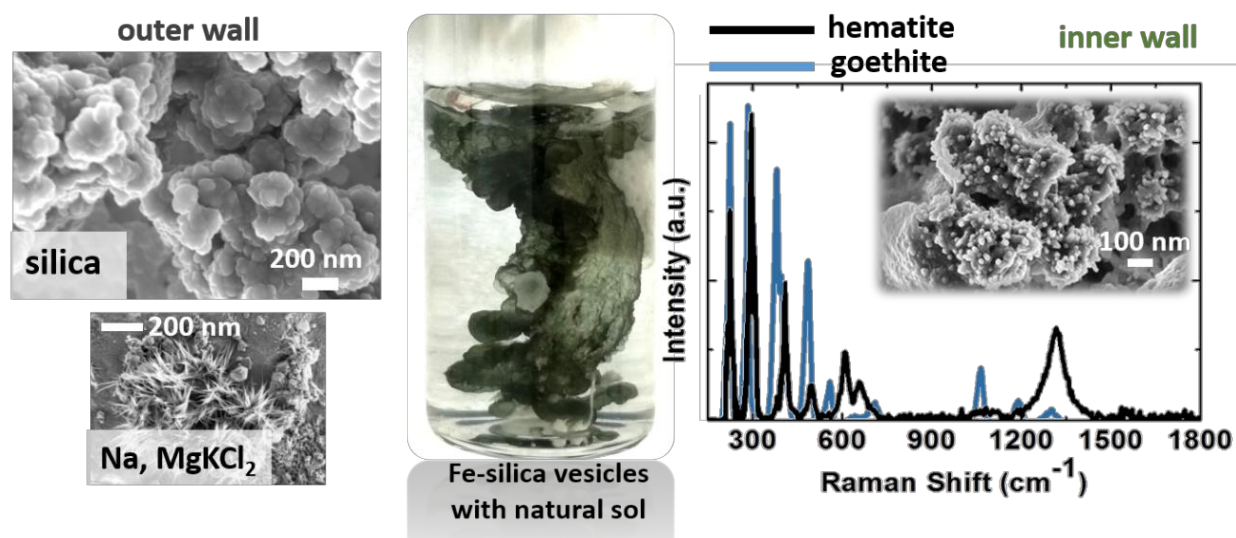


Figure 17. SEM images and Raman spectra of iron-silica membranes in the form of botryoidal vesicles grown by mixing of the Dallol water and a silicate solution. As in the typical iron-silica membranes the outer part is silica-rich and the inner iron-rich composed of hematite, akaganeite and goethite as shown by Raman.

3.4. Findings and concluding remarks

- This thesis chapter reports on a terrestrial polyextreme hydrothermal system that combines hyperacidic to hypersaline conditions though to impose a geochemical barrier to life, known as the ‘Dallol dome’ in NE Ethiopia.
- In situ measurements and hydrochemical analysis of the fluids showed that the Dallol brines are hyperacidic (near to zero pH and down to -1.7), hypersaline (< 30%) and oxygen-free, containing up to 150 g/L of iron.
- To determine the redox state across the aqueous system of Dallol I measured the concentration of Fe(II) and Fe(III) species, in different spring solutions and related pools by using UV-Vis spectroscopy.
- Also, UV-Vis and Raman spectroscopies were used for the identification of the species responsible for the colors of the brines. The light green color of the spring and upper pools is owed to ferrous species, mainly associated with the $[\text{FeII}(\text{H}_2\text{O})_6]^{2+}$ complex. Moving from the upper green to the lower yellow pools, the $[\text{FeII}(\text{H}_2\text{O})_6]^{2+}$ is oxidized and the hexaquairon complex $[\text{FeIII}(\text{H}_2\text{O})_6]^{3+}$ undergoes hydrolysis to form progressive hydroxo-species, namely $[\text{Fe}(\text{OH})(\text{H}_2\text{O})_5]^{2+}$ and $[\text{Fe}(\text{OH})_2(\text{H}_2\text{O})_4]^+$ with the accompanying pH drop.
- In contrast to other hydrothermal systems, such as Yellowstone, where the color is clearly associated to microbial biofilms, the entire color palette of Dallol is the result of inorganic processes.
- In situ incubations of isotopically-labeled enriched oxygen and urea in the hydrothermal pools were performed for 48h to detect in situ heterotrophic and autotrophic activity but no biologic activity was detected. Likewise, no microorganisms were observed in microscopic study of fixed filter samples from the hydrothermal terraces and brines. Recent microbiological studies confirmed the absence of any microbial activity in the brines of Dallol.

- The amount of organic matter in the dome is practically zero except for one spring system of gray color rich in dissolved diatoms and partially graphitized, organic matter. Isotopic analysis of the $\delta^{13}\text{C}$ values of the organic matter (-13‰) showed they are typical of marine algae, therefore, both silica and organic matter are considered remnants of fossil diatoms trapped in the evaporitic sequence.
- The mineralogy of precipitates, patterns and biomorphic structures was investigated by using a series of techniques (PXRD, in situ Raman, micro-Raman, FESEM-EDS, TEM). Regarding the solids halite is the dominant macro-crystalline phase found all over the Dallol dome, producing an impressive array of complex mineral patterns. Among them are: i) hydrothermal salt-pillars up to 4 meters high, ii) water-lily structures forming in subaqueous springs, iii) flower-like crystals growing in lower pools by extreme evaporation, iv) egg-shaped thin crusts, hollow twisted tubes and pearl-like spheres around active gas gateways, v) various types of efflorescences, and vi) polygonal cracking patterns resembling pieces in a chocolate bar.
- Apart from halite crystals, microcrystals of Na-/K-/Ca-/Mg-salts, such as, gypsum ($\text{CaSO}_4 \cdot 2\text{H}_2\text{O}$), sodium-sulfates, sylvite (KCl) and carnallite ($\text{KMgCl}_3 \cdot 6\text{H}_2\text{O}$) were common.
- Fe-(oxy)hydroxides/sulfates, mainly jarosite ($\text{KFe}_3 + 3(\text{SO}_4)_2(\text{OH})_6$) and akaganeite ($\beta\text{-Fe}_3 + \text{O}(\text{OH}, \text{Cl})$) form a colorful veil over all the mineral patterns and are responsible for the color diversity and color evolution of the solids with time.
- Hydrochemical, isotopic, spectroscopic and mineralogical study demonstrated that the hyperacidic pH, the brine evolution, the color palette and the mineral paragenesis are controlled by inorganic processes, related to ferrous iron oxidation and iron complexation with chlorides and sulfates.
- At Dallol iron cycling, iron oxidation and mineral precipitation are abiotic, unlike other submarine and terrestrial hydrothermal systems where microorganisms actively interfere in the elemental cycling and mineral precipitation.

- If microorganisms are ever found in Dallol polyextreme hydrothermal brines their existence would expand the limit of life supporting habitance on Earth and Earth-like planets, as we currently understand it, rendering Dallol a site of unique astrobiological significance. Until then, Dallol is the only present-day site we currently know of where we can witness iron mineral self-organization and progressive oxidation as possibly occurred at the early Earth when life was neither affecting, nor, inducing mineralization.
- Finally, the growth of iron-silica membranes from the Dallol water demonstrates that iron-silica mineral self-organization can occur even at the hydrochemical extremes, as long as the two main reacting species are iron cations and silicate anions. This finding, amplifies the environments where self-organizing mineral membranes may have at some moment assisted the adsorption, catalysis and organization of organic molecules as discussed in the previous chapter.

References

- Agusto, M.R., Caselli, A., Daga, R., Varekamp, J., Trinelli, A., Dos Santos Afonso, M., Velez, M.L., Euillades, P., Ribeiro Guevara, S., 2016. The crater lake of Copahue volcano (Argentina): geochemical and thermal changes between 1995 and 2015, in: Ohba, T., Capaccioni, B., Caudron, C. (Eds.), *Geochemistry and Geophysics of Active Volcanic Lakes*. Geological Society, London, Special Publications, pp. 107-130.
- Amils, R., Fernandez-Remolar, D., The Ipbsl, T., 2014. Rio tinto: a geochemical and mineralogical terrestrial analogue of Mars. *Life* 4, 511-534.
- Bekker, A., Holland, H.D., Wang, P.L., Rumble Iii, D., Stein, H.J., Hannah, J.L., Coetzee, L.L., Beukes, N.J., 2004. Dating the rise of atmospheric oxygen. *Nature* 427, 117.
- Belilla, J., Moreira, D., Jardillier, L. et al., 2019. Hyperdiverse archaea near life limits at the polyextreme geothermal Dallol area. *Nat Ecol Evol* 3, 1552–1561, doi:10.1038/s41559-019-1005-0.
- Berhanu, B., Seleshi, Y., and Melesse, A.M., 2014. Surface Water and Groundwater Resources of Ethiopia: Potentials and Challenges of Water Resources Development, in: A. M. Melesse et al. (eds.) (Ed.), Nile River Basin, Ecohydrological Challenges, Climate Change and Hydropolitics. Springer.
- Bishop, J.L., Murad, E., Dyar, M.D., 2015. Akaganeite and schwertmannite: Spectral properties and geochemical implications of their possible presence on Mars. *American Mineralogist* 100, 738-746.
- Bonatti, E., Fisher, D.E., Joensuu, O., Rydell, H.S., Beyth, M., 1972. Iron-Manganese-Barium Deposit from the Northern Afar Rift (Ethiopia). *Econ. Geol.* 67, 717-730.
- Canfield, D.E., 2005. The early history of atmospheric oxygen Homage to Robert M. Garrels. *Annual Review of Earth and Planetary Sciences* 33, 1-36.
- Carniel, R., Jolis, E.M., Jones, J., 2010. A geophysical multi-parametric analysis of hydrothermal activity at Dallol, Ethiopia. *Journal of African Earth Sciences* 58, 812-819.
- Christenson, B.W., Wood, C.P., 1993. Evolution of a vent-hosted hydrothermal system beneath Ruapehu Crater Lake, New Zealand. *Bull Volcanol* 55, 547-565.
- Colvin, A., Rose, W.I., Varekamp, J.C., Palma, J.L., Escobar, D., Gutierrez, E., Montalvo, F., and Maclean, A., 2013. Crater lake evolution at Santa Ana Volcano (El Salvador) following the 2005 eruption, in: Rose, W.I., Palma, J.L., Delgado Granados, H., and Varley, N., eds. (Ed.), Understanding Open-Vent Volcanism and Related Hazards: Geological Society of America Special Paper 498, *Geological Society of America*, pp. p. 23–43.
- Craig, H., 1961. Isotopic Variations in Meteoric Waters. *Science* 133, 1702-1703.
- Craig, H., 1969. Geochemistry and origin of the Red Sea brines, in: Degens, E.T., Ross, D.A. (Eds.), Hot brines and recent heavy metal deposits in the Red Sea, A geochemical and geophysical account. Springer, pp. 208-242.
- Craig, H., et al., 1977. Geochemistry and Hydrology of Geothermal Waters in the Ethiopian Rift Valley, Isotope Lab Scripps Institution of Oceanography, University of California at San Diego, USA, California, San Diego, USA, p. 140.

- Darrah, T.H., Tedesco, D., Tassi, F., Vaselli, O., Cuoco, E., Poreda, R.J., 2013. Gas chemistry of the Dallol region of the Danakil Depression in the Afar region of the northern-most East African Rift. *Chemical Geology* 339, 16-29.
- Delmelle, P., Bernard, A., 2000. Downstream composition changes of acidic volcanic waters discharged into the Banyupahit stream, Ijen caldera, Indonesia. *J. Volcanol. Geotherm. Res.* 95, 55-75.
- Ebinger, C.J., Casey, M., 2001. Continental breakup in magmatic provinces: An Ethiopian Example. *Geology* 29, 527-530.
- Fazzini, M., Bisci, C., Billi, P., 2015. The climate of Ethiopia, in: (ed.), P.B. (Ed.), *Landscapes and Landforms of Ethiopia*. Springer.
- Fernández-Remolar, D.C., Morris, R.V., Gruener, J.E., Amils, R., Knoll, A.H., , 2005. The Rio Tinto Basin, Spain: Mineralogy, sedimentary geobiology, and implications for interpretation of outcrop rocks at Meridiani Planum, Mars. . *Earth Planet. Sci. Lett.* 240, , 149-167.
- Grande, K.D., Williams, P.J.L., Marra, J., Purdie, D.A., Heinemann, K., Eppley, R.W., Bender, M.L., 1989. Primary production in the North Pacific gyre: a comparison of rates determined by the ¹⁴C, O₂ concentration and ¹⁸O methods. *Deep Sea Research Part A. Oceanographic Research Papers* 36, 1621-1634.
- Gómez, F., Cavalazzi, B., Rodríguez, N. et al., 2019. Ultra-small microorganisms in the polyextreme conditions of the Dallol volcano, Northern Afar, Ethiopia. *Sci Rep* 9, 7907, doi:10.1038/s41598-019-44440-8.
- Halevy, I., Alesker, M., Schuster, E.M., Popovitz-Biro, R., Feldman, Y., 2017. A key role for green rust in the Precambrian oceans and the genesis of iron formations. *Nature Geoscience* 10, 135-139.
- Harrison, J.P., Gheeraert, N., Tsigelnitskiy, D., Cockell, C.S., 2013. The limits for life under multiple extremes. *Trends Microbiol* 21, 204-212.
- Harrison, W.G., Head, E.J.H., Conover, R.J., Longhurst, A.R., Sameoto, D.D., 1985. The distribution and metabolism of urea in the eastern Canadian Arctic. *Deep Sea Research Part A. Oceanographic Research Papers* 32, 23-42.
- Heinrich, C.A., Seward, T.M., 1990. A spectrophotometric study of aqueous iron (II) chloride complexing from 25 to 200°C. *Geochimica et Cosmochimica Acta* 54, 2207-2221.
- Holwerda, J.G., Hutchinson, R.W., 1968. Potash-bearing evaporites in the Danakil Region, Ethiopia. *Econ. Geol.* 63, 124-150.
- Hovland, M., Rueslåtten, H.G., Johnsen, H.K., Kvamme, B., Kuznetsova, T., 2006. Salt formation associated with sub-surface boiling and supercritical water. *Marine and Petroleum Geology* 23, 855-869.
- Inguaggiato, C., Censi, P., Zuddas, P., Londoño, J.M., Chacón, Z., Alzate, D., Brusca, L., D'Alessandro, W., 2015. Geochemistry of REE, Zr and Hf in a wide range of pH and water composition: The Nevado del Ruiz volcano-hydrothermal system (Colombia). *Chemical Geology* 417, 125-133.
- Kalacheva, E., Taran, Y., Kotenko, T., Hattori, K., Kotenko, L., Solis-Pichardo, G., 2016. Volcano–hydrothermal system of Ebeko volcano, Paramushir, Kuril Islands: Geochemistry and

solute fluxes of magmatic chlorine and sulfur. *Journal of Volcanology and Geothermal Research* 310, 118-131.

Kanno, H., Iraishi, J., 1982. A Raman study of aqueous solutions of Ferric Nitrate, Ferrous Chloride and Ferric Chloride in the Glassy State. *J. of Raman Spectroscopy* 12, 224-227.

Keir, D., Bastow, I.D., Pagli, C., Chambers, E.L., 2013. The development of extension and magmatism in the Red Sea rift of Afar. *Tectonophysics* 607, 98-114.

Klingelhofer, G., Morris, R.V., Bernhardt, B., Schroder, C., Rodionov, D.S., de Souza, P.A., Jr., Yen, A., Gellert, R., Evlanov, E.N., Zubkov, B., Foh, J., Bonnes, U., Kankeleit, E., Gutlich, P., Ming, D.W., Renz, F., Wdowiak, T., Squyres, S.W., Arvidson, R.E., 2004. Jarosite and hematite at Meridiani Planum from Opportunity's Mössbauer Spectrometer. *Science* 306, 1740-1745.

Koyama, Y., Umemoto, Y., Akamatsu, A., Uehara, K., Tanaka, M., 1986. Raman spectra of chlorophyll forms. *Journal of Molecular Structure* 146, 273-287.

Kyser, T.K., 1986. Stable isotope variations in the mantle. *Reviews in Mineralogy and Geochemistry* 16, 141-164.

Lyons, T.W., Reinhard, C.T., Planavsky, N.J., 2014. The rise of oxygen in Earth's early ocean and atmosphere. *Nature* 506, 307-315.

Makris, J., Ginzburg, A., 1987. The Afar Depression: transition between continental rifting and sea-floor spreading. *Tectonophysics* 141, 199-214.

Merino, N., Aronson, H.S., Bojanova, D.P., Feyhl-Buska, J., Wong, M.L., Zhang, S., Giovannelli, D., 2019. Living at the Extremes: Extremophiles and the Limits of Life in a Planetary Context, *Frontiers in Microbiology*, 10, 780.

Mesa, E., Delgado-Huertas, A., Carrillo-de-Albornoz, P., Garcia-Corral, L.S., Sanz-Martin, M., Wassmann, P., Reigstad, M., Sejr, M., Dalsgaard, T., Duarte, C.M., 2017. Continuous daylight in the high-Arctic summer supports high plankton respiration rates compared to those supported in the dark. *Scientific reports* 7, 1247.

Millero, F.J., 1986. The thermodynamics and kinetics of the hydrogen sulfide system in natural waters. *Marine Chemistry* 18, 121-147.

Nobile, A., Pagli, C., Keir, D., Wright, T.J., Ayele, A., Ruch, J., Acocella, V., 2012. Dike-fault interaction during the 2004 Dallol intrusion at the northern edge of the Erta Ale Ridge (Afar, Ethiopia). *Geophysical Research Letters* 39, L19305.

Nordstrom, D.K., Alpers, C.N., Ptacek, K.J., Blowers, D.W., 2000. Negative pH and Extremely Acidic Mine Waters from Iron Mountain, California. *Environ. Sci. Technol.* 34, 254-258.

Nugent, P.W., Shaw, J.A., Vollmer, M., 2015. Colors of thermal pools at Yellowstone National Park. *Appl Opt* 54, B128-139.

Oerter, E.J., Singleton, M., Davisson, M.L., 2018. Hydrogen and oxygen stable isotope dynamics of hyper-saline and salt-saturated aqueous solutions. *Geochimica et Cosmochimica Acta* 238, 316-328.

Ohmoto, H., Lasaga, A.C., 1982. Kinetics of reactions between aqueous sulfates and sulfides in hydrothermal systems. *Geochimica et Cosmochimica Acta* 46, 1727-1745.

- Pagli, C., Wright, T.J., Ebinger, C.J., Yun, S.-H., Cann, J.R., Barnie, T., Ayele, A., 2012. Shallow axial magma chamber at the slow-spreading Erta Ale Ridge. *Nature Geoscience* 5, 284-288.
- Pehkonen, S., 1995. Determination of the Oxidation States of Iron in Natural Waters. *Analyst* 120, 2655-2663.
- Pérez, E., Chebude, Y., 2017. Chemical Analysis of Gaet'ale, a Hypersaline Pond in Danakil Depression (Ethiopia): New Record for the Most Saline Water Body on Earth. *Aquatic Geochemistry* 23, 109-117.
- Pittwell, L.R., 1972. Some coordination effects in natural waters of Ethiopia. *Journal of Hydrology* 17, 225-228.
- Prodehl, C.M., J., 1991. Crustal thinning in relationship to the evolution of the Afro-Arabian rift system: a review of seismic refraction data. *Tectonophysics* 198, 311-327.
- Radajewski, S., Ineson, P., Parekh, N.R., Murrell, J.C., 2000. Stable-isotope probing as a tool in microbial ecology. *Nature* 403, 646-649.
- Rampelotto, P.H., 2013. Extremophiles and extreme environments. *Life* 3, 482-485.
- Raven, J.A., Walker, D.I., Johnston, A.M., Handley, L.L., xfc, bler, J.E., 1995. Implications of ¹³C natural abundance measurements for photosynthetic performance by marine macrophytes in their natural environment. *Marine Ecology Progress Series* 123, 193-205.
- Rodríguez, A., van Bergen, M.J., 2017. Superficial alteration mineralogy in active volcanic systems: An example of Poás volcano, Costa Rica. *Journal of Volcanology and Geothermal Research* 346, 54-80.
- Rodríguez, A., Varekamp, J.C., van Bergen, M.J., Kading, T.J., Oonk, P., Gammons, C.H., Gilmore, M., 2016. Acid Rivers and Lakes at Cavihue-Copahue Volcano as Potential Terrestrial Analogues for Aqueous Paleo-Environments on Mars, in: (eds.), F.T.e.a. (Ed.), Copahue Volcano, *Active Volcanoes of the World*, pp. 141-172.
- Rothschild, L.J., Mancinelli, R.L., 2001. Life in extreme environments. *Nature* 409, 1092-1101.
- Rowe, G.L., Brantley, S.L., Fernandez, M., Fernandez, J.F., Borgia, A., Barquero, J., 1992. Fluid-volcano interaction in an active stratovolcano: the crater lake system of Poás volcano, Costa Rica. *Journal of Volcanology and Geothermal Research* 49, 23-51.
- Rudolph, W., Brooker, M.H., Tremaine, P.R., 1997. Raman Spectroscopic Investigation of Aqueous FeSO₄ in Neutral and Acidic Solutions from 25 C to 303 C Inner and Outer-Sphere Complexes. *Journal of Solution Chemistry* 26, 757-767.
- Rull, F., Sobrón, F., 1994. Band profile analysis of the Raman spectra of sulphate ions in aqueous solutions. *J. of Raman Spectroscopy* 25, 693-698.
- Rye, R.O., O'Neil, J.R., 1968. The O18 content of water in primary fluid inclusions from Providencia, north-central Mexico. *Economic Geology* 63, 232-238.
- Salata, G.G., Roelke, L. A. & Cifuentes, L. A. , 2000. A rapid and precise method for measuring stable carbon isotope ratios of dissolved inorganic carbon. *Marine Chemistry* 69, 153-161.

- Savidge, G., Hutley, H.T., 1977. Rates of remineralization and assimilation of urea by fractionated plankton populations in coastal waters. *Journal of Experimental Marine Biology and Ecology* 28, 1-16.
- Sharp, Z.D., Atudorei, V. & Durakiewicz, T., 2001. A rapid method for determination of hydrogen and oxygen isotope ratios from water and hydrous minerals. *Chemical Geology* 178, 197–210.
- Sheppard, S.M., Nielsen, R.L., Taylor, H.P., 1971. Hydrogen and oxygen isotope ratios in minerals from porphyry copper deposits. *Economic Geology* 66, 515-542.
- Sheppard, S.M.F., 1986. Characterization and isotopic variations in natural waters, in: Alley, J.W., Taylor, H.P.J., J.R., O.N. (Eds.), *Stable Isotopes in High Temperature Geological Processes*, pp. 165–184.
- Snyder, G., Poreda, R., Fehn, U., Hunt, A., 2003. Sources of nitrogen and methane in Central American geothermal settings: Noble gas and ^{129}I evidence for crustal and magmatic volatile components. *Geochemistry, Geophysics, Geosystems* 4, 1-28.
- Sofer, Z., Gat, J., 1975. The isotope composition of evaporating brines: effect of the isotopic activity ratio in saline solutions. *Earth Planet. Sci. Lett.* 26, 179-186.
- Stefánsson, A., Seward, T.M., 2008. A spectrophotometric study of iron(III) hydrolysis in aqueous solutions to 200 °C. *Chemical Geology* 249, 227-235.
- Varekamp, J.C., Ouimette, A.P., Herman, S.W., Flynn, K.S., Bermudez, A., Delpino, D., 2009. Naturally acid waters from Copahue volcano, Argentina. *Applied Geochemistry* 24, 208-220.
- Warren, J.K., 2015. Danakil Potash, Ethiopia: Beds of Kainite-Carnallite, Part 2 of 4, Danakil Potash, Ethiopia.
- Withnall, R., Chowdhry, B.Z., Edwards, S.J., F., d.O.L., 2003. Raman spectra of carotenoids in natural products. *Spectrochim Acta A Mol. Biomol. Spectrosc.* 59, 2207-2212.

Chapter 4

General conclusions, limitations and open questions

4.1. Iron-silica membranes geochemical plausibility and catalytic potential

Fe-silica self-organized membranes are life-mimicking nanostructures that arise when mixing an alkaline silicate solution with an iron-salt solution/pellet. The spontaneous formation of these membranes compartmentalizes two very distinct chemical environments; an outer, alkaline and silica-rich from an inner, acidic and iron-rich. As a result, ionic and pH gradients are generated across the membrane compartments that remain active for several hours during the membrane growth. These gradients give rise to an electrochemical voltage that was postulated to have played a crucial role in proto-biochemistry (Russell et al., 1994; Glaab et al., 2012; Barge et al., 2015a,b). Fueling this hypothesis, it was shown recently that iron membranes are capable to yield amino acids, carboxylic acids and nucleobases through formamide condensation (Saladino et al., 2016; 2019; Bizzari et al., 2018), and produce lactate and/or alanine in the presence of pyruvate (Barge et al., 2019). At the same time, it was shown that these membranes provide shielding from UV radiation (Saladino et al., 2016). Hence, the aforementioned results have sparked interest in the geochemical plausibility of these membranes and their possible role in prebiotic chemical reactions of the early Earth.

To better understand the possible role of Fe silica gardens in prebiotic chemistry, natural Fe-silica self-organized membranes, analogous to the model Fe-silica gardens, were grown from alkaline and silica-rich spring water deriving from a serpentinization environment (García-Ruiz et al., 2017; Boschetti et al., 2018). Following their synthesis, a detailed nanoscale characterization of the anatomy and mineralogy of synthetic and natural membranes was conducted by imaging FIB-milled sections using a combination of TEM, HR-HAADF and EELS. This nanoscale study was complemented by specific surface area measurements of both membrane types (BET analysis).

The obtained results showed that iron-silica self-organization brings two different surfaces together in one membrane; an outer amorphous silica wall and an inner iron-rich wall. The inner wall is composed of nanosized akaganeite, magnetite and goethite particles (5-10 nm particles and rosettes of 100-150 nm), which display significant intra- and inter-particle porosity. Moreover, this investigation brought to light a previously overlooked important property of these membranes; their bilayer structure. This comprises hydrophilic silica layers enclosing the hydrophobic, iron nanoparticles, providing an inorganic analogue of an organic bilayer membrane. Previous studies have attributed the remarkable catalytic properties of these membranes solely to the generation of an electrochemical voltage across the membrane's surface. Here it is argued that the mineral

chemistry and structure, as well as the properties of the nanoparticles building these membrane, dictate their catalytic capacity. As discussed here, the precipitation of the Fe-silica membranes in early Earth hydrothermal environments could have catalyzed the production of Fischer-Tropsch type organic molecules or other organics present on early Earth, such as, formamide and pyruvate, yielding amino acids, nucleobases and carboxylic acids (Saladino et al., 2016; Bizzari et al., 2018; Barge et al., 2019). At the same time, these membranes could have provided a template for the concentration and organization of organic molecules in a bilayer membrane, by a self-propagating mechanism (Fig.11). The fact that iron-silica membranes can be formed using natural water supports the geochemical plausibility of these membranes, and the role they might have played in catalyzing the building blocks of early life from simple organics produced in hydrothermal settings (McCollom and Seewald, 2007; Saladino et al., 2016; Niether et al., 2016; Bizzari et al., 2018; Barge et al., 2019). Furthermore, these results suggest that iron-silica self-organization could have been a rather common phenomenon on the primitive Earth and Earth-like planets, where ferrous iron and silica saturated waters are thought to have been widespread (Siever, 1992; Fischer and Knoll, 2009; Tosca et al., 2016; Halevy et al., 2017; Russell, 2018; Ménez et al., 2018).

It is also worth noting that understanding the interactions between ferrous iron and silica may offer key insight into the redox chemistry of the Precambrian seawater and iron formations (Grenne and Slack, 2003; Konhauser et al., 2007; Fischer and Knoll, 2009; Bekker et al., 2014; Rasmussen et al., 2015). The growth and characterization of iron-silica membranes in anoxic conditions that was performed in this work showed that they are composed of mixed valence iron oxyhydroxides, greenalites and amorphous silica. Greenalites are a group of Al-free, Fe-serpentine that are hypothesized to be the main precipitates of the Archean, ferrous- and silica-rich, oceans and they have been identified in many Proterozoic iron formations (Klein, 2005; Beukes and Klein, 1990; Simonson, 2003; Rasmussen et al., 2015; Pufahl et al., 2014; Tosca et al., 2016; Jonson et al., 2018).

Finally, the morphological and mineralogical resemblance of the iron-silica tubular membranes, obtained from purely inorganic reactions, to biogenic iron filaments considered as the oldest remnants of life on this planet, further blurs the boundaries between geochemical and biological morphologies. Thus, the Fe-silica membranes present a noteworthy duality; on the one hand these membranes should not be misinterpreted as remnants of life, while on the other, they probably played a critical role in the geochemical origin of life itself.

4.1.1. On the Fe-silica membranes precipitation in natural environments

In this context, a question that immediately rises, without having nonetheless a straightforward answer, is if iron-silica membranes -or Me-silica membranes in general- have been encountered in natural environments. So far, there has been only one report of iron-silica filaments recognized as inorganic membranes, from the Cero Colorado terraces of Rio Tinto in Spain (Barge et al., 2016). However, this does not mean that this is the single report of Fe-silica filaments in sediments and rocks. On the contrary, a wealth of studies have described such structures from a variety of settings of different ages and origins (see chapter 3.9 and references therein), but, they have been proven or presumed to be biogenic. It is assumed that for some of these cases the criterion of the biogenicity was merely the result of lack of knowledge that a purely inorganic mechanism can produce Fe-silica filaments, both chemically and morphologically, similar to the biologic ones (McMahon, 2019; Johannessen et al., 2020). By studying at the nanoscale the mineralogy and the anatomy of Fe-silica membranes it was shown that they can be mineralogically and morphologically identical to their biologic counterparts. As was shown here, their growth from natural solutions is geochemically plausible in a range of silica (0.6 M to 6.5 M) and iron concentrations (0.1 M- 5M) and in a temperature range of 20-80 ° C. Also, the very high ionic strength of the solutions and the water activity do not seem to affect the membrane growth -just slow it down- as long as the main reacting species are the iron cations and the silicate anions. Nonetheless, certain environmental prerequisites need to be met, since for the Fe-silica membranes to precipitate and endure, a low energy environment is required. This can be an isolated shallow water body, i.e. pond, lake etc., a shallow-sea hydrothermal system where diffuse venting prevails over vigorous venting, or even a protective niche, e.g., mineral pore, cavities, etc., within a high energy environment.

Several early Earth settings might have offered the required conditions for the Fe-silica membrane growth. With the currently available information on the Hadean it is believed that water condensed on the surface of the planet soon after solidification of the first ultramafic crust (Mojzsis et al., 2001; Wilde et al., 2001). The thermally-driven interaction between water and ultramafic minerals, known as serpentinization, would have created an alkaline, and reduced hydrosphere (Holm and Charlou, 2001; Sleep et al., 2004). Because of the high geothermal gradient, these reactions might have been easily associated with Fischer-Tropsch type synthesis of organic molecules (Holm and Andersson, 2005). By the same period, Earth's crust became more differentiated, forming tonalite-trondjemite-granite (TTG) series, alongside ultramafic and mafic rocks, resulting either from intense intraplate melting (Kemp et al., 2010), or from arc-like settings at the onset of proto plate-

tectonics (Harrison et al., 2005). The interaction of alkaline waters with granites/gabbro produced alkaline and silica-rich water, owing to the very high silica solubility at high pH. In these settings, that can be shallow lakes or ponds, reaction with iron particles of terrestrial input should have led to Fe-silica membrane formation. Other sources of iron and organics could have been generated by meteorites impact on the alkaline silica rich “oceans”, that would also result in iron-silica self-organized membranes. Recent silicon isotope studies have shown that Archean crustal rocks were unusually rich in ^{30}Si , which is enriched in cherts (André et al., 2019; Deng et al., 2019). This signature is interpreted to indicate subduction of cherts and mass transfer of silica from the subsiding slab into the newly formed felsic crust. If this interpretation is correct, these results indicate that the global pre-Archean ocean must have been particularly high in silica. Thus, terrigenous input of iron particles or hydrothermal input of iron nanoparticles would provide another plausible scenario for iron-silica membrane precipitation to have occurred.

Following crustal differentiation, global serpentinization rates would slow down and the change of atmospheric composition to higher pCO_2 would drive the decrease of the pH of seawater. This would trigger further silicification until a new steady state established itself (García-Ruiz et al., 2020). During the transitional period the increased CO_2 flux into an ocean-atmosphere system still heavily affected by serpentinization reactions might have boosted methanogens ($\text{CO}_2 + 4\text{H}_2 \rightarrow \text{CH}_4 + 2\text{H}_2\text{O}$). Eventually the increasing CO_2 mantle flux surpassed H_2 production by the throttled serpentinization and pCO_2 was able to build up in the atmosphere. As a consequence of the pH drop of the oceans, the concentrations of dissolved ferrous iron would have been high, resulting from secondary minerals as ferrous hydroxides and would lead to an iron enrichment of the oceans (Halevy et al., 2017). During the Great Oxidation Event (GOE) the pH of the oceans would further decrease owing to ferrous iron oxidation ($\text{Fe}^{2+} + 0.25 \text{O}_{2(\text{aq})} + 2.5 \text{H}_2\text{O} \rightarrow \text{Fe}(\text{OH})_3 + 2\text{H}^+$) leading to more silica precipitation ($\text{H}^+ + \text{H}_3\text{SiO}_4^- = \text{SiO}_2 \cdot 2 \text{H}_2\text{O}$) (García-Ruiz et al., 2020).

In a nutshell, various settings and periods existed during the Hadean-Early Archean, where highly alkaline and silica-rich aquatic environments could react with iron sources, in both local and global scales, provoking the precipitation of iron-silica self-organized membranes.

Beyond Earth, several planetary bodies could have ongoing serpentinization in a subsurface ocean, including Enceladus, Titan, Ceres, and Europa, and serpentinization reactions could be widespread in the cosmos (Holm et al., 2015; Barge, 2018). Mars might also have serpentinization occurring in the subsurface or had serpentinization occurring millions of years ago, as indicated by the

observation of hydrated minerals, such as serpentine phases, on the surface of Mars (Ehlmann et al., 2010). Serpentinite-hosted sites on planetary bodies could likely support chemoautotrophic life, such as methanogens (McCollom, 1999). In addition to organic molecules being synthesized on Earth, organics may also have arrived from space by meteorites and cosmic dust particles, where the synthesis would have occurred under very different environmental conditions from those prevailing on early Earth. Extreme cold temperatures, vacuum-like pressures, and high UV radiation conditions would have been present in space. And, organic molecule synthesis may also be possible under conditions on other planets and their satellites, such as Enceladus and Titan (two moons of Saturn)(Sahai et al., 2016). This hypothesis, given their interest as prebiotic catalysts, amplifies the environments where self-organizing mineral reactors may have at some moment assisted the adsorption, catalysis and organization of organic molecules.

4.1.2. Fe-silica membranes and microfossils

Reaching a verdict about the biogenicity of iron tubular structures found in silica-rich rocks has become even more complicated considering that geochemically plausible environments for the formation of Fe-silica membranes may also host abiotic organics. As has been demonstrated, isotopic signatures of carbon compounds formed by mineral reactions, such as, Fischer–Tropsch (FT) cycles and siderite decomposition are very similar to those appearing in biological reactions and it is not uncommon for inorganic reactions to overprint the biologic ones (van Zuilen et al., 2002, 2003; McCollom and Seewald, 2006; van Zuilen et al., 2007). In this case, following diagenesis and/or deformation-metamorphism would result in a quite similar chemical print of these organics to biologic ones (García-Ruiz et al., 2003). Nevertheless, aiming to resolve this dilemma future studies should focus on comparing the morphological, chemical and isotopic signatures of iron-silica inorganic membranes in presence of abiotic organics to biologic iron filaments found in silica precipitates during diagenesis, low and upper grade metamorphism (autoclave experiments).

4.2. The polyextreme hydrothermal system of Dallol; an analogue-site for abiotic iron minerals' formation and oxidation

In this PhD dissertation a terrestrial hydrothermal system that discharges hyperacidic (near to zero pH and down to -1.7), hypersaline and oxygen-free brines that contain up to 150 g/L of iron was studied in detail. It is demonstrated that the hyperacidic pH, the brine evolution, the color palette and the mineral paragenesis are controlled by purely inorganic processes, related to ferrous iron oxidation and iron complexation with chlorides and sulfates. This stands in stark contrast with most submarine and terrestrial hydrothermal systems, where iron cycling and iron mineral precipitation are biologically controlled/influenced. Recent microbiological studies confirmed the absence of active microbial activity in the brines of Dallol, supporting the results presented here. Owing to the reducing and sterile conditions of Dallol is a unique real-time laboratory for abiotic precipitation of iron minerals and formations. Adding to this, Dallol brines are anoxic and CO₂-rich, thus may simulate early Earth's or Martian atmospheres.

4.2.1. Analogue-site

An analogue-site is a terrestrial place that exhibits geologic or atmospheric characteristics which are close to those that prevailed on early Earth or have been observed on other celestial bodies. The term also includes terrestrial sites that can be used for space mission simulations, e.g., to test sampling or drilling equipment, space suits, or the performance of astronauts. By definition, there can be no ideal -modern- terrestrial analogue-site for the early Earth, as there can also be no ideal terrestrial analogue-site for other planets and moons.

Dallol is developed at the extension of the Ertu Ale volcanic chain in the Main Ethiopian Rift, a result of the highly active extensional regime of what is known as the 'Afar Triangle'. At Dallol, the presence of a shallow magmatic body developed within a marine evaporitic sequence that is overlying flood basalts, results in the generation of an unique combination of hyperacidic and hypersaline conditions. These geodynamical conditions are singular on modern Earth and may not be similar to early Earth geological settings. However, Dallol may be considered as an analogue-site for abiotic iron mineral precipitation relevant for early Earth and Martian environments, taking into account that at Dallol mineral processes and elemental cycling are purely inorganic. In fact, Dallol is the only terrestrial site where there is liquid water and no life, therefore, it takes the lead on other Martian analogue-sites that are under biologic and anthropogenic influence (e.g. Rio Tinto, Spain or Iron Mt, California)(Fernández-Remolar, et al., 2004; Sobron and Alpers, 2013).

If microorganisms are ever found in Dallol polyextreme hydrothermal brines their existence would expand the limit of life supporting habitance on Earth and Earth-like planets, as we currently understand it, rendering Dallol a site of unique astrobiological significance. Until then, Dallol is the only present-day site where we can witness iron mineral precipitation, self-organization and progressive oxidation as possibly resembling processes that occurred during the complex redox history of the early Earth, when life was neither influencing, nor, inducing mineralization.

4.2.2. Dallol hydrothermal brine: un utterly complex fluid

In such an utterly complex fluid such as the Dallol brines, conducting reliable in situ measurements such as determining the pH or performing chemical analysis can be a tedious task. The salinity of the Dallol brines was determined to be around 380 g/L, while Belilla et al., 2019 measured water activity < 0.4 for the Dallol spring water. Apart from the extreme chloride concentration, sodium (90 g/L), iron (26-150 g/L) and potassium (11 g/L) are also extremely high. Besides the very high ionic strength, another extreme parameter of the Dallol brines is the pH, the values of which are near and below zero, impeding analytical issues for the chemical and isotopic analyses. These two parameters, along with the high temperature of the fluids, ranging from 32 to 108 ° C, render in situ measurements and pH determination challenging. Taking into account the Nordstrom et al., (2000) discussion on negative pH, the pH meter was calibrated with the following buffers: 4, 2, 1.68 and 0.8. The latter was prepared by using a 3.5 M HCl solution of $d=1.19$ g/mL and activity 'a' of 1.5 m/(mol kg⁻¹). Due to the difficulty of determining the pH in highly concentrated acidic brines, the pH meter was calibrated before every measurement, repeating each measurement three times and re-measuring the values for every site in different days. Also, we compared the in situ pH measurements with the calculation of the pH by charge balance difference, considering that the hydrogen ion is the major cation. The difference between measured and calculated pH values ranged from ± 0.05 for the spring water (in situ pH: 0.1) to ± 0.2 for the most acidic pool water (in situ pH: -1.7). Another approach would be a liquid junction- free cell containing specific ion electrodes to measure the activities of protons and chloride ions. This approach might be preferable for acid mine waters provided that a reliable sulfate, or bisulfate, ion-selective electrode will be used (Nordstrom et al., 2000).

References

- André, L., Abraham, K., Hofmann, A., Monin, L., Kleinhanns, I.C., Foley, S., 2019. Early continental crust generated by reworking of basalts variably silicified by seawater. *Nature Geoscience*, 12, 769-773.
- Barge, L.M., Doloboff, I.J., White, L.M., Stucky, G.D., Russell, M.J., Kanik, I., 2012. Characterization of iron-phosphate-silicate chemical garden structures. *Langmuir : the ACS journal of surfaces and colloids* 28, 3714-3721.
- Barge, L.M., Abedian, Y., Russell, M.J., Doloboff, I.J., Cartwright, J.H., Kidd, R.D., Kanik, I., 2015a. From Chemical Gardens to Fuel Cells: Generation of Electrical Potential and Current Across Self-Assembling Iron Mineral Membranes. *Angewandte Chemie* 54, 8184-8187.
- Barge, L.M., Cardoso, S.S., Cartwright, J.H., Cooper, G.J., Cronin, L., De Wit, A., Doloboff, I.J., Escribano, B., Goldstein, R.E., Haudin, F., Jones, D.E., Mackay, A.L., Maselko, J., Pagano, J.J., Pantaleone, J., Russell, M.J., Sainz-Diaz, C.I., Steinbock, O., Stone, D.A., Tanimoto, Y., Thomas, N.L., 2015b. From Chemical Gardens to Chemobrionics. *Chemical reviews* 115, 8652-8703.
- Barge, L.M., Cardoso, S.S., Cartwright, J.H., Doloboff, I.J., Flores, E., Macias-Sanchez, E., Sainz-Diaz, C.I., Sobron, P., 2016. Self-assembling iron oxyhydroxide/oxide tubular structures: laboratory-grown and field examples from Rio Tinto. *Proceedings. Mathematical, physical, and engineering sciences* 472, 20160466.
- Barge, L.M., 2018. Considering planetary environments in origin of life studies. *Nature Communications*, 9, 5170.
- Barge, L.M., Flores, E., Baum, M.M., VanderVelde, D.G., Russell, M.J., 2019. Redox and pH gradients drive amino acid synthesis in iron oxyhydroxide mineral systems, *Proc Natl Acad Sci USA*, 116, 4828-4833; DOI: 10.1073/pnas.1812098116.
- Bekker, A., Holland, H.D., Wang, P.L., Rumble III, D., Stein, H.J., Hannah, J.L., Coetsee, L.L., Beukes, N.J., 2004. Dating the rise of atmospheric oxygen. *Nature* 427, 117.
- Belilla, J., Moreira, D., Jardillier, L. et al., 2019. Hyperdiverse archaea near life limits at the polyextreme geothermal Dallol area. *Nat Ecol Evol* 3, 1552–1561, doi:10.1038/s41559-019-1005-0.
- Beukes, N.J., Klein, C., 1990. Geochemistry and sedimentology of a facies transition -from microbanded to granular iron-formation - in the early Proterozoic Transvaal Supergroup, South Africa, *Precambrian Research*, 47, 99-139.
- Bizzarri, B.M., Botta, L., Perez-Valverde, M.I., Saladino, R., Di Mauro, E., Garcia Ruiz, J.M., 2018. Silica metal-oxide vesicles catalyze comprehensive prebiotic chemistry. *Chem. Eur. J.* 2018, 24, 8126.
- Boschetti T, Etiope G, Pennisi M, Romain M, Toscani L (2013a) Boron, lithium and methane isotope composition of hyperalkaline waters (Northern Apennines, Italy): terrestrial serpentinization or mixing with brine? *Appl Geochem* 32:17–25. doi:10.1016/j.apgeochem.2012.08.018.
- Cartwright, J.H.E., Escribano, B., Sainz-Díaz, C.I., 2011. Chemical-Garden Formation, Morphology, and Composition. I. Effect of the Nature of the Cations. *Langmuir : the ACS journal of surfaces and colloids* 27, 3286-3293.

- Cartwright, J.H.E., Garia-Ruiz, J.M., Novella, M.L., Otálora, F., 2002. Formation of Chemical Gardens. *J. Colloid Interface Sci.* 256, 351-359.
- Corti, G., Bastow, I. D., Keir, D., and Pagli, C., 2015. “Rift-related morphology of the Afar Depression,” in *Landscapes and Landforms of Ethiopia*, ed. P. Billi, (Dordrecht: Springer Science Business Media), 251–274. doi: 10.1007/978-94-017-8026-1.
- Darrah, T.H., Tedesco, D., Tassi, F., Vaselli, O., Cuoco, E., Poreda, R.J., 2013. Gas chemistry of the Dallol region of the Danakil Depression in the Afar region of the northern-most East African Rift. *Chemical Geology* 339, 16-29.
- Deng, Z., Chaussidon, M., Guitreau, M., Puchtel, I.S, Dauphas, N., Moynier, F., 2019. An oceanic subduction origin for Archaean granitoids revealed by silicon isotopes. *Nature Geoscience*, 12, 774-8.
- Ehlmann, B.L., Mustard, J.F., S. L. Murchie, S.L., 2010. Geologic setting of serpentine deposits on Mars, *Geophys. Res. Lett.*, 37, L06201, doi:10.1029/2010GL042596.
- Eugster, H.P., 1967. Hydrous Sodium Silicates from Lake Magadi, Kenya: Precursors of Bedded Chert. *Science*, 157, 1177-1180. DOI: 10.1126/science.157.3793.1177.
- Fernández-Remolar, D.C., Morris, R.V., Gruener, J.E., Amils, R., Knoll, A.H., 2005. The Río Tinto Basin, Spain: Mineralogy, sedimentary geobiology, and implications for interpretation of outcrop rocks at Meridiani Planum, Mars, *Earth and Planetary Science Letters*, 1, 149-167.
- Fischer, W.W., Knoll, A.H., 2009. An iron shuttle for deepwater silica in Late Archean and early Paleoproterozoic iron formation. *GSA Bulletin* 121, 222-235.
- Franzson, H., Helgadóttir, H. M., and Óskarsson, F., 2015. Surface exploration and first conceptual model of the Dallol geothermal area, northern Afar, Ethiopia, in Proceedings *World Geothermal Congress* 2015, Melbourne, 11.
- García-Ruiz, J.M., Hyde, S.T., Carnerup, A.M., Christy, A.G., Van Kranendonk, M.J., Welham, N.J., 2003. Self-assembled silica-carbonate structures and detection of ancient microfossils. *Science* 302, 1194-1197.
- García-Ruiz, J.M., Melero-Garcia, E., Hyde, S.T., 2009. Morphogenesis of self-assembled nanocrystalline materials of barium carbonate and silica. *Science* 323, 362-365.
- García-Ruiz, J.M., Nakouzi, E., Kotopoulou, E., Tamborrino, L., Steinbock, O., 2017. Biomimetic mineral self-organization from silica-rich spring waters. *Science Advances* 3, e1602285.
- García-Ruiz, J.M., van Zuilen, M., Bach, W., 2020. Mineral self-organization on a lifeless planet, *Physics of Life Reviews*, in press.
- Glaab, F., Kellermeier, M., Kunz, W., Morallon, E., Garcia-Ruiz, J.M., 2012. Formation and evolution of chemical gradients and potential differences across self-assembling inorganic membranes. *Angewandte Chemie* 51, 4317-4321.
- Glaab, F., Rieder, J., Garcia-Ruiz, J.M., Kunz, W., Kellermeier, M., 2016. Diffusion and precipitation processes in iron-based silica gardens. *Physical chemistry chemical physics : PCCP* 18, 24850-24858.

- Glaab, F., Rieder, J., Klein, R., Choquesillo-Lazarte, D., Melero-Garcia, E., Garcia-Ruiz, J.M., Kunz, W., Kellermeier, M., 2017. Precipitation and Crystallization Kinetics in Silica Gardens. *Chemphyschem : a European journal of chemical physics and physical chemistry* 18, 338-345.
- Grenne, T., Slack, J. F., 2003. Paleozoic and Mesozoic silica-rich seawater: Evidence from hematitic chert (jasper) deposits, *Geology* 31, 319–322.
- Halevy, I., Alesker, M., Schuster, E.M., Popovitz-Biro, R., Feldman, Y., 2017. A key role for green rust in the Precambrian oceans and the genesis of iron formations. *Nature Geoscience* 10, 135-139.
- Harrison, T.M, Blichert-Toft, J, Muller, W, Albarede, F, Holden, P, Mojzsis, S.J., 2005. Heterogeneous Hadean hafnium: Evidence of continental crust at 4.4 to 4.5 Ga. *Science*, 310, 1947-50.
- Holm, N.G, Charlou, J.L., 2001. Initial indications of abiotic formation of hydrocarbons in the Rainbow ultramafic hydrothermal system, Mid-Atlantic Ridge. *Earth and Planetary Science Letters*, 191, 1-8.
- Holm, N.G., Andersson, E., 2005. Hydrothermal simulation experiments as a tool for studies of the origin of life on earth and other terrestrial planets: A review. *Astrobiology*, 5, 444-60.
- Holm, N. G., Oze, C., Mousis, O., Waite, J. H., & Guilbert-Lepoutre, A. (2015). Serpentinization and the Formation of H₂ and CH₄ on Celestial Bodies (Planets, Moons, Comets). *Astrobiology*, 15(7), 587–600. doi:10.1089/ast.2014.1188,
- Johannessen, K.C., McLoughlin, N., Vullum, P.E., Thorseth, I.H., 2020. On the biogenicity of Fe-oxyhydroxide filaments in silicified low-temperature hydrothermal deposits: Implications for the identification of Fe-oxidizing bacteria in the rock record. *Geobiology* 18, 31-53.
- Johnson, J. E., Muhling, J. R., Cosmidis, J., Rasmussen, B., & Templeton, A. S., 2018. Low-Fe(III) Greenalite was a primary mineral from Neoproterozoic oceans. *Geophysical Research Letters*, 45, 3182– 3192. <https://doi.org/10.1002/2017GL076311>.
- Keir, D., Bastow, I. D., Pagli, C., and Chambers, E. L., 2013. The development of extension and magmatism in the Red Sea rift of Afar. *Tectonophysics* 607, 98–114. doi: 10.1016/j.tecto.2012.10.015.
- Kellermeier, M., Glaab, F., Melero-Garcia, E., Garcia-Ruiz, J.M., 2013. Experimental techniques for the growth and characterization of silica biomorphs and silica gardens. *Methods in enzymology* 532, 225-256.
- Kemp, AIS, Wilde, S.A, Hawkesworth, C.J, Coath, C.D, Nemchin, A., Pidgeon, R.T., et al., 2010. Hadean crustal evolution revisited: New constraints from Pb-Hf isotope systematics of the Jack Hills zircons. *Earth and Planetary Science Letters*, 296, 45-56.
- Klein. C., 2005. Some Precambrian banded iron-formations (BIFs) from around the world: Their age, geologic setting, mineralogy, metamorphism, geochemistry, and origins. *American Mineralogist* 90, 1473–1499.
- Konhauser KO, Amskold L, Lalonde SV, Posth NR, Kappler A, Anbar A., 2007. Decoupling photochemical Fe(II) oxidation from shallow-water BIF deposition. *Earth and Planetary Science Letters* 258, 87–100.

- López-García J.M., Moreira, D., Benzerara, K., Grunewald, O., and López-García, P., 2020. Origin and Evolution of the Halo-Volcanic Complex of Dallol: Proto-Volcanism in Northern Afar (Ethiopia). *Front. Earth Sci.* 7:351. doi: 10.3389/feart.2019.00351.
- McCollom, T.M., Ritter, G., Simoneit, B.R.T., 1999. Lipid Synthesis Under Hydrothermal Conditions by Fischer-Tropsch-Type Reactions. *Origins of life and evolution of the biosphere* 29, 153-166.
- McCollom, T.M., Seewald, J.S., 2007. Abiotic Synthesis of Organic Compounds in Deep-Sea Hydrothermal Environments. *Chem. Rev.* 107, 382-401.
- McMahon, S., 2019. Earth's earliest and deepest purported fossils may be iron-mineralized chemical gardens. *Proc. R. Soc. B* 286, 20192410.
- Ménez, B., Pisapia, C., Andreani, M., Jamme, F., Vanbellingen, Q.P., Brunelle, A., Richard, L., Dumas, P., Refregiers, M., 2018. Abiotic synthesis of amino acids in the recesses of the oceanic lithosphere. *Nature* 564, 59-63.
- Mojzsis SJ, Harrison TM, Pidgeon RT., 2001. Oxygen-isotope evidence from ancient zircons for liquid water at the Earth's surface 4,300 Myr ago. *Nature*, 409, 178-81.
- Niether, D. Afanasenkau, J. K. Dhont, S. Wiegand, Accumulation of formamide in hydrothermal pores to form prebiotic nucleobases, 2016, *Proc. Natl. Acad. Sci. USA.*, 113, 4272–4277.
- Nobile, A., Pagli, C., Keir, D., Wright, T. J., Ayele, A., Ruch, J., et al., 2012. Dike-fault interaction during the 2004 Dallol intrusion at the northern edge of the Erta Ale Ridge (Afar, Ethiopia). *Geophys. Res. Lett.* 39, 2–7. doi: 10.1029/2012GL053152.
- Nordstrom, D.K., Alpers, C.N., Ptacek, K.J., Blowers, D.W., 2000. Negative pH and Extremely Acidic Mine Waters from Iron Mountain, California. *Environ. Sci. Technol.* 34, 254-258.
- Pagli, C., Wright, T. J., Ebinger, C. J., Yun, S.-H., Cann, J. R., Barnie, T., et al. (2012). Shallow axial magma chamber at the slow-spreading Erta Ale Ridge. *Nat. Geosci.* 5, 284–288. doi: 10.1038/ngeo1414.
- Pérez, E., Chebude, Y., 2017. Chemical Analysis of Gaet'ale, a Hypersaline Pond in Danakil Depression (Ethiopia): New Record for the Most Saline Water Body on Earth. *Aquatic Geochemistry* 23, 109-117.
- Pufahl, P.K., Anderson, S. L., Hiatt, E.E., 2014. Dynamic sedimentation of Paleoproterozoic continental margin iron formation, Labrador Trough, Canada: Paleoenvironments and sequence stratigraphy, *Sedimentary Geology*, 309, 48-65.
- Russell, M.J., Daniel, R.M.D., Hall, A.J., Sherringham, J.A., 1994. A Hydrothermally Precipitated Catalytic Iron Sulphide Membrane as a First Step Toward Life. *J Mol Evol* 39, 231-243.
- Russell, M.J., 2018. Green Rust: The Simple Organizing 'Seed' of All Life? *Life* 8, 35; <https://doi.org/10.3390/life8030035>.
- Sahai, N., Kaddour, H., Dalai, P., 2016. The Transition from Geochemistry to Biogeochemistry, *Elements*, 12, 389-394.
- Saladino, R., Botta, G., Bizzarri, B.M., Di Mauro, E., Garcia Ruiz, J.M., 2016. A Global Scale Scenario for Prebiotic Chemistry: Silica-Based Self-Assembled Mineral Structures and Formamide. *Biochemistry* 55, 2806-2811.

- Saladino, R., Di Mauro, E., Garcia-Ruiz, J.M., 2019. A Universal Geochemical Scenario for Formamide Condensation and Prebiotic Chemistry. *Chem. Eur. J.* 25, 3181 – 3189.
- Sánchez, M., Sabio, L., Gálvez, N., Capdevila, M., Dominguez-Vera, J.M., 2017. Iron chemistry at the service of life. *Life*, 69, 382-388.
- Siever, R., 1992. The silica cycle in the Precambrian. *Geochimica et Cosmochimica Acta* 56, 3265-3272.
- Simonson, B. M., 2003. Origin and evolution of large Precambrian formations, in *Extreme Depositional Environments: Mega End Members in Geologic Time*, (eds.) Chan, M.A., Archer, W.A., Geological society of America, Special Paper 370.
- Sleep, N.H, Meibom, A, Fridriksson, T, Coleman, R.G, Bird, D.K., 2004. H₂-rich fluids from serpentinization: Geochemical and biotic implications. *Proceedings of the National Academy of Sciences of the United States of America*, 101, 12818-23.
- Sobron, P., Alpers, C. N., 2013. Raman Spectroscopy of Efflorescent Sulfate Salts from Iron Mountain Mine Superfund Site, California. *Astrobiology* 13, 270-278.
- Rasmussen, B., Krapež, B., Muhling, J.R., Suvorova, A., 2015. Precipitation of iron silicate nanoparticles in early Precambrian oceans marks Earth's first iron age. *Geology* 43, 303-306.
- Tosca, N.J., Guggenheim, S., Pufahl, P.K., 2016. An authigenic origin for Precambrian greenalite: Implications for iron formation and the chemistry of ancient seawater. *GSA Bulletin* 128, 511-530
- Varekamp, J.C., Ouimette, A.P., Herman, S.W., Flynn, K.S., Bermudez, A., Delpino, D., 2009. Naturally acid waters from Copahue volcano, Argentina. *Applied Geochemistry* 24, 208-220.
- Wilde, S.A, Valley, J.W, Peck, W.H, Graham, C.M., 2001. Evidence from detrital zircons for the existence of continental crust and oceans on the Earth 4.4 Gyr ago. *Nature*, 409, 175-8.

APPENDIX

I. Supplementary Information

Chapter 3.

Table S1

| Sample name | $\delta^{13}\text{C}$ ‰ (V-PDB) | $\delta^{15}\text{N}$ ‰ (AIR) | $\delta^{17}\text{O}$ ‰ (V-SMOW) | $\delta^{18}\text{O}$ ‰ (V-SMOW) | $\delta^{36}\text{Ar}$ ‰ (AIR) | $\delta^{38}\text{Ar}$ ‰ (AIR) |
|--------------------|---|---|--|--|--|--|
| S1 | -6.76 | -0.14 | 14.11 | 25.78 | 8.2 | 4.6 |
| S3 | -4.51 | -0.66 | 17.26 | 22.94 | 2.93 | 32.73 |
| YL1 | -3.4 | 4.15 | 27.11 | 22.64 | 17.03 | 135.08 |
| YL2 | -3.16 | 1.63 | 16.21 | 22.37 | 4.6 | 47.59 |
| SS3 | -4.42 | 1.02 | 19.4 | 23.82 | 4.9 | 67.28 |
| S2 | -4.12 | 1.38 | 33.83 | 28.45 | 4.58 | 101.73 |
| BL1 | -6.9 | 0.18 | 12.51 | 23.26 | 0.94 | 8.89 |
| SS4 | -4.46 | 0.99 | 21.87 | 25.6 | 1.75 | 70.75 |
| SS5 | -4.01 | 2.31 | | | 15.06 | 190.69 |
| S4 | -5.04 | 0.25 | 15.08 | 25.08 | 9.9 | 160.17 |
| SS6 | -3.91 | 2.45 | | | 0.21 | 13.06 |

| Sample name | $\delta(32/28)$ ‰ (AIR) | $\delta(32/40)$ ‰ (AIR) | $\delta(28/40)$ ‰ (AIR) | 32/40 | 28/40 |
|--------------------|---|---|---|--------------|--------------|
| S1 | 335 | 262.37 | 2.16 | 28.3101 | 83.782 |
| S3 | -202.14 | -212.26 | -18.62 | 17.6659 | 82.0449 |
| YL1 | -27.76 | -125.88 | -105.57 | 19.603 | 74.7761 |
| YL2 | -29.46 | -64.53 | -39.22 | 20.9789 | 80.3232 |
| SS3 | -198.08 | -231.74 | -48.75 | 17.2291 | 79.5265 |
| S2 | -329.01 | -335.75 | -19.98 | 14.8965 | 81.9311 |
| BL1 | -32.06 | -25.01 | 5.58 | 21.8653 | 84.0679 |
| SS4 | -232.98 | -239.26 | -15.07 | 17.0604 | 82.3418 |
| SS5 | -132.82 | -185.89 | -67.14 | 18.2573 | 77.9888 |
| S4 | -229.73 | -287.54 | -83.55 | 20.302 | 84.0524 |
| SS6 | -102.29 | -94.72 | 5.39 | 15.9778 | 76.6168 |

| Sample name | 44/40 | 40Ar/36Ar | 38Ar/36Ar | 40Ar/38Ar |
|-------------|---------|-----------|-----------|-----------|
| S1 | 23.575 | 293.75 | 0.18696 | 1571.20 |
| S3 | 232.936 | 295.29 | 0.19321 | 1528.40 |
| YL1 | 552.173 | 291.20 | 0.20941 | 1390.59 |
| YL2 | 360.165 | 294.80 | 0.19566 | 1506.72 |
| SS3 | 416.214 | 294.72 | 0.19928 | 1478.92 |
| S2 | 559.461 | 294.81 | 0.20578 | 1432.68 |
| BL1 | 31.18 | 295.88 | 0.18912 | 1564.52 |
| SS4 | 157.793 | 295.64 | 0.20055 | 1474.13 |
| SS5 | 473.37 | 291.77 | 0.22009 | 1325.64 |
| S4 | 35.291 | 293.26 | 0.21555 | 1360.51 |
| SS6 | 857.685 | 296.10 | 0.19004 | 1558.08 |

| Sample name | % O ₂ | % N ₂ | % Ar | % CO ₂ |
|-------------|------------------|------------------|-------|-------------------|
| S1 | 20.715 | 61.304 | 0.732 | 17.25 |
| S3 | 5.295 | 24.59 | 0.3 | 69.82 |
| YL1 | 3.027 | 11.548 | 0.154 | 85.27 |
| YL2 | 4.536 | 17.368 | 0.216 | 77.88 |
| SS3 | 3.352 | 15.473 | 0.195 | 80.98 |
| S2 | 2.266 | 12.465 | 0.152 | 85.12 |
| BL1 | 15.831 | 60.869 | 0.724 | 22.58 |
| SS4 | 6.608 | 31.891 | 0.387 | 61.11 |
| SS5 | 3.2 | 13.667 | 0.175 | 82.96 |
| S4 | 14.435 | 59.762 | 0.711 | 25.09 |
| SS6 | 1.68 | 8.054 | 0.105 | 90.16 |

Table S1. Oxygen, nitrogen, argon and carbon stable isotopes and atomic ratios in free gases from springs of Dallol and Black and Yellow Lake waters (sampling 2017). Hydrothermal springs (S1, S2, S3, S4) and subaqueous springs (SS1, SS2, SS3, SS4) of Dallol hydrothermal system and the Black lake (BL1) and Yellow (YL1, YL2) Lake waters.

Table S2

| Sample name | δD ‰ (V-SMOW) | $\delta^{18}O$ ‰ (V-SMOW) | δD excess "d" † | $\delta^{13}C_{DIC}$ ‰ (V-PDB) | DIC [] ppm C |
|---|--------------------------|------------------------------|----------------------------|-----------------------------------|------------------|
| Ambo Ethiopia with CO ₂ (*) | -22.0 | -4.84 | 16.7 | -25.98 | 787.8 |
| Dera (*) | -12.4 | -1.09 | -3.6 | -13.95 | 6.2 |
| Alage Merci (*) | -13.5 | -1.77 | 0.7 | -22.35 | 3.6 |
| Kool CO ₂ (*) | -13.0 | -1.07 | -4.4 | -30.12 | 576.9 |
| Kool CO ₂ | -13.0 | -1.54 | -0.6 | -30.39 | 568.5 |
| PA (*) | | | | | 58.7 |
| 25 L hotel | -4.2 | -2.29 | 14.1 | -5.85 | |
| Nice (*) | -20.7 | -4.33 | 13.9 | -15.87 | 5.5 |
| SPA (*) | -7.7 | -1.94 | 7.8 | -14.73 | 5.4 |
| Mekele tap water | -3.3 | -1.81 | 11.2 | -7.23 | 42.1 |
| Yara- Potash mine | -9.2 | -3.34 | 17.5 | -4.85 | 23.3 |
| Ahmedela tap water | -6.3 | -2.42 | 13.1 | -6.58 | 16.8 |
| CR1 | 1.7 | -0.54 | 6.0 | -9.0 | 16.8 |
| CR2 | 7.8 | 0.83 | 1.1 | -11.56 | 4.2 |
| C1 | 19.5 | 8.64 | -49.6 | -6.30 | 6.9 |
| C1** | -24.2 | -4.74 | | | |
| S1 | -20.9 | 4.97 | -60.6 | | 0.5 |
| S2 | -15.6 | 5.94 | -63.1 | -5.83 | 11.42 |
| S3 | -8.9 | 5.50 | -52.9 | -4.00 | 44.85 |
| S4 | -11.5 | 4.92 | -50.9 | | 0.5 |
| S5 | -8.2 | 6.31 | -58.7 | -6.41 | 0.7 |
| S6 | -9.8 | 7.78 | -72.1 | -0.35 | 0.5 |
| S7 | -20.8 | 5.33 | -63.4 | -5.00 | 21.79 |
| S8 | -17.7 | 6.10 | -66.5 | -6.45 | 2.33 |
| SS1 | -8.6 | 8.09 | -73.3 | | |
| SS2 | -9.3 | 9.18 | -82.7 | | |
| P1 | -5.7 | 9.26 | -79.7 | | 5.43 |

| | | | | | |
|-------|-------|-------|-------|-------|-------|
| P2 | -11.3 | 10.75 | -97.3 | -0.15 | 1.14 |
| P3 | -10.2 | 10.33 | -92.8 | -4.33 | 0.91 |
| P4 | -2.8 | 10.65 | -88.0 | -1.37 | 0.9 |
| P5 | -15.1 | 8.13 | -80.1 | -5.76 | 0.98 |
| P7 | -15.0 | 8.04 | -79.3 | -5.66 | 11.10 |
| P8 | -14.0 | 8.77 | -84.2 | -6.84 | 94.36 |
| P2S3 | -6.2 | 6.02 | -54.4 | | 0.5 |
| P18 | -9.9 | 6.24 | -59.8 | | 0.5 |
| PB1 | 3.2 | 9.54 | -73.1 | -3.26 | 0.62 |
| YL1 | -45.2 | -6.50 | 6.8 | | 0.5 |
| BL1 | -23.8 | -1.15 | -14.6 | | |
| S1** | -9.4 | 7.99 | -73.3 | | |
| S2** | -7.2 | 9.94 | -86.7 | | |
| S3** | -8.0 | 7.76 | -70.1 | | |
| P1** | -16.6 | 8.03 | -80.8 | | |
| P2** | -15.5 | 8.54 | -83.8 | | |
| P3** | -15.9 | 7.01 | -71.9 | | |
| BL2** | -24.4 | -0.88 | -17.4 | | |
| YL3** | -31.8 | -7.18 | 25.6 | | |

Table S2. Stable isotopes in H₂O and DIC (Dissolved Inorganic Carbon) for Dallol hydrothermal brines compared to water from the wider area. Dallol spring (S1-S8, S1**-S3**), subaqueous spring (SS1-SS2), and pool (P1-P5, P7-P8, P18, PB, P2S3, P1**-P3**) water, Black (BL1, BL2**) and Yellow Lake (YL1, YL3**) waters, cave water from the salt canyon of Dallol (C1, C1**), well water from the salt mine of the Danakil (Yara potash mine), creek water from the wider area of NE Ethiopia (CR1, CR2), mineral waters from Ethiopia (*) and tap water from Mekele and Ahmedela were analyzed as references in the plot context of the meteoric water line (MWL) and Addis Ababa meteoric water line (AAMWL)⁸. ** samples of the field campaign of 2016.

Table S3

| Sample name | $\delta^{15}\text{N}$ ‰ | $\delta^{36}\text{Ar}$ ‰ | $\delta^{38}\text{Ar}$ ‰ | $\delta(32/28)$ ‰ | $\delta(32/40)$ ‰ | $\delta(28/40)$ ‰ | $\delta(44/40)$ ‰ |
|--------------------|---|--|--|---|---|---|---|
| P6 | 0.22 | -14.24 | 3.31 | -723 | -818 | -436 | 771192 |
| P1 | 0.17 | -14.7 | 8.64 | -775 | -824 | -328 | 2144381 |
| P2 | 0.19 | -17.06 | 0.15 | -765 | -846 | -457 | 314623 |
| P3 | 0.39 | -16.23 | 2.03 | -747 | -844 | -492 | 200870 |
| P4 | 0.29 | -16.51 | 8.55 | -757 | -844 | -472 | 200483 |
| S5 | -0.06 | -16.22 | -10.06 | -921 | -911 | -205 | 648180 |
| S3 | -1.05 | -7.64 | 1.1 | -790 | -843 | -370 | 18307424 |
| PS3 | 0.05 | -16.88 | -8.04 | -886 | -891 | -272 | 200465 |
| S9 | -0.11 | -14.03 | -8.89 | -880 | -890 | -293 | 239165 |
| PB1 | 0.01 | -12.77 | 17 | -905 | -889 | -94 | 128721 |
| YL1 | 0.11 | 5.15 | 59.4 | 173 | -295 | -401 | 76752772 |
| S1 | -1.1 | -10.73 | -3.34 | -915 | -905 | -191 | 5791443 |
| S2 | -1.67 | -8.79 | -6.13 | -812 | -857 | -379 | 4526856 |
| BL1 | -0.88 | 6.45 | 128.83 | -466 | -641 | -364 | 193325443 |
| P5 | -0.98 | -14 | -6.43 | -830 | -876 | -431 | 345556 |
| P7 | -0.52 | -16.69 | -12.86 | -846 | -885 | -432 | 4461316 |
| P8 | 0.3 | -13.77 | 6.01 | -865 | -881 | -312 | 49446823 |
| S7 | -1.59 | -9.04 | -5.95 | -630 | -801 | -528 | 12301404 |
| S8 | -1.29 | -10.65 | 8.5 | -809 | -867 | -445 | 743965 |

| Sample name | 32/28 | 32/40 | 28/40 | 44/40 | 40/36 | 38/3 | 40/38 |
|--------------------|--------------|--------------|--------------|--------------|--------------|-------------|--------------|
| P6 | 0.0743 | 4.083 | 47.1372 | 31.83 | 300.44 | 0.19097 | 1573.22 |
| P1 | 0.0603 | 3.9375 | 56.1398 | 88.434 | 300.58 | 0.19207 | 1564.90 |
| P2 | 0.063 | 3.4625 | 45.4003 | 13.01 | 301.30 | 0.19092 | 1578.19 |
| P3 | 0.0678 | 3.4901 | 42.4848 | 8.321 | 301.05 | 0.19111 | 1575.23 |
| P4 | 0.0653 | 3.4958 | 44.1403 | 8.305 | 301.13 | 0.19241 | 1565.04 |
| S5 | 0.0211 | 1.9869 | 66.4351 | 26.76 | 301.04 | 0.18880 | 1594.47 |

| | | | | | | | |
|-----|--------|---------|---------|---------|--------|---------|---------|
| S3 | 0.0563 | 3.5319 | 52.6768 | 754.683 | 298.44 | 0.18928 | 1576.69 |
| PS3 | 0.0305 | 2.4438 | 60.8881 | 8.305 | 301.25 | 0.18932 | 1591.22 |
| S9 | 0.0321 | 2.4773 | 59.0655 | 9.9 | 300.37 | 0.18861 | 1592.58 |
| PB1 | 0.0254 | 2.4935 | 75.7555 | 5.347 | 299.99 | 0.19329 | 1552.04 |
| YL1 | 0.3147 | 15.8042 | 50.0599 | 3163.83 | 294.64 | 0.19776 | 1489.92 |
| S1 | 0.0228 | 2.1202 | 67.6378 | 238.768 | 299.37 | 0.18903 | 1583.72 |
| S2 | 0.0505 | 3.1977 | 51.9508 | 186.641 | 298.79 | 0.18813 | 1588.16 |
| BL1 | 0.1432 | 8.0571 | 53.1809 | 7969.02 | 294.26 | 0.21045 | 1398.28 |
| P5 | 0.0455 | 2.773 | 47.5803 | 14.285 | 300.37 | 0.18907 | 1588.64 |
| P7 | 0.0414 | 2.5717 | 47.482 | 183.94 | 301.19 | 0.18836 | 1598.99 |
| P8 | 0.0362 | 2.6789 | 57.481 | 2038.27 | 300.30 | 0.19139 | 1569.00 |
| S7 | 0.0993 | 4.4553 | 39.4891 | 507.11 | 298.86 | 0.18822 | 1587.87 |
| S8 | 0.0512 | 2.991 | 46.4079 | 30.708 | 299.35 | 0.19126 | 1565.12 |

| Sample name | % O ₂ | % N ₂ | % Ar | % CO ₂ |
|-------------|------------------|------------------|-------|-------------------|
| P6 | 4.858 | 56.082 | 1.19 | 37.87 |
| P1 | 2.634 | 37.549 | 0.669 | 59.149 |
| P2 | 5.507 | 72.21 | 1.591 | 20.693 |
| P3 | 6.312 | 76.831 | 1.808 | 15.048 |
| P4 | 6.139 | 77.519 | 1.756 | 14.586 |
| S5 | 2.066 | 69.073 | 1.04 | 27.822 |
| S3 | 0.435 | 6.488 | 0.123 | 92.954 |
| PS3 | 3.364 | 83.826 | 1.377 | 11.433 |
| S9 | 3.42 | 81.534 | 1.38 | 13.666 |
| PB1 | 2.948 | 89.549 | 1.182 | 6.321 |
| YL1 | 0.489 | 1.55 | 0.031 | 97.93 |
| S1 | 0.685 | 21.852 | 0.323 | 77.14 |
| S2 | 1.317 | 21.397 | 0.412 | 76.874 |
| BL1 | 0.1 | 0.662 | 0.012 | 99.225 |
| P5 | 4.225 | 72.488 | 1.523 | 21.763 |
| P7 | 1.094 | 20.206 | 0.426 | 78.274 |
| P8 | 0.128 | 2.738 | 0.048 | 97.087 |

| | | | | |
|----|-------|--------|-------|--------|
| S7 | 0.807 | 7.153 | 0.181 | 91.859 |
| S8 | 3.688 | 57.218 | 1.233 | 37.861 |

Table S3. Oxygen, nitrogen, argon and carbon stable isotopes and atomic ratios in dissolved gases from Dallol brines and Black and Yellow Lake waters. Hydrothermal springs (S1-S3, S5, S7-S8) and pools (P1-P8, PS3, PB1) of Dallol hydrothermal system and the Black (BL1) and Yellow (YL1) Lake waters.

Table S4

| Sample name | $\delta^{13}\text{C} \text{ ‰ (V-PDB) I}$ | $\delta^{13}\text{C} \text{ ‰(V-PDB) I}$ |
|---|---|--|
| P1 | 966 | 5813 |
| P2 | 7051 | 26039 |
| P3 | 8071 | 26410 |
| P4 | 9573 | 30438 |
| P6 | 1732 | 10195 |
| P18 | 112 | 2520 |
| FeCl ₂ (100 mg/12 ml) | - | 780 |
| FeCl ₂ (600 mg/12 ml) | - | 1332 |
| FeCl ₃ (100 mg/12 ml) | - | 2726 |
| FeCl ₃ (300 mg/12 ml) | - | 2739 |
| FeCl ₃ (600 mg/12 ml) | - | 2330 |
| 0.1 ml (NH ₄) ₂ S ₂ O ₈ (200g/L) | - | 127263 |
| 0.5 ml (NH ₄) ₂ S ₂ O ₈ (200g/L) | - | 198241 |
| 1 ml (NH ₄) ₂ S ₂ O ₈ (sol 200g/L) | - | 150910 |
| sterilized P3 | - | 8087 |

Table S4. First and second batch of measurements of $\delta^{13}\text{C}_{\text{DIC}} \text{ ‰}$ of isotopically labeled Urea for incubations performed in selected samples of Dallol pools and sterilized solutions of FeCl₂, FeCl₃, (NH₄)₂S₂O₈.

II. Publications directly related to this thesis

1. Garcia-Ruiz, J.M., Nakouzi, E., **Kotopoulou E.**, Tamborrino, L., Steinbock, O., 2017. Biomimetic mineral self-organization from silica-rich spring waters, *Science Advances* **3**, e1602285, DOI: 10.1126/sciadv.1602285, **21** citations by December 2019.

SCIENCE ADVANCES | RESEARCH ARTICLE

GEOLOGY

Biomimetic mineral self-organization from silica-rich spring waters

Juan Manuel García-Ruiz,^{1*} Elias Nakouzi,² Electra Kotopoulou,¹ Leonardo Tamborrino,^{1†} Oliver Steinbock²

Purely inorganic reactions of silica, metal carbonates, and metal hydroxides can produce self-organized complex structures that mimic the texture of biominerals, the morphology of primitive organisms, and that catalyze prebiotic reactions. To date, these fascinating structures have only been synthesized using model solutions. We report that mineral self-assembly can be also obtained from natural alkaline silica-rich water deriving from serpentinization. Specifically, we demonstrate three main types of mineral self-assembly: (i) nanocrystalline biomorphs of barium carbonate and silica, (ii) mesocrystals and crystal aggregates of calcium carbonate with complex biomimetic textures, and (iii) osmosis-driven metal silicate hydrate membranes that form compartmentalized, hollow structures. Our results suggest that silica-induced mineral self-assembly could have been a common phenomenon in alkaline environments of early Earth and Earth-like planets.

INTRODUCTION

Living organisms and their biochemical products affect the crystallization of minerals, such as calcium carbonate and calcium phosphate, forming hybrid (organic-inorganic) composite materials, called biominerals, with shapes and textures significantly different from their purely inorganic counterparts (1, 2). These properties were thought to be solely life-originated and are the rationale behind the use of morphology for detection of the oldest remnants of life on this planet and elsewhere (3–5). This view was challenged by the discovery that silica severely affects the crystallization of some carbonates inducing self-assembled inorganic-inorganic composite materials named “biomorphs” (6) that mimic the morphology and chemical signature of the putative microfossils found in Archean cherts (7–9) and the textures of some calcitic biominerals (10). This phenomenon of self-assembly occurs when carbonate minerals precipitate from silica-rich solutions under alkaline conditions, namely, in pH ranging from 9.5 to 12.5 (fig. S1), with a source of carbonate, such as atmospheric CO₂, in temperature ranging from 4° to 100°C.

Likewise, metal silicate hydrate (MSH) membranes, also known as silica gardens, precipitate upon reaction of silica-rich solutions and Me salt solutions (or solids) at a pH range of 11.4 to 12.5 (fig. S1), giving rise to membranous forms of life-like tubes or film-like structures with important catalytic properties (11, 12). It is now known that these membranes show space compartmentalization, separating the inner and outer environments of distinct chemical and textural

Here, we have tested the precipitation of silica-carbonate biomorphs, calcium carbonate mesocrystals, and MSH membranes using natural water collected from the Ney spring (California, USA) (17, 18). The alkaline Ney spring is located in Siskiyou County at the contact between the Trinity Ophiolite Complex and the albite-rich dacitic facies of the Tertiary basaltic-andesitic volcanic deposits. We measured a pH of 11.89 and a silica concentration of 4236 parts per million (fig. S1, table S1, and movie S1) that fulfill the requirements for silica-induced mineral self-assembly. The extremely high pH value of Ney’s water arises from serpentinization (18), a geological process known to produce simple abiotic organic molecules, whereas the high-silica content is due to percolation through silica-rich volcanic rocks (see the Supplementary Materials for details).

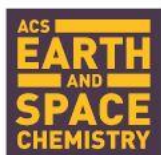
RESULTS AND DISCUSSION

Figure 1 (A to K) shows the biomimetic structures of barium carbonate and silica, grown from the Ney water. Despite some structural differences, these materials conform to the main properties of silica-carbonate biomorphs (6, 19, 20). First, they exhibit smoothly curved surfaces that are not restricted to crystallographic geometries. For example, the Ney biomorphs grow irregular shapes with “appendages” that extend to millimeter-length scales (Fig. 1, A and B, and fig. S2, A and B) and thin sheets that often show topographic oscillations on the order of few micrometers (Fig. 1, E and F, and fig. S2, C and D), a signature of regular, laboratory-grown biomorphs (19). Perhaps the

2017 © The Authors, some rights reserved; exclusive licensee American Association for the Advancement of Science. Distributed under a Creative Commons Attribution NonCommercial License 4.0 (CC BY-NC).

Downloaded from <http://advances.sciencemag.org/> on March 21, 2017

2. Kotopoulou et al., 2019. A Polyextreme Hydrothermal System Controlled by Iron: The Case of Dallol at the Afar Triangle. *ACS Earth and Space Chemistry* Cover 2019 **3** (1), 90-99, DOI: 10.1021/acsearthspacechem.8b00141, 6 citations by December 2019.



Article

Cite This: *ACS Earth Space Chem.* 2019, 3, 90–99

<http://pubs.acs.org/journal/aescq>

A Polyextreme Hydrothermal System Controlled by Iron: The Case of Dallol at the Afar Triangle

Electra Kotopoulou,[†] Antonio Delgado Huertas,[†] Juan Manuel Garcia-Ruiz,^{*,†} Jose M. Dominguez-Vera,[‡] Jose Maria Lopez-Garcia,[§] Isabel Guerra-Tschuschke,^{||} and Fernando Rull[⊥]

[†]Instituto Andaluz de Ciencias de la Tierra, (IACT), 18100 Granada, Spain

[‡]Departamento de Química Inorganica- Instituto de Biotecnología, Universidad de Granada (UGR), 18071 Granada, Spain

[§]Instituto Geológico y Minero de España (IGME), 07006 Palma de Mallorca, Spain

^{||}Centro de Instrumentación Científica, Universidad de Granada (UGR), 18071 Granada, Spain

[⊥]Unidad Asociada UVa-CSIC al Centro de Astrobiología, University of Valladolid, 47002 Valladolid, Spain

Supporting Information

ABSTRACT: One of the latest volcanic features of the Erta Ale range at the Afar Triangle (NE Ethiopia) has created a polyextreme hydrothermal system located at the Danakil depression on top of a protovolcano known as the dome of Dallol. The interaction of the underlying basaltic magma with the evaporitic salts of the Danakil depression has generated a unique, high-temperature (108 °C), hypersaline (NaCl supersaturated), hyperacidic (pH values from 0.1 to -1.7), oxygen-free hydrothermal site containing up to 150 g/L of iron. We find that the colorful brine pools and mineral patterns of Dallol derive from the slow oxygen diffusion and progressive oxidation of the dissolved ferrous iron, the iron-chlorine/-sulfate complexation, and the evaporation. These inorganic processes induce the precipitation of nanoscale jarosite-group minerals and iron(III)-oxyhydroxides over a vast deposition of halite displaying complex architectures. Our results suggest that life, if present under such conditions, does not play a dominant role in the geochemical cycling and mineral precipitation at Dallol as opposed to other hydrothermal sites. Dallol, a hydrothermal system controlled by iron, is a present-day laboratory for studying the precipitation and progressive oxidation of iron minerals, relevant for geochemical processes occurring at early Earth and Martian environments.

KEYWORDS: hyperacidic, hydrothermal, iron oxidation, Dallol, polyextreme, early Earth, Martian analogue-site



3. Kotopoulou et al., 2020. Nanoscale anatomy of Fe-silica self-organized membranes: implications for prebiotic chemistry. *Angew. Chem. (submitted)*.

WILEY-VCH

RESEARCH ARTICLE

Nanoscale anatomy of Fe-silica self-organized membranes: implications for prebiotic chemistry

Electra Kotopoulou^[a], Dr. Miguel Lopez Haro^[b], Prof. Jose Juan Calvino Gamez^[b], and Prof. Juan Manuel Garcia Ruiz^[a]

[a] Instituto Andaluz de Ciencias de la Tierra, Consejo Superior de Investigaciones Científicas- Universidad de Granada, Avda. de las Palmeras 4, 18100, Granada, Spain

[b] Departamento de Ciencia de los Materiales e Ingeniería Metalúrgica y Química Inorgánica, Facultad de Ciencias, Universidad de Cádiz, Campus Río San Pedro, Puerto Real, 11510-Cádiz, Spain

Supporting information for this article is given via a link at the end of the document.

Abstract: Iron-silica self-organized membranes, so-called chemical gardens, behave as fuel cells and catalyze the formation of amino-carboxylic acids and RNA nucleobases from organics that were available on early Earth. Despite their relevance for prebiotic chemistry, little is known about their structure and mineralogy at the nanoscale. Here we studied FIB-milled sections of iron-silica membranes grown from synthetic and natural, alkaline, serpentinization-derived fluids, thought to be widespread on early Earth. Advanced electron microscopy tools show they are composed of amorphous silica and iron nanoparticles of large surface areas and inter-/intra-particle porosity. Their building resembles that of a heterogeneous catalyst, but they also exhibit a bilayer structure. Additional surface area measurements suggest that membranes grown from natural waters hold even higher catalytic potential. Considering their geochemically plausible precipitation in the early hydrothermal systems where abiotic organics were also produced, iron-silica membranes might have assisted the generation and organization of the first biologically relevant organics.

Introduction

One of the most critical steps in the emergence of life on Earth was the concentration and oligomerization of the biologically relevant organic molecules. But, the information available about water bodies/primitive oceans on Hadean-Early Archean earth strongly suggests that concentrations of the abiotic building blocks (e.g. amides, lipids, amino acids, etc.) were too dilute for significant oligomerization to occur. To solve this conundrum, absorption on mineral surfaces has been put forward as a plausible mechanism for the significant concentration of the first organic molecules [1-3]. In this context, multiple studies examined the role of mineral surfaces in the chemical polymerization reactions that might have taken place at early Earth, and in the formation of a proto-cellular membrane by allowing amphiphilic molecules, such as fatty acids, to interact with clays, silica, pyrite, iron-oxides, iron-sulfides etc., assisting the formation of a vesicle [4-10]. Based on these, and other works, it is now generally accepted that mineral-mediated membranes may have provided a geochemical pathway to the transition from inorganic chemistry to biology.

Among all mineral-mediated pathways that have been explored

a concentrated Me-source (e.g. soluble Me-salt particle or Me-salt solution), due to a reaction-diffusion controlled precipitation process [11, 12]. This leads to the formation of a diaphragm membrane with compartmentalized spaces, separating two very distinct chemical environments in terms of pH and ions concentrations. It has been shown that these drastic differences across the membrane generate electrochemical potential and electrical current, able to endure for several hours/days (as long as the system remains far from equilibrium), thus, presenting battery-like properties [13, 14]. Owing to the generated pH-Eh interface, these membranes have been paralleled to hydrothermal chimneys [15, 16, 17], although the precipitation mechanism is quite different, i.e. in chemical gardens the cations directly react with silicate (or other anions) and hydroxide ions to yield metal-silica hydrates, whereas mineral precipitation in chimneys occurs due to pressure/temperature decrease and mixing with seawater. Nonetheless, these membranes are thought to have served as electron/proton conductors and redox catalysts at the early Earth hydrothermal vents environments [15, 16, 18]. Hydrothermal settings have been shown to generate abiotic organics and have been proposed as possible niches for the emergence of metabolism [19, 20].

Although a wide variety of synthetic and natural Me-membranes can be produced [21, 22, 23], those made with Fe(II/III) soluble particles/solutions are by far the most relevant for early Earth geochemistry and prebiotic chemistry. Iron is the fourth most abundant element in Earth's crust that has been readily available in early Earth (in the reduced form), being a primary component of the early oceans, sediments and hydrothermal precipitates [24, 25]. The role of ferrous iron in prebiotic chemistry was recently highlighted by [26] that demonstrated that by mixing it with pyruvate and glycinate (two products of abiotic CO₂ reduction) they can build up nine of the eleven intermediates of the biological Krebs cycle, including all five universal metabolic precursors, supporting the theory for a geochemical origin of the metabolism. With respect to the Me-silica membranes, those made with iron-salts/salt solutions have been found to show the highest battery-like performance, generating more than 550 mV enduring for several hours [21, 22]. Moreover, it was demonstrated that iron membranes can catalyze the condensation of formamide (CH₃NO) -a critical intermediary in Miller-type reactions thought to be widespread in early Earth- yielding the four nucleobases of RNA, three amino acids and several carboxylic acids in a single experiment at 80 °C

III. Publications non related to this thesis

1. F. Otálora, A. Mazurier, J.M. García-Ruiz, M.J. Van Kranendonk, **E. Kotopoulou**, A. El Albani, and C. J. Garrido, 2018. A crystallographic study of crystalline casts and pseudomorphs from the 3.5 Ga Dresser Formation, Pilbara Craton (Australia). *J. Appl. Cryst.* (2018). 51, 1050–1058 (Cover), 6 citations by January 2020.

research papers



JOURNAL OF
APPLIED
CRYSTALLOGRAPHY

ISSN 1600-5767

A crystallographic study of crystalline casts and pseudomorphs from the 3.5 Ga Dresser Formation, Pilbara Craton (Australia)

Fermin Otálora,^a A. Mazurier,^b J. M. Garcia-Ruiz,^{a*} M. J. Van Kranendonk,^c E. Kotopoulou,^a A. El Albani^b and C. J. Garrido^a

Received 16 October 2017
Accepted 15 May 2018

Edited by J. Hajdu, Uppsala University, Sweden, and The European Extreme Light Infrastructure, Czech Republic

Keywords: aragonite; pseudomorphs; crystal morphology; X-ray tomography; precambrian.

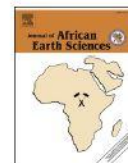
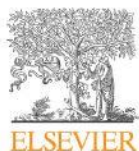
Supporting information: this article has supporting information at journals.iucr.org/j

^aLaboratorio de Estudios Cristalográficos, Instituto Andaluz de Ciencias de la Tierra (CSIC-UGR), Avenida de las Palmeras, 4, Armilla, Granada, Spain, ^bIC2MP, UMR CNRS 7285, Equipe E2 HydrASA, Université de Poitiers, 5 rue Albert Turpain, Bâtiment B8, TSA 51106, 86073 Poitiers Cedex 9, France, and ^cSchool of Biological, Earth and Environmental Sciences and Australian Centre for Astrobiology, University of New South Wales Sydney, Kensington, NSW 2052, Australia.

*Correspondence e-mail: juanmanuel.garcia@csic.es

Crystallography has a long history of providing knowledge and methods for applications in other disciplines. The identification of minerals using X-ray diffraction is one of the most important contributions of crystallography to earth sciences. However, when the crystal itself has been dissolved, replaced or deeply modified during the geological history of the rocks, diffraction information is not available. Instead, the morphology of the crystal cast provides the only crystallographic information on the original mineral phase and the environment of crystal growth. This article reports an investigation of crystal pseudomorphs and crystal casts found in a carbonate-chert facies from the 3.48 Ga-old Dresser Formation (Pilbara Craton, Australia), considered to host some of the oldest remnants of life. A combination of X-ray microtomography, energy-dispersive X-ray spectroscopy and crystallographic methods has been used to reveal the original phases of these Archean pseudomorphs. It is found with a high degree of confidence that the original crystals forming in Archean times were hollow aragonite, the high-temperature polymorphs of calcium carbonate, rather than other possible alternatives such as gypsum ($\text{CaSO}_4 \cdot 2\text{H}_2\text{O}$) and nahcolite (NaHCO_3). The methodology used is described in detail.

2. Margariti, E., Stathopoulou, E.T., Sanakis, Y., **Kotopoulou E.**, Pavlakis, P., Godelitsas, A., 2019. A geochemical approach to fossilization processes in Miocene vertebrate bones from Sahabi, NE Libya, *Journal of African Earth Sciences*, **149**, 1-18. 1 citation by January 2020.



A geochemical approach to fossilization processes in Miocene vertebrate bones from Sahabi, NE Libya



E. Margariti^{a,*}, E.T. Stathopoulou^a, Y. Sanakis^b, E. Kotopoulou^{a,c}, P. Pavlakis^a, A. Godelitsas^a

^a Department of Geology and Geoenvironment, National and Kapodistrian University of Athens, Zographou Campus, 15784, Athens, Greece

^b Institute of Nanoscience and Nanotechnology (INN), NCSR "Demokritos", 15310 Aghia Paraskevi, Athens, Greece

^c Instituto Andaluz de Ciencias de la Tierra, Laboratorio de Estudios Cristalográficos, Avda. de Las Palmeras, 4, 18100, Armilla (Granada), Spain

ARTICLE INFO

Keywords:

Sahabi
Libya
Fossil bones
Miocene
Bioapatite

ABSTRACT

In the present paper a multi-technique approach was followed in order to study the diagenetic alterations of fifteen fossil bones derived from the Miocene site of Sahabi in NE Libya. Specifically, X-ray Diffraction (XRD) supplemented by the Rietveld method, Scanning Electron Microscopy (SEM), Energy Dispersive X-ray Analysis (EDS), Electron Probe Microanalysis (EPMA) and Fourier Transform Infrared Spectroscopy in the Mid-IR (FTIR, Mid-IR), were performed on fossilized bone fragments belonging mainly to artiodactyl mammals. From the qualitative observation of bone histology by means of SEM, a moderate preservation of the internal bone morphology and limited microbial attack were inferred. The high percentage (wt.%) of F concentration that the EPMA analyses yielded, combined: (a) with the absorbance bands of carbonate anions in the FTIR spectra and (b) the structural parameters calculated by the Rietveld method, revealed the partial substitution of F^- for OH^- and CO_3^{2-} for PO_4^{3-} in the apatite structure. As a result, one of the basic diagenetic trends was the preservation of the inorganic part of the studied samples as carbonate fluorapatite. Additionally, according to our infrared spectra, CO_3^{2-} substituted for OH^- and a carbonate species known to be labile was also present. Apart from F, EPMA also detected S and Fe. Sulfur speciation was studied by micro-XANES, that confirmed the presence of S^{6+} (sulfates). Iron speciation was investigated with Mössbauer spectroscopy, which indicated the possible presence of goethite-type ($FeOOH$) submicroscopic inclusions. In nearly all specimens, quartz and gypsum were identified as the main secondary phases.

3. **E. Kotopoulou et al.,** 2020. Geochemistry and nanomineralogy of Fe-sulfides from As-rich shallow-sea hydrothermal sediments. *Marine Chemistry* (under review).

Geochemistry and nanomineralogy of Fe-sulfides from As-rich shallow-sea hydrothermal sediments

E. Kotopoulou^{1*}, A. Godelitsas¹, J. Göttlicher², R. Steininger², R. Price³, D. A. Fike⁴, J.P. Amend⁵, W.P. Gilhooly III⁶, G. Druschell⁶, P. Nomikou¹, P. Gamaletsos⁷, S. Lozios¹

¹*Department of Geology and Geoenvironment, National and Kapodistrian University of Athens, Zografou Campus, GR-15784 Athens, Greece (*corresponding author ikotopoulou@geol.uoa.gr, current address ekotopoulou@iact.ugr-csic.es)*

²*ANKA Synchrotron Radiation Facility, Karlsruhe Institute of Technology, Karlsruhe, Germany*

³*SUNY Stony Brook, School of Marine and Atmospheric Sciences, Stony Brook, New York, USA*

⁴*Department of Earth and Planetary Sciences, Washington University in St. Louis, St. Louis, MO, USA*

⁵*Department of Earth Sciences, University of Southern California, Los Angeles, CA, USA*

⁶*Department of Earth Sciences, Indiana University-Purdue University Indianapolis, Indianapolis, IN, USA*

⁷*Center for Electron Nanoscopy, Technical University of Denmark, Denmark*

ABSTRACT

Nanosized Fe-sulfides fuel Fe, S and C biogeochemical cycles in modern marine environments and hydrothermal vents. In addition, these minerals have been proposed as key catalytic phases of prebiotic reactions in hydrothermal settings of early Earth. Yet, the majority of studies have focused on synthetic Fe-sulfides and at present we lack knowledge about the occurrence of natural Fe:S nanophases (i.e. nanominerals and amorphous

Curriculum Vitae

PERSONAL INFORMATION

Name: Ilektra E. Kotopoulou
Date of birth: 26.07.1989
Nationality: Greek
Languages: English (C2), Michigan University (2004);
Spanish (equivalent to C1); Greek (mother tongue)
e-mail addresses: ekotopoulou@iact.ugr-csic.es,
geoelectra.kotopoulou@gmail.com
contact telephone: +34 722208257,
@GeoElectra

EDUCATION

2020

PhD student in Earth Sciences at CSIC (Spanish National Research Council) – UGR (University of Granada, Spain) studying “**Mineral Self-Organization in Extreme Geochemical Environments: Implications for Prebiotic Chemistry and Life Detection**”, under the supervision of Prof. J.M. Garcia-Ruiz, in the framework of Prometheus ERC grant agreement no. 340863.

Maternity break between November 2018 to November 2019

2015

MSc in Applied Environmental Geology by the School of Science, University of Athens (Greece), grade excellent (9.46/10.00). Master thesis entitled “**Mineralogy and Biogeochemistry of the Shallow-sea Hydrothermal System off SE Milos Island (Greece)**”, under the supervision of Assoc. Prof. A. Godelitsas, in collaboration with the ANKA Synchrotron Radiation Facility-KIT (Germany), Stony Brook (USA), University of Southern California (USA), Washington University in St. Luis (USA) and Indiana University-Purdue University Indianapolis (USA) in the framework of the IKY-DAAD grant 7/2015 awarded to A. Godelitsas and J. Göttlicher, and the US National Science Foundation grants (OCE-1061476) awarded to D. A. Fike and J. Amend, and (OCE-1261424) to G. Druschel.

2014

BSc in Geology and Geoenvironment (2014). School of Science, National and Kapodistrian University of Athens/Greece, grade very good.

PUBLICATIONS

Peer-reviewed International Journals

2020

1. Kotopoulou, E., Lopez-Haro, M, Calvino, J.J., Garcia-Ruiz., J.M. **Nanoscale anatomy of Fe-silica self-organized membranes: implications for prebiotic chemistry** *Angew. Chem.* (submitted).
2. Kotopoulou, E., Godelitsas, A., Göttlicher, J., Steininger, R., Price, R., Fike, D.A, Amend, J.P., Gillhooly III, W.P., Druschel, G.K., Nomikou, P., Gamaletsos, P., Lozios, S., **Geochemistry and nanomineralogy of Fe-sulfides from As-rich shallow-sea hydrothermal sediments** *Marine Chemistry* (under review).
Kotopoulou, E., Rull., F., Garcia-Ruiz., J.M. **Raman spectral study of mineral precipitates from the hydrothermal brines of Dallol, Ethiopia: a mineralogical Martian analogue-site** (to be submitted).

2019

3. Kotopoulou, E., Delgado-Huertas, A., Garcia-Ruiz., J.M., Dominguez-Vera, J.M., Garcia-Lopez, J.M., Guerra-Tschuscke, I., Rull., F. **A poly-extreme hydrothermal system under the control of iron: The case of Dallol at the Afar Triangle.** *ACS Earth and Space Chemistry (cover)*, 2019, 3, 1, 90-99. DOI: 10.1021/acsearthspacechem.8b00141.
4. Margariti, E., Stathopoulou, E.T., Sanakis, Y., Kotopoulou, E., Pavlakis, P., Godelitsas, A. **A geochemical approach to fossilization processes in Miocene vertebrate bones from Sahabi, NE Libya.** *Journal of African Earth Sciences*, 2018, DOI: 10.1016/j.jafrearsci.2018.07.019.

2018

5. Otálora, F., Mazurier, A., García-Ruiz, JM., Van Kranendonk, M.J., Kotopoulou, E., El Albani, A., Garrido, C.J. **A crystallographic study of crystalline casts and pseudomorphs from the 3.5 Ga Dresser Formation, Pilbara Craton (Australia),** *Journal of Applied Crystallography (cover)*, 51, 1050-1058, DOI: 10.1107/S1600576718007343.

2017

6. Garcia-Ruiz, J.M., Nakouzi, E., Kotopoulou, E., Tamborrino, L. and Steinbock, O., 2017. **Biomimetic mineral self-organization from silica-rich spring waters.** *Science Advances*, 3, e1602285, DOI: 10.1126/sciadv.16022817.

International Conferences

2018

1. Kotopoulou, E., Lopez-Haro, M., Calvino Gamez, J.J., Van Zuilen, M., Garcia-Ruiz, J.M., 2018. **Precipitation of self-organized Fe-silica membranes on early Earth: Friend or Foe?** Abstract, 28th Annual **Goldschmidt** Conference, Session: *Prebiotic chemistry and the Archean record of early life* (oral).

2017

2. Kotopoulou, E., Garcia-Ruiz, J.M., Delgado-Huertas, A., Lopez-Garcia, J.M., Dominquez-Vera, J.M., Guerra, I., 2017. **Geochemistry and mineralogy of the hyperacidic hydrothermal system of Dallol, Ethiopia.** Abstract, 27th Annual **Goldschmidt** Conference, Session: *Hydrothermal biogeochemistry and geobiology* (oral).
3. Garcia Ruiz, J.M., Kotopoulou, E., Nakouzi, E., Steinbock, O., Van Zuilen, M., 2017. **Geochemical Plausibility of Silica Self-Assembly and its Relation to Life Detection Studies and Prebiotic Chemistry.** Abstract, 27th Annual **Goldschmidt** Conference, Session: *Chemistry versus Biology – How to distinguish traces of life on Earth and Beyond* (oral).

2015

4. E. Kotopoulou, A. Godelitsas, J. Göttlicher, R. Steininger, R. Price, D.A. Fike, J.P. Amend, W.P. Gilhooly III, G.K. Druschel, T.J. Mertzimekis, P. Gamaletsos, F.-C. A. Kafantaris, 2015. **Sulfur Mineralogy and Speciation in the Shallow-sea Hydrothermal Sediments off Milos**

Island (Greece). Abstract, 25th Annual **Goldschmidt** Conference, Session: *Sulfur Geomicrobiology* (poster).

5. **E. Kotopoulou**, T.J. Mertzimekis, A. Godelitsas, R. Price, D.A. Fike, J.P. Amend, W.P. Gillhooly III, G.K. Druschel, 2015. **Natural Radioactivity Levels in the Shallow-sea Hydrothermal System off Milos Island, Greece.** **ENVIRA2015**, International Conference on Environmental Radioactivity (poster).

FIELDWORK

Rio Tinto, SW Spain (2018)

Sampling of liquids, acid mine effluents and mineral precipitates from Rio Tinto acid mine drainage system/astrobiological site.

Ney springs - continental serpentinization site, NE California (2017)

Sampling of water, mineral precipitates and gases from the hyperalkaline silica-rich springs of the Ney, in Trinity Ophiolite complex, Shasta Mt., Siskiyou County, California.

Dallol hyperacidic hydrothermal system, Afar Triangle, NE Ethiopia (2016-2017)

Two international multi-disciplinary field campaigns at the Dallol hyperacidic hydrothermal system in the Danakil Depression for the sampling of hydrothermal brines, precipitates and gases.

Soda lakes of the Rift Valley, Kenya (2016)

Sampling of lake water, hydrothermal brines, gases and mineral precipitates from the soda lakes of Kenya: Magadi, Elementaita-Nakuru-Naivasha, Bogoria, Baringo- Ol Kokwe Island.

RESEARCH PROJECTS

ERC Prometheus advanced grant: **Geochemical self-organized pathways to mineral-organic chemical coupling and the origin of life**, under the scientific coordination of Prof. Garcia Ruiz, Spanish National Research Council (CSIC)- University of Granada (UGR) <http://prometheus-erc.eu/>, October 2015- February 2020.

IKY-DAAD: Biogenic sulfur minerals in the environment of eastern Mediterranean volcanoes: the case of shallow-sea hydrothermal vents off Milos Island, Greece of the University of Athens/Greece and ANKA Synchrotron Radiation Facility-KIT/Germany, Scientific Coordinators: Dr. A. Godelitsas (UoA) and Dr. J. Goettlicher (KIT, ANKA), September 2014- December 2015.

GR-FR Bilateral Project: Study of the sea level changes in Cyclades islands (Greece) during the Late Holocene of the University of Athens/Greece - Aix-Marseille University (AMU)/France “EMerChanCy” - supported by the General Secretariat for Research and Technology of Greece. Scientific coordinators Prof. Evelpidou (UoA) and Prof. Morhange (AMU), October 2013- October 2015.

SCHOLARSHIPS - GRANTS - AWARDS

Oral Presentation Award for “Geochemical plausibility of iron-silica self-assembled biomimetic structures” during the international PhD Students’ Conference organized by the Institute de Physique du Globe de Paris (IPGP), March 2017.

Poster Presentation Award for “Self-assembled structures of iron silicate hydrates from alkaline springs” during the 5th International School on Crystallization: Minerals, New Materials, Drugs, Foods, Agrochemicals, (Granada, ISC2016), May 2016.

Student Journal Award by the IUCr (International Union of Crystallography) and the COSPAR (Committee of Space Research), for the project of “Characterization of rock samples” undertaken during the “Crystallography for Space Sciences” training school, April 2015.

IKYDA (IKY-DAAD) research scholarship for training on **Synchrotron-based Spectroscopy (μ -XRF mapping, S-Fe-As μ -XANES, μ -XRD)** at SUL-X beamline of ANKA Synchrotron Radiation Facility, Karlsruhe Institute of Technology (KIT), March 2015.

STSM (Short Term Scientific Mission) grant for training on **Optically Stimulated Luminescence (OSL) dating method**, in Leibniz Institute for Applied Geophysics in Hannover (LIAG, Germany) by the European Program COST Action ES0701, December 2011.

INTERNATIONAL TRAINING SCHOOLS

European Summer Workshop “**TEM-UCA 2017 - Transmission Electron Microscopy of Nanomaterials, Imaging and Spectroscopic Techniques**”, 17 - 21 July, Cádiz (Spain) organized by the University of Cadiz (UCA), Spain.

“**5th International School on Crystallization: Minerals, New Materials, Drugs, Foods, Agrochemicals**”, Granada ISC2016, May 2016, organized by the Laboratory of Crystallographic Studies of Granada (LEC) and the International Union of Crystallography (IUCr).

International Training School on “**Crystallography for Space Sciences 2016**” organized by the Committee of Space Research (COSPAR), the International Union of Crystallography (IUCr) and the International Astronomical Union (IAU) at INAOE and BUAP, Puebla-Mexico. April 17-29, 2016.

COST International Training School on “Glacial Isostatic Adjustment (GIA) modeling” in Gävle (Sweden), July 2011, by the European Programme COST action ES0701, Improved Constraints on Models of GIA.

ANALYTICAL TECHNIQUES

Microscopies: Scanning and Transmission Electron Microscopy (EDS, HR-TEM, HR-HAADF, SAED, EELS)

Spectroscopies: IR, micro-Raman, UV-Vis, Gamma-ray, Synchrotron-based micro-XRF/micro-XRD/micro-XANES

X-ray Diffraction: PXRD

Dating: Optically Stimulated Luminescence

Crystallization: Crystallization in Gels

SCIENTIFIC OUTREACH

‘Women in STEM’ presentation to students of secondary schools from the province of Granada for the celebration of the International Day of Women and Girls in Science, 11th of February, 2018, at the EEZ-CSIC Institute, Granada, Spain.

Participation in the scientific documentary: ‘Dallol Volcano - On the frontiers of life’ <https://vimeo.com/169516179> by Olivier Grunewald, Camera Lucida Productions and CPB International, 2017.

Science week 7th -11th November 2016 – Scicom talk on the ‘Fieldtrip to another planet: Dallol’ at the Instituto Andaluz de Ciencias de la Tierra (IACT-CSIC), Granada, Spain.

Participation in the jury committee of the ‘Crystallization contest of secondary schools of Andalucía, Spain’ 2016 and 2017 editions.

MEMBER OF SCIENTIFIC SOCIETIES AND GROUPS

European Association of Geochemistry (**EAG**)

Geological Society of America (**GSA**)

International Association of Volcanology and Chemistry of the Earth's Interior (**IAVCEI**)

International Union of Crystallography (**IUCr**)

Committee on Space Research (**COSPAR**)



ugr

Universidad
de Granada



European Research Council
Established by the European Commission



CSIC

CONSEJO SUPERIOR DE INVESTIGACIONES CIENTÍFICAS



IACT

INSTITUTO ANDALUZ DE CIENCIAS DE LA TIERRA